

# On peristaltic transport with heat transfer and rotation aspects



*By*

*Hina Zahir*

**Department of Mathematics  
Quaid-I-Azam University  
Islamabad, Pakistan  
2018**

# On peristaltic transport with heat transfer and rotation aspects



By

*Hina Zahir*

Supervised By

*Prof. Dr. Tasawar Hayat*

Department of Mathematics  
Quaid-I-Azam University  
Islamabad, Pakistan  
2018

# On peristaltic transport with heat transfer and rotation aspects



By

*Hina Zahir*

A DISSERTATION SUBMITTED IN THE PARTIAL FULFILLMENT OF THE REQUIREMENT  
FOR THE DEGREE OF  
DOCTOR OF PHILOSOPHY  
IN  
MATHEMATICS

Supervised By

*Prof. Dr. Tasawar Hayat*

Department of Mathematics  
Quaid-I-Azam University  
Islamabad, Pakistan  
2018

## Author's Declaration

I Hina Zahir hereby state that my PhD thesis titled On Peristaltic transport with heat transfer and rotation aspects is my own work and has not been submitted previously by me for taking any degree from the Quaid-i-Azam University Islamabad, Pakistan or anywhere else in the country/world.

At any time if my statement is found to be incorrect even after my graduate the university has the right to withdraw my PhD degree.

*Hina*

Name of Student: Hina Zahir

Date: 20-08-2018



### Plagiarism Undertaking

I solemnly declare that research work presented in the thesis titled "On Peristaltic transport with heat transfer and rotation aspects" is solely my research work with no significant contribution from any other person. Small contribution/help wherever taken has been duly acknowledged and that complete thesis has been written by me.

I understand the zero tolerance policy of the HEC and Quaid-i-Azam University towards plagiarism. Therefore, I as an Author of the above titled thesis declare that no portion of my thesis has been plagiarized and any material used as reference is properly referred/cited.

I undertake that if I am found guilty of any formal plagiarism in the above titled thesis even afterward of PhD degree, the University reserves the rights to withdraw/revoke my PhD degree and that HEC and the University has the right to publish my name on the HEC/University Website on which names of students are placed who submitted plagiarized thesis.

Student/Author Signature: \_\_\_\_\_

Hina  
20/08/2018

Name: Hina Zahir

# On Peristaltic transport with heat transfer and rotation aspects

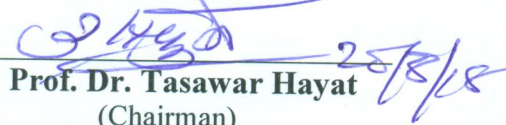
By

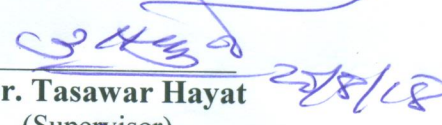
*Hina Zahir*


## CERTIFICATE

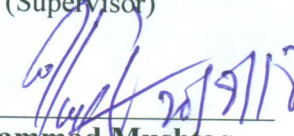
A DISSERTATION SUBMITTED IN THE PARTIAL FULFILLMENT OF THE  
REQUIREMENTS FOR THE DEGREE OF THE DOCTOR OF  
PHILOSOPHY

We accept this dissertation as conforming to the required standard

1.  25/8/18  
**Prof. Dr. Tasawar Hayat**  
(Chairman)

2.  25/8/18  
**Prof. Dr. Tasawar Hayat**  
(Supervisor)

3.   
**Dr. Rahmat Ellahi**  
Associate Professor  
Department of Mathematics & Statistics  
International Islamic University  
H-10 Islamabad  
(External Examiner)

4.  25/9/18  
**Dr. Muhammad Mushtaq**  
Associate Professor  
Department of Mathematics  
COMSATS, Park Road Chak Shahzad,  
Islamabad  
(External Examiner)

**Department of Mathematics  
Quaid-I-Azam University  
Islamabad, Pakistan**

**2018**



## Certificate of Approval

This is to certify that the research work presented in this thesis entitled **On Peristaltic transport with heat transfer and rotation aspects** was conducted by Ms. **Hina Zahir** under the supervision of **Prof. Dr. Tasawar Hayat**. No part of this thesis has been submitted anywhere else for any other degree. This thesis is submitted to the Department of Mathematics, Quaid-I-Azam University, Islamabad in partial fulfillment of the requirements for the degree of Doctor of Philosophy in Field of Mathematics from Department of Mathematics, Quaid-I-Azam University Islamabad, Pakistan.

Student Name: **Hina Zahir**

Signature: Hina  
20/08/2018

External committee:

a) **External Examiner 1:**

Signature:

Name: **Dr. Rahmat Ellahi**

Designation: Associate Professor

Office Address: Department of Mathematics , IIU Islamabad

R. Ellahi

b) **External Examiner 2:**

Signature: \_\_\_\_\_

Name: **Dr. Muhammad Mushtaq**

Designation: Associate Professor

Office Address: Department of Mathematics , COMSATS, Islamabad

M. Mushtaq  
20/08/18

c) **Internal Examiner :**

Signature: \_\_\_\_\_

Name: **Dr. Tasawar Hayat**

Designation: Professor

Office Address: Department of Mathematics, QAU Islamabad.

T. Hayat  
25/8/18

**Supervisor Name:**

Signature: \_\_\_\_\_

**Prof. Dr. Tasawar Hayat**

T. Hayat  
25/8/18

**Name of Dean/ HOD**

Signature: \_\_\_\_\_

**Prof. Dr. Tasawar Hayat**

T. Hayat  
25/8/18

*Dedicated*  
*To*  
*My Parents and*  
*Supervisor*



# Acknowledgments

Although it is just my name mentioned on the cover, many people have contributed to this research in their own particular way and for that I want to give them special thanks. First I am thankful to **Allah**, who supplied me with the courage, the guidance and the love to complete this research. I also express my sincere gratitude to **Prophet Hazrat Mohammed S.A.W.** for His guidance through teachings of patience, motivation and immense knowledge.

Special appreciation goes to my Supervisor and Chairman of Mathematics Department, **Prof. Dr. Tasawar Hayat**, for his supervision and constant support. His invaluable help of constructive comments and suggestions throughout the research work have contributed to the success of this thesis. I am very grateful for him since he gave me the chance to work on an interesting and practical topic. In short, his tireless work, unique personality and dedication to profession cannot be expressed in words.

I would also like to acknowledge all the teachers I learnt from since my childhood. I would not have been here without their guidance, blessing and support. I also express my gratitude to respected post graduate professors **Prof. Dr. Muhammad Yousaf Malik Prof. Dr. Muhammad Ayub, Prof. Dr. Sohail Nadeem and Dr. Masood Khan** for their valuable and constructive suggestions in all aspects.

I wish to express my deep and sincere gratitude to my family for their continuous and unparalleled love, help and support. I am especially grateful to my parents **Mr. and Mrs. Zahir Muhammad**, who supported me emotionally and financially. Especially after my father's death, my mother understands me like friends and supports me everywhere. May Allah give her healthy long life (Ameen). I am grateful to my **brothers, sisters, brothers in law and bhabhis** for always being there for me as a friends. They selflessly encouraged me to explore new directions in life and seek my own destiny. How can I forget to thank little angels **Nephews** and **Nieces** for the love and care they gave me. This journey would not have been possible without my family and I dedicate this milestone to them as well.

To my friends **Sadia Ayub** and **Anum Tanveer** thank you for listening, offering me advice and supporting me through this entire process. The debates, breakfast, lunches, long drives as well as editing advises, visit to shopping malls and different universities are general help and this friendship were all greatly appreciated. Special thanks for their prayers well wishes, phone calls, e-mails, texts and being their whenever I needed a friend. The mind refreshing music, entertaining games which has also shared part of itself in accomplishment of my work. I would also like to thank my all lab fellows for their valuable and polite discussions.

I would also like to thank **Zahoor bhae, Sajid bhae, Safdar bhae, Sheraz sahib** and all other office staff of the department for their administrative support throughout the completion of Ph.D.

May Allah bless health and wealth to all those who pray for me (Ameen).

**Hina Zahir**  
**(20-08-2018)**

# Preface

Importance of peristalsis is recognized for numerous physiological and industrial applications which include swallowing food through oesophagus, capillaries and arterioles, in the vasomotion of venules, in sanitary fluid transportation, toxic liquid transport in the nuclear industry, digestive system catastalsis, ureteral tract, carrying of bile from gallbladder to duodenum, blood pumping, ovum transport, peristaltic pumps, locomotion of worms, roller and finger pumps etc. The waves of constant wavelength and amplitude (periodic waves) traveling along the tube give rise peristaltic excitation in human physiology. Further peristaltic transport of fluid with heat transfer is quite significant in oxygenation, hemodialysis, conduction of tissues, radiation between environment and its surface and heat convection for blood flow from the pores of tissues. As heat transfer fundamentally refers to the exchange of thermal energy between the different components of a physical system. Heat transfer rate depends upon temperature of different components and the physical properties of the medium through which heat transfer takes place. Heat transfer is further important in many processes including the design of chemical processing equipment, food processing and cooling towers, power generation, distribution of moisture over grove fields and many others. Further in rotating frame the study of fluid flow has vital applications in astronomy, geophysics, atmospheric science, stellar dynamics and earth sciences. Phenomenon of rotation can be understood by ocean circulation, flight dynamics, formation of galaxies and amusement rides, which gives rise to the effects of Coriolis and centrifugal force in addition to inertial forces. Peristalsis in presence of rotation has relevance with saline water, blood and bio fluid such as intestines, arterioles and ureters.

Keeping all such facts in mind, the objective here is to develop fluid flows through periodic wave transport in channels. Such considerations are focused particularly for human tubular organs functioning to inspect the outcomes of different effects. Modeling and analysis are carried out by using basic laws and different techniques. Finally the present thesis is structured as follows:

Chapter one provides literature review for peristaltic mechanism under different aspects. This chapter also consists of fundamental expressions.

The peristaltic flow of viscous fluid in a rotating channel is discussed in chapter two.

*Channel walls are compliant. MHD effect is present. Hall current and Joule heating are taken into account. Convective conditions for heat transfer in the formulation are adopted. Lubrication approach is followed. Axial and secondary velocities are computed and analyzed. Results of this chapter are published in **Results in Physics 7 (2016) pp. 2831-2836.***

*Chapter three extends the research work of chapter two for heat and mass transfer. Thermophoresis, chemical reaction heat source/sink and thermal radiation are considered. Exact solutions to resulting problems invoking lubrication approach are established. The axial and secondary velocities and temperature are analyzed. Graphs are sketched for a parametric study for effects of thermophoretic, chemical, non-uniform heat source/sink, radiation and rotation parameters. The findings of this chapter are published in **Results in Physics 6 (2016) pp. 1044-1050.***

*Chapter four aims to examine the magnetohydrodynamic (MHD) peristaltic transport of Prandtl fluid in a rotating medium. The channel walls satisfy wall properties. The relevant formulation is made on the basis of long wavelength approximations. Numerical solutions for axial and secondary velocities, temperature and heat transfer coefficient are presented. The contents of this chapter are published in **Computers in Biology and Medicine 79 (2016) pp. 215-221.***

*Chapter five examines peristalsis transport of Prandtl fluid in a rotating channel. In fact results of chapter four here are modified for Soret and Dufour effects. The governing equations have been modeled and simplified using lubrication approach. The solution expressions are approximated numerically for the graphical results. The findings of this chapter have been published in **Results in Physics 8 (2018) 1291-1300.***

*The purpose of chapter six is twofold. Firstly to explore peristaltic flow of an incompressible Ree-Eyring fluid. Secondly to inspect non-uniform heat source/sink effect. Convective conditions for heat transfer in the formulation are also adopted. Closed form solutions for axial and secondary velocities, pressure rise per wavelength, flow rate due to secondary flow and temperature are obtained by considering small Reynolds number and long wavelength approximation. The results obtained in this chapter are published in **Chinese Journal of Physics 55 (2017) pp. 1894-1907.***

*The objective of chapter seven is to analyze peristalsis of Ree-Eyring fluid in a rotating channel. Interest here is covered by three concepts. Firstly to examine the influence of Hall current and ion slip effects. Secondly to examine the influence of heat transfer*



with viscous and Ohmic dissipation. Thirdly to address the impact of convective conditions. The relevant problems are formulated. Out coming problems through lubrication approach are solved. Attention is focused to the temperature, velocities and heat transfer coefficient. Material of this chapter is submitted for publication in *Journal of Theoretical and Applied Mechanics*.

Chapter eight investigates the peristalsis Couple stress fluid in a non-uniform rotating channel. The generation of fluid temperature due to thermal radiation and non-uniform heat source/sink effects is recorded. The flow and heat transfer are discussed in presence of wall slip conditions. Numerical technique is applied to solve the non-linear system. Attention is focused for the temperature, both axial and secondary velocities, heat transfer coefficient and streamlines. The research presented in this chapter is published in *Results in Physics 7 (2017) pp. 2865-2873*.

Chapter nine is intended to study effects of heat transfer in peristaltic flow when both the system and fluid are rotating. Third grade fluid is taken in convectively heated channel. Nonlinear radiation is discussed. This study is motivated towards investigating the physiological flows in rotating frame. Lubrication approach is adopted for problem formulation. Impact of various emerging physical parameters on the velocity, temperature and heat transfer coefficient is described. Estimated results are discussed in graphical representation. Material of this chapter is published in *Canadian Journal of Physics*.

In thermal engineering processes many researchers have shown that second law of thermodynamics is more efficient in optimizing the system than first law. Since first law of thermodynamics does not determine the fluctuations in energy and only manipulates the accounting of energy. Therefore in chapter ten we analyze the entropy generation on the peristaltic flow of Casson fluid in a symmetric rotating channel. Heat transfer is examined for thermal radiation and viscous dissipation effects. Velocity and thermal slip effects at the channel boundaries are also considered. The fluid parameter, Taylor and Brinkman number, radiation and wall parameters effects on the axial and secondary velocities, temperature and entropy generation are discussed in detail. Main points of the resulting problem have been highlighted. The contents of this chapter are published in *Results in Physics 7 (2017) pp. 3668-3677*.

# Contents

<b>1 Literature review and basic laws</b>	<b>5</b>
1.1 Literature survey . . . . .	5
1.2 Basic equations . . . . .	14
1.2.1 Mass conservation . . . . .	14
1.2.2 Momentum conservation . . . . .	15
1.2.3 Energy conservation . . . . .	15
1.2.4 Concentration conservation . . . . .	15
1.2.5 Transformations and volume flow rate . . . . .	16
1.2.6 Dimensionless parameters . . . . .	17
<b>2 Hall current and Joule heating impacts in peristaltic transport of rotating liquid</b>	<b>19</b>
2.1 Introduction . . . . .	19
2.2 Problem development . . . . .	19
2.3 Solution methodology . . . . .	22
2.4 Discussion . . . . .	22
2.4.1 Axial velocity . . . . .	22
2.4.2 Secondary velocity . . . . .	24
2.4.3 Temperature . . . . .	25
2.4.4 Heat transfer coefficient . . . . .	27
2.5 Conclusions . . . . .	28

<b>3</b>	<b>Impact of thermal radiation and thermophoresis on peristalsis in rotating frame</b>	<b>30</b>
3.1	Introduction . . . . .	30
3.2	Problem development . . . . .	31
3.3	Solution methodology . . . . .	34
3.4	Discussion . . . . .	34
3.5	Conclusions . . . . .	40
<b>4</b>	<b>Peristaltic activity of rotating Prandtl fluid</b>	<b>42</b>
4.1	Introduction . . . . .	42
4.2	Definition . . . . .	42
4.3	Analysis . . . . .	45
4.4	Conclusions . . . . .	53
<b>5</b>	<b>MHD peristaltic flow of rotating Prandtl fluid with Soret and Dufour effects</b>	<b>54</b>
5.1	Introduction . . . . .	54
5.2	Problem development . . . . .	54
5.3	Solution methodology . . . . .	58
5.4	Discussion . . . . .	58
5.4.1	Axial velocity . . . . .	58
5.4.2	Secondary velocity . . . . .	60
5.4.3	Temperature . . . . .	62
5.4.4	Concentration . . . . .	65
5.4.5	Heat transfer coefficient . . . . .	68
5.5	Conclusions . . . . .	70
<b>6</b>	<b>Heat transfer analysis on peristalsis of Ree-Eyring fluid</b>	<b>71</b>
6.1	Introduction . . . . .	71
6.2	Problem development . . . . .	71
6.3	Solution methodology . . . . .	75
6.4	Discussion . . . . .	76

6.5	Conclusions . . . . .	82
<b>7</b>	<b>Numerical analysis for ionslip and Hall current on peristaltic transport of rotating Ree-Eyring fluid</b>	<b>84</b>
7.1	Introduction . . . . .	84
7.2	Problem development . . . . .	84
7.3	Solution methodology . . . . .	87
7.4	Discussion . . . . .	88
7.5	Conclusions . . . . .	92
<b>8</b>	<b>Peristalsis of couple stress liquid in a non-uniform rotating geometry</b>	<b>93</b>
8.1	Introduction . . . . .	93
8.2	Problem development . . . . .	93
8.3	Solution methodology . . . . .	96
8.4	Discussion . . . . .	97
	8.4.1 Axial velocity . . . . .	97
	8.4.2 Secondary velocity . . . . .	98
	8.4.3 Temperature profile . . . . .	100
	8.4.4 Heat transfer rate . . . . .	101
	8.4.5 Streamlines . . . . .	103
8.5	Conclusions . . . . .	104
<b>9</b>	<b>Peristaltic motion of third grade fluid subject to nonlinear radiation</b>	<b>106</b>
9.1	Introduction . . . . .	106
9.2	Problem statement . . . . .	106
9.3	Solution methodology . . . . .	109
9.4	Discussion . . . . .	109
	9.4.1 Velocity profile . . . . .	109
	9.4.2 Heat transfer . . . . .	111
9.5	Conclusions . . . . .	115



<b>10 Entropy generation impact on peristaltic motion in a rotating frame</b>	<b>116</b>
10.1 Introduction . . . . .	116
10.2 Problem definition . . . . .	116
10.3 Entropy generation . . . . .	120
10.4 Solution methodology . . . . .	120
10.5 Discussion . . . . .	121
10.5.1 Entropy generation . . . . .	128
10.5.2 Trapping . . . . .	131
10.6 Conclusions . . . . .	132

# Chapter 1

## Literature review and basic laws

This chapter deals with literature review related to peristalsis and transfer of heat with different effects in a rotating frame. Some fundamental equations for fluids flow are also presented in this chapter.

### 1.1 Literature survey

Peristalsis in human physiological systems has gained much attention of the researchers. Engelman [1] was the first to investigate the existence of peristaltic waves in ureter. After his initial work, several other researchers like Lapidés [2], Kiil [3] and Boyarsky [4] put their efforts to extend this study. The phenomenon of peristaltic pumping was discussed by Latham [5]. Shapiro et al. [6] presented experimental work by considering the inertia free flow in a flexible tube. The pioneer work of Latham [5] and Shapiro et al. [6] opened new ways for further advancements in peristaltic transport. After the confirmation of Shapiro's theory based on long wavelength and low Reynolds number approximation by Eckstein [7] and Weinberg [8], a number of attempts have been made for advancements in this direction. Further the ureteral system as peristaltic pump by imposing different waves on ureteral walls was analyzed by Weinberg et al. [9] and Lykoudis [10]. Zein and Ostrach [11] investigated significance of peristalsis in ureteral system. Afterwards, Fung [12, 13] discussed the effect of biomechanical forces on dynamics of urethral muscles. Peristalsis of viscous liquid in both symmetric and asymmetric configurations is explored by Burns and Parkes [14]. Lubrication approach was adopted by Hanin [15] along with

consideration of small amplitude ratio. An investigation on studying the impact of low Reynolds number on peristalsis in a tube of roller pump is carried out by Megininiss [16]. Peristaltic flow of viscous fluid through circular tube is addressed by Yin and Fung [17]. Lew and Fung [18, 19] explored asymmetric flow of viscous fluid in a cylindrical tube. Their investigation presents the importance of fluid motion inside vessels of living organisms. Barton et al. [20] discussed the peristaltic motion in tubes. An analysis on peristalsis of viscous fluid subject to inertial and streamline curvature is conducted by Jaffrin [21]. Tong and Vawter [22] adopted finite element method to analyze the peristaltic transport through a tube. Movement of spermatozoa in tube is mathematically investigated by Semleser et al. [23]. Mitra and Parsad managed to determine the impact of Poiseuille flow on peristalsis in a two dimensional channel [24]. Liron [25] developed the series solution by double expansion about long wavelength and Reynolds number for peristalsis in pipe and channel. He studied the efficiency of biological functions in terms of peristaltic flow. Assumption of small wave number is invoked in his analysis. Impacts of wave amplitude and wavelength on flow field was first presented by Brown and Hung [26]. He observed that reflux occurs on the axis of the tube for short wavelengths. However reflux occurs off the axis for longer wavelengths. A detailed examination of peristaltic flow through pipe and channel is carried out by Srivastava and Srivastava [27]. Nakanishi [28] numerically investigated a two-dimensional model of peristalsis of viscous fluid through a channel with progressive waves of wall contraction. Takabatake et al. [29] adopted finite difference scheme for analyzing the peristaltic pumping through a tube. Peristalsis of incompressible viscous fluid through uniform and non-uniform annulus is elaborated by Makheimer [30]. Inertia and curvature effects on peristalsis in asymmetric geometry is explored by Rao and Mishra [31]. Viscous fluid flow subject to compliant walls has been analyzed by Hayat et al. [32].

There is no doubt that many realistic liquids are different than viscous fluids. Non-Newtonian characteristics have been exhibited by peristalsis transport of chyme in [33] and contraction and expansion of blood vessels in [34]. The classical Navier Stokes relations are unable to describe the nature of rheological complex liquids such as lubricants, hydrocarbons, industrial oils, shampoo, muds, petroleum and blood etc. Non-Newtonian fluids have wide utility in many phenomena. In order to investigate the non-Newtonian behavior of fluids, many models have been formulated by the investigators. Patel and Timol [35] mentioned the stress strain relation-

ship for non-Newtonian fluids. Akbar et al. [36] performed an analysis for flow of Carreau fluid through asymmetric channel. A study on peristaltic transport of Jeffrey fluid through rectangular duct is commenced by Ellahi and Hussain [37]. Jeffrey fluid flow with simplest mathematical form is capable of relating the retardation and relaxation times effects. Bhatti and Abbas [38] investigated peristaltic blood flow by considering Jeffrey model saturating porous medium. Application of low Reynolds number on peristaltic motion of micropolar fluid was discussed by Devi and Devanathan [39]. Adomian decomposition method was adopted by Sheikholeslami et al. [40] in order to investigate Jeffrey-Hamel flow analytically. Long wavelength assumption is employed on two-dimensional peristalsis of non-Newtonian fluid by Rahakrishnamacharya [41]. Srivastava and Saxena [42] observed the peristaltic transport of blood through a tube of uniform diameter. They employed constitutive relation of Casson fluid for blood. Elshehawey et al. [43] scrutinized the peristaltic motion of Carreau fluid by invoking the lubrication approach and employing the perturbation technique for small Weissenberg number. An analytical discussion on flow properties of Carreau fluid in a compliant rectangular duct is commenced by Riaz et al. [44]. Sisko fluid is one of the most important non-Newtonian fluids comprised of shear thinning as well as shear thickening attributes. Sisko fluid model has tendency to represent the properties of Newtonian and non-Newtonian fluids for suitable choice of material fluid parameter. An analysis for porosity and magnetic field effects on flow of Sisko fluid is provided by Hayat et al. [45, 46]. Zaman et al. [47] managed to study blood flow through vessel by assuming the blood as Sisko fluid. Hayat et al. [48] reported a numerical investigation of peristalsis of non-Newtonian Carreau-Yasuda fluid under the influence of Hall effect. Mernone and Mazumdar [49] provided a detailed theoretical investigation of Casson fluid through an axisymmetric channel. Eytan and Elad [50] inspected the motion of intrauterine fluid motion due to myometric contraction as peristaltic transport. Nadeem and Akram [51] scrutinized two-dimensional peristaltic flow of hyperbolic tangent fluid and simplified the problem under lubrication approach. Hina et al. [52] examined the wall properties on peristalsis in a curved channel by considering pseudo-plastic fluid and heat and mass transfer. They discussed the shear-thinning/thickening effects followed by lubrication approach. Akbar et al. [53] employed non-Newtonian Williamson fluid for numerical study of peristalsis in an axisymmetric channel. Peristalsis of Prandtl fluid under long wavelength assumption has been reported by Riaz et al. [54]. This work is extended by



Hayat et al. [55] with Hall and chemical reaction effects.

Viscoelastic non-Newtonian fluids have tremendous applications in physiology and industry. Ree-Eyring can be reduced to Newtonian fluid model for both high and low shear rates. Also its constitutive equation can be obtained from kinetic theory of fluids instead of empirical relation. Ketchup, polymer solutions, ketchup, nail polish and wiped cream are some of the relevant examples. Physiological fluids movement like blood also contains such characteristics. Pulsatile flow of Ree-Eyring fluid in a channel is discussed by Shawky et al. [56]. Bhatti et al. [57] discussed blood flow in a vessel by considering Ree-Eyring fluid. Abbasi et al. [58] worked out flow of Eyring Powell liquid in curved channel. This work was extended by Hina et al. [59] in presence of heat and mass transfer. Theory of micropolar fluid was explained by Eringen [60] and characteristics like body couples, microinertial effects, couple stresses and microrotation are illustrated in details. Johnson and Segalman [61] introduced the theory for viscoelastic fluids expressing non-affine deformation. Chaturani and samy [62] analyzed the blood flow through arteries. Bohme and Friedrich [63] modeled a problem for investigating attributes of an incompressible viscoelastic fluid in a planar channel without any inertial force. Chaturani and Samy performed an analysis for peristalsis of blood through stenosed artery [64]. Flow of Eyring Powell fluid model through straight channel is demonstrated by Hayat et al. [64]. Alvi et al. [65] examined impact of non-constant viscosity on peristaltic activity of Jeffrey fluid containing nanoparticles. Latif et al. [66] discussed the peristalsis of third order liquid with variable properties. Also Fosdick and Rajagopal [67] presented thermodynamics analysis for third grade fluid. Tripathi et al. [68] explored the peristalsis of fractional Maxwell fluid in a channel. Couple stress fluid model is intended for the body couples and couple stresses in the medium of fluid. It has applications to understand many physical problems as it possesses the rheological convoluted fluid phenomena. Coating of paper, plasma, nuclear fuel slurries, polymers, fossil fuels, lubrication with heavy oils and greases carry such rheological characteristics. From industry point of view, many applications e.g., colloidal fluids, extrusion of polymer fluids, exotic lubricants, metallic plate cooling in bath and solidification of liquid crystals are related to this fluid. In the lubrication of engine rod bearings and tribology of thrust bearings, this fluid is also important. Couple stress model has been used to discuss biomedical phenomena such as infected urine from a diseased kidney and human and animal

blood. Peristalsis of couple stress liquid in an endoscope was investigated by Mekheimer and Abd elaboud [69]. Then his work is extended by Shit and Roy [70] through inclined channel. The problem is solved analytically by taking long wavelength and low Reynolds number assumptions. Ramesh [71] stated the rheology of couple stresses in transport of fluids.

Importance of heat transfer in medical and industrial applications cannot be ignored. Particularly, the heat transfer phenomenon in human body is an important area of research. Due to its wide spread significance in human tissues, many biomedical engineers are attracted towards human thermoregulation system [72] and thermotherapy [73]. In humans heat transfer take place as conduction in cancer tissues, metabolic heat generation, dilution technique in examining blood flow, perfusion of arterial-venous blood through the pores of the tissues and vasodilation. Transfer of heat with the interaction of peristaltic fluid flows is significant in hemodialysis, oxygenation, laser therapy and thermal energy storage. Radhakrishnamacharaya et al. [74] and Vajravelu et al. [75] analyzed the heat transfer on peristaltic flow of viscous fluid in non-uniform channel and tube. Peristaltic flows of viscous and non-Newtonian fluids in the presence of magnetic field is significant in physiological processes such as medicine and bio-engineering. Many phenomena are based on MHD principles such as design of heat exchangers, flow meters, radar systems, MHD compressor operation etc. Such effects is useful in the development of magnetic devices, hyperthermia [76], blood reduction during surgeries and cancer tumor treatment, MHD drug targeting [77], micro-circulation flows [78] and biomedical flow control, separation devices [79], in treatment of the pathologies e.g., gastroenric pathologies, rheumatisms, constipation and hypertension. Another important aspect of MHD is related to Hall and ionslip effects. Hall current is much more significant for higher externally applied magnetic field. Further when the electron-atom-collision frequency is high then ionslip effect cannot be ignored. Some applications which basically lie on Hall and ionslip currents include MHD generators, electric transformers, power generators, Hall accelerators, heating elements, refrigeration coils and flight MHD. In addition flow of fluid is much affected by the presence of Joule heating. The study of heat transfer with Joule heating effects has immense applications in biomedical engineering and food industries. Effect of Joule heating arises from the fluid electrical resistivity and applied electric field. One of the applications of electro osmosis is the fluid delivery in lab-on-a-chip devices, where one deals with thermally labile samples. Temperature

rise due to Joule heating can result in low column separation efficiency, reduction of analysis resolution and even loss of injected samples. Therefore several investigations regarding these effects in peristalsis are performed. Sud et al. [80] discussed the magnetic field effect for blood flow. Peristaltic activity of blood flow in equally branched channel is investigated by Agrawal et al. [81]. Their study concludes that during cardiac surgeries the magnetic field may be used in blood pump. Radhakrishnamacharya and Murty [82] examined the MHD aspects of peristaltic flow in a non-uniform channel. Wang et al. [83] discussed magnetohydrodynamics effects on peristaltic motion of Sisko fluid in symmetric channel. Hayat et al. [84] canvassed the peristaltic flow of MHD hyperbolic tangent fluid with Joule heating and slip conditions. Awais et al. [85] examined convective heat transfer on MHD peristaltic flow in a symmetric channel. Abbasi et al. [86] observed MHD peristaltic flow of Carreau fluid in curved channel under long wavelength and low Reynolds number assumptions. Further his work was extended by Ellahi et al. [87] by employing a uniform duct of rectangular cross section. Analytical solutions are obtained by employing a perturbation method. They also compared their results by numerical solutions. Heat transfer phenomenon with Ohmic heating is discussed by Asghar et al. [88]. They also considered the Hall and ionslip effects in their analysis. Hayat et al. [89] extended the work of Asghar et al. [88] for Jeffrey nanofluid. Nowar [90] investigated peristaltic flow of nanofluid saturating porous space inside the channel with Hall effect. In a non-uniform rectangular duct Pop et al. [91] observed the peristaltic flow of non-Newtonian fluid with magnetic and ionslip effects. Blood flow of Powell Eyring fluid in a porous medium with ionslip effect is studied by Bhatti et al. [92]. Noreen and Qasim [93] analyzed the flow of pseudoplastic fluid in presence of Hall current.

In many environmental and scientific processes, thermal radiation plays a significant role. Radiative heat transfer occurs when electromagnetic waves propagate across pore-air spaces. Heating and cooling of chambers, astrophysical flows, solar power technology and water evaporation from open reservoirs are useful applications of this effect. Thermal insulation, cooling of nuclear reactors, combustion, fluidized bed heat exchanger, biological tissues, turbid water bodies, furnace design, gas turbines, power generation systems, high temperature plasmas, fire spreads, solar fans, solar collectors, cancer therapy are such significant examples of thermal radiation. In addition heat generation/absorption effect is quite useful in thermal performance

of working fluids. Radiation can control the excess heat generation inside the body since high temperatures pose serious stresses for the human body placing it in serious danger of injury or even death. Further the involvement of heat generation/absorption effect in heat transfer is encountered frequently in many fields such as engineering, aerosol technology and industrial sector. It is also quite useful in the manufacture of plastic and rubber sheets, food stuff storage, disposal of radioactive waste material and dislocating of fluids in packed bed reactors. Having all such in mind the representative studies for non-uniform heat source/sink and radiation of nonlinear fluids have been addressed by number of researchers [94 – 102].

Mass transfer mechanism involves transfer of mass from one location to another. Mass transfer occurs in variety of engineering process. Specifically in chemical industry, mass transfer has widespread applications such as diffusion of chemical impurities, distillation process, reverse osmosis and membrane separation process. The rate of mass transfer rely on diffusivity and flow pattern of fluid. Investigation of combined heat and mass transfer species is important in seeking better understanding of various physical phenomena. Heat and mass transfer is not only responsible for energy distribution in the system but these also influence the system mechanics. Peristalsis with heat and mass transfer has vital position in biomedical sciences and industry. Few relevant applications are food processing [103], fog dispersion [104], metal purification [105], vasodilation, perspiration in hot weather, blood transfusions [106], heat convection occurring due to blood flow through pores of tissues, food drying [107], nuclear power generation [108], underground disposal of nuclear waste and extraction of geothermal energy. Energy flux induced by concentration gradient is referred as Dufour effect whereas mass flux produced by temperature gradient is known as Soret effect. Importance of Soret-Dufour effect cannot be neglected in isotopes separation, catalytical reactor, reservoir engineering and paper industry. Ogulu [109] put forward his efforts in investigating fluid and mass transfer flow of blood through single vessel. Nadeem and Akbar [110] discussed peristalsis of Jeffrey-six constant fluid filled with heat and mass transfer simultaneously. Hayat et al. [111] scrutinized heat and mass transfer effects on peristaltic transport of pseudoplastic in the presence of induced magnetic field. Shaaban and Abou-zeid [112] performed a comprehensive study on MHD peristaltic flow of Eyring-Powell fluid. Hayat et al. [113] examined Joule heating aspects on mixed convective peristaltic flow of viscous nano fluid with Soret-Dufour effects. Mustafa et al.



[114] focused their attention on study of peristalsis of fourth grade fluid under the influence of Dufour and Soret effects. They adopted Keller-box method for numerical solution of non-linear boundary value problem. Hayat et al. [115] discussed Soret and Dufour effects on peristalsis of pseudoplastic fluid through a tapered channel. Farooq et al. [116] considered the mathematical aspects of Soret and Dufour phenomena on MHD peristalsis of Jeffrey fluid. He performed his analysis subject to variable viscosity. Hayat et al. [117] accounted the Soret-Dufour impacts on peristalsis of Bingham plastic fluid by regular perturbation technique for series solution of problem.

Chemical reaction is another phase of mass transfer. Investigation of heat and mass transfer problems with chemical reaction has promising applications in industry such as burning of fuels, making cheese, solar collector, combustion system, smelting iron and brewing beer. Chemical reactions are integral part of many complicated processes of living organisms. Mustafa et al. [118] addressed heat and mass transfer on mixed convective peristalsis of fourth grade fluid. Hayat et al. [119] attempted to investigate the peristaltic transport of Casson fluid under the influence of chemical reaction and Soret-Dufour effect. Sankad and Dhange [120] modeled peristaltic transport of incompressible viscous fluid with flexible walls and chemical reaction. He computed the mean effective coefficient of dispersion through Taylor's limit and long wavelength hypothesis. Muthuraj et al. [121] performed a comprehensive examination on peristaltic pumping of dusty fluid in the presence of chemical reaction and wall properties. Impact of thermal deposition and chemical reaction on peristalsis of Carreau-Yasuda fluid is reported by Hayat et al. [122]. Machireddy and Kattamreddy [123] commenced a study for Joule heating and chemical reaction effects on peristaltic flow through porous medium. Influence of chemical reaction on hydromagnetic peristaltic pumping of radiating and reacting couple stress fluid passing through an inclined channel is explored by Reddy et al. [124]. Mishra et al. [125] explained impact of chemical reactions on peristalsis of physiological fluids with temperature dependent properties.

Thermophoresis is a kind of mass transfer that occurs due to movement of colloidal particles due to macroscopic temperature. Small suspended particles are more likely to travel in the direction of decreasing temperature when temperature gradient is maintained in the gas. This phenomenon arises due to difference of average velocities of particles. The most common

applications of thermophoresis are stone statue erosion, eliminate the particles from gas stream, silicon thin film deposition and blackening of glass of kerosene lantern. The novel features of Joule heating and thermophoresis on MHD peristaltic pumping of viscous nanofluid are elaborated by Shehzad et al. [126]. Hayat et al. [127] scrutinized the effects of thermophoresis and rotations on MHD peristalsis of Jeffrey fluid with non-uniform heat source/sink and flexible wall channel. Ali et al. [128] considered fourth grade for peristaltic transport through asymmetric channel of convective walls with concentration and thermophoresis effects. Analytic solution of problem is approximated through perturbation technique.

Analysis of heat transfer in fluid flow by movement of particles is known as convection. In many physical processes such as gas turbines, thermal storage and nuclear fluid transport, macroscopic fluid transportation produces development in heat transfer. Transfer of heat between static fluid and solid boundary through physical contact is referred as conduction. In case of moving fluids, heat transfer occurs through conduction as well as convection. For such problems boundary conditions can be modified by Fourier law of heat conduction and the Newton's law of cooling. These conditions are referred as convective boundary conditions [129, 130]. Hemodialysis and oxygenation, hypothermia treatment, sanitary fluid transport, blood pump in heart-lung machines, transport of corrosive fluids, laser therapy and coldness cryosurgery are some practical applications. In view of such importance various researchers studied the peristaltic flow subject to convective boundary condition [131 – 135].

Flow pattern with slip boundary characteristics has special significance in many applications. Undoubtedly due to the wetted wall, a loss of adhesion by fluid is presented which compels it to slide along the wall. In fluid-solid interaction situations, slip effect is meaningful in describing the macroscopic effects of certain molecular phenomena. Some daily life applications of slip are rarefied fluid, polishing of internal cavities and artificial heart valves, fluid motion within human body, flow on multitudinal interfaces and thin film. However less devotion towards slip relative to peristalsis is shown in the literature. Ali et al. [136] examined the slip effects on MHD peristaltic flow of viscous fluid with variable viscosity. Hayat et al. [137, 138] captured the effect of slip under peristaltic flow of Jeffrey and viscous materials respectively. Couple stress fluid flow with peristalsis through porous medium comprising slip effects has been reported by Ramesh [139]. Hina et al. [140] studied peristalsis of Johnson-Segalman fluid in curved

geometry subject to slip conditions. Yildirim and Sezer [141] discussed partial slip on MHD peristalsis of viscous fluid in an asymmetric channel. Peristaltic motion of power-law model is analyzed by Kumar et al. [142]. Ellahi and Hussain [143] discussed peristaltic flow in a rectangular duct with slip effects. Some more investigations for slip effect are reported via studies [144 – 149].

Existing literature on peristaltic mechanism were done in straight or curved channels. However literature peristalsis of viscous and non-Newtonian fluids in rotating channel is scarce. Flow of fluid in rotating frame has gained much importance amongst the researchers. It is because of its vast applications in ocean circulation, gas turbines, medical equipment, galaxies formation, aircraft, rotational spectroscopy, rotational air cleaner and geophysical flows. This phenomenon through rigid body rotation give rise to effects of centrifugal and Coriolis force in addition of inertial forces. Few aspects for peristalsis with rotating frame are discussed in the attempts [150 – 156].

## 1.2 Basic equations

Here the basic laws for mass, momentum, energy and concentration are presented.

### 1.2.1 Mass conservation

The mass conservation equation in differential form is

$$\frac{\partial \rho}{\partial t} + \nabla \cdot (\rho \mathbf{V}) = 0. \quad (1.1)$$

Here  $\rho$  denotes the density,  $\mathbf{V}$  the velocity and  $\nabla$  represents gradient operator. For incompressible material

$$\nabla \cdot \mathbf{V} = 0. \quad (1.2)$$

### 1.2.2 Momentum conservation

Generalized equation of motion is

$$\rho \frac{d\mathbf{V}}{dt} = \nabla \cdot \boldsymbol{\tau} + \rho \mathbf{f}, \quad (1.3)$$

$$\boldsymbol{\tau} = -p\mathbf{I} + \mathbf{S}, \quad (1.4)$$

where  $\boldsymbol{\tau}$  represents Cauchy-stress tensor,  $\mathbf{f}$  body force,  $\mathbf{I}$  identity tensor,  $\mathbf{S}$  extra stress tensor,  $\frac{d}{dt}$  the material time differentiation, and  $p$  the pressure. Equation of momentum in rotating is written as:

$$\rho \frac{d\mathbf{V}}{dt} + \rho [2(\boldsymbol{\Omega} \times \mathbf{V}) + \boldsymbol{\Omega} \times (\boldsymbol{\Omega} \times \mathbf{r})] = \nabla \cdot \boldsymbol{\tau} + \rho \mathbf{f}, \quad (1.5)$$

where on left hand side second and third terms present the Coriolis and centrifugal force respectively. Here  $\boldsymbol{\Omega}$  denotes angular velocity.

### 1.2.3 Energy conservation

The energy equation is

$$c_p \rho \frac{dT}{dt} = -\nabla \cdot (-\kappa \text{grad } T) + Q_t, \quad (1.6)$$

where  $T$  shows temperature,  $c_p$  specific heat and  $\kappa$  fluid's thermal conductivity. First and second term on right side stands for energy flux and source term related to transport of energy. For the modification of heat transport characteristics the source term is responsible for consideration of velocity components, radiative heat flux, surface heating cooling, and viscous dissipation. Moreover, it also stands for other physical phenomena such as Joule heating and Dufour effects.

### 1.2.4 Concentration conservation

Suppose  $C$  be the mass concentration of fluid per unit volume, then equation of mass can be given as:

$$\frac{dC}{dt} = D_m \nabla^2 C + \frac{D_m R_T}{T_r} \nabla^2 T \quad (1.7)$$

in which  $R_T$  presents the thermal-diffusion ratio,  $D_m$  stands for mass diffusion coefficient and  $T_r$  is the mean temperature.

### 1.2.5 Transformations and volume flow rate

In present thesis we use Galilean transformations for flow analysis from laboratory to wave frames of reference. The variables are designed as

$$\begin{aligned} x &= \hat{x} - ct, \quad y = \hat{y}, \quad z = \hat{z}, \quad p = \hat{p}(\hat{x}, \hat{y}, \hat{z}), \\ u(x, y, z) &= \hat{u}(\hat{x}, \hat{y}, \hat{z}) - c, \quad v(\hat{x}, \hat{y}, \hat{z}) = \hat{v}(\hat{x}, \hat{y}, \hat{z}), \quad w(\hat{x}, \hat{y}, \hat{z}) = \hat{w}(\hat{x}, \hat{y}, \hat{z}), \end{aligned} \quad (1.8)$$

where  $p, u, v, w$  are the pressure and velocity components with respect to wave frame.

The dimensionless volume flow rate for asymmetric channel in fixed and wave frames is given by

$$\bar{Q} = \int_{\bar{H}_2(\hat{x}, \hat{t})}^{\bar{H}_1(\hat{x}, \hat{t})} \hat{u}(\hat{x}, \hat{y}, \hat{z}) d\hat{z}, \quad \bar{q} = \int_{h_2(x)}^{h_1(x)} u(x, y, z) dz. \quad (1.9)$$

Using Eq. (1.8), the volume flow rate can be related by

$$\bar{Q} = \bar{q} + ch_1(x) - ch_2(x). \quad (1.10)$$

The time mean flow at a fixed position  $\hat{x}$  over a period (say  $t_p$ ) is

$$\bar{\Theta} = \frac{1}{t_p} \int_0^{t_p} \bar{Q} dt. \quad (1.11)$$

Putting Eq. (1.10) into Eq. (1.11) and then evaluating the integral we get

$$\bar{\Theta} = \bar{q} + cb_1 + cb_2. \quad (1.12)$$

Now defining nondimensional mean time flow in fixed and wave frames respectively

$$Q = \frac{\bar{\Theta}}{cb_1}, \quad F_1 = \frac{\bar{q}}{cb_1}, \quad (1.13)$$

finally we obtain

$$Q = F_1 + 1 + \eta, \quad (1.14)$$



in which

$$F_1 = \int_{h_2(x)}^{h_1(x)} u(x, y, z) dz. \quad (1.15)$$

Similarly for symmetric channel the flow rate is given by

$$F_1 = \int_0^{h(x)} u(x, y, z) dz. \quad (1.16)$$

### 1.2.6 Dimensionless parameters

The non-dimensionless parameters occurring in whole thesis are defined as

$$\begin{aligned} T' &= \frac{\text{Re} \bar{\Omega} d}{c}, \quad m = \frac{\sigma B_0}{en_e}, \quad H = \frac{\sigma B_0^2}{\mu}, \quad Br = EPr, \\ E &= \frac{c^2}{T_0 c_p}, \quad \text{Pr} = \frac{\mu c_p}{k_T}, \quad \epsilon_i = \frac{a_i}{d_i} (i = 1, 2), \quad Bi_1 = \frac{\hat{h}_1 d}{k_T}, \\ Bi_2 &= \frac{\hat{h}_2 d}{D}, \quad E_1 = -\frac{\tau d^3}{\lambda^3 \mu c}, \quad E_2 = \frac{m_1^* c d^3}{\lambda^3 \mu}, \quad E_3 = \frac{d^3 d'}{\mu \lambda^2} \\ R_n &= \frac{16 \sigma^*}{3 k_T k^*} T_0^3, \quad S = \frac{Q_0 d^2}{k_T}, \quad \tau' = -\frac{k^{**} T_0}{T_r}, \quad \delta = \frac{d}{\lambda}, \quad \text{Re} = \frac{cd}{\nu}, \\ Du &= \frac{D k' C_0}{\mu c_p C_s T_0}, \quad Sc = \frac{\mu}{\rho D}, \quad Sr = \frac{\rho D k' T_0}{\mu T_m C_0}, \quad k = \frac{K}{d_1}, \quad \gamma = \frac{k_1 d^2}{\nu}. \end{aligned} \quad (1.17)$$

Here  $\text{Re}$  denotes the Reynolds number,  $\bar{\Omega}$  the angular velocity,  $d_i$  the displacement,  $c$  the wave speed,  $\lambda$  the wavelength,  $\rho$  the fluid density,  $\nu$  the kinematic viscosity,  $\sigma$  the electrical conductivity,  $B_0$  the magnetic field strength,  $e$  the electron,  $n_e$  the cyclotron frequency,  $\mu$  the dynamic viscosity,  $C_0$  concentration at walls,  $T_0$  temperature at walls,  $c_p$  the specific heat,  $k_T$  thermal conductivity,  $a_i$  the amplitudes,  $\hat{h}_1, \hat{h}_2$  heat and mass transfer coefficient,  $\tau$  the elastic tension,  $m_1^*$  the mass per unit area,  $d'$  the damping coefficient,  $\sigma^*$  the Stephen Boltzman constant,  $k^*$  the mean absorption coefficient,  $Q_0$  non-uniform heat source/sink coefficient,  $k^{**}$  the thermophoretic coefficient,  $T_r$  the reference temperature,  $D$  the mass diffusivity coefficient,  $C_s$  concentration susceptibility,  $T_m$  mean fluid temperature,  $k'$  thermal diffusion ratio,  $k_1$  the chemical reaction coefficient,  $K$  non-uniform channel coefficient,  $T'$  denotes the Taylor number,  $m$  the Hall parameter,  $H$  the Hartman number,  $Br$  Brinkman number,  $E$  Eckert number,  $\text{Pr}$

Prandtl number,  $\epsilon_i$  amplitude ratio variable,  $Bi_1$  heat transfer Biot number,  $Bi_2$  mass transfer Biot number,  $E_i (i = 1, 2, 3)$  the wall parameters,  $R_n$  the radiation variable,  $S$  the non-uniform heat source/sink parameter,  $\tau'$  thermophoretic parameter,  $\delta$  wavelength,  $Re$  Reynolds number,  $Sc$  Schmidt number,  $k$  non-uniform channel parameter,  $Du$  Dufour number,  $\gamma$  chemical reaction parameter and  $Sr$  Soret number.

## Chapter 2

# Hall current and Joule heating impacts in peristaltic transport of rotating liquid

### 2.1 Introduction

The present chapter is arranged to study the Hall current and Joule heating effects on peristaltic flow of viscous fluid. Channel with flexible boundaries is considered. System consisting of liquid and channel behaves like a rigid body. Convective conditions for heat transfer in the formulation are adopted. Viscous dissipation in energy expression is taken into account. Resulting differential systems after invoking small Reynolds number and long wavelength considerations are numerically solved. Runge-Kutta scheme of order four is implemented temperature, axial and secondary velocities and heat transfer coefficient. Comparison with previous limiting studies is shown. Outcome of new parameters of interest is analyzed.

### 2.2 Problem development

We choose channel with compliant boundaries. Viscous liquid is electrically conducted. Electric field effect is not considered. However the Hall and Joule heating effects are accounted. Both the channel and fluid rotates with a uniform angular velocity  $\bar{\Omega}$  about the  $z$ -axis. The channel

walls are convectively heated. Viscous dissipation impact is accounted. The sinusoidal waves propagating along the channel walls (at  $z = \pm\eta$ ) are

$$z = \pm\eta(x, t) = \pm \left[ d + a \sin \frac{2\pi}{\lambda}(x - ct) \right], \quad (2.1)$$

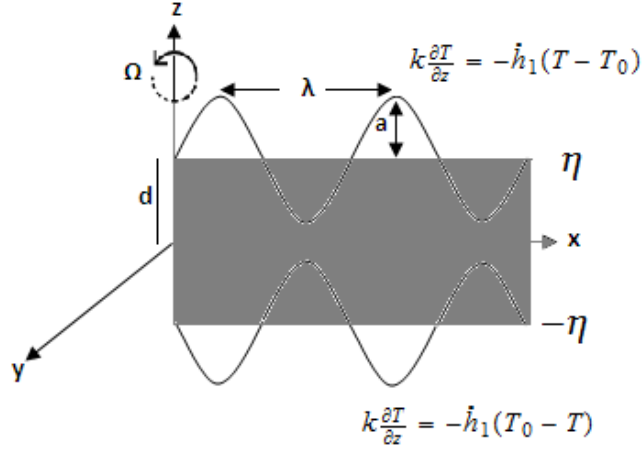


Fig. 2.1: Geometry of problem.

where  $a$ ,  $\lambda$ ,  $c$  and  $t$ , represent the wave amplitude, wavelength, wave speed and time respectively.

The equations in rotating frame can be put as follows:

$$\frac{\partial u}{\partial x} + \frac{\partial w}{\partial z} = 0, \quad (2.2)$$

$$\rho \frac{du}{dt} - 2\rho\bar{\Omega}v = -\frac{\partial \tilde{p}}{\partial x} + \mu \left[ \frac{\partial^2}{\partial x^2} + \frac{\partial^2}{\partial z^2} \right] u + \frac{\sigma B_0^2}{1+m^2}(-u + mv), \quad (2.3)$$

$$\rho \frac{dv}{dt} + 2\rho\bar{\Omega}u = -\frac{\partial \tilde{p}}{\partial y} + \mu \left[ \frac{\partial^2}{\partial x^2} + \frac{\partial^2}{\partial z^2} \right] v - \frac{\sigma B_0^2}{1+m^2}(v + mu), \quad (2.4)$$

$$\rho \frac{dw}{dt} = -\frac{\partial \tilde{p}}{\partial z} + \mu \left[ \frac{\partial^2}{\partial x^2} + \frac{\partial^2}{\partial z^2} \right] w, \quad (2.5)$$

$$\rho c_p \frac{dT}{dt} = k_T \nabla^2 T + \frac{\sigma B_0^2}{1+m^2}(u^2 + w^2) + \mu \left[ 2 \left\{ \left( \frac{\partial u}{\partial z} \right)^2 + \left( \frac{\partial w}{\partial x} \right)^2 \right\} + \left( \frac{\partial u}{\partial z} + \frac{\partial w}{\partial x} \right)^2 \right]. \quad (2.6)$$

The conditions for present problem are

$$k_T \frac{\partial T}{\partial z} = -\dot{h}_1(T - T_0) \text{ at } z = \eta, \quad (2.7)$$

$$k_T \frac{\partial T}{\partial z} = -\dot{h}_1(T_0 - T) \text{ at } z = -\eta, \quad (2.8)$$

$$u = 0, v = 0 \text{ at } z = \pm\eta \quad (2.9)$$

and compliant wall condition is

$$\frac{\partial}{\partial x} G(\eta) = \frac{\partial p}{\partial x} = -\rho \frac{du}{dt} + \left[ \frac{\partial^2}{\partial x^2} + \frac{\partial^2}{\partial z^2} \right] u + \frac{\sigma B_0^2}{1+m^2}(-u + mv) + 2\rho\bar{\Omega}v \text{ at } z = \pm\eta, \quad (2.10)$$

$$G = -\tau \frac{\partial^2}{\partial x^2} + m_1^* \frac{\partial^2}{\partial t^2} + d' \frac{\partial}{\partial t},$$

where  $\tilde{p} = p - \frac{1}{2}\rho\Omega^2(x^2 + y^2)$ .

If  $\psi(x, z, t)$  is the stream function then

$$u = \psi_z, w = -\delta\psi_x. \quad (2.11)$$

Define the dimensionless variables as:

$$\begin{aligned} x^* &= \frac{x}{\lambda}, y^* = \frac{y}{\lambda}, z^* = \frac{z}{d}, p^* = \frac{d^2\tilde{p}}{c\mu\lambda}, t^* = \frac{ct}{\lambda}, \\ u^* &= \frac{u}{c}, v^* = \frac{v}{c}, w^* = \frac{w}{c}, \eta^* = \frac{\eta}{d}, \\ \theta &= \frac{T - T_0}{T_1 - T_0}. \end{aligned} \quad (2.12)$$

The problems subject to long wavelength and small Reynolds number become

$$p_x = \psi_{zzz} - \frac{H^2}{1+m^2}\psi_z + \left( 2T' + \frac{H^2m}{1+m^2} \right) v, \quad (2.13)$$

$$p_y = v_{zz} - \frac{H^2}{1+m^2}(v + m\psi_z) - 2T'\psi_z, \quad (2.14)$$

$$p_z = 0, \quad (2.15)$$

$$\theta_{zz} + Br\psi_{zz}^2 - Br\frac{H^2}{1+m^2}\psi_z^2 = 0, \quad (2.16)$$

$$\eta = 1 + \epsilon \sin 2\pi(x - t), \quad (2.17)$$

$$\theta_z + Bi_1\theta = 0 \text{ at } z = \eta,$$

$$\theta_z - Bi_1\theta = 0 \text{ at } z = -\eta, \quad (2.18)$$

$$\psi_z = 0, v = 0 \text{ at } z = \pm\eta, \quad (2.19)$$

$$\left[ E_1 \frac{\partial^3}{\partial x^3} + E_2 \frac{\partial^3}{\partial x \partial t^2} + E_3 \frac{\partial^2}{\partial x \partial t} \right] \eta = \psi_{zz} - \frac{H^2}{1+m^2}\psi_z + \left( 2T' + \frac{H^2 m}{1+m^2} \right) v \text{ at } z = \pm\eta. \quad (2.20)$$

From equation (2.15)  $p \neq p(z)$  so equations (2.13) and (2.14) yield

$$\psi_{zzzz} + \left( 2T' + \frac{H^2 m}{1+m^2} \right) v_z - \frac{H^2}{1+m^2}\psi_{zz} = 0, \quad (2.21)$$

$$v_{zz} - \frac{H^2}{1+m^2}(v + m\psi_z) - 2T'\psi_z = 0. \quad (2.22)$$

Here the pressure term is neglected because of secondary flow which is produced due to rotation.

## 2.3 Solution methodology

Now our interest is to solve equations (2.16), (2.21) and (2.22) subject to the conditions (2.17) – (2.20). Therefore we apply a numerical technique (shooting technique with fourth order Runge-Kutta integration) built in command of Mathematica. The graphical outcomes of velocities  $(u, v)$ , temperature  $(\theta)$  and heat transfer coefficient  $(Z)$  have been discussed in detail for the sundry parameters.

## 2.4 Discussion

### 2.4.1 Axial velocity

Figs. (2.2 – 2.5) are plotted to see the effects of  $H$ ,  $T'$ ,  $m$  and  $E_1$ ,  $E_2$ ,  $E_3$  on axial velocity  $u(z)$ . The impact of Hartman number  $H$  on velocity profile  $u$  is sketched in Fig. 2.2. Result in Fig. shows decaying behavior of  $u$  via larger  $H$ . It is due to the resistive nature of Lorentz force.

Impact of Taylor number  $T'$  on velocity profile is displayed in Fig. 2.3. It is evident from Fig. 2.3 that velocity is enhanced by increasing rotation. The reason behind this fact is that the rotation of fluid induced the secondary flow which causes decrease in velocity. The result matches with the study [155]. On the other hand Fig. 2.4 shows the increasing impact of axial velocity for increasing Hall parameter  $m$ . In fact for larger values of  $m$  the effective conductivity decreases. It causes decrease in magnetic damping force and hence axial velocity enhances. Variation in  $u$  for wall parameters is depicted in Fig. 2.5. The velocity increases for larger  $E_1$  and  $E_2$  while it decays for increasing damping parameter  $E_3$ .

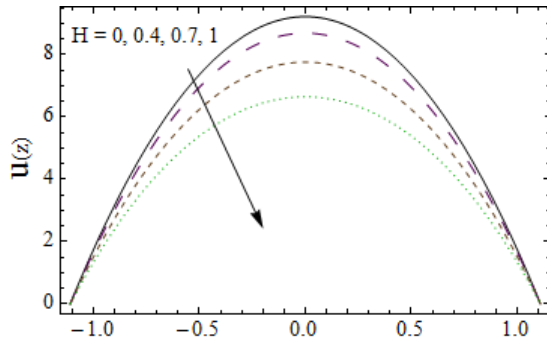


Fig. 2.2

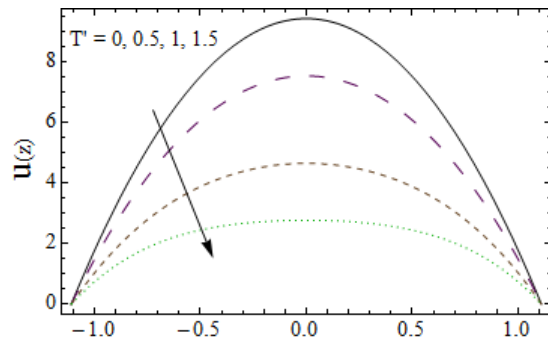


Fig. 2.3

Fig. 2.2: Axial velocity  $u$  for  $H$  with  $x = 0.2$ ,  $\epsilon = 0.2$ ,  $t = 0.1$ ,  $E_1 = 0.3$ ,  $E_2 = 0.1$ ,  $E_3 = 0.1$ ,  
 $m = 0.5$ ,  $T' = 0.2$ ,  $Bi_1 = 2$ ,  $Br = 0.3$ .

Fig. 2.3: Axial velocity  $u$  for  $T'$  with  $x = 0.2$ ,  $\epsilon = 0.2$ ,  $t = 0.1$ ,  $E_1 = 0.3$ ,  $E_2 = 0.1$ ,  $E_3 = 0.1$ ,  
 $m = 0.5$ ,  $H = 0.2$ ,  $Bi_1 = 2$ ,  $Br = 0.3$ .

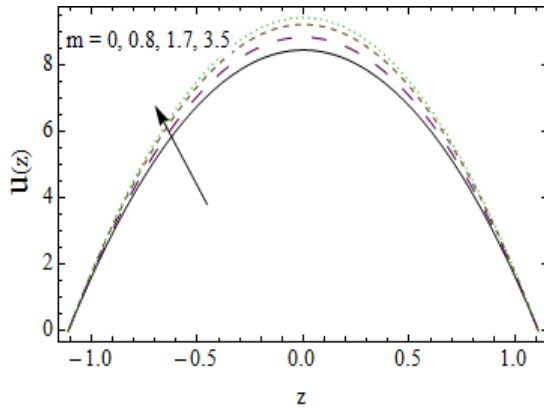


Fig. 2.4

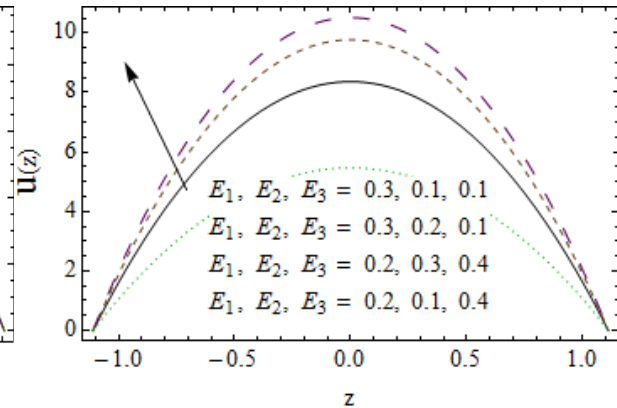


Fig. 2.5

Fig. 2.4: Axial velocity  $u$  for  $m$  with  $x = 0.2$ ,  $\epsilon = 0.2$ ,  $t = 0.1$ ,  $E_1 = 0.3$ ,  $E_2 = 0.1$ ,  $E_3 = 0.1$ ,  
 $H = 0.2$ ,  $T' = 0.2$ ,  $Bi_1 = 2$ ,  $Br = 0.3$ .

Fig. 2.5: Axial velocity  $u$  for  $E_1$ ,  $E_2$ ,  $E_3$  with  $x = 0.2$ ,  $\epsilon = 0.2$ ,  $t = 0.1$ ,  $m = 0.5$ ,  $H = 0.2$ ,  
 $T' = 0.2$ ,  $Bi_1 = 2$ ,  $Br = 0.3$ .

### 2.4.2 Secondary velocity

Figs. (2.6 – 2.9) are sketched for the outcome of emerging parameters on secondary velocity  $v(z)$ . In Fig. 2.6 secondary velocity decreases for increasing Hartman number  $H$ . Fig. 2.7 depicts that for larger Taylor number  $T'$  the secondary velocity increases. It is because of the fact that secondary velocity is enhanced due to an increase in rotation. This result also agrees with previous studies of Hayat et al. [155] and Mahmoud [154]. Also Fig. 2.7 shows no variation when  $T' = 0$ . In Fig. 2.8 the effect of Hall current parameter  $m$  on  $v(z)$  is depicted. Larger  $m$  lead to secondary velocity enhancement. The result shows that  $m$  resists the change in fluid caused by an increase in the applied magnetic field strength. Fig. 2.9 witnesses that  $v$  is enhanced for greater values of  $E_1$  and  $E_2$  whereas it has reversed behavior for  $E_3$ .

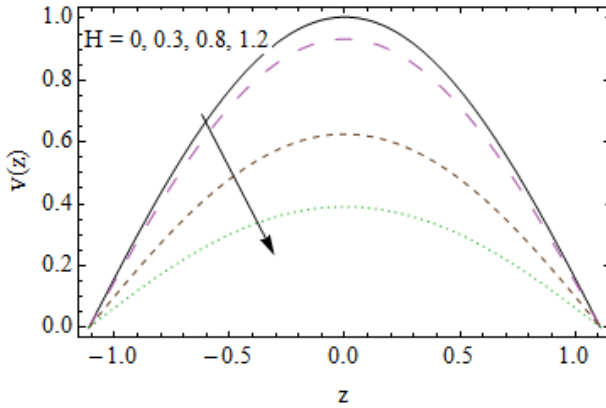


Fig. 2.6

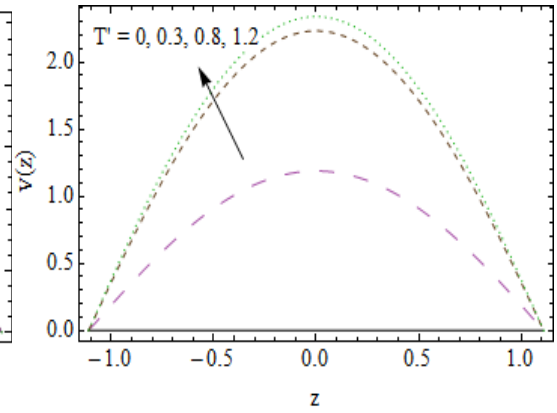


Fig. 2.7

Fig. 2.6: Secondary velocity  $v$  for  $H$  with  $x = 0.5$ ,  $\epsilon = 0.1$ ,  $t = 0.1$ ,  $E_1 = 0.3$ ,  $E_2 = 0.1$ ,  
 $E_3 = 0.1$ ,  $m = 0.4$ ,  $T' = 0.2$ ,  $Bi_1 = 2$ ,  $Br = 0.3$ .

Fig. 2.7: Secondary velocity  $v$  for  $T'$  with  $x = 0.5$ ,  $\epsilon = 0.1$ ,  $t = 0.1$ ,  $E_1 = 0.3$ ,  $E_2 = 0.1$ ,  
 $E_3 = 0.1$ ,  $m = 0.5$ ,  $H = 0.5$ ,  $Bi_1 = 2$ ,  $Br = 0.3$ .



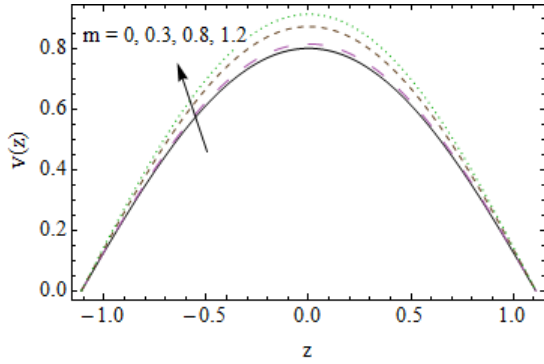


Fig. 2.8

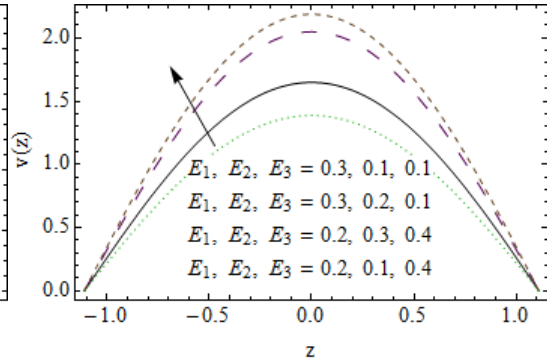


Fig. 2.9

Fig. 2.8: Secondary velocity  $v$  for  $m$  with  $x = 0.5$ ,  $\epsilon = 0.1$ ,  $t = 0.1$ ,  $E_1 = 0.3$ ,  $E_2 = 0.1$ ,  
 $E_3 = 0.1$ ,  $H = 0.5$ ,  $T' = 0.2$ ,  $Bi_1 = 2$ ,  $Br = 0.3$ .

Fig. 2.9: Secondary velocity  $v$  for  $E_1, E_2, E_3$  with  $x = 0.5$ ,  $\epsilon = 0.2$ ,  $t = 0.1$ ,  $m = 0.4$ ,  $H = 0.5$ ,  
 $T' = 0.2$ ,  $Bi_1 = 2$ ,  $Br = 0.3$ .

### 2.4.3 Temperature

Variations of temperature distribution  $\theta$  plotted against  $z$  for several interesting parameters are observed through Figs. 2.10– 2.14. Temperature decays as we increase Hartman number  $H$  and rotation parameter  $T'$  (see Figs. 2.10 and 2.11). In Fig. 2.12 the temperature reduces when heat transfer Biot number  $Bi_1$  increases. The obtained result indicates that the thermal conductivity of the fluid reduces with the increase in  $Bi_1$  and thus temperature decreases. Fig. 2.13 reveals that temperature increases for larger Brinkman number  $Br$ . In fact minimum heat conduction is produced by viscous dissipation. The increasing behaviors of temperature for elastic parameters  $E_1$  and  $E_2$  and decreasing behavior for damping parameter  $E_3$  are shown in Fig. 2.14.

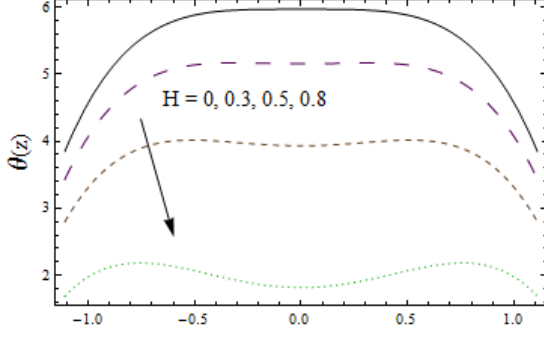


Fig. 2.10

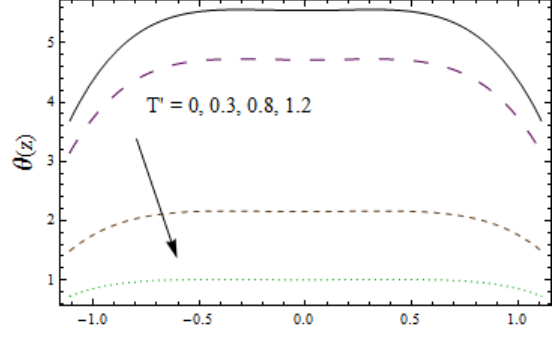


Fig. 2.11

Fig. 2.10: Temperature  $\theta$  for  $H$  with  $x = 0.2$ ,  $\epsilon = 0.1$ ,  $t = 0.1$ ,  $E_1 = 0.3$ ,  $E_2 = 0.1$ ,  $E_3 = 0.1$ ,  
 $m = 0.4$ ,  $T' = 0.2$ ,  $Bi_1 = 2$ ,  $Br = 0.3$ .

Fig. 2.11: Temperature  $\theta$  for  $T'$  with  $x = 0.2$ ,  $\epsilon = 0.1$ ,  $t = 0.1$ ,  $E_1 = 0.3$ ,  $E_2 = 0.1$ ,  $E_3 = 0.1$ ,  
 $m = 0.4$ ,  $H = 0.5$ ,  $Bi_1 = 2$ ,  $Br = 0.3$ .

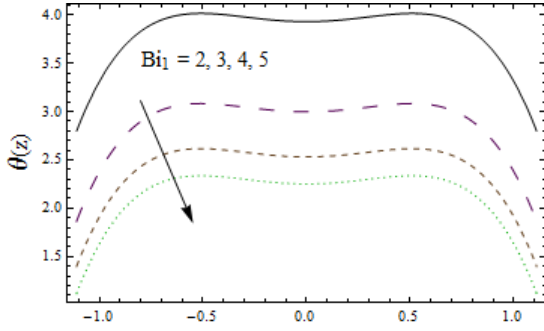


Fig. 2.12

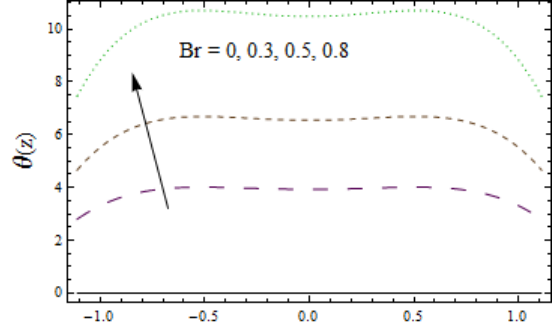


Fig. 2.13

Fig. 2.12: Temperature  $\theta$  for  $Bi_1$  with  $x = 0.2$ ,  $\epsilon = 0.1$ ,  $t = 0.1$ ,  $E_1 = 0.3$ ,  $E_2 = 0.1$ ,  $E_3 = 0.1$ ,  
 $H = 0.5$ ,  $T' = 0.2$ ,  $m = 0.4$ ,  $Br = 0.2$ .

Fig. 2.13: Temperature  $\theta$  for  $Br$  with  $x = 0.2$ ,  $\epsilon = 0.1$ ,  $t = 0.1$ ,  $E_1 = 0.3$ ,  $E_2 = 0.1$ ,  $E_3 = 0.1$ ,  
 $H = 0.5$ ,  $T' = 0.2$ ,  $m = 0.4$ ,  $Bi_1 = 2$ .

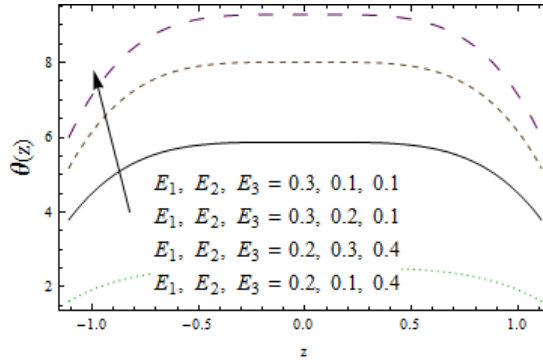


Fig. 2.14

Fig. 2.14: Temperature  $\theta$  for  $E_1, E_2, E_3$  with  $x = 0.2, \epsilon = 0.1, t = 0.1, m = 0.4, H = 0.1, T' = 0.2, Bi_1 = 2, Br = 0.3$ .

#### 2.4.4 Heat transfer coefficient

The impacts of  $H, T', Br$  and  $E_1, E_2, E_3$  on rate of heat transfer at channel walls are portrayed in Figs. 2.15 – 2.18. Fig. 2.15 shows oscillatory behavior for increasing Hartman number  $H$ . Here  $Z$  shows decreasing behavior for increasing Taylor number (see Fig. 2.16). In Fig. 2.17 the rate of heat transfer coefficient  $Z$  is enhanced for larger Brinkman number  $Br$  due to stronger viscous dissipation effect. The magnitude of heat transfer coefficient  $Z$  near centerline increases for wall parameters whereas it decreases near the boundaries of the channel (see Fig. 2.18).

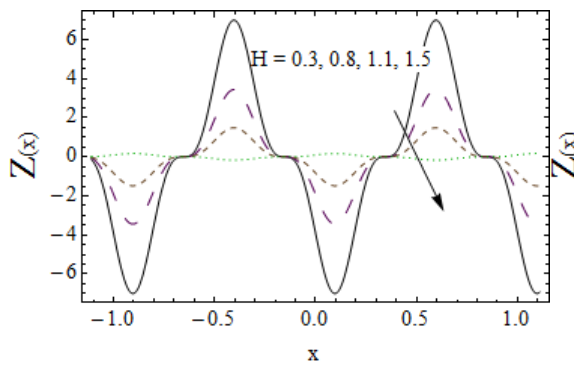


Fig. 2.15

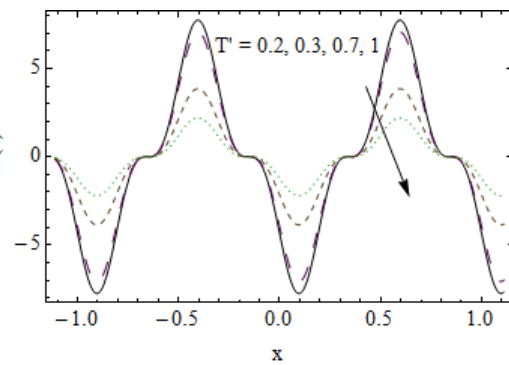


Fig. 2.16

Fig. 2.15: Heat transfer coefficient  $Z$  for  $H$  with  $\epsilon = 0.2$ ,  $t = 0.1$ ,  $E_1 = 0.3$ ,  $E_2 = 0.1$ ,  
 $E_3 = 0.1$ ,  $m = 0.5$ ,  $T' = 0.2$ ,  $Bi_1 = 2$ ,  $Br = 0.3$ .

Fig. 2.16: Heat transfer coefficient  $Z$  for  $T'$  with  $\epsilon = 0.2$ ,  $t = 0.1$ ,  $E_1 = 0.3$ ,  $E_2 = 0.1$ ,  
 $E_3 = 0.1$ ,  $m = 0.5$ ,  $H = 0.2$ ,  $Bi_1 = 2$ ,  $Br = 0.3$ .

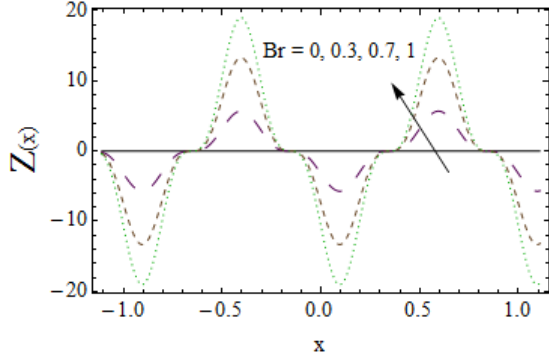


Fig. 2.17

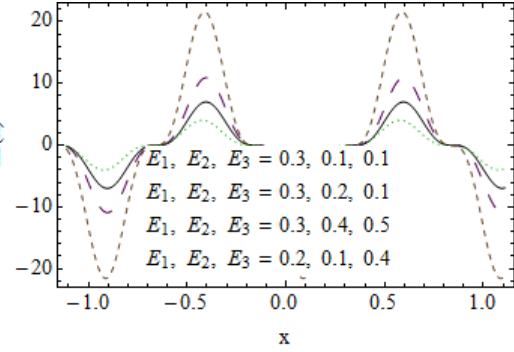


Fig. 2.18

Fig. 2.17: Heat transfer coefficient  $Z$  for  $Br$  with  $\epsilon = 0.1$ ,  $t = 0.1$ ,  $E_1 = 0.3$ ,  $E_2 = 0.1$ ,  
 $E_3 = 0.1$ ,  $H = 0.5$ ,  $T' = 0.2$ ,  $m = 0.4$ ,  $Bi_1 = 2$ .

Fig. 2.18: Heat transfer coefficient  $Z$  for  $E_1, E_2, E_3$  with  $\epsilon = 0.2$ ,  $t = 0.1$ ,  $m = 0.4$ ,  $H = 0.5$ ,  
 $T' = 0.2$ ,  $Bi_1 = 2$ ,  $Br = 0.3$ .

## 2.5 Conclusions

Hall current and Ohmic heating effects on peristaltic flow in a rotating frame are analyzed. The major key findings are:

- Impact of Hartman and Taylor numbers on the axial velocity are found similar.
- Both axial and secondary velocities are increasing functions of Hall parameter.
- Opposite behavior of Taylor number on axial and secondary velocities is observed.
- The axial and secondary velocities show similar behavior for wall parameters.
- Rotation parameter leads to an enhancement of temperature.

- Temperature decays for increasing  $Bi_1$  while it enhances for Brinkman number, Hartman number and wall parameters.
- Hartman and Taylor numbers outcomes on heat transfer rates are opposite to that of Brinkman number and wall parameters.

## Chapter 3

# Impact of thermal radiation and thermophoresis on peristalsis in rotating frame

### 3.1 Introduction

Thermal radiation effect on peristaltic activity of rotating flow in a channel is addressed in this chapter. The influences of thermophoresis and chemical reaction are taken into account. Convective heat and mass transfer conditions in formulation are adopted. In addition, the non-uniform heat source/sink effect is included in heat transfer analysis. Exact solutions for stream function and temperature are obtained. Numerical solution for concentration of developed mathematical model are obtained by considering low Reynolds number and long wavelength. The effects of emerging physical parameters are analyzed through graphical illustrations. It is found that influences of thermophoretic and thermal radiation parameters on temperature and concentration are quite opposite. Further heat transfer coefficient decays when rotation is increased.

### 3.2 Problem development

Consider an incompressible viscous fluid in a channel with width  $2d$ . Both the channel and fluid rotates with a uniform angular velocity  $\bar{\Omega}$  about the  $z$  - *axis*. Mathematical expression for wave propagation along the channel walls at  $\hat{z} = \pm\bar{H}$  is given by

$$\bar{H}(\hat{x}, \hat{t}) = d + a \sin \frac{2\pi}{\lambda}(\hat{x} - c\hat{t}). \quad (3.1)$$

In a rotating frame the governing equations are given by

$$\frac{\partial \hat{u}}{\partial \hat{x}} + \frac{\partial \hat{w}}{\partial \hat{z}} = 0, \quad (3.2)$$

$$\rho \frac{d\hat{u}}{d\hat{t}} - 2\rho\Omega\hat{v} = -\frac{\partial \tilde{p}}{\partial \hat{x}} + \mu \left[ \frac{\partial^2}{\partial \hat{x}^2} + \frac{\partial^2}{\partial \hat{y}^2} + \frac{\partial^2}{\partial \hat{z}^2} \right] \hat{u}, \quad (3.3)$$

$$\rho \frac{d\hat{v}}{d\hat{t}} + 2\rho\Omega\hat{u} = -\frac{\partial \tilde{p}}{\partial \hat{y}} + \mu \left[ \frac{\partial^2}{\partial \hat{x}^2} + \frac{\partial^2}{\partial \hat{y}^2} + \frac{\partial^2}{\partial \hat{z}^2} \right] \hat{v}, \quad (3.4)$$

$$\rho \frac{d\hat{w}}{d\hat{t}} = -\frac{\partial \tilde{p}}{\partial \hat{z}} + \mu \left[ \frac{\partial^2}{\partial \hat{x}^2} + \frac{\partial^2}{\partial \hat{y}^2} + \frac{\partial^2}{\partial \hat{z}^2} \right] \hat{w}, \quad (3.5)$$

$$\begin{aligned} \rho c_p \frac{dT}{d\hat{t}} &= k_T \left[ \frac{\partial^2}{\partial \hat{x}^2} + \frac{\partial^2}{\partial \hat{y}^2} + \frac{\partial^2}{\partial \hat{z}^2} \right] T + \mu \left[ \left( \frac{\partial \hat{u}}{\partial \hat{z}} + \frac{\partial \hat{w}}{\partial \hat{x}} \right)^2 \right] \\ &\quad - \frac{\partial (q_r)_{\hat{z}}}{\partial \hat{z}} + Q_0(T - T_0), \end{aligned} \quad (3.6)$$

$$\frac{dC}{d\hat{t}} = D \left[ \frac{\partial^2}{\partial \hat{x}^2} + \frac{\partial^2}{\partial \hat{y}^2} + \frac{\partial^2}{\partial \hat{z}^2} \right] C - \frac{\partial (V_T(C - C_0))}{\partial \hat{z}} - k_1(C - C_0). \quad (3.7)$$

Using Rosseland heat flux approximation we have

$$q_r = -\frac{4\sigma^*}{3k^*} \frac{\partial}{\partial \hat{z}} T^4, \quad (3.8)$$

where  $k^*$  and  $\sigma^*$  represent the Rosseland mean absorption coefficient and Stefan-Boltzmann respectively. Expanding  $T^4$  about  $T_0$  and ignoring higher order terms of  $(T - T_0)$ . Then

$$V_T = -\frac{k^{*\nu}}{T_r} \frac{\partial T}{\partial \hat{z}}, \quad (3.9)$$

where  $\nu$ ,  $k^{**}$  and  $T_r$  denote the kinematic viscosity, thermophoretic coefficient and reference temperature respectively.

The conditions for present problem are

$$\hat{u}_z = 0, \hat{v}_z = 0, k_T \frac{\partial T}{\partial \hat{z}} = 0, D \frac{\partial C}{\partial \hat{z}} = 0 \text{ at } \hat{z} = 0, \quad (3.10)$$

$$\hat{u} = 0, \hat{v} = 0, k_T \frac{\partial T}{\partial \hat{z}} = -\hat{h}_1(T_0 - T), D \frac{\partial C}{\partial \hat{z}} = -\hat{h}_2(C_0 - C) \text{ at } \hat{z} = \hat{h}, \quad (3.11)$$

in which  $\hat{h}_1$  and  $\hat{h}_2$  indicate the heat and mass transfer coefficients respectively.

Putting Eqs. (3.8) and (3.9) in Eqs. (3.6) and (3.77) and then using the wave frame transformations

$$\begin{aligned} x &= \hat{x} - ct, \quad y = \hat{y}, \quad z = \hat{z}, \quad p = \hat{p}(\hat{x}, \hat{y}, \hat{z}), \\ u(x, y, z) &= \hat{u}(\hat{x}, \hat{y}, \hat{z}) - c, \quad v(\hat{x}, \hat{y}, \hat{z}) = \hat{v}(\hat{x}, \hat{y}, \hat{z}), \quad w(\hat{x}, \hat{y}, \hat{z}) = \hat{w}(\hat{x}, \hat{y}, \hat{z}). \end{aligned} \quad (3.12)$$

Eqs. (3.2) – (3.7) become

$$\frac{\partial u}{\partial x} + \frac{\partial w}{\partial z} = 0, \quad (3.13)$$

$$\left[ (u + c) \frac{\partial u}{\partial x} + v \frac{\partial u}{\partial y} + w \frac{\partial u}{\partial z} - 2\Omega v \right] = -\frac{\partial p}{\partial x} + \mu \left[ \frac{\partial^2 u}{\partial x^2} + \frac{\partial^2 u}{\partial y^2} + \frac{\partial^2 u}{\partial z^2} \right], \quad (3.14)$$

$$\left[ (u + c) \frac{\partial v}{\partial x} + v \frac{\partial v}{\partial y} + w \frac{\partial v}{\partial z} + 2\Omega u \right] = -\frac{\partial p}{\partial y} + \mu \left[ \frac{\partial^2 v}{\partial x^2} + \frac{\partial^2 v}{\partial y^2} + \frac{\partial^2 v}{\partial z^2} \right], \quad (3.15)$$

$$\left[ (u + c) \frac{\partial w}{\partial x} + v \frac{\partial w}{\partial y} + w \frac{\partial w}{\partial z} \right] = -\frac{\partial p}{\partial z} + \mu \left[ \frac{\partial^2 w}{\partial x^2} + \frac{\partial^2 w}{\partial y^2} + \frac{\partial^2 w}{\partial z^2} \right], \quad (3.16)$$

$$\begin{aligned} \rho c_p \frac{dT}{dt} &= k \left[ \frac{\partial^2}{\partial x^2} + \frac{\partial^2}{\partial y^2} + \frac{\partial^2}{\partial z^2} \right] T + \mu \left[ \left( \frac{\partial u}{\partial z} + \frac{\partial w}{\partial x} \right)^2 \right] \\ &\quad + \frac{16\sigma^*}{3k^*} T_0^3 \frac{\partial^2}{\partial z^2} + Q_0(T - T_0), \end{aligned} \quad (3.17)$$

$$\frac{dC}{dt} = D \left[ \frac{\partial^2}{\partial x^2} + \frac{\partial^2}{\partial y^2} + \frac{\partial^2}{\partial z^2} \right] C + \frac{k^{**}\nu}{T_r} \left[ \frac{\partial}{\partial z} \left( \frac{\partial T}{\partial z} (C - C_0) \right) \right] - k_1(C - C_0). \quad (3.18)$$



Using dimensionless variables

$$\begin{aligned}
x^* &= \frac{x}{\lambda}, \quad y^* = \frac{y}{\lambda}, \quad z^* = \frac{z}{d}, \quad t^* = \frac{ct}{\lambda}, \quad p^* = \frac{d^2 p}{\mu c \lambda}, \\
u^* &= \frac{u}{c}, \quad v^* = \frac{v}{c}, \quad w^* = \frac{w}{c}, \quad \eta^* = \frac{\eta}{d}, \quad \theta = \frac{T - T_0}{T_0}, \\
\phi &= \frac{C - C_0}{C_0}, \quad \delta = \frac{d}{\lambda}, \quad \text{Re} = \frac{cd}{\nu}.
\end{aligned} \tag{3.19}$$

$$u = \psi_z, w = -\delta\psi_x, \tag{3.20}$$

and applying lubrication approach, the Eqs. (3.14) – (3.18) give

$$p_x - \psi_{zzz} - 2T'v = 0, \tag{3.21}$$

$$p_y - v_{zz} + 2T'(\psi_z + 1) = 0, \tag{3.22}$$

$$p_z = 0, \tag{3.23}$$

$$(1 + R_n \text{Pr})\theta_{zz} + Br\psi_{zz}^2 + S\theta = 0, \tag{3.24}$$

$$\phi_{zz} - \tau' Sc [\theta_{zz}\phi + \theta_z\phi_z] - \gamma\phi = 0 \tag{3.25}$$

and the conditions in non-dimensional form are

$$h(x) = 1 + \epsilon \sin 2\pi x, \tag{3.26}$$

$$\psi = 0, \quad \psi_{zz} = 0, \quad v_z = 0, \quad \frac{\partial\theta}{\partial z} = 0, \quad \frac{\partial\phi}{\partial z} = 0 \quad \text{at } z = 0, \tag{3.27}$$

$$\psi = F_1, \quad \psi_z = -1, \quad v = 0, \quad \frac{\partial\theta}{\partial z} - Bi_1\theta = 0, \quad \frac{\partial\phi}{\partial z} - Bi_2\phi = 0 \quad \text{at } z = h, \tag{3.28}$$

where the stream function  $\psi$  gives

$$F_1 = \int_0^h \psi_z dz$$

From Eq. (3.23)  $p \neq p(z)$ , thus Eq. (3.21) becomes

$$\psi_{zzzz} + 2T'v_z = 0 \tag{3.29}$$

and due to rotational effect, we neglect pressure term caused by secondary flow. Therefore Eq.

(3.22) becomes

$$v_{zz} - 2T'(\psi_z + 1) = 0. \quad (3.30)$$

### 3.3 Solution methodology

The closed form solutions of Eqs. (3.29), (3.30) and (3.24) and boundary conditions (3.26) – (3.27) are

$$\begin{aligned} \psi(z) = & \left( \sin 2h\sqrt{T'} - \sinh 2h\sqrt{T'} \right)^{-1} [-z \sin 2h\sqrt{T'} - A_1(2(F_1 + h) \cosh z\sqrt{T'} \sin z\sqrt{T'} \\ & - 2F_1 \cos z\sqrt{T'} \sinh z\sqrt{T'} - 2h \cos z\sqrt{T'} \sinh z\sqrt{T'}) + z \sinh 2h\sqrt{T'} \\ & + (1 + i)(F_1 + h)A_2(\sin(1 + i)z\sqrt{T'} - \sinh(1 + i)z\sqrt{T'})], \end{aligned} \quad (3.31)$$

$$\begin{aligned} v(z) = & \left( \sin 2h\sqrt{T'} - \sinh 2h\sqrt{T'} \right)^{-1} [2(F_1 + h)(\cos 2h\sqrt{T'} - \cosh^2 h\sqrt{T'} \\ & - 2A_3 \cos z\sqrt{T'} \cosh z\sqrt{T'}) + \sinh^2 h\sqrt{T'} + A_4 \sin z\sqrt{T'} \sinh z\sqrt{T'}], \end{aligned} \quad (3.32)$$

$$\begin{aligned} \theta(z) = & (B_1 + B_2) \cosh B_3 z + (B_1 - B_2) \sinh B_3 z + B_4[(\cosh B_5 - \sinh B_5) \\ & (C_l \cos C_m z + D_n \cosh D_p z + E_q \sin C_m z + G_r \sinh D_p z)], \end{aligned} \quad (3.33)$$

where  $A_j$  ( $j = 1 - 4$ ),  $B_k$  ( $k = 1 - 5$ ),  $C_{l,m}$  ( $l, m = 1 - 32$ ),  $D_{n,p}$  ( $n = 1 - 32$ ),  $E_q$  ( $q = 1 - 32$ ) and  $G_r$  ( $r = 1 - 32$ ) have been computed algebraically. Eq. (25) is solved numerically using NDSolve built in MATHEMATICA.

### 3.4 Discussion

The Taylor number  $T'$  effect on axial velocity is sketched in Fig. 3.1. It is noticed from Fig. that velocity is decreasing function of  $T'$  in the upper half of the channel whereas it shows an increasing behavior in lower half of channel. It is because of the fact that the secondary flow is produced by rotation which causes decay of velocity. Fig. 3.2 depicts that for increasing Taylor number  $T'$  the secondary velocity increases. In fact secondary velocity is enhanced due to an

increase in rotation.

Figs. 3.3– 3.7 are plotted to observe the effect of temperature distribution  $\theta$  for several parameters. Temperature rapidly decays as we increase rotation parameter  $T'$  (see Fig. 3.3). The reason behind this fact is that as we increase  $T'$  the motion of the fluid particles increases which causes decrease in  $\theta$ . Effect of increasing non-uniform source/sink parameter  $S$  on  $\theta$  is observed in Fig. 3.4. We noticed that temperature distribution rises for larger  $S$ . The distribution of temperature is portrayed for different values of  $R_n$  in Fig. 3.5. It is noticed that for larger radiation parameter  $R_n$  the temperature decreases. It is in fact due to the loss of heat. Effect of Brinkman number  $Br$  is shown in Fig. 3.6. Here temperature enhances for increasing Brinkman number  $Br$ . Involvement of viscous dissipation effect in  $Br$  produced minimum heat conduction which results rise in  $\theta$ . In Fig. 3.7 the temperature reduces when heat transfer Biot number  $Bi_1$  increases. The obtained result indicates that the thermal conductivity of fluid reduces with an increase in  $Bi_1$  and so decay in  $\theta$  is noticed.

The impacts of  $T'$ ,  $S$ ,  $R_n$ ,  $Br$  and  $Bi_1$  on heat transfer rate  $Z$  at channel walls are portrayed in Figs. 3.8 – 3.12. Fig. 3.8 predicts that  $Z$  increases for larger  $T'$  when rotation increases. Opposite behavior for heat generation/absorption  $S$  is shown in Fig. 3.9. This indicates that  $Z$  is higher for  $S > 0$ . In Fig. 3.10 the magnitude of heat transfer coefficient  $Z$  near centerline enhances for radiation parameter whereas it decreases near the channel boundaries. In Fig. 3.11 due to stronger viscous dissipation effect the rate of heat transfer coefficient  $Z$  rises for larger Brinkman number  $Br$ . Influence of  $Bi_1$  on heat transfer rate  $Z$  is illustrated in Fig. 3.12. Decrease in  $Z$  is seen for larger values of  $Bi_1$ .

Effect of different emerging parameters on dimensionless concentration  $\phi$  are demonstrated through Figs. 3.13 – 3.17. As temperature and concentration have inverse relation so concentration shows opposite behavior for sundry parameters. In Fig. 3.13 we observed that concentration  $\phi$  increases for larger Taylor number  $T'$ . An enhancement of  $\phi$  is shown in Fig. 3.14 for increasing values of heat generation/absorption  $S$ . Similar graphical result of concentration field  $\phi$  is obtained in Fig. 3.15 for growing values of chemical reaction parameter  $\gamma$ . Since chemical effect increases the rate of interfacial mass transfer and thus reduces the local concentration which in turn increases concentration flux when we have constructive chemical reaction. Here Fig. 3.16 is plotted to analyze the behavior of thermophoretic parameter  $\tau$

on concentration  $\phi$ . It is noticed that larger values of thermophoresis parameter increases the concentration for a small range. In fact larger temperature gradient increases  $\tau'$  which causes an enhancement in concentration profile. Fluctuation in  $\phi$  for mass transfer Biot number  $Bi_2$  is portrayed in Fig. 3.17. Concentration of fluid increases when we take larger values of  $Bi_2$ .

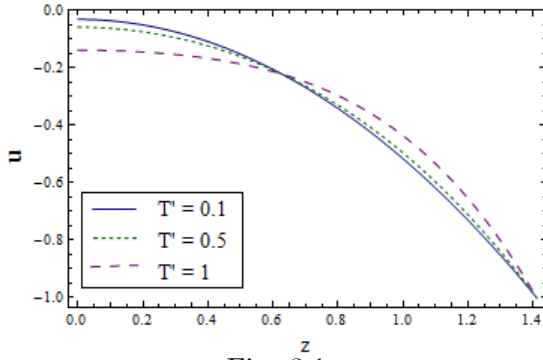


Fig. 3.1

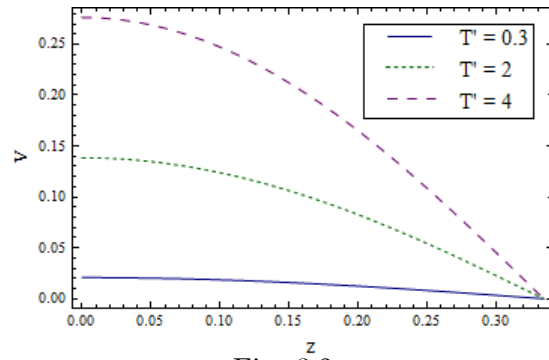


Fig. 3.2

Fig. 3.1: Plot of  $u$  via  $T'$  when  $\epsilon = 0.7$ ,  $x = 0.1$ ,  $\eta = 0.5$ .

Fig. 3.2: Plot of  $v$  via  $T'$  when  $\epsilon = 0.7$ ,  $x = 0.5$ ,  $\eta = 0.5$ .

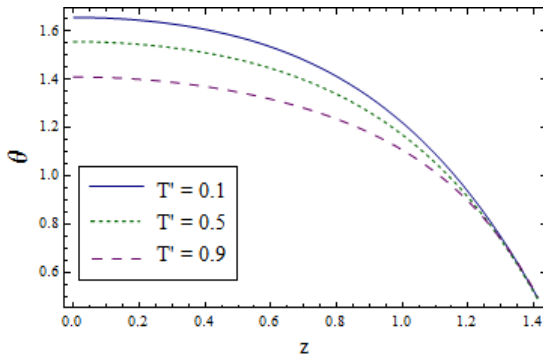


Fig. 3.3

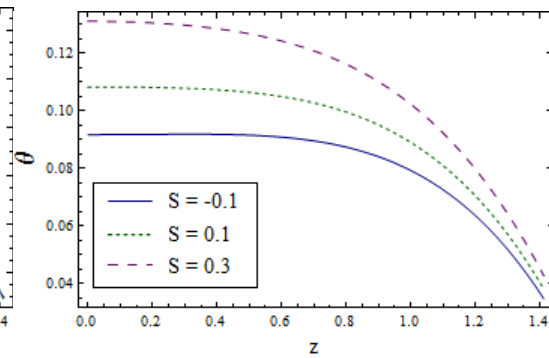


Fig. 3.4

Fig. 3.3: Plot of  $\theta$  via  $T'$  when  $\epsilon = 0.7$ ,  $x = 0.1$ ,  $\eta = 0.7$ ,  $Pr = 0.5$ ,  $Bi_1 = 5$ ,  $Br = 2$ ,  $R_n = 0.3$ ,  $S = 0.5$ .

Fig. 3.4: Plot of  $\theta$  via  $S$  when  $\epsilon = 0.7$ ,  $x = 0.1$ ,  $\eta = 0.7$ ,  $Pr = 0.5$ ,  $Bi_1 = 5$ ,  $Br = 2$ ,  $R_n = 0.3$ ,

$$T' = 0.2.$$

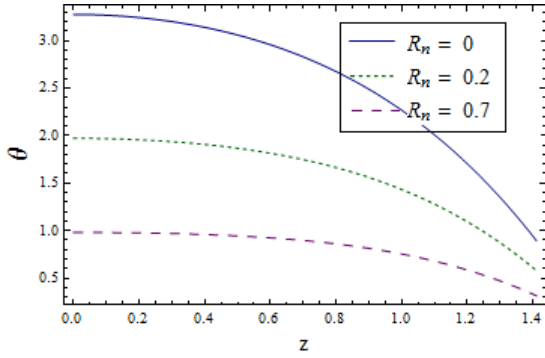


Fig. 3.5

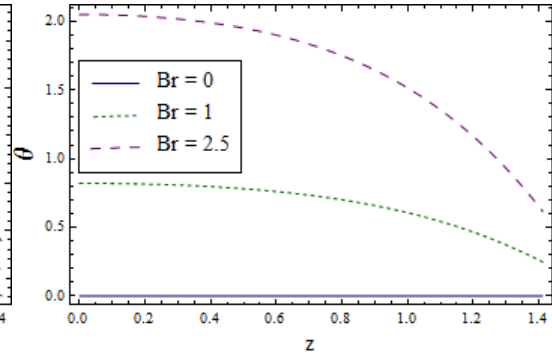


Fig. 3.6

Fig. 3.5: Plot of  $\theta$  via  $R_n$  when  $\epsilon = 0.7$ ,  $x = 0.1$ ,  $\eta = 0.7$ ,  $Pr = 0.5$ ,  $Bi_1 = 5$ ,  $Br = 2$ ,  $S = 0.5$ ,

$$T' = 0.2.$$

Fig. 3.6: Plot of  $\theta$  via  $Br$  when  $\epsilon = 0.7$ ,  $x = 0.1$ ,  $\eta = 0.7$ ,  $Pr = 0.5$ ,  $Bi_1 = 5$ ,  $R_n = 0.3$ ,

$$S = 0.5, T' = 0.2.$$

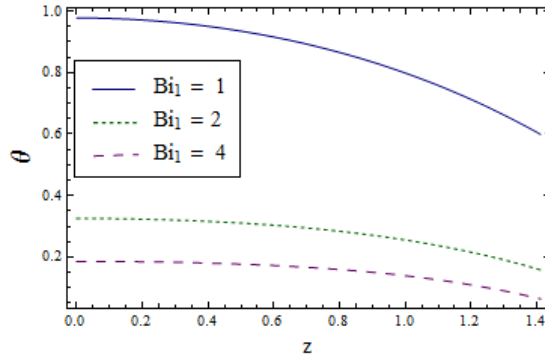


Fig. 3.7

Fig. 3.7: Plot of  $\theta$  via  $Bi_1$  when  $\epsilon = 0.7$ ,  $x = 0.1$ ,  $\eta = 0.7$ ,  $Pr = 0.5$ ,  $Br = 0.2$ ,  $R_n = 0.3$ ,

$$S = 0.5, T' = 0.2.$$

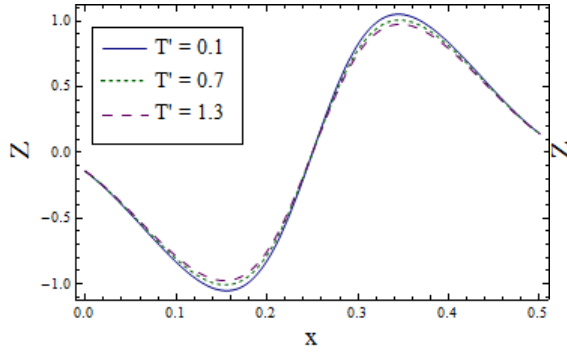


Fig. 3.8

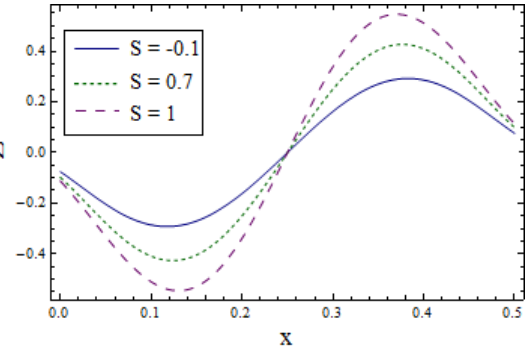


Fig. 3.9

Fig. 3.8: Plot of  $Z$  via  $T'$  when  $\epsilon = 0.3$ ,  $\eta = 0.1$ ,  $Pr = 1.5$ ,  $Bi_1 = 5$ ,  $Br = 2$ ,  $S = 1.4$ ,  $R_n = 0.3$ .

Fig. 3.9: Plot of  $Z$  via  $S$  when  $\epsilon = 0.3$ ,  $\eta = 0.1$ ,  $Pr = 1.5$ ,  $Bi_1 = 5$ ,  $Br = 2$ ,  $R_n = 0.3$ ,  $T' = 0.2$ .

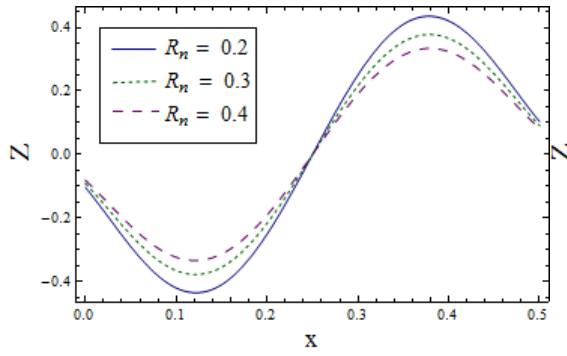


Fig. 3.10

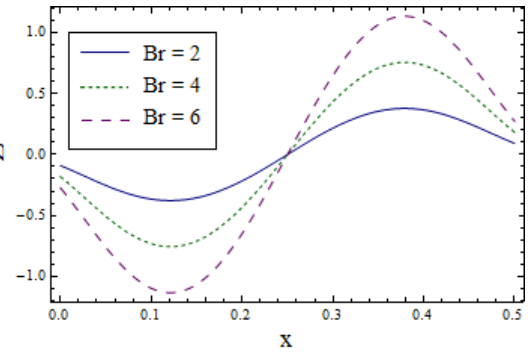


Fig. 3.11

Fig. 3.10: Plot of  $Z$  via  $R_n$  when  $\epsilon = 0.3$ ,  $\eta = 0.1$ ,  $Pr = 1.5$ ,  $Bi_1 = 5$ ,  $Br = 2$ ,  $T' = 0.2$ ,

$S = 0.5$ .

Fig. 3.11: Plot of  $Z$  for via  $Br$  when  $\epsilon = 0.3$ ,  $\eta = 0.1$ ,  $Pr = 1.5$ ,  $Bi_1 = 5$ ,  $R_n = 0.3$ ,  $T' = 0.2$ ,

$$S = 0.5.$$

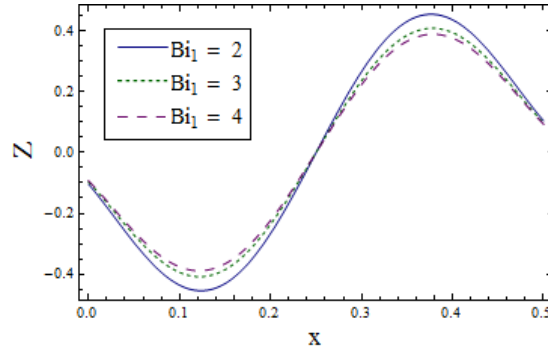


Fig. 3.12

Fig. 3.12: Plot of  $Z$  via  $Bi_1$  when  $\epsilon = 0.3$ ,  $\eta = 0.1$ ,  $Pr = 1.5$ ,  $Br = 2$ ,  $R_n = 0.3$ ,  $T' = 0.2$ ,  $S = 0.5$ .

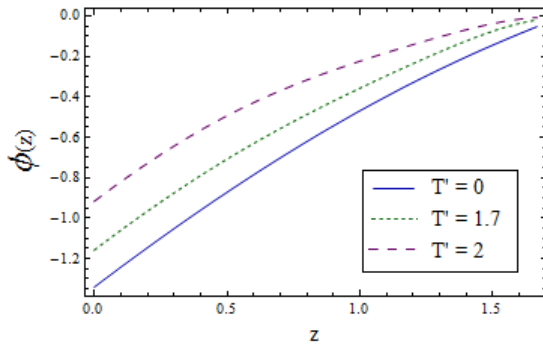


Fig. 3.13

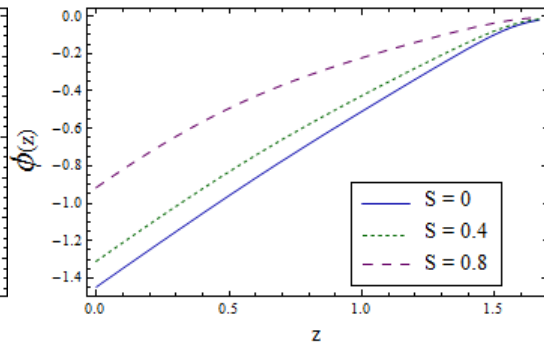


Fig. 3.14

Fig. 3.13: Plot of  $\phi$  via  $T'$  when  $\epsilon = 0.3$ ,  $x = 0.2$ ,  $\eta = 0.7$ ,  $Bi_1 = 10$ ,  $Bi_2 = 10$ ,  $Pr = 0.7$ ,  $Br = 2$ ,  $R_n = 1$ ,  $S = 0.8$ ,  $\tau' = 0.7$ ,  $Sc = 0.2$ ,  $\gamma = 0.3$ .

Fig. 3.14: Plot of  $\phi$  via  $S$  when  $\epsilon = 0.3$ ,  $x = 0.2$ ,  $\eta = 0.7$ ,  $Bi_1 = 10$ ,  $Bi_2 = 10$ ,  $Pr = 0.7$ ,  $Br = 2$ ,  $R_n = 1$ ,  $\tau' = 0.7$ ,  $Sc = 0.2$ ,  $\gamma = 0.3$ ,  $T' = 0.2$ .

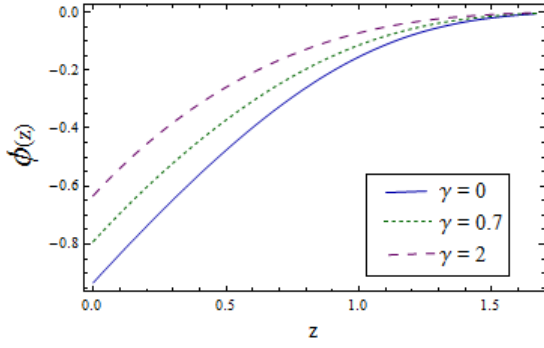


Fig. 3.15

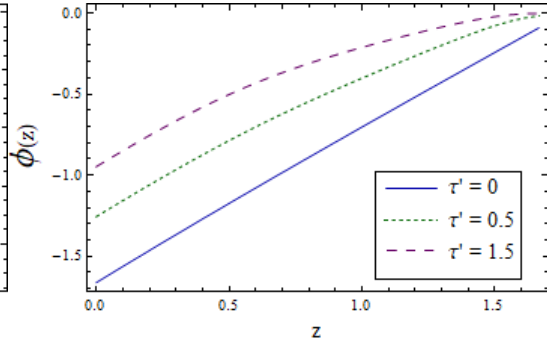


Fig. 3.16

Fig. 3.15: Plot of  $\phi$  via  $\gamma$  when  $\epsilon = 0.3$ ,  $x = 0.2$ ,  $\eta = 1.5$ ,  $Bi_1 = 10$ ,  $Bi_2 = 10$ ,  $Pr = 0.7$ ,

$$Br = 2, R_n = 1, \tau' = 0.7, Sc = 0.2, S = 0.5, T' = 0.2.$$

Fig. 3.16: Plot of  $\phi$  via  $\tau'$  when  $\epsilon = 0.3$ ,  $x = 0.2$ ,  $\eta = 0.7$ ,  $Bi_1 = 10$ ,  $Bi_2 = 10$ ,  $Pr = 0.7$ ,

$$Br = 2, R_n = 0.8, \gamma = 0.3, Sc = 0.2, S = 0.5, T' = 2.$$

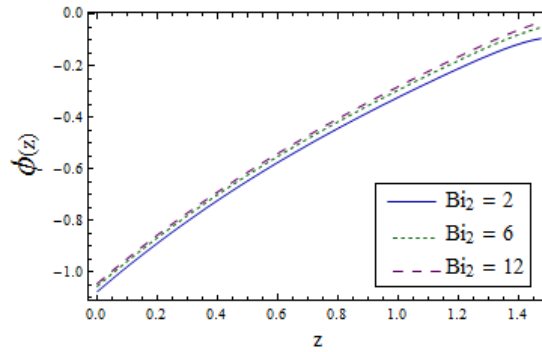


Fig. 3.17

Fig. 3.17: Plot of  $\phi$  via  $Bi_2$  when  $\epsilon = 0.3$ ,  $x = 0.2$ ,  $\eta = 0.7$ ,  $Bi_1 = 10$ ,  $\tau = 0.1$ ,  $Pr = 0.7$ ,

$$Br = 2, R_n = 0.8, \gamma = 0.3, Sc = 0.2, S = 0.5, T' = 2.$$

### 3.5 Conclusions

Influences of thermal radiation and thermophoresis on peristaltic rotating flow are focused. Key findings of present analysis are:

- Dual effect of Taylor number on  $u$  is observed.



- Secondary velocity is an increasing function of Taylor number.
- Similar behavior of temperature is noticed for rotation and radiation parameters.
- Temperature is an increasing function of heat generation/absorption and Brinkman number.
- Opposite behavior of temperature and concentration is noticed for emerging parameters.
- Heat transfer rate decreases by increasing  $T'$ ,  $R_n$  and  $Bi_1$  whereas it enhances for  $S$  and  $Br$ .

## Chapter 4

# Peristaltic activity of rotating Prandtl fluid

### 4.1 Introduction

Peristaltic motion of MHD rotating flow of Prandtl fluid in channel with flexible characteristics is discussed. Constant angular velocity is adopted. Channel is convectively heated. Numerical results are obtained. Axial and secondary velocities, temperature and heat transfer coefficient are examined.

### 4.2 Definition

Consider peristaltic motion of MHD Prandtl fluid in a uniform channel of thickness  $2d$ . Uniform magnetic field  $B_0$  is applied. Effect of electric field is not retained. Convectively heated channel has flexible walls. The wall surface satisfies

$$z = \pm\eta(x, t) = \pm \left[ d + a \sin \frac{2\pi}{\lambda}(x - ct) \right]. \quad (4.1)$$

For Prandtl fluid, the general constitutive equations are represented as:

$$\boldsymbol{\tau} = -p\mathbf{I} + \mathbf{S}, \quad (4.2)$$

$$\mathbf{S}_{ij} = \dot{A}_1 \left[ \frac{\sin^{-1} \left( \sum_{m=1}^3 \sum_{n=1}^3 \frac{\epsilon_{mn}\epsilon_{nm}}{2\dot{A}_2^2} \right)^{\frac{1}{2}}}{\left( \sum_{m=1}^3 \sum_{n=1}^3 \frac{\epsilon_{mn}\epsilon_{nm}}{2\dot{A}_2^2} \right)^{\frac{1}{2}}} \right] e_{ij}, \quad (4.3)$$

where

$$e_{ij} = \frac{1}{2} \left( \frac{\partial u}{\partial x_i} + \frac{\partial u}{\partial x_j} \right).$$

Using Patel et. al. [35] we have

$$S_{xz} = \frac{\dot{A}_1 \sin^{-1} \left[ \frac{1}{\dot{A}_2} \left[ \left( \frac{\partial u}{\partial z} \right)^2 + \left( \frac{\partial w}{\partial x} \right)^2 \right]^{1/2} \right] \frac{\partial u}{\partial z}}{\left[ \left( \frac{\partial u}{\partial z} \right)^2 + \left( \frac{\partial w}{\partial x} \right)^2 \right]^{1/2}},$$

$$S_{yz} = \frac{\dot{A}_1 \sin^{-1} \left[ \frac{1}{\dot{A}_2} \left[ \left( \frac{\partial v}{\partial z} \right)^2 + \left( \frac{\partial u}{\partial y} \right)^2 \right]^{1/2} \right] \frac{\partial v}{\partial z}}{\left[ \left( \frac{\partial v}{\partial z} \right)^2 + \left( \frac{\partial u}{\partial y} \right)^2 \right]^{1/2}},$$

where  $\dot{A}_1$  and  $\dot{A}_2$  are material constants relating to Prandtl fluid. Considering velocity components  $u$ ,  $v$ ,  $w$  in  $x$ ,  $y$ ,  $z$  directions, we have

$$\mathbf{V} = [u(x, z, t), v(x, z, t), w(x, z, t)]. \quad (4.4)$$

Mass, momentum and energy conservation equations in rotating frame are

$$\frac{\partial u}{\partial x} + \frac{\partial w}{\partial z} = 0, \quad (4.5)$$

$$\rho \frac{du}{dt} - 2\rho\Omega v = -\frac{\partial \tilde{p}}{\partial x} + \frac{\partial S_{xx}}{\partial x} + \frac{\partial S_{xy}}{\partial y} + \frac{\partial S_{xz}}{\partial z} - \sigma B_0^2 u, \quad (4.6)$$

$$\rho \frac{dv}{dt} + 2\rho\Omega u = -\frac{\partial \tilde{p}}{\partial y} + \frac{\partial S_{yx}}{\partial x} + \frac{\partial S_{yy}}{\partial y} + \frac{\partial S_{yz}}{\partial z} - \sigma B_0^2 v, \quad (4.7)$$

$$\rho \frac{dw}{dt} = -\frac{\partial \tilde{p}}{\partial z} + \frac{\partial S_{zx}}{\partial x} + \frac{\partial S_{zy}}{\partial y} + \frac{\partial S_{zz}}{\partial z}, \quad (4.8)$$

$$\rho c_p \frac{dT}{dt} = k_T \left[ \frac{\partial^2 T}{\partial x^2} + \frac{\partial^2 T}{\partial y^2} + \frac{\partial^2 T}{\partial z^2} \right] + S_{xx} \frac{\partial u}{\partial x} + S_{xz} \left( \frac{\partial u}{\partial z} + \frac{\partial w}{\partial x} \right) + S_{zz} \frac{\partial w}{\partial z}, \quad (4.9)$$

with conditions

$$k_T \frac{\partial T}{\partial z} = -\dot{h}_1(T - T_0) \text{ at } z = \eta, \quad (4.10)$$

$$k_T \frac{\partial T}{\partial z} = -\dot{h}_1(T_0 - T) \text{ at } z = -\eta, \quad (4.11)$$

$$u = 0, v = 0 \text{ at } z = \pm\eta, \quad (4.12)$$

$$\frac{\partial}{\partial x} G(\eta) = \frac{\partial p}{\partial x} = -\rho \frac{du}{dt} + \frac{\partial S_{xx}}{\partial x} + \frac{\partial S_{xy}}{\partial y} + \frac{\partial S_{xz}}{\partial z} - \sigma B_0^2 u + 2\rho\Omega v \text{ at } z = \pm\eta, \quad (4.13)$$

where

$$G = -\tau \frac{\partial^2}{\partial x^2} + m_1^* \frac{\partial^2}{\partial t^2} + d' \frac{\partial}{\partial t}.$$

Consider

$$\begin{aligned} x^* &= \frac{x}{\lambda}, y^* = \frac{y}{\lambda}, z^* = \frac{z}{d}, t^* = \frac{ct}{\lambda}, p^* = \frac{d^2 \tilde{p}}{\mu c \lambda}, \\ u^* &= \frac{u}{c}, v^* = \frac{v}{c}, w^* = \frac{w}{c}, \eta^* = \frac{\eta}{d}, \mathbf{S}^* = \frac{d\mathbf{S}}{\mu c}, \\ \theta &= \frac{T - T_0}{T_0}, \delta = \frac{d}{\lambda}, \text{Re} = \frac{cd}{\nu}. \end{aligned} \quad (4.14)$$

Defining the stream function ( $\psi$ ) by

$$u = \psi_z, w = -\delta \psi_x \quad (4.15)$$

and invoking lubrication technique one obtains from (4.5) – (4.9) as

$$-2T'v = -\frac{\partial p}{\partial x} + \frac{\partial S_{xz}}{\partial z} - H^2 \psi_z, \quad (4.16)$$

$$2T' \psi_z = -\frac{\partial p}{\partial y} + \frac{\partial S_{yz}}{\partial z} - H^2 v, \quad (4.17)$$

$$0 = -\frac{\partial p}{\partial z} + \frac{\partial S_{zz}}{\partial z}, \quad (4.18)$$

$$\frac{\partial^2 \theta}{\partial z^2} + Br S_{xz} \psi_{zz} = 0. \quad (4.19)$$

Through Eq. (4.3) we can write

$$S_{xz} = \alpha_1 \psi_{zz} + \frac{\alpha_2}{6} \psi_{zz}^3, \quad (4.20)$$

$$S_{yz} = \alpha_1 v_z + \frac{\alpha_2}{6} v_z^3, \quad (4.21)$$

$$S_{zz} = 0, \quad (4.22)$$

with the dimensionless conditions

$$\eta = 1 + \epsilon \sin 2\pi(x - t), \quad (4.23)$$

$$\begin{aligned} \frac{\partial \theta}{\partial z} + Bi_1 \theta &= 0 \text{ at } z = \eta, \\ \frac{\partial \theta}{\partial z} - Bi_1 \theta &= 0 \text{ at } z = -\eta, \end{aligned} \quad (4.24)$$

$$\psi_z = 0, \quad v = 0 \text{ at } z = \pm \eta, \quad (4.25)$$

$$\left[ E_1 \frac{\partial^3}{\partial x^3} + E_2 \frac{\partial^3}{\partial x \partial t^2} + E_3 \frac{\partial^2}{\partial x \partial t} \right] \eta = \frac{\partial S_{xz}}{\partial z} - H^2 \psi_z + 2T'v \text{ at } z = \pm \eta. \quad (4.26)$$

In above expressions  $\alpha_1 = \frac{A_1}{\mu A_2}$  and  $\alpha_2 = \frac{\alpha_1 c^2}{A_2^2 d^2}$  denote the Prandtl fluid parameters.

Equations (4.18) and (4.22) indicate  $p \neq p(z)$ . Following arguments of previous chapters we have

$$\frac{\partial}{\partial z} \left[ \frac{\partial S_{xz}}{\partial z} - H^2 \psi_z + 2T'v \right] = 0, \quad (4.27)$$

$$\frac{\partial S_{yz}}{\partial z} - H^2 v - 2T' \psi_z = 0. \quad (4.28)$$

Our interest is now to find numerical solution by shooting technique with fourth order Runge-Kutta scheme.

### 4.3 Analysis

Various pertinent parameters effects on  $u(z)$  are concluded via Figs. 4.1 (a – e). Figs. 4.1(a) and (b) depict a visible reduction in velocity profile with the increase in  $\alpha_1$  and  $\alpha_2$  respectively. Higher Prandtl fluid parameters  $\alpha_1$  and  $\alpha_2$  characterize an increase in viscosity. Consequently a decreasing velocity profile is captured. Same results are reported by Riaz et al. [54] and Hayat

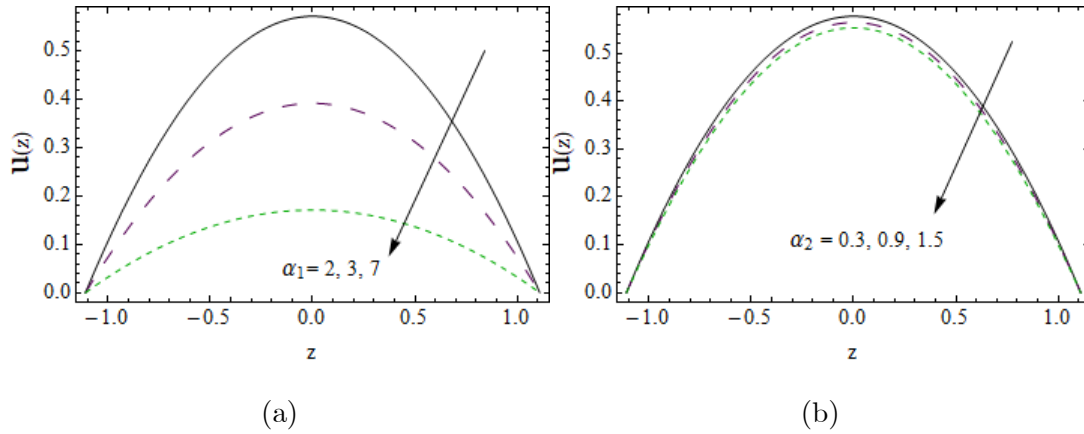
et al. [55]. Externally applied magnetic field helps in aligning the fluid particles. Fluid velocity is decreased. This effect of magnetic field makes it valuable in biomedical applications like GMR (see Fig. 4.1(c)). A numerical study using Runge-Kutta Fehlberg method presented by Akbar et al. [52] approves the present finding via larger Hartman number. Velocity against wall parameters is presented via Fig. 4.1(d). The obtained result illustrates velocity enhancement against  $E_1$  and  $E_2$ . However velocity is decreased by  $E_3$ . Larger  $E_1$  and  $E_2$  give less resistance to flow and so velocity decreases for  $E_3$ . Results of [53] also confirm these outcomes. Rotation in system induces a secondary flow. This secondary flow is perceived to yield decrease in axial velocity (shown by Fig. 4.1(e)). Accordingly the axial velocity is quite high in the absence of rotation parameter  $T'$ . The Taylor number ( $T'$ ) is a dimensionless quantity which characterizes the importance of centrifugal forces due to rotation of fluid relative to viscous forces.

Figs. 4.2(a – e) indicate secondary velocity  $v$  by rotation about  $z$ -axis. Secondary velocity for  $\alpha_1$  and  $\alpha_2$  has similar behavior to that of axial velocity (see Figs. 4.2(a) and 4.2(b)). Fig. 4.2(c) depicts decay in secondary for larger Hartman number  $H$ . Externally applied magnetic field acts as drag force and so resists the fluid flow. In Fig. 4.2(d) the wall parameters have similar impact on secondary velocity when compared to that of axial velocity. Impact of Taylor number  $T'$  on  $v$  is shown via Fig. 4.2(e). An interesting fact worth mentioning here is the opposite behavior of secondary velocity in response to rotation. Secondary velocity, in contrast to axial velocity, enhances in the presence of rotation. For authenticity the results of  $T'$  can be compared with Mahmoud [154] and Hayat et al. [155]. However secondary velocity vanishes for  $T' = 0$ .

Figs. 4.3 (a – g) are included to elaborate the behavior of temperature distribution  $\theta$ . From Figs. 4.3(a) and (b) it is observed that fluid cools down for fluid parameters  $\alpha_1$  and  $\alpha_2$ . Parabolic temperature profile is observed in these figures, referring to the fact that fluid has the highest velocity and temperature, at centre of channel. Fig. 4.3(c) concludes a decreasing behavior when  $H$  is enhanced. Fig. 4.3(d) illustrates the impact of wall parameters. Variation of wall parameter leads to temperature enhancement. Average kinetic energy is known as temperature. The velocity and temperature have similar effects. Temperature is decreased for larger  $Bi_1$  (see Fig. 4.3(e)). Note that dissipation effect leads to Brinkman number. Clearly such dissipation generates heat in channel. There is temperature enhancement when Br enhances (see Fig.

4.3(f)). Temperature is decreased via  $T'$  (see Fig. 4.3(g)).

Behavior of heat transfer coefficient  $Z$  for parameters  $\alpha_1$ ,  $\alpha_2$ ,  $H$ ,  $Bi_1$ ,  $Br$ ,  $T'$  and wall parameters  $E_i$  are shown through Figs. 4.4 (a – g). Heat transfer coefficient defined by  $Z = \eta_x \theta(\eta)$ , involves temperature of the fluid as well as position of channel walls. It is found from Figs. 4.4(a) and (b) that larger fluid parameters  $\alpha$  and  $\beta$  ensure lower heat transfer rate. Hartman number  $H$  decays magnitude of heat transfer coefficient  $Z$  near channel centre whereas it increases near the boundaries (see Fig. 4.4(c)). From Fig. 4.4(d) it is noticed that  $Z$  increases for  $E_1$  and  $E_2$ . Effects of  $E_3$  on  $Z$  is different to that of  $E_1$  and  $E_2$ . Fig. 4.4(e) depicts no absolute value of heat transfer coefficient when  $Bi_1$  varies. The obtained result from Fig. 4.4(f) shows increasing behavior of  $Br$ . Heat transfer rate between wall and fluid decays for larger rotation (see in Fig. 4.4(g)).



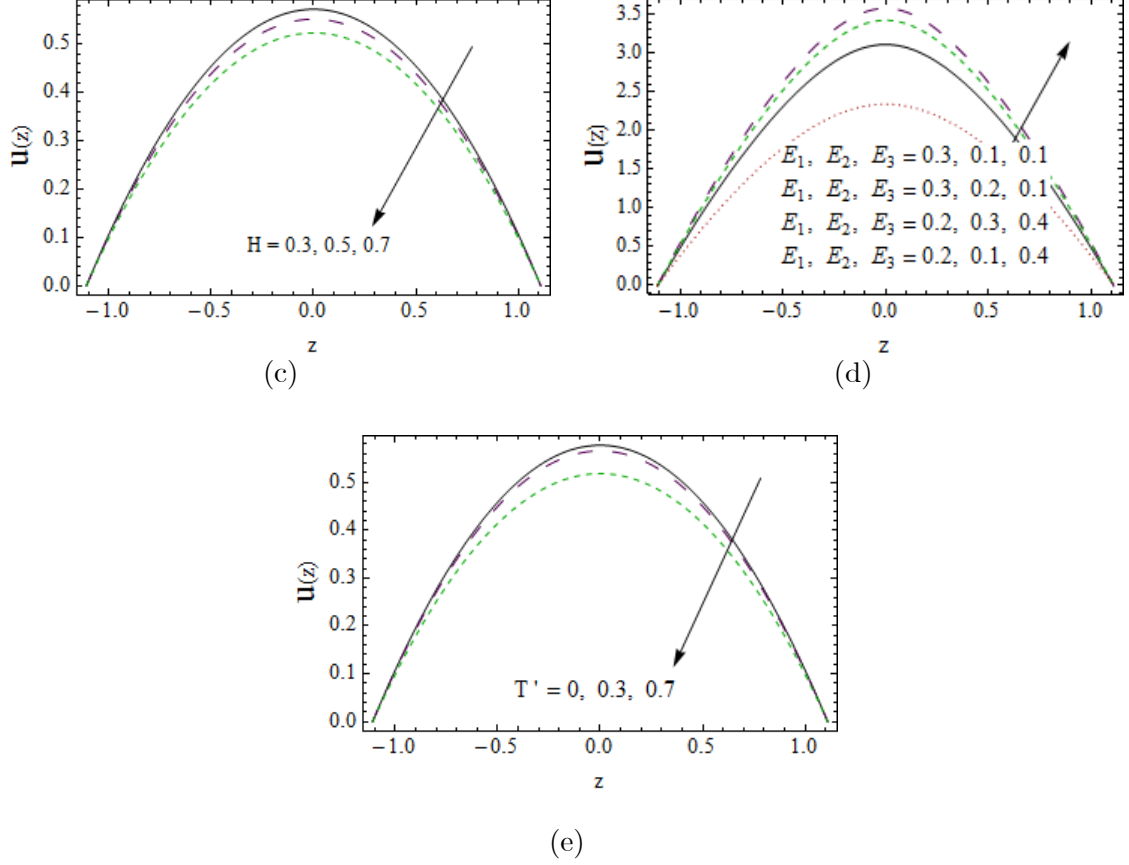


Fig. 4.1: Axial velocity  $u$  for (a) Prandtl fluid parameter  $\alpha_1$  when  $E_1 = 0.03$ ,  $E_2 = 0.02$ ,  $E_3 = 0.01$ ,  $\epsilon = 0.2$ ,  $t = 0.1$ ,  $x = 0.2$ ,  $\alpha_2 = 0.5$ ,  $Br = 0.3$ ,  $Bi_1 = 2$ ,  $T' = 0.2$ ,  $H = 0.3$  (b) Prandtl fluid parameter  $\alpha_2$  when  $E_1 = 0.03$ ,  $E_2 = 0.02$ ,  $E_3 = 0.01$ ,  $\epsilon = 0.2$ ,  $t = 0.1$ ,  $x = 0.2$ ,  $\alpha_1 = 2$ ,  $Br = 0.3$ ,  $Bi_1 = 2$ ,  $T' = 0.2$ ,  $H = 0.3$  (c) Hartman number  $H$  when  $E_1 = 0.03$ ,  $E_2 = 0.02$ ,  $E_3 = 0.01$ ,  $\epsilon = 0.2$ ,  $t = 0.1$ ,  $x = 0.2$ ,  $\alpha_2 = 0.5$ ,  $Br = 0.3$ ,  $Bi_1 = 2$ ,  $T' = 0.2$ ,  $\alpha_1 = 2$  (d) wall parameters  $E_1, E_2, E_3$  when  $\alpha_1 = 2$ ,  $t = 0.1$ ,  $x = 0.2$ ,  $\alpha_2 = 0.5$ ,  $Br = 0.3$ ,  $Bi_1 = 2$ ,  $T' = 0.2$ ,  $H = 0.3$  (e) Taylor number  $T'$  when  $E_1 = 0.03$ ,  $E_2 = 0.02$ ,  $E_3 = 0.01$ ,  $\epsilon = 0.2$ ,  $t = 0.1$ ,  $x = 0.2$ ,  $\alpha_2 = 0.5$ ,  $Br = 0.3$ ,  $Bi_1 = 2$ ,  $H = 0.3$ ,  $\alpha_1 = 2$ .



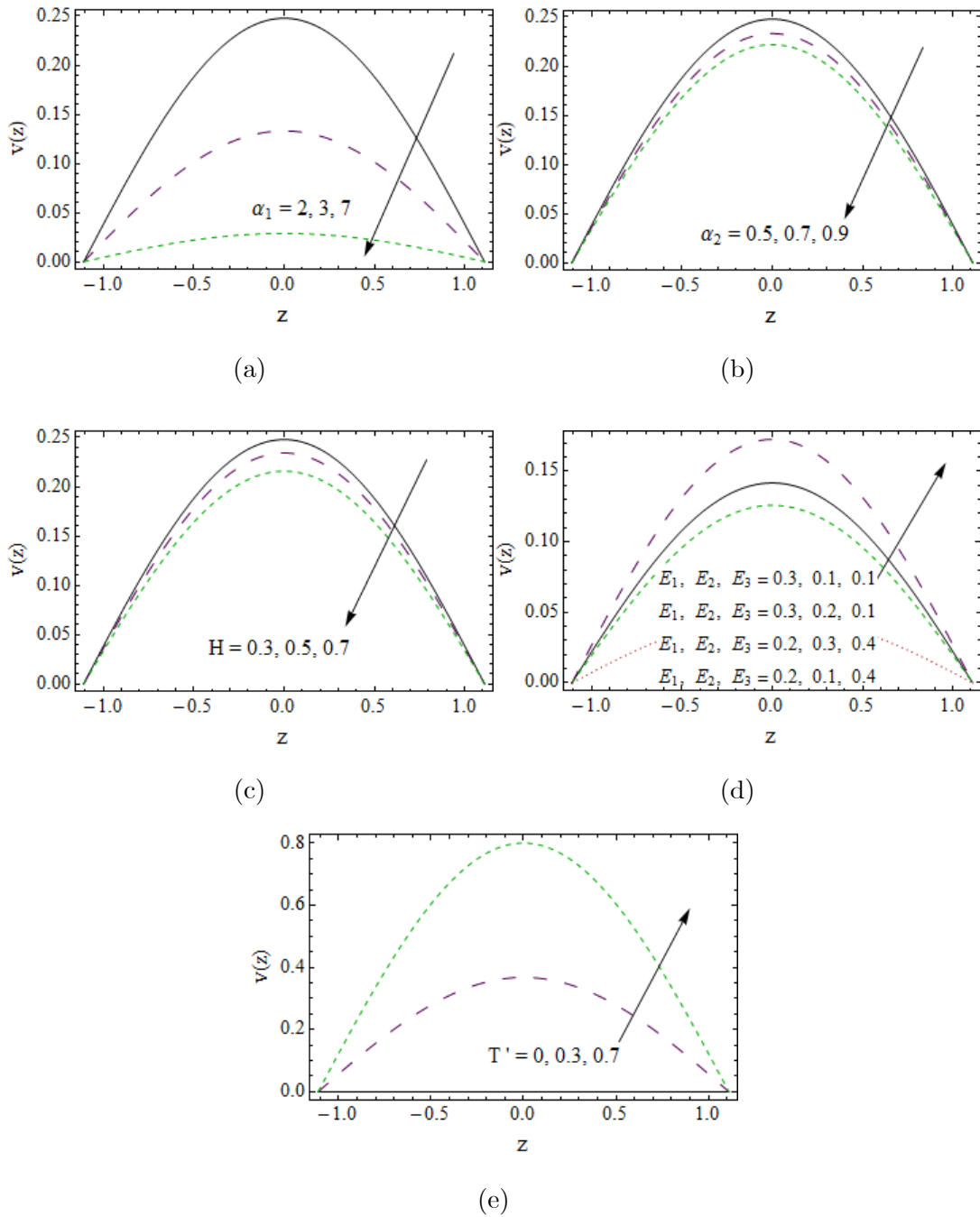
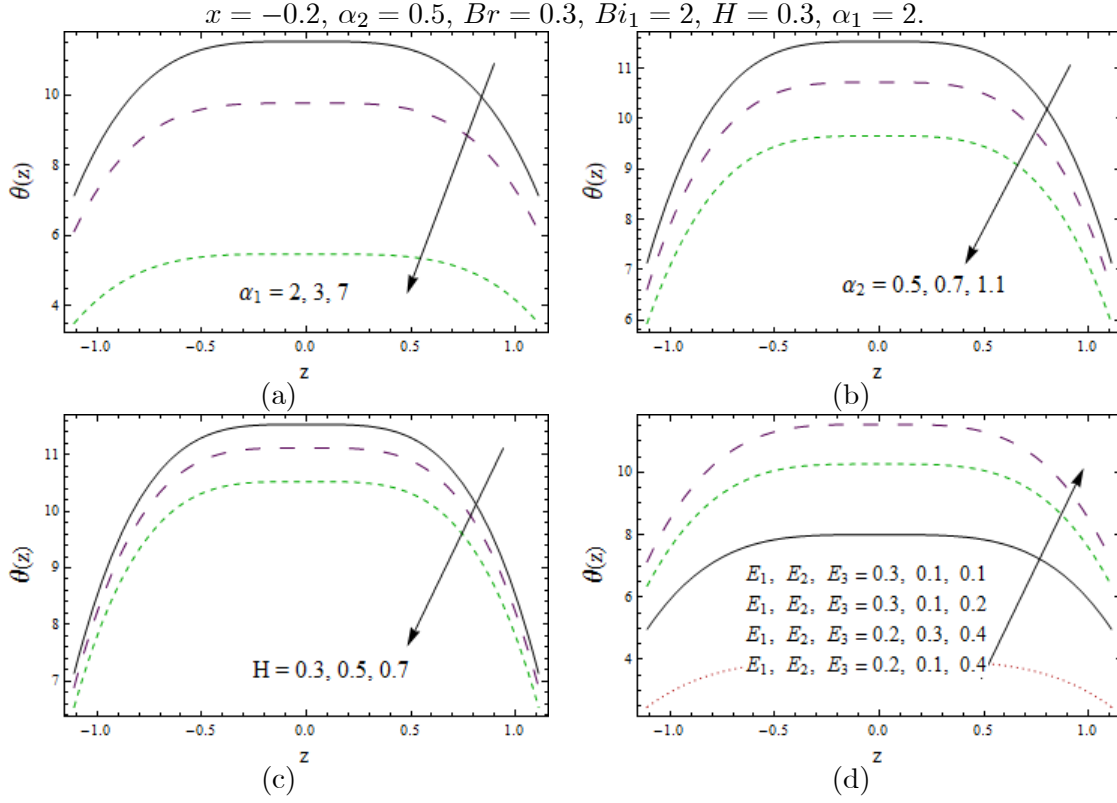


Fig. 4.2: Secondary velocity  $v$  for (a) Prandtl fluid parameter  $\alpha_1$  when  $E_1 = 0.5$ ,  $E_2 = 0.4$ ,  $E_3 = 0.3$ ,  $\epsilon = 0.2$ ,  $t = 0.1$ ,  $x = -0.2$ ,  $\alpha_2 = 0.5$ ,  $Br = 0.3$ ,  $Bi_1 = 2$ ,  $T' = 0.2$ ,  $H = 0.3$  (b) Prandtl fluid parameter  $\alpha_2$  when  $E_1 = 0.5$ ,  $E_2 = 0.4$ ,  $E_3 = 0.3$ ,  $\epsilon = 0.2$ ,  $t = 0.1$ ,  $x = -0.2$ ,  $\alpha_1 = 2$ ,  $Br = 0.3$ ,  $Bi_1 = 2$ ,  $T' = 0.2$ ,  $H = 0.3$  (c) Hartman number  $H$  when  $E_1 = 0.5$ ,

$E_2 = 0.4, E_3 = 0.3, \epsilon = 0.2, t = 0.1, x = -0.2, \alpha_2 = 0.5, Br = 0.3, Bi_1 = 2, T' = 0.2, \alpha_1 = 2$   
 (d) wall parameters  $E_1, E_2, E_3$  when  $\alpha_1 = 2, t = 0.1, x = -0.2, \alpha_2 = 0.5, Br = 0.3, Bi_1 = 2, T' = 0.2, H = 0.3$  (e) Taylor number  $T'$  when  $E_1 = 0.5, E_2 = 0.4, E_3 = 0.3, \epsilon = 0.2, t = 0.1,$



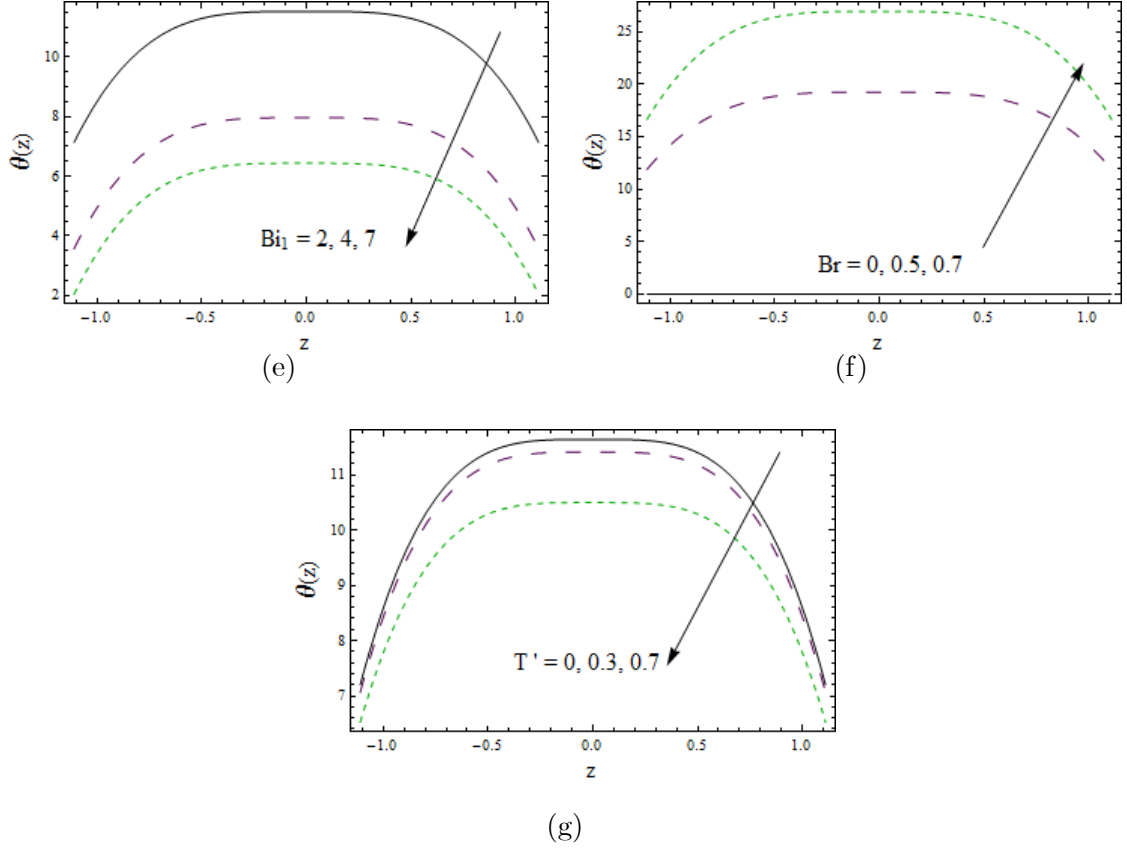
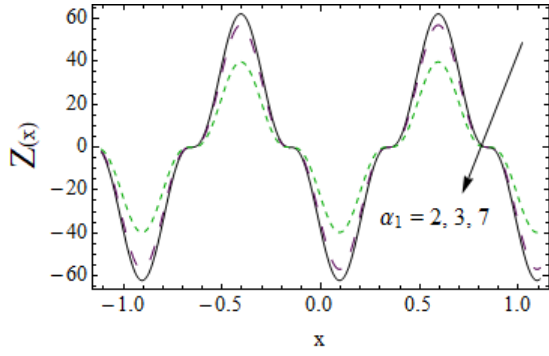
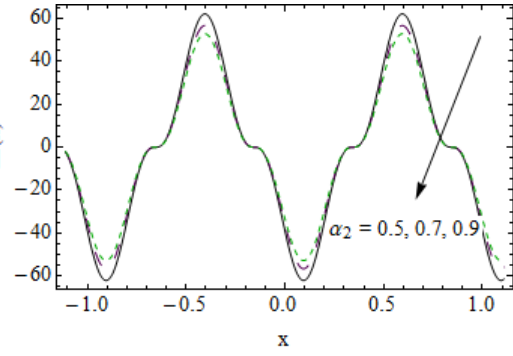


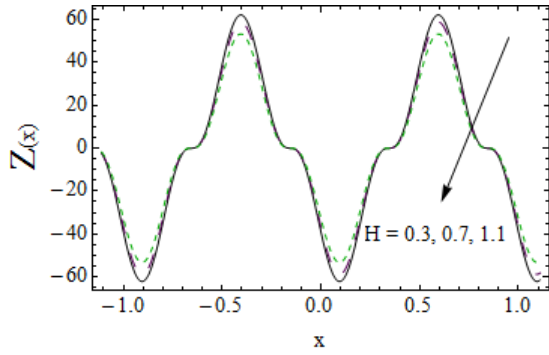
Fig. 4.3: Temperature  $\theta$  for (a) Prandtl fluid parameter  $\alpha_1$  when  $E_1 = 0.3$ ,  $E_2 = 0.2$ ,  $E_3 = 0.1$ ,  $\epsilon = 0.2$ ,  $t = 0.1$ ,  $x = 0.2$ ,  $\alpha_2 = 0.5$ ,  $Br = 0.3$ ,  $Bi_1 = 2$ ,  $T' = 0.2$ ,  $H = 0.3$  (b) Prandtl fluid parameter  $\alpha_2$  when  $E_1 = 0.3$ ,  $E_2 = 0.2$ ,  $E_3 = 0.1$ ,  $\epsilon = 0.2$ ,  $t = 0.1$ ,  $x = 0.2$ ,  $\alpha_1 = 2$ ,  $Br = 0.3$ ,  $Bi_1 = 2$ ,  $T' = 0.2$ ,  $H = 0.3$  (c) Hartman number  $H$  when  $E_1 = 0.3$ ,  $E_2 = 0.2$ ,  $E_3 = 0.1$ ,  $\epsilon = 0.2$ ,  $t = 0.1$ ,  $x = 0.2$ ,  $\alpha_2 = 0.5$ ,  $Br = 0.3$ ,  $Bi_1 = 2$ ,  $T' = 0.2$ ,  $\alpha_1 = 2$  (d) wall parameters  $E_1$ ,  $E_2$ ,  $E_3$  when  $\alpha_1 = 2$ ,  $t = 0.1$ ,  $x = 0.2$ ,  $\alpha_2 = 0.5$ ,  $Br = 0.3$ ,  $Bi_1 = 2$ ,  $T' = 0.2$ ,  $H = 0.3$  (e) Biot number  $Bi_1$  when  $E_1 = 0.3$ ,  $E_2 = 0.2$ ,  $E_3 = 0.1$ ,  $\epsilon = 0.2$ ,  $t = 0.1$ ,  $x = 0.2$ ,  $\alpha_2 = 0.5$ ,  $Br = 0.3$ ,  $H = 0.3$ ,  $T' = 0.2$ ,  $\alpha_1 = 2$  (f) Brinkman  $Br$  when  $E_1 = 0.3$ ,  $E_2 = 0.2$ ,  $E_3 = 0.1$ ,  $\epsilon = 0.2$ ,  $t = 0.1$ ,  $x = 0.2$ ,  $\alpha_2 = 0.5$ ,  $Bi_1 = 2$ ,  $H = 0.3$ ,  $T' = 0.2$ ,  $\alpha_1 = 2$  (g) Taylor number  $T'$  when  $E_1 = 0.3$ ,  $E_2 = 0.2$ ,  $E_3 = 0.1$ ,  $\epsilon = 0.2$ ,  $t = 0.1$ ,  $x = 0.2$ ,  $\alpha_2 = 0.5$ ,  $Br = 0.3$ ,  $Bi_1 = 2$ ,  $H = 0.3$ ,  $\alpha_1 = 2$ .



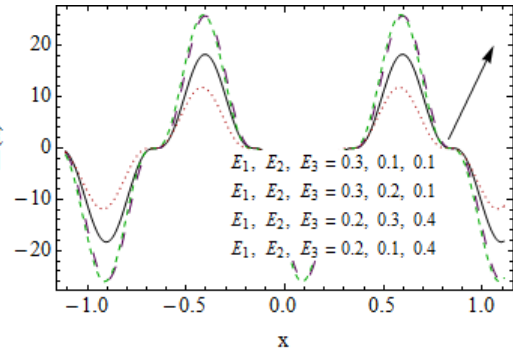
(a)



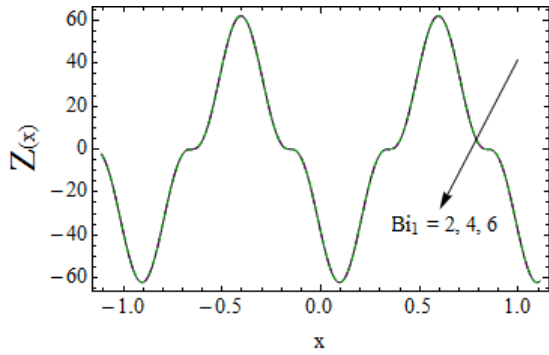
(b)



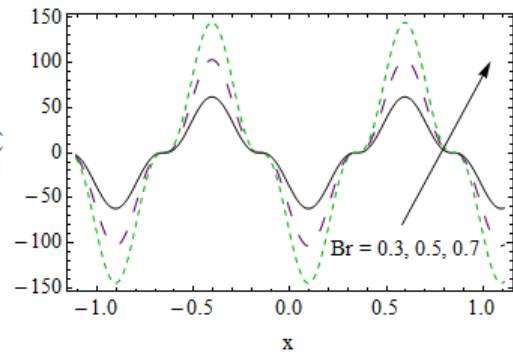
(c)



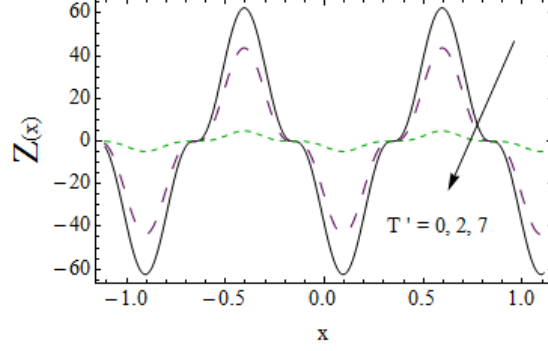
(d)



(e)



(f)



(g)

Fig. 4.4: Heat transfer coefficient  $Z$  (a) Prandtl fluid parameter  $\alpha_1$  when  $E_1 = 0.5$ ,  $E_2 = 0.4$ ,  $E_3 = 0.3$ ,  $\epsilon = 0.2$ ,  $t = 0.1$ ,  $x = 0.2$ ,  $\alpha_2 = 0.5$ ,  $Br = 0.3$ ,  $Bi_1 = 2$ ,  $T' = 0.2$ ,  $H = 0.3$  (b) Prandtl fluid parameter  $\alpha_2$  when  $E_1 = 0.5$ ,  $E_2 = 0.4$ ,  $E_3 = 0.3$ ,  $\epsilon = 0.2$ ,  $t = 0.1$ ,  $x = 0.2$ ,  $\alpha_1 = 2$ ,  $Br = 0.3$ ,  $Bi_1 = 2$ ,  $T' = 0.2$ ,  $H = 0.3$  (c) Hartman number  $H$  when  $E_1 = 0.5$ ,  $E_2 = 0.4$ ,  $E_3 = 0.3$ ,  $\epsilon = 0.2$ ,  $t = 0.1$ ,  $x = 0.2$ ,  $\alpha_2 = 0.5$ ,  $Br = 0.3$ ,  $Bi_1 = 2$ ,  $T' = 0.2$ ,  $\alpha_1 = 2$  (d) wall parameters  $E_1$ ,  $E_2$ ,  $E_3$  when  $\alpha_1 = 2$ ,  $t = 0.1$ ,  $x = 0.2$ ,  $\alpha_2 = 0.5$ ,  $Br = 0.3$ ,  $Bi_1 = 2$ ,  $T' = 0.2$ ,  $H = 0.3$  (e) Biot number  $Bi_1$  when  $E_1 = 0.5$ ,  $E_2 = 0.4$ ,  $E_3 = 0.3$ ,  $\epsilon = 0.2$ ,  $t = 0.1$ ,  $x = 0.2$ ,  $\alpha_2 = 0.5$ ,  $Br = 0.3$ ,  $H = 0.3$ ,  $T' = 0.2$ ,  $\alpha_1 = 2$  (f) Brinkman  $Br$  when  $E_1 = 0.5$ ,  $E_2 = 0.4$ ,  $E_3 = 0.3$ ,  $\epsilon = 0.2$ ,  $t = 0.1$ ,  $x = 0.2$ ,  $\alpha_2 = 0.5$ ,  $Bi_1 = 2$ ,  $H = 0.3$ ,  $T' = 0.2$ ,  $\alpha_1 = 2$  (g) Taylor number  $T'$  when  $E_1 = 0.5$ ,  $E_2 = 0.4$ ,  $E_3 = 0.3$ ,  $\epsilon = 0.2$ ,  $t = 0.1$ ,  $x = 0.2$ ,  $\alpha_2 = 0.5$ ,  $Br = 0.3$ ,  $Bi_1 = 2$ ,  $H = 0.3$ ,  $\alpha_1 = 2$ .

## 4.4 Conclusions

Important findings here are

- Axial and secondary velocities via rotation have opposite effects.
- Similar response of Prandtl fluid parameters on  $u$ ,  $v$ ,  $\theta$  and  $Z$  is seen.
- Both velocities are enhanced for flexible characteristics.
- Decay in  $u$ ,  $\theta$  and  $Z$  is observed for Hartman number.
- Brinkman and Biot numbers for temperature and heat transfer coefficient have opposite effects.

## Chapter 5

# MHD peristaltic flow of rotating Prandtl fluid with Soret and Dufour effects

### 5.1 Introduction

The purpose here is to examine Soret/Dufour effects in MHD peristaltic flows of rotating Prandtl liquid in a channel with flexible boundaries. Formulation for heat and mass transfer is arranged using convective conditions. Large wavelength and small Reynolds number are utilized. The numerical solution of resulting problems are obtained and analyzed in detail.

### 5.2 Problem development

We examine peristaltic flow of Prandtl liquid in a rotating system. Channel of width  $2d$  is considered. The channel and liquid rotate by constant angular velocity  $\boldsymbol{\Omega} = \Omega \hat{k}$  ( $\hat{k}$  is unit vector parallel to  $z$  - axis). Magnetic field of strength  $B_0$  is applied. The wall surface in mathematical form is

$$z = \pm \eta(x, t) = \pm \left[ d + a \sin \frac{2\pi}{\lambda}(x - ct) \right]. \quad (5.1)$$

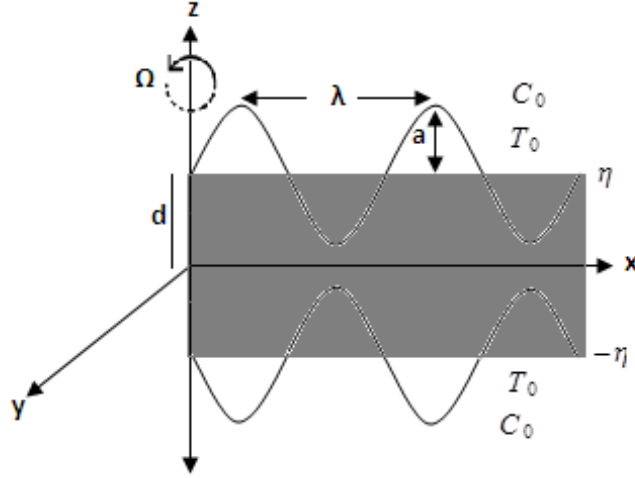


Fig. 5.1: Sketch of problem.

For Prandtl fluid, the Cauchy stress tensor  $\tau$  is represented by:

$$\tau = -p\mathbf{I} + \mathbf{S}, \quad (5.2)$$

$$\mathbf{S}_{ij} = \dot{A}_1 \left[ \frac{\sin^{-1} \left( \sum_{m=1}^3 \sum_{n=1}^3 \frac{\epsilon_{mn}\epsilon_{nm}}{2\dot{A}_2^2} \right)^{\frac{1}{2}}}{\left( \sum_{m=1}^3 \sum_{n=1}^3 \frac{\epsilon_{mn}\epsilon_{nm}}{2\dot{A}_2^2} \right)^{\frac{1}{2}}} \right] e_{ij}, \quad (5.3)$$

where

$$e_{ij} = \frac{1}{2} \left( \frac{\partial u}{\partial x_i} + \frac{\partial u}{\partial x_j} \right)$$

and  $(\dot{A}_1, \dot{A}_2)$  are material constants.

For present rotating flow, the governing equations are

$$\frac{\partial u}{\partial x} + \frac{\partial w}{\partial z} = 0, \quad (5.4)$$

$$\rho \frac{du}{dt} - 2\rho\Omega v = -\frac{\partial \tilde{p}}{\partial x} + \frac{\partial S_{xx}}{\partial x} + \frac{\partial S_{xy}}{\partial y} + \frac{\partial S_{xz}}{\partial z} - \sigma B_0^2 u, \quad (5.5)$$

$$\rho \frac{dv}{dt} + 2\rho\Omega u = -\frac{\partial \tilde{p}}{\partial y} + \frac{\partial S_{yx}}{\partial x} + \frac{\partial S_{yy}}{\partial y} + \frac{\partial S_{yz}}{\partial z} - \sigma B_0^2 v, \quad (5.6)$$

$$\rho \frac{dw}{dt} = -\frac{\partial \tilde{p}}{\partial z} + \frac{\partial S_{zx}}{\partial x} + \frac{\partial S_{zy}}{\partial y} + \frac{\partial S_{zz}}{\partial z}, \quad (5.7)$$

Energy and concentration equations are

$$\rho c_p \frac{dT}{dt} = k_T \nabla^2 T + \frac{Dk'}{C_s} \nabla^2 C + S_{xx} \frac{\partial u}{\partial x} + S_{xz} \left( \frac{\partial u}{\partial z} + \frac{\partial w}{\partial x} \right) + S_{zz} \frac{\partial w}{\partial z}, \quad (5.8)$$

$$\frac{dC}{dt} = D \nabla^2 C + \frac{Dk'}{T_m} \nabla^2 T \quad (5.9)$$

in which  $T_m$ ,  $D$ ,  $k'$ ,  $C_s$ , represent mean fluid temperature, mass diffusivity coefficient, thermal diffusion ratio and concentration susceptibility respectively. The conditions are

$$k_T \frac{\partial T}{\partial z} = -\dot{h}_1 (T - T_0) \quad \text{at } z = \eta, \quad (5.10)$$

$$k_T \frac{\partial T}{\partial z} = -\dot{h}_1 (T_0 - T) \quad \text{at } z = -\eta, \quad (5.11)$$

$$D \frac{\partial C}{\partial z} = -\dot{h}_2 (C - C_0) \quad \text{at } z = \eta, \quad (5.12)$$

$$D \frac{\partial C}{\partial z} = -\dot{h}_2 (C_0 - C) \quad \text{at } z = -\eta, \quad (5.13)$$

$$u = 0, \quad v = 0 \quad \text{at } z = \pm\eta, \quad (5.14)$$

$$\frac{\partial}{\partial x} G(\eta) = \frac{\partial p}{\partial x} = -\rho \frac{du}{dt} + \frac{\partial S_{xx}}{\partial x} + \frac{\partial S_{xy}}{\partial y} + \frac{\partial S_{xz}}{\partial z} - \sigma B_0^2 u + 2\rho\Omega v \quad \text{at } z = \pm\eta, \quad (5.15)$$

$$G = -\tau \frac{\partial^2}{\partial x^2} + m_1^* \frac{\partial^2}{\partial t^2} + d' \frac{\partial}{\partial t},$$

where  $(\dot{h}_1, \dot{h}_2)$  and  $T$  represent the coefficient of heat and mass transfer and fluid temperature.

Employing

$$\begin{aligned} x^* &= \frac{x}{\lambda}, \quad y^* = \frac{y}{\lambda}, \quad z^* = \frac{z}{d}, \quad t^* = \frac{ct}{\lambda}, \quad p^* = \frac{d^2 \tilde{p}}{\mu c \lambda}, \\ u^* &= \frac{u}{c}, \quad v^* = \frac{v}{c}, \quad w^* = \frac{w}{c}, \quad \eta^* = \frac{\eta}{d}, \quad \mathbf{S}^* = \frac{d\mathbf{S}}{\mu c}, \quad \theta = \frac{T - T_0}{T_0}, \\ \phi &= \frac{C - C_0}{C_0}, \quad k = \frac{R^*}{d}, \quad \delta = \frac{d}{\lambda}, \quad \text{Re} = \frac{cd}{\nu}. \end{aligned} \quad (5.16)$$

$$u = \psi_z, \quad w = -\delta \psi_x, \quad (5.17)$$

Eqs. (5.5) – (5.9) takes the given form after using long wavelength and low Reynolds number



considerations,

$$-2T'v = -\frac{\partial p}{\partial x} + \frac{\partial S_{xz}}{\partial z} - H^2\psi_z, \quad (5.18)$$

$$2T'\psi_z = -\frac{\partial p}{\partial y} + \frac{\partial S_{yz}}{\partial z} - H^2v, \quad (5.19)$$

$$\frac{\partial p}{\partial z} = 0, \quad (5.20)$$

$$\theta_{zz} + \text{Pr} Du\phi_{zz} + \text{Br}S_{xz}\psi_{zz} = 0, \quad (5.21)$$

$$\phi_{zz} + \text{Sc}Sr\phi_{zz} = 0. \quad (5.22)$$

Non-dimensional extra stress components through Eq. (5.3) are

$$S_{xz} = \alpha_1\psi_{zz} + \frac{\alpha_2}{6}\psi_{zz}^3, \quad (5.23)$$

$$S_{yz} = \alpha_1v_z + \frac{\alpha_2}{6}v_z^3, \quad (5.24)$$

with  $\alpha_1 = \frac{\dot{A}_1}{\mu\dot{A}_2}$  and  $\alpha_2 = \frac{\alpha_1 c^2}{\dot{A}_2^2 d^2}$  are Prandtl fluid parameters. The corresponding dimensionless conditions are

$$\eta = 1 + \epsilon \sin 2\pi(x - t), \quad (5.25)$$

$$\begin{aligned} \frac{\partial \theta}{\partial z} + Bi_1\theta &= 0 \text{ at } z = \eta, \\ \frac{\partial \theta}{\partial z} - Bi_1\theta &= 0 \text{ at } z = -\eta, \end{aligned} \quad (5.26)$$

$$\begin{aligned} \frac{\partial \phi}{\partial z} + Bi_2\phi &= 0 \text{ at } z = \eta, \\ \frac{\partial \phi}{\partial z} - Bi_2\phi &= 0 \text{ at } z = -\eta, \end{aligned} \quad (5.27)$$

$$\psi_z = 0, \quad v = 0 \text{ at } z = \pm\eta, \quad (5.28)$$

$$\left[ E_1 \frac{\partial^3}{\partial x^3} + E_2 \frac{\partial^3}{\partial x \partial t^2} + E_3 \frac{\partial^2}{\partial x \partial t} \right] \eta = \frac{\partial S_{xz}}{\partial z} - H^2\psi_z + 2T'v \text{ at } z = \pm\eta. \quad (5.29)$$

From equation (5.20)  $p \neq p(z)$ , equation (5.18) becomes

$$\frac{\partial}{\partial z} \left[ \frac{\partial S_{xz}}{\partial z} - H^2\psi_z + 2T'v \right] = 0 \quad (5.30)$$

and equation (5.19) gives

$$\frac{\partial S_{yz}}{\partial z} - H^2 v - 2T' \psi_z = 0. \quad (5.31)$$

Here we neglect the pressure term due to secondary flow which is caused by rotation.

### 5.3 Solution methodology

We solve equations (5.21), (5.22), (5.30) and (5.31) numerically in Mathematica using built in command ND-Solve. Physical quantities of interest with respect to emerging parameters are discussed.

### 5.4 Discussion

#### 5.4.1 Axial velocity

First of all axial velocity  $u(z)$  is displayed in Figs. 5.2 – 5.6. Impact of  $\alpha_1$  and  $\alpha_2$  on velocity is presented in Figs. 5.2 and 5.3. The obtained results show the decreasing behavior of velocity via larger parameters. Fig. 5.4 is portrayed to observe the behavior of Hartman number  $H$  on  $u$ . It is evident that velocity decreases by increasing  $H$ . As expected the magnetic field resists the flow. For increasing Taylor number  $T'$ , the axial velocity decays as shown in Fig. 5.5. In fact secondary flow due to rotation decayed the velocity. In absence of rotation, we observed that velocity is maximum. In Fig. 5.6 variation in velocity is depicted for wall parameters. For increment in elastic parameters  $E_1$  and  $E_2$ ,  $u$  increases while for enhancement in damping parameter  $E_3$ ,  $u$  decays.

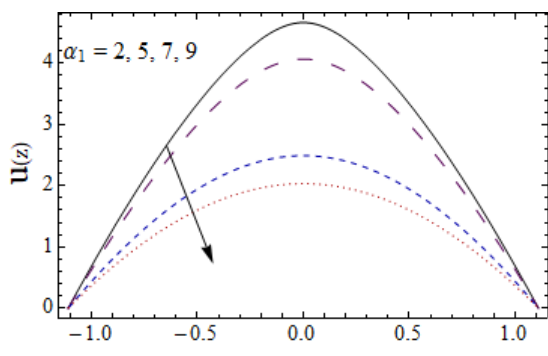


Fig. 5.2

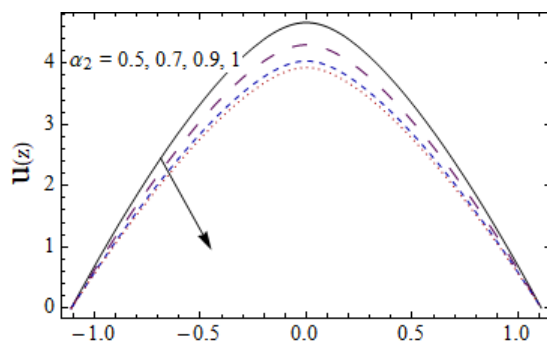


Fig. 5.3

Fig. 5.2: Sketch of  $u$  versus  $\alpha_1$  when  $x = 0.2$ ,  $\epsilon = 0.2$ ,  $t = 0.1$ ,  $E_1 = 0.3$ ,  $E_2 = 0.1$ ,  $E_3 = 0.1$ ,  
 $H = 0.3$ ,  $T' = 0.2$ ,  $\alpha_2 = 0.5$ ,  $Bi_1 = 2$ ,  $Bi_2 = 5$ ,  $Pr = 0.2$ ,  $Sr = 0.4$ ,  $Du = 0.4$ ,  $Sc = 0.3$ ,  
 $Br = 0.2$ .

Fig. 5.3: Sketch of  $u$  versus  $\alpha_2$  when  $x = 0.2$ ,  $\epsilon = 0.2$ ,  $t = 0.1$ ,  $E_1 = 0.3$ ,  $E_2 = 0.1$ ,  $E_3 = 0.1$ ,  
 $H = 0.3$ ,  $T' = 0.2$ ,  $\alpha_1 = 2$ ,  $Bi_1 = 2$ ,  $Bi_2 = 5$ ,  $Pr = 0.2$ ,  $Sr = 0.4$ ,  $Du = 0.4$ ,  $Sc = 0.3$ ,  
 $Br = 0.2$ .

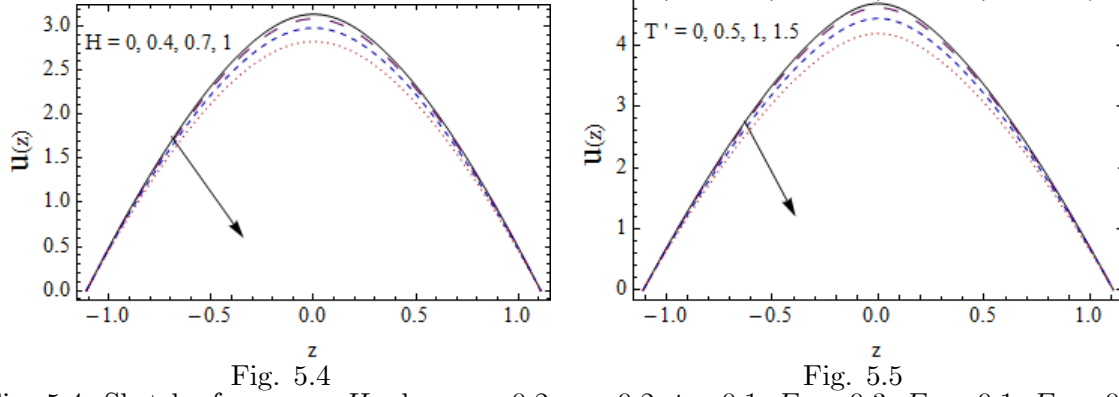


Fig. 5.4: Sketch of  $u$  versus  $H$  when  $x = 0.2$ ,  $\epsilon = 0.2$ ,  $t = 0.1$ ,  $E_1 = 0.3$ ,  $E_2 = 0.1$ ,  $E_3 = 0.1$ ,  
 $\alpha_2 = 0.5$ ,  $T' = 0.2$ ,  $\alpha_1 = 2$ ,  $Bi_1 = 2$ ,  $Bi_2 = 5$ ,  $Pr = 0.2$ ,  $Sr = 0.4$ ,  $Du = 0.4$ ,  $Sc = 0.3$ ,  
 $Br = 0.2$ .

Fig. 5.5: Sketch of  $u$  versus  $T'$  when  $x = 0.2$ ,  $\epsilon = 0.2$ ,  $t = 0.1$ ,  $E_1 = 0.3$ ,  $E_2 = 0.1$ ,  $E_3 = 0.1$ ,  
 $H = 0.3$ ,  $\alpha_2 = 0.5$ ,  $\alpha_1 = 2$ ,  $Bi_1 = 2$ ,  $Bi_2 = 5$ ,  $Pr = 0.2$ ,  $Sr = 0.4$ ,  $Du = 0.4$ ,  $Sc = 0.3$ ,  
 $Br = 0.2$ .

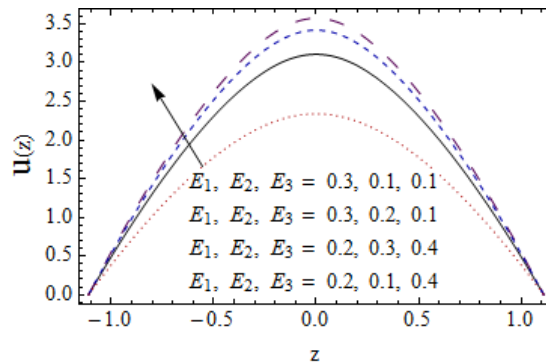


Fig. 5.6

Fig. 5.6: Sketch of  $u$  versus  $E_1$ ,  $E_2$ ,  $E_3$  when  $x = 0.2$ ,  $\epsilon = 0.2$ ,  $t = 0.1$ ,  $\alpha_1 = 2$ ,  $H = 0.3$ ,

$$T' = 0.2, \alpha_2 = 0.5, Bi_1 = 2, Bi_2 = 5, Pr = 0.2, Sr = 0.4, Du = 0.4, Sc = 0.3, Br = 0.2.$$

### 5.4.2 Secondary velocity

Influence of emerging physical parameters on secondary velocity  $v$  are sketched in Figs. 5.7 – 5.11. For increasing  $\alpha_1$  and  $\alpha_2$ , axial velocity shows decreasing behavior (see Figs. 5.7 and 5.8). Secondary velocity decreases for increasing Hartman number  $H$  as depicted in Fig. 5.9. In Fig. 5.10 the effect of Taylor number  $T'$  on  $v$  is depicted. Increasing rotation enhances secondary velocity. Also we observe that there is no secondary velocity when  $T' = 0$ . From Fig. 5.11 we see that  $v$  is increased by  $E_i (i = 1, 2)$  and reverse effect is noticed for  $E_3$ .

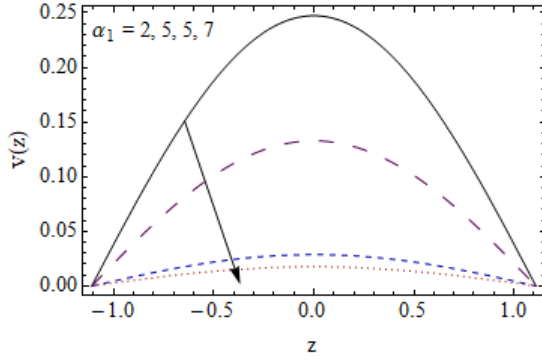


Fig. 5.7

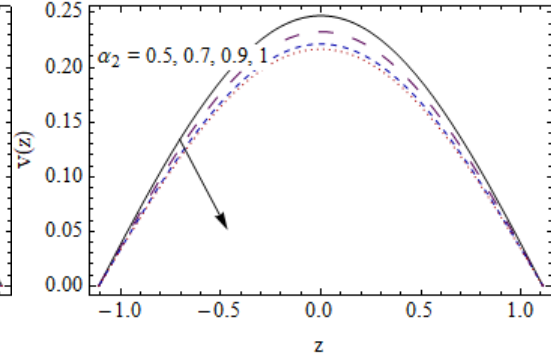


Fig. 5.8

Fig. 5.7: Secondary velocity  $v$  for Prandtl fluid parameter  $\alpha_1$  when  $x = -0.2, \epsilon = 0.2, t = 0.1, E_1 = 0.5, E_2 = 0.3, E_3 = 0.1, H = 0.3, T' = 0.2, \alpha_2 = 0.5, Bi_1 = 2, Bi_2 = 5, Pr = 0.2, Sr = 0.4, Du = 0.4, Sc = 0.3, Br = 0.2$ .

Fig. 5.8: Secondary velocity  $v$  for Prandtl fluid parameter  $\alpha_2$  when  $x = -0.2, \epsilon = 0.2, t = 0.1, E_1 = 0.5, E_2 = 0.3, E_3 = 0.1, H = 0.3, T' = 0.2, \alpha_1 = 2, Bi_1 = 2, Bi_2 = 5, Pr = 0.2, Sr = 0.4, Du = 0.4, Sc = 0.3, Br = 0.2$ .

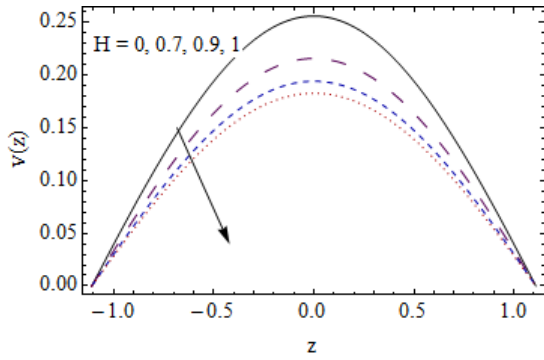


Fig. 5.9

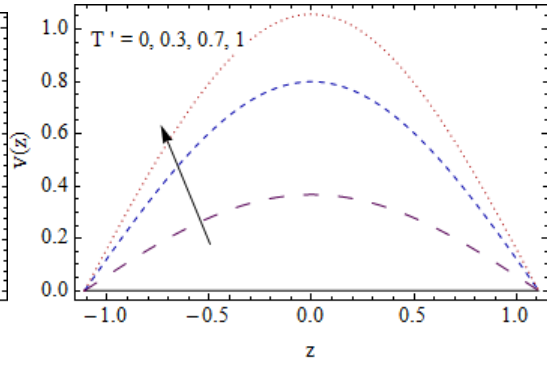


Fig. 5.10

Fig. 5.9: Secondary velocity  $v$  for Hartman number  $H$  when  $x = -0.2$ ,  $\epsilon = 0.2$ ,  $t = 0.1$ ,  $E_1 = 0.5$ ,  $E_2 = 0.3$ ,  $E_3 = 0.1$ ,  $\alpha_2 = 0.5$ ,  $T' = 0.2$ ,  $\alpha_1 = 2$ ,  $Bi_1 = 2$ ,  $Bi_2 = 5$ ,  $Pr = 0.2$ ,  $Sr = 0.4$ ,  $Du = 0.4$ ,  $Sc = 0.3$ ,  $Br = 0.2$ .

Fig. 5.10: Secondary velocity  $v$  for Taylor number  $T'$  when  $x = -0.2$ ,  $\epsilon = 0.2$ ,  $t = 0.1$ ,  $E_1 = 0.5$ ,  $E_2 = 0.3$ ,  $E_3 = 0.1$ ,  $H = 0.3$ ,  $\alpha_2 = 0.5$ ,  $\alpha_1 = 2$ ,  $Bi_1 = 2$ ,  $Bi_2 = 5$ ,  $Pr = 0.2$ ,  $Sr = 0.4$ ,  $Du = 0.4$ ,  $Sc = 0.3$ ,  $Br = 0.2$ .

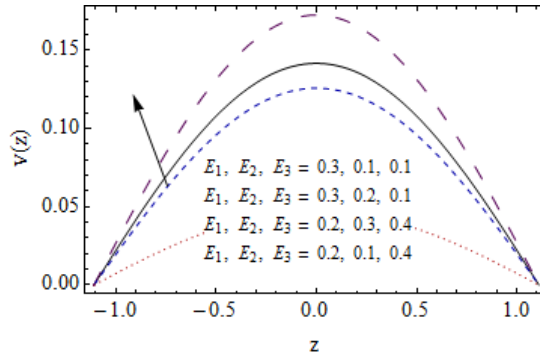


Fig. 5.11

Fig. 5.11: Secondary velocity  $v$  for walls parameter  $E_1$ ,  $E_2$ ,  $E_3$  when  $x = -0.2$ ,  $\epsilon = 0.2$ ,  $t = 0.1$ ,  $\alpha_1 = 2$ ,  $H = 0.3$ ,  $T' = 0.2$ ,  $\alpha_2 = 0.5$ ,  $Bi_1 = 2$ ,  $Bi_2 = 5$ ,  $Pr = 0.2$ ,  $Sr = 0.4$ ,  $Du = 0.4$ ,  $Sc = 0.3$ ,  $Br = 0.2$ .

### 5.4.3 Temperature

The temperature  $\theta$  with  $z$  for  $\alpha_1$ ,  $\alpha_2$ ,  $Bi_1$ ,  $Bi_2$ ,  $T'$ ,  $Sr$ ,  $Du$ ,  $Br$ ,  $Sc$  and  $Pr$  are plotted in Figs. 5.12– 5.22. As we increase fluid parameters  $\alpha_1$  and  $\alpha_2$ ,  $\theta$  decays (see Figs. 5.12 and 5.13). The effects of  $Bi_1$  and  $Bi_2$  on temperature are shown in Figs. 5.14 and 5.15. For increasing heat transfer Biot number  $Bi_1$ , temperature decays. In fact thermal conductivity of fluid is reduced. No variation in  $\theta$  is seen for increasing mass transfer Biot number  $Bi_2$ . Due to fluid resistance, temperature falls for larger  $H$  (see Fig. 5.16). In Fig. 5.17 temperature decreases for increasing  $T'$ . In Figs. 5.18 and 5.19 temperature rises by increasing Soret  $Sr$  and Dufour  $Du$  numbers. It is due to increase in thermal diffusion. Impact of Brinkman number  $Br$  on  $\theta$  is portrayed in Fig. 5.20. Temperature increases due to less heat conduction produced by viscous dissipation. Temperature is increasing function of  $Sc$  and  $Pr$  as exhibited in Figs. 5.21 and 5.22. It is because of the fact that for larger  $Sc$ , mass diffusivity decays and hence  $\theta$  enhances. Specific heat of fluid enhances when we increase  $Pr$  which results in rise of temperature.

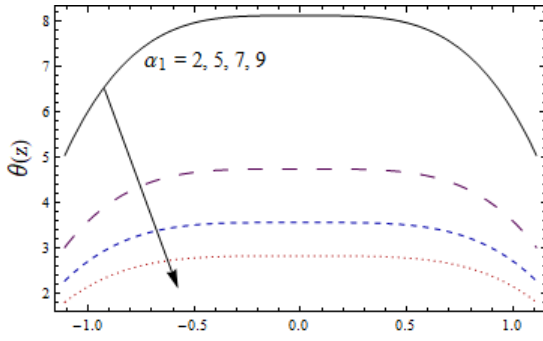


Fig. 5.12

Fig. 5.12: Temperature  $\theta$  for Prandtl fluid parameter  $\alpha_1$  when  $x = 0.2$ ,  $\epsilon = 0.2$ ,  $t = 0.1$ ,  $E_1 = 0.3$ ,  $E_2 = 0.1$ ,  $E_3 = 0.1$ ,  $H = 0.3$ ,  $T' = 0.2$ ,  $\alpha_2 = 0.5$ ,  $Bi_1 = 2$ ,  $Bi_2 = 5$ ,  $Pr = 0.2$ ,  $Sr = 0.4$ ,  $Du = 0.4$ ,  $Sc = 0.3$ ,  $Br = 0.2$ .

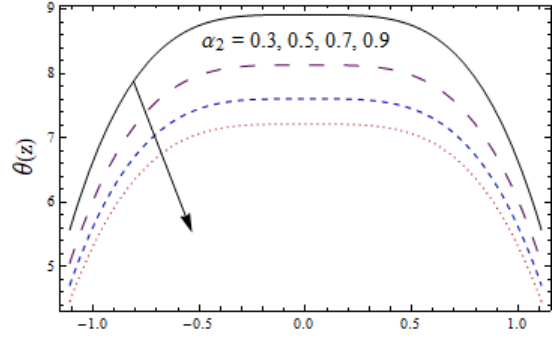


Fig. 5.13

Fig. 5.13: Temperature  $\theta$  for Prandtl fluid parameter  $\alpha_2$  when  $x = 0.2$ ,  $\epsilon = 0.2$ ,  $t = 0.1$ ,  $E_1 = 0.3$ ,  $E_2 = 0.1$ ,  $E_3 = 0.1$ ,  $H = 0.3$ ,  $T' = 0.2$ ,  $\alpha_1 = 2$ ,  $Bi_1 = 2$ ,  $Bi_2 = 5$ ,  $Pr = 0.2$ ,  $Sr = 0.4$ ,  $Du = 0.4$ ,  $Sc = 0.3$ ,  $Br = 0.2$ .

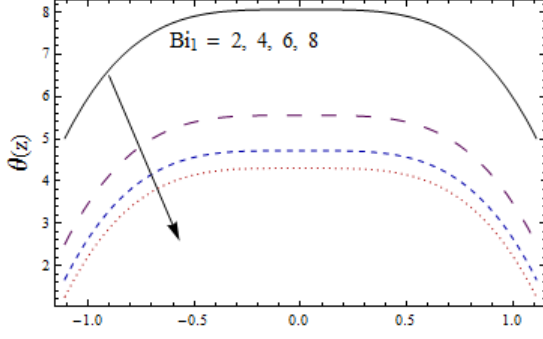


Fig. 5.14

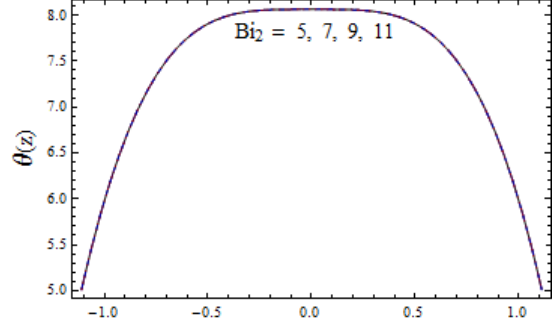


Fig. 5.15

Fig. 5.14: Temperature  $\theta$  for heat Biot number  $Bi_1$  when  $x = 0.2$ ,  $\epsilon = 0.2$ ,  $t = 0.1$ ,  $E_1 = 0.3$ ,  $E_2 = 0.1$ ,  $E_3 = 0.1$ ,  $H = 0.3$ ,  $T' = 0.2$ ,  $\alpha_2 = 0.5$ ,  $\alpha_1 = 2$ ,  $Bi_2 = 5$ ,  $Pr = 0.2$ ,  $Sr = 0.4$ ,  $Du = 0.4$ ,  $Sc = 0.3$ ,  $Br = 0.2$ .

Fig. 5.15: Temperature  $\theta$  for mass Biot number  $Bi_2$  when  $x = 0.2$ ,  $\epsilon = 0.2$ ,  $t = 0.1$ ,  $E_1 = 0.3$ ,  $E_2 = 0.1$ ,  $E_3 = 0.1$ ,  $H = 0.3$ ,  $T' = 0.2$ ,  $\alpha_1 = 2$ ,  $Bi_1 = 2$ ,  $\alpha_2 = 0.5$ ,  $Pr = 0.2$ ,  $Sr = 0.4$ ,  $Du = 0.4$ ,  $Sc = 0.3$ ,  $Br = 0.2$ .

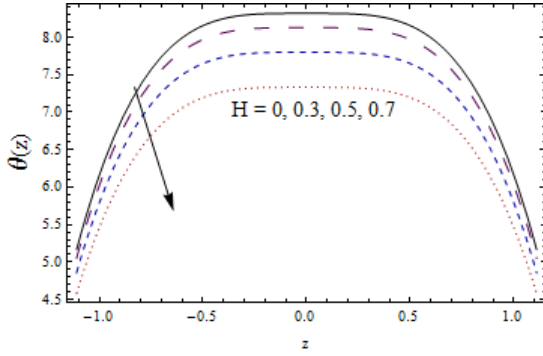


Fig. 5.16

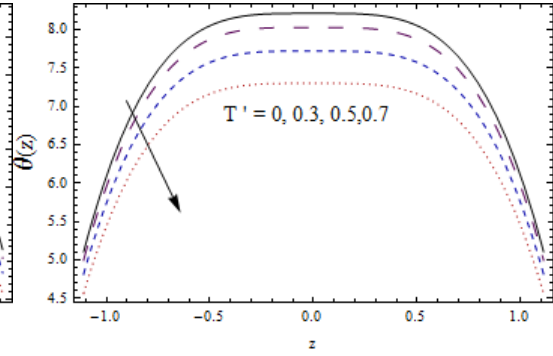


Fig. 5.17

Fig. 5.16: Temperature  $\theta$  for Hartman number  $H$  when  $x = 0.2$ ,  $\epsilon = 0.2$ ,  $t = 0.1$ ,  $E_1 = 0.3$ ,  $E_2 = 0.1$ ,  $E_3 = 0.1$ ,  $\alpha_2 = 0.5$ ,  $T' = 0.2$ ,  $\alpha_1 = 2$ ,  $Bi_1 = 2$ ,  $Bi_2 = 5$ ,  $Pr = 0.2$ ,  $Sr = 0.4$ ,  $Du = 0.4$ ,  $Sc = 0.3$ ,  $Br = 0.2$ .

Fig. 5.17: Temperature  $\theta$  for Taylor number  $T'$  when  $x = 0.2$ ,  $\epsilon = 0.2$ ,  $t = 0.1$ ,  $E_1 = 0.3$ ,  $E_2 = 0.1$ ,  $E_3 = 0.1$ ,  $H = 0.3$ ,  $\alpha_2 = 0.5$ ,  $\alpha_1 = 2$ ,  $Bi_1 = 2$ ,  $Bi_2 = 5$ ,  $Pr = 0.2$ ,  $Sr = 0.4$ ,  $Du = 0.4$ ,  $Sc = 0.3$ ,  $Br = 0.2$ .

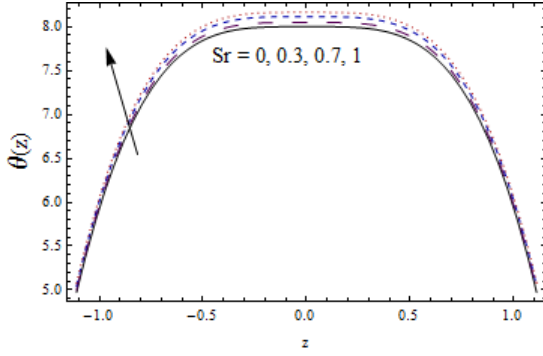


Fig. 5.18

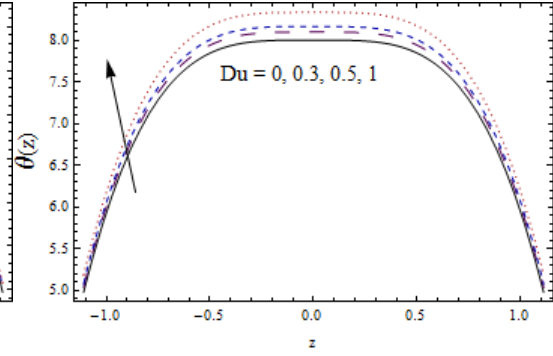


Fig. 5.19

Fig. 5.18: Temperature  $\theta$  for Soret number  $Sr$  when  $x = 0.2$ ,  $\epsilon = 0.2$ ,  $t = 0.1$ ,  $E_1 = 0.3$ ,  $E_2 = 0.1$ ,  $E_3 = 0.1$ ,  $\alpha_2 = 0.5$ ,  $T' = 0.2$ ,  $\alpha_1 = 2$ ,  $Bi_1 = 2$ ,  $Bi_2 = 5$ ,  $Pr = 0.2$ ,  $H = 0.3$ ,  $Du = 0.4$ ,  $Sc = 0.3$ ,  $Br = 0.2$ .

Fig. 5.19: Temperature  $\theta$  for Dufour number  $Dr$  when  $x = 0.2$ ,  $\epsilon = 0.2$ ,  $t = 0.1$ ,  $E_1 = 0.3$ ,  $E_2 = 0.1$ ,  $E_3 = 0.1$ ,  $H = 0.3$ ,  $\alpha_2 = 0.5$ ,  $\alpha_1 = 2$ ,  $Bi_1 = 2$ ,  $Bi_2 = 5$ ,  $Pr = 0.2$ ,  $Sr = 0.4$ ,  $T' = 0.2$ ,  $Sc = 0.3$ ,  $Br = 0.2$ .

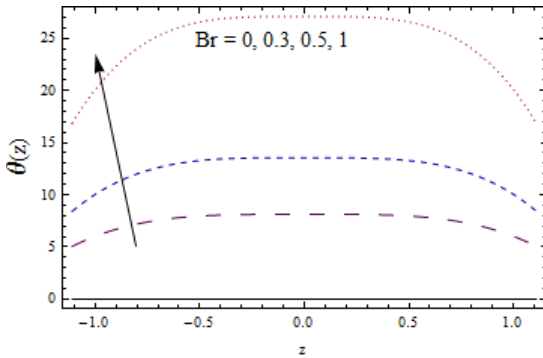


Fig. 5.20

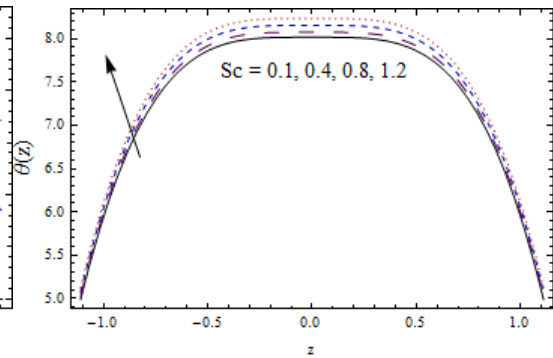


Fig. 5.21

Fig. 5.20: Temperature  $\theta$  for Brinkman number  $Br$  when  $x = 0.2$ ,  $\epsilon = 0.2$ ,  $t = 0.1$ ,  $E_1 = 0.3$ ,  $E_2 = 0.1$ ,  $E_3 = 0.1$ ,  $\alpha_2 = 0.5$ ,  $T' = 0.2$ ,  $\alpha_1 = 2$ ,  $Bi_1 = 2$ ,  $Bi_2 = 5$ ,  $Pr = 0.2$ ,  $H = 0.3$ ,  $Du = 0.4$ ,  $Sc = 0.3$ ,  $Sr = 0.4$ .

Fig. 5.21: Temperature  $\theta$  for Schmidt number  $Sc$  when  $x = 0.2$ ,  $\epsilon = 0.2$ ,  $t = 0.1$ ,  $E_1 = 0.3$ ,  $E_2 = 0.1$ ,  $E_3 = 0.1$ ,  $H = 0.3$ ,  $\alpha_2 = 0.5$ ,  $\alpha_1 = 2$ ,  $Bi_1 = 2$ ,  $Bi_2 = 5$ ,  $Pr = 0.2$ ,  $Sr = 0.4$ ,



$$T' = 0.2, Du = 0.4, Br = 0.2.$$

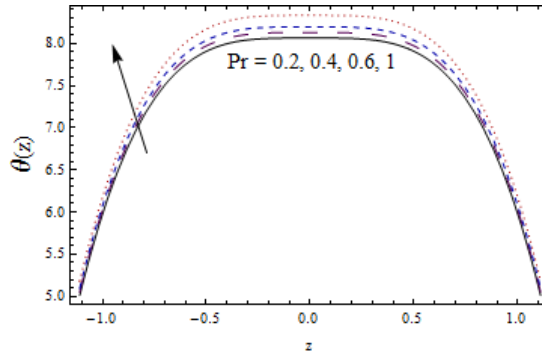


Fig. 5.22

Fig. 5.22: Temperature  $\theta$  for Prandtl number  $Pr$  when  $x = 0.2$ ,  $\epsilon = 0.2$ ,  $t = 0.1$ ,  $E_1 = 0.3$ ,  $E_2 = 0.1$ ,  $E_3 = 0.1$ ,  $H = 0.3$ ,  $\alpha_2 = 0.5$ ,  $\alpha_1 = 2$ ,  $Bi_1 = 2$ ,  $Bi_2 = 5$ ,  $Sc = 0.3$ ,  $Sr = 0.4$ ,  $T' = 0.2$ ,  $Du = 0.4$ ,  $Br = 0.2$ .

#### 5.4.4 Concentration

This section provides the behavior of involved parameters in the expressions of concentration  $\phi$ . For increasing fluid parameters  $\alpha_1$  and  $\alpha_2$ , decreasing effect in  $\phi$  is noticed (see Figs. 5.23 and 5.24). Fig. 5.25 shows no variation for  $Bi_1$  on  $\phi$ . On other hand in Fig. 5.26 the role of  $Bi_2$  on the concentration field  $\phi$  is increasing rapidly due to decrease in mass diffusivity. Similar pattern is observed on  $\phi$  for Soret  $Sr$  and Dufour  $Du$  numbers on  $\phi$  in Figs. 5.27 and 5.28. Concentration is decreased by  $Sr$  and  $Du$ .

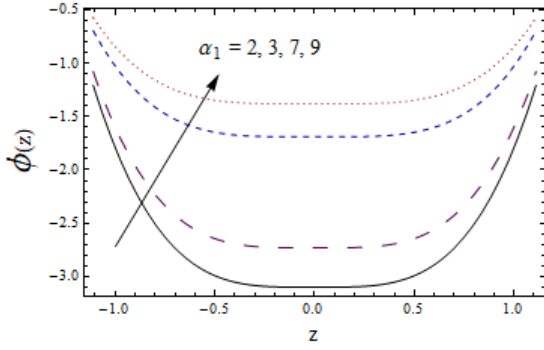


Fig. 5.23

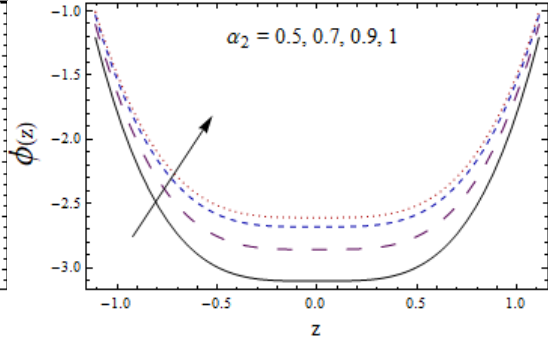


Fig. 5.24

Fig. 5.23: Concentration  $\phi$  for Prandtl fluid parameter  $\alpha_1$  when  $x = 0.2$ ,  $\epsilon = 0.2$ ,  $t = 0.1$ ,  $E_1 = 0.3$ ,  $E_2 = 0.1$ ,  $E_3 = 0.1$ ,  $H = 0.3$ ,  $T' = 0.2$ ,  $\alpha_2 = 0.5$ ,  $Bi_1 = 2$ ,  $Bi_2 = 5$ ,  $Pr = 0.2$ ,  $Sr = 0.4$ ,  $Du = 0.4$ ,  $Sc = 0.3$ ,  $Br = 0.2$ .

Fig. 5.24: Concentration  $\phi$  for Prandtl fluid parameter  $\alpha_2$  when  $x = 0.2$ ,  $\epsilon = 0.2$ ,  $t = 0.1$ ,  $E_1 = 0.3$ ,  $E_2 = 0.1$ ,  $E_3 = 0.1$ ,  $H = 0.3$ ,  $T' = 0.2$ ,  $\alpha_1 = 2$ ,  $Bi_1 = 2$ ,  $Bi_2 = 5$ ,  $Pr = 0.2$ ,  $Sr = 0.4$ ,  $Du = 0.4$ ,  $Sc = 0.3$ ,  $Br = 0.2$

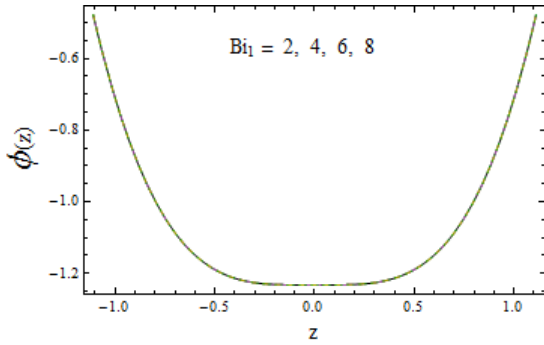


Fig. 5.25

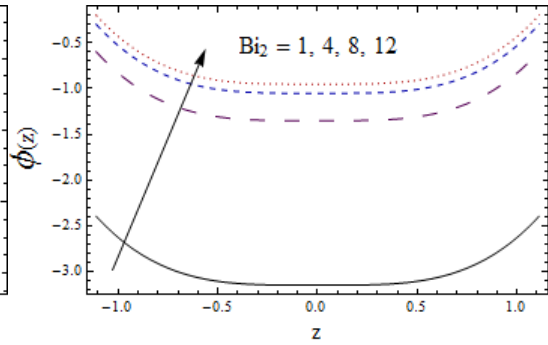


Fig. 5.26

Fig. 5.25: Concentration  $\phi$  for heat Biot number  $Bi_1$  when  $x = 0.2$ ,  $\epsilon = 0.2$ ,  $t = 0.1$ ,  $E_1 = 0.3$ ,  $E_2 = 0.1$ ,  $E_3 = 0.1$ ,  $H = 0.3$ ,  $T' = 0.2$ ,  $\alpha_2 = 0.5$ ,  $\alpha_1 = 2$ ,  $Bi_2 = 5$ ,  $Pr = 0.2$ ,  $Sr = 0.4$ ,  $Du = 0.4$ ,  $Sc = 0.3$ ,  $Br = 0.2$ .

Fig. 5.26: Concentration  $\phi$  for mass Biot number  $Bi_{12}$  when  $x = 0.2$ ,  $\epsilon = 0.2$ ,  $t = 0.1$ ,  $E_1 = 0.3$ ,  $E_2 = 0.1$ ,  $E_3 = 0.1$ ,  $H = 0.3$ ,  $T' = 0.2$ ,  $\alpha_1 = 2$ ,  $Bi_1 = 2$ ,  $\alpha_2 = 0.5$ ,  $Pr = 0.2$ ,

$$Sr = 0.4, Du = 0.4, Sc = 0.3, Br = 0.2.$$

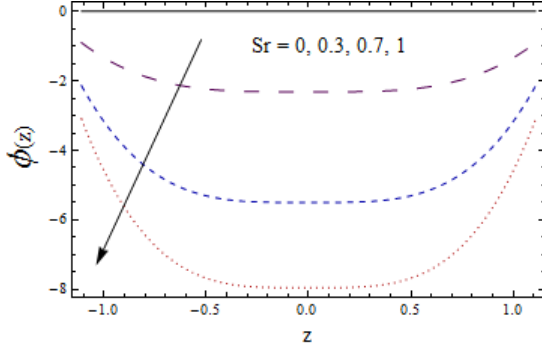


Fig. 5.27

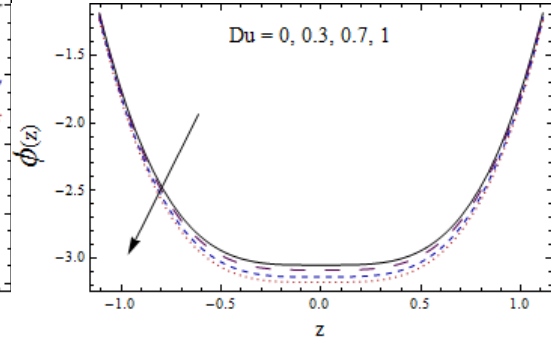


Fig. 5.28

Fig. 5.27: Concentration  $\phi$  for Soret number  $Sr$  when  $x = 0.2$ ,  $\epsilon = 0.2$ ,  $t = 0.1$ ,  $E_1 = 0.3$ ,  $E_2 = 0.1$ ,  $E_3 = 0.1$ ,  $\alpha_2 = 0.5$ ,  $T' = 0.2$ ,  $\alpha_1 = 2$ ,  $Bi_1 = 2$ ,  $Bi_2 = 5$ ,  $Pr = 0.2$ ,  $H = 0.3$ ,  $Du = 0.4$ ,  $Sc = 0.3$ ,  $Br = 0.2$ .

Fig. 5.28: Concentration  $\phi$  for Dufour number  $Dr$  when  $x = 0.2$ ,  $\epsilon = 0.2$ ,  $t = 0.1$ ,  $E_1 = 0.3$ ,  $E_2 = 0.1$ ,  $E_3 = 0.1$ ,  $H = 0.3$ ,  $\alpha_2 = 0.5$ ,  $\alpha_1 = 2$ ,  $Bi_1 = 2$ ,  $Bi_2 = 5$ ,  $Pr = 0.2$ ,  $Sr = 0.4$ ,  $T' = 0.2$ ,  $Sc = 0.3$ ,  $Br = 0.2$ .

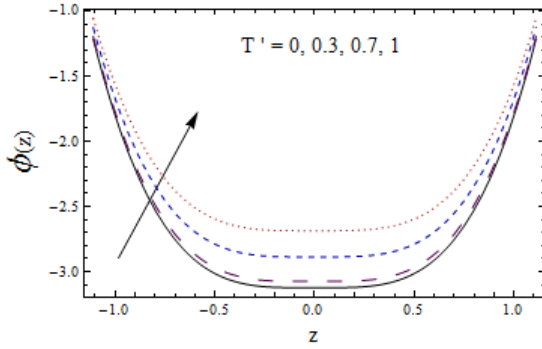


Fig. 5.29

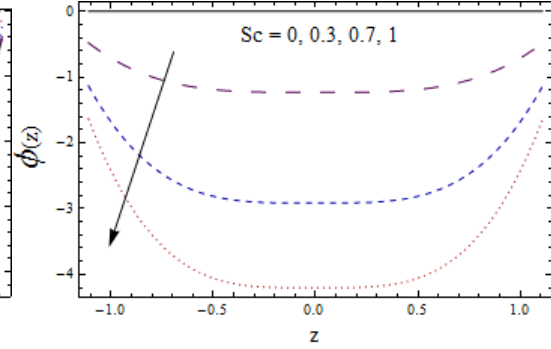


Fig. 5.30

Fig. 5.29: Concentration  $\phi$  for Taylor number  $T'$  when  $x = 0.2$ ,  $\epsilon = 0.2$ ,  $t = 0.1$ ,  $E_1 = 0.3$ ,  $E_2 = 0.1$ ,  $E_3 = 0.1$ ,  $E_3 = 0.1$ ,  $H = 0.3$ ,  $\alpha_2 = 0.5$ ,  $\alpha_1 = 2$ ,  $Bi_1 = 2$ ,  $Bi_2 = 5$ ,  $Pr = 0.2$ ,  $Sr = 0.4$ ,  $Du = 0.4$ ,  $Sc = 0.3$ ,  $Br = 0.2$ .

Fig. 5.30: Concentration  $\phi$  for Schmidt number  $Sc$  when  $x = 0.2$ ,  $\epsilon = 0.2$ ,  $t = 0.1$ ,  $E_1 = 0.3$ ,

$$E_2 = 0.1, E_3 = 0.1, H = 0.3, \alpha_2 = 0.5, \alpha_1 = 2, Bi_1 = 2, Bi_2 = 5, Pr = 0.2, Sr = 0.4,$$

$$T' = 0.2, Du = 0.4, Br = 0.2.$$

### 5.4.5 Heat transfer coefficient

In Figs. 5.31 – 5.36, the heat transfer coefficient  $Z$  is plotted for parameters  $\alpha_1$ ,  $\alpha_2$ ,  $H$ ,  $T'$ ,  $Sr$  and  $Du$ . Heat transfer coefficient has oscillatory character. It is expected in view of waves propagation along channel boundaries.  $Z$  shows a decreasing behavior for increasing  $\alpha_1$  and  $\alpha_2$  (see Figs. 5.31 and 5.32). The oscillatory nature is captured in Figs. 5.33 and 5.34 for Hartman  $H$  and Taylor  $T'$  numbers. Here  $Z$  decays for larger  $H$  due to strong magnetic strength whereas it increases for larger  $T'$ . In Figs. 5.35 and 5.36,  $Z$  increases for  $Sr$  and  $Du$  near the centerline whereas it decays near boundaries.

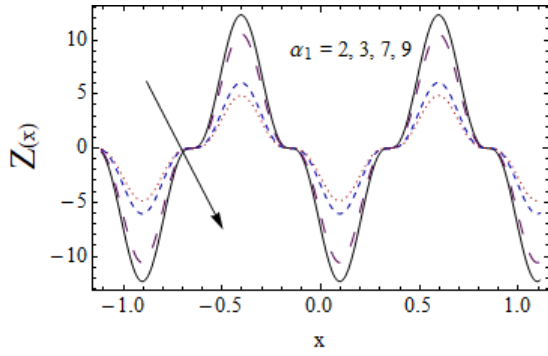


Fig. 5.31

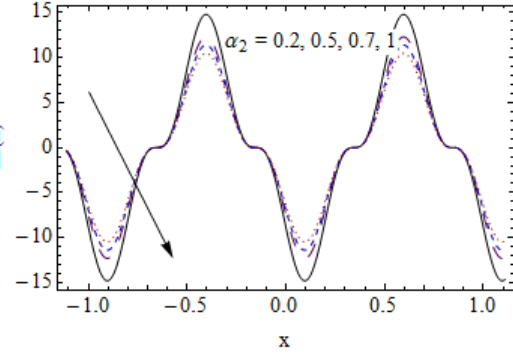


Fig. 5.32

Fig. 5.31: Heat transfer coefficient  $Z$  for  $\alpha_1$  when  $x = 0.2$ ,  $\epsilon = 0.2$ ,  $t = 0.1$ ,  $E_1 = 0.3$ ,  $E_2 = 0.1$ ,  $E_3 = 0.1$ ,  $H = 0.3$ ,  $T' = 0.2$ ,  $\alpha_2 = 0.5$ ,  $Bi_1 = 2$ ,  $Bi_2 = 5$ ,  $Pr = 0.2$ ,  $Sr = 0.4$ ,  $Du = 0.4$ ,  $Sc = 0.3$ ,  $Br = 0.2$ .

Fig. 5.32: Heat transfer coefficient  $Z$  for  $\alpha_2$  when  $x = 0.2$ ,  $\epsilon = 0.2$ ,  $t = 0.1$ ,  $E_1 = 0.3$ ,  $E_2 = 0.1$ ,  $E_3 = 0.1$ ,  $H = 0.3$ ,  $T' = 0.2$ ,  $\alpha_1 = 2$ ,  $Bi_1 = 2$ ,  $Bi_2 = 5$ ,  $Pr = 0.2$ ,  $Sr = 0.4$ ,  $Du = 0.4$ ,  $Sc = 0.3$ ,  $Br = 0.2$

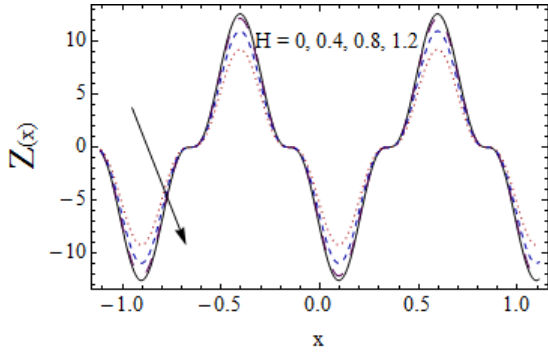


Fig. 5.33

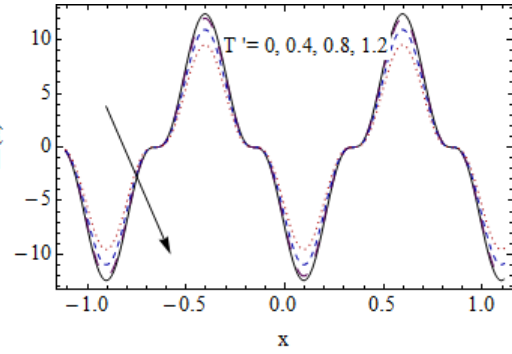


Fig. 5.34

Fig. 5.33: Heat transfer coefficient  $Z$  for  $H$  when  $x = 0.2$ ,  $\epsilon = 0.2$ ,  $t = 0.1$ ,  $E_1 = 0.3$ ,  $E_2 = 0.1$ ,  $E_3 = 0.1$ ,  $\alpha_2 = 0.5$ ,  $T' = 0.2$ ,  $\alpha_1 = 2$ ,  $Bi_1 = 2$ ,  $Bi_2 = 5$ ,  $Pr = 0.2$ ,  $Sr = 0.4$ ,  $Du = 0.4$ ,  $Sc = 0.3$ ,  $Br = 0.2$ .

Fig. 5.34: Heat transfer coefficient  $Z$  for  $T'$  when  $x = 0.2$ ,  $\epsilon = 0.2$ ,  $t = 0.1$ ,  $E_1 = 0.3$ ,  $E_2 = 0.1$ ,  $E_3 = 0.1$ ,  $H = 0.3$ ,  $\alpha_2 = 0.5$ ,  $\alpha_1 = 2$ ,  $Bi_1 = 2$ ,  $Bi_2 = 5$ ,  $Pr = 0.2$ ,  $Sr = 0.4$ ,  $Du = 0.4$ ,  $Sc = 0.3$ ,  $Br = 0.2$ .

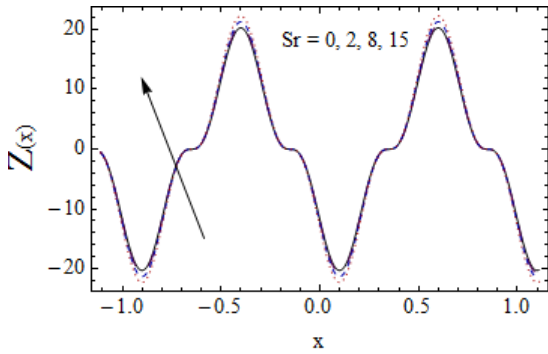


Fig. 5.35

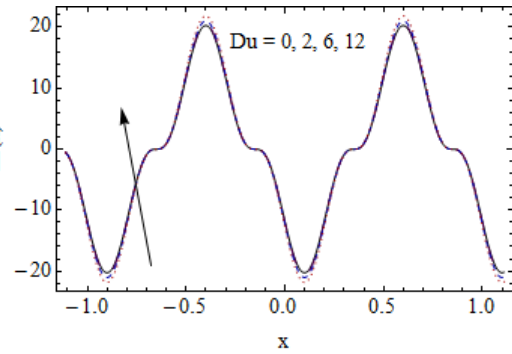


Fig. 5.36

Fig. 5.35: Heat transfer coefficient  $Z$  for  $Sr$  when  $x = 0.2$ ,  $\epsilon = 0.2$ ,  $t = 0.1$ ,  $E_1 = 0.5$ ,  $E_2 = 0.01$ ,  $E_3 = 0.01$ ,  $\alpha_2 = 0.5$ ,  $T' = 0.2$ ,  $\alpha_1 = 2$ ,  $Bi_1 = 2$ ,  $Bi_{12} = 5$ ,  $Pr = 0.2$ ,  $H = 0.3$ ,  $Du = 0.4$ ,  $Sc = 0.3$ ,  $Br = 0.2$ .

Fig. 5.36: Heat transfer coefficient  $Z$  for  $Dr$  when  $x = 0.2$ ,  $\epsilon = 0.2$ ,  $t = 0.1$ ,  $E_1 = 0.5$ ,  $E_2 = 0.01$ ,  $E_3 = 0.01$ ,  $H = 0.3$ ,  $\alpha_2 = 0.5$ ,  $\alpha_1 = 2$ ,  $Bi_1 = 2$ ,  $Bi_{12} = 5$ ,  $Pr = 0.2$ ,  $Sr = 0.4$ ,

$$T' = 0.2, Sc = 0.3, Br = 0.2.$$

## 5.5 Conclusions

Influences of Soret and Dufour on peristaltic flow in a rotating channel subject to compliant walls are discussed. Main observations are

- Decreasing behavior of  $\alpha_1$ ,  $\alpha_2$  on  $(u, v)$ ,  $\theta$  and  $Z$  is noticed while for  $\phi$  increasing effect is observed.
- Velocity, temperature and heat transfer coefficient are decreasing functions of Hartman number. However Hartman number leads to an enhancement of concentration.
- Both velocities shows opposite behavior for rotation parameter.
- Impact of wall parameters on both velocities are identical.
- For increasing Taylor parameter  $T'$  the temperature decreases .
- Temperature increases for  $Sr$ ,  $Du$ ,  $Br$ ,  $Sc$  and  $Pr$ .
- By increasing  $Bi_1$ ,  $\theta$  decays whereas for  $Bi_2$ ,  $\phi$  increases.
- Heat transfer rate is increasing function of  $Sr$  and  $Du$  while it is decreasing function of  $H$  and  $T'$ .

## Chapter 6

# Heat transfer analysis on peristalsis of Ree-Eyring fluid

### 6.1 Introduction

The peristaltic activity of Ree-Eyring fluid in a rotating frame is studied. Heat transfer analysis with viscous dissipation and heat source/sink is taken into account. Convective conditions for heat transfer in the formulation are adopted. Closed form solutions for axial and secondary velocities, pressure rise per wavelength, flow rate due to secondary flow and temperature are obtained by considering small Reynolds number and long wavelength. The variation for different physical parameters are shown through graphical illustrations. This study reveals that influence of rotation parameter causes significant fluctuations in axial and secondary velocities. It is also found that presence of non-uniform heat source in energy equation causes enhancement in rate of heat transfer coefficient.

### 6.2 Problem development

Here we address an incompressible Ree-Eyring material in a channel of width  $2d$ . Both the channel and fluid rotates with a uniform angular velocity  $\bar{\Omega}$  about the  $\hat{z}$  - axis. Mathematical

expression for wave propagation along the channel walls at ( $\hat{z} = \pm\bar{H}$ ) is given by

$$\bar{H}(\hat{x}, \hat{t}) = d + a \sin \frac{2\pi}{\lambda} (\hat{x} - c\hat{t}). \quad (6.1)$$

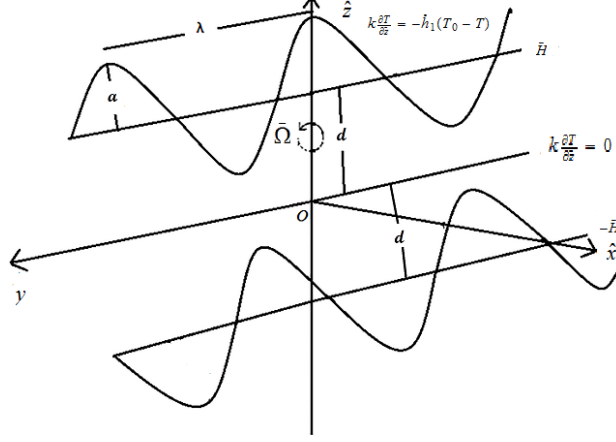


Fig. 6.1: Geometry of the problem.

Extra stress tensor of Ree- Eyring fluid model is defined as [56, 57] :

$$\mathbf{S}_{ij} = \mu \frac{\partial \hat{\mathbf{V}}_i}{\partial \hat{x}_j} + \frac{1}{\dot{A}_3} \sinh^{-1} \left( \frac{1}{\dot{A}_4} \frac{\partial \hat{\mathbf{V}}_i}{\partial \hat{x}_j} \right). \quad (6.2)$$

Since  $\sinh^{-1} \hat{x} \approx \hat{x}$  for  $|\hat{x}| \leq 1$  then

$$\mathbf{S}_{ij} = \mu \frac{\partial \hat{\mathbf{V}}_i}{\partial \hat{x}_j} + \frac{1}{\dot{A}_3} \left( \frac{1}{\dot{A}_4} \frac{\partial \hat{\mathbf{V}}_i}{\partial \hat{x}_j} \right), \quad (6.3)$$

where  $\mu$  is the fluid viscosity,  $\dot{A}_3$  and  $\dot{A}_4$  are material constants and

$$\begin{aligned} \hat{\mathbf{V}}_i &= (\hat{u}, \hat{v}, \hat{w}), \\ \hat{x}_j &= (\hat{x}, \hat{y}, \hat{z}). \end{aligned}$$

The governing equations of continuity, momentum and energy for incompressible fluid flow in a rotating frame are

$$\frac{\partial \hat{u}}{\partial \hat{x}} + \frac{\partial \hat{w}}{\partial \hat{z}} = 0, \quad (6.4)$$



$$\rho \frac{d\hat{u}}{d\hat{t}} - 2\rho\Omega\hat{v} = -\frac{\partial\tilde{p}}{\partial\hat{x}} + \frac{\partial S_{\hat{x}\hat{x}}}{\partial\hat{x}} + \frac{\partial S_{\hat{x}\hat{y}}}{\partial\hat{y}} + \frac{\partial S_{\hat{x}\hat{z}}}{\partial\hat{z}}, \quad (6.5)$$

$$\rho \frac{d\hat{v}}{d\hat{t}} + 2\rho\Omega\hat{u} = -\frac{\partial\tilde{p}}{\partial\hat{y}} + \frac{\partial S_{\hat{y}\hat{x}}}{\partial\hat{x}} + \frac{\partial S_{\hat{y}\hat{y}}}{\partial\hat{y}} + \frac{\partial S_{\hat{y}\hat{z}}}{\partial\hat{z}}, \quad (6.6)$$

$$\rho \frac{d\hat{w}}{d\hat{t}} = -\frac{\partial\tilde{p}}{\partial\hat{z}} + \frac{\partial S_{\hat{z}\hat{x}}}{\partial\hat{x}} + \frac{\partial S_{\hat{z}\hat{y}}}{\partial\hat{y}} + \frac{\partial S_{\hat{z}\hat{z}}}{\partial\hat{z}}, \quad (6.7)$$

$$\begin{aligned} \rho c_p \frac{dT}{d\hat{t}} &= k_T \left[ \frac{\partial^2 T}{\partial\hat{x}^2} + \frac{\partial^2 T}{\partial\hat{y}^2} + \frac{\partial^2 T}{\partial\hat{z}^2} \right] + S_{\hat{x}\hat{x}} \frac{\partial\hat{u}}{\partial\hat{x}} + S_{\hat{x}\hat{z}} \left( \frac{\partial\hat{u}}{\partial\hat{z}} + \frac{\partial\hat{w}}{\partial\hat{x}} \right) + S_{\hat{z}\hat{z}} \frac{\partial\hat{w}}{\partial\hat{z}} \\ &+ Q_0(T - T_0). \end{aligned} \quad (6.8)$$

The conditions are

$$\hat{u}_{\hat{z}} = 0, \hat{v}_{\hat{z}} = 0, k_T \frac{\partial T}{\partial\hat{z}} = 0 \text{ at } \hat{z} = 0, \quad (6.9)$$

$$\hat{u} = 0, \hat{v} = 0, k_T \frac{\partial T}{\partial\hat{z}} = -\hat{h}_1(T_0 - T) \text{ at } \hat{z} = \hat{h}, \quad (6.10)$$

in which  $\hat{h}_1$  indicates the heat transfer coefficient and  $T_0$  the temperature at walls.

Putting Eqs. (6.8) and (6.9) in Eqs. (6.6) and (6.7) and then using the wave frame transformations

$$\begin{aligned} x &= \hat{x} - c\hat{t}, \quad y = \hat{y}, \quad z = \hat{z}, \quad p = \hat{p}(\hat{x}, \hat{y}, \hat{z}), \\ u(x, y, z) &= \hat{u}(\hat{x}, \hat{y}, \hat{z}) - c, \quad v(\hat{x}, \hat{y}, \hat{z}) = \hat{v}(\hat{x}, \hat{y}, \hat{z}), \quad w(\hat{x}, \hat{y}, \hat{z}) = \hat{w}(\hat{x}, \hat{y}, \hat{z}), \end{aligned} \quad (6.11)$$

Eqs. (6.2) – (6.7) become

$$\frac{\partial u}{\partial x} + \frac{\partial w}{\partial z} = 0, \quad (6.12)$$

$$\left[ (u + c) \frac{\partial u}{\partial x} + \bar{v} \frac{\partial u}{\partial y} + w \frac{\partial u}{\partial z} - 2\Omega v \right] = -\frac{\partial p}{\partial x} + \frac{\partial S_{xx}}{\partial x} + \frac{\partial S_{xy}}{\partial y} + \frac{\partial S_{xz}}{\partial z}, \quad (6.13)$$

$$\left[ (u + c) \frac{\partial v}{\partial x} + v \frac{\partial v}{\partial y} + w \frac{\partial v}{\partial z} + 2\Omega(u + c) \right] = -\frac{\partial p}{\partial y} + \frac{\partial S_{yx}}{\partial x} + \frac{\partial S_{yy}}{\partial y} + \frac{\partial S_{yz}}{\partial z}, \quad (6.14)$$

$$\left[ (u + c) \frac{\partial w}{\partial x} + v \frac{\partial w}{\partial y} + w \frac{\partial w}{\partial z} \right] = -\frac{\partial p}{\partial z} + \frac{\partial S_{zx}}{\partial x} + \frac{\partial S_{zy}}{\partial y} + \frac{\partial S_{zz}}{\partial z}, \quad (6.15)$$

$$\begin{aligned} \rho c_p \frac{dT}{dt} = & k_T \left[ \frac{\partial^2 T}{\partial x^2} + \frac{\partial^2 T}{\partial y^2} + \frac{\partial^2 T}{\partial z^2} \right] + S_{xx} \frac{\partial u}{\partial x} + S_{xz} \left( \frac{\partial u}{\partial z} + \frac{\partial w}{\partial x} \right) + S_{zz} \frac{\partial w}{\partial z} \\ & + Q_0(T - T_0). \end{aligned} \quad (6.16)$$

Using dimensionless variables

$$\begin{aligned} x^* &= \frac{x}{\lambda}, \quad y^* = \frac{y}{\lambda}, \quad z^* = \frac{z}{d}, \quad t = \frac{ct}{\lambda}, \quad p^* = \frac{d^2 p}{\mu c \lambda}, \\ u^* &= \frac{u}{c}, \quad v^* = \frac{v}{c}, \quad w^* = \frac{w}{c}, \quad \eta^* = \frac{\eta}{d}, \quad \theta = \frac{T - T_0}{T_0}, \\ \mathbf{S}_{ij}^* &= \frac{d \mathbf{S}_{ij}}{\mu c}, \quad k = \frac{R}{d}, \quad \delta = \frac{d}{\lambda}, \quad \text{Re} = \frac{cd}{\nu}. \end{aligned} \quad (6.17)$$

$$u = \psi_z, \quad w = -\delta \psi_x \quad (6.18)$$

and the Eqs. (6.14) – (6.18) after invoking lubrication approach give

$$\frac{\partial p}{\partial x} - \frac{\partial S_{xz}}{\partial z} - 2T'v = 0, \quad (6.19)$$

$$\frac{\partial p}{\partial y} - \frac{\partial S_{yz}}{\partial z} + 2T' \left( \frac{\partial \psi}{\partial z} + 1 \right) = 0, \quad (6.20)$$

$$\frac{\partial p}{\partial z} = 0, \quad (6.21)$$

$$\frac{\partial^2 \theta}{\partial z^2} + Br S_{xz} \psi_{zz} + S\theta = 0, \quad (6.22)$$

$$S_{xz} = (1 + \alpha_3) \psi_{zz}, \quad (6.23)$$

$$S_{yz} = (1 + \alpha_3) v_z. \quad (6.24)$$

The dimensionless conditions are

$$h = 1 + \epsilon \sin 2\pi x, \quad (6.25)$$

$$\psi = 0, \quad \psi_{zz} = 0, \quad v_z = 0, \quad \frac{\partial \theta}{\partial z} = 0 \quad \text{at } z = 0, \quad (6.26)$$

$$\psi = F_1, \quad \psi_z = -1, \quad v = 0, \quad \frac{\partial \theta}{\partial z} - Bi_1 \theta = 0 \quad \text{at } z = h, \quad (6.27)$$

where

$$F_1 = \int_0^h \psi_z dz. \quad (6.28)$$

Here  $\alpha_3 = \frac{1}{\mu A_3 A_4}$  denotes the fluid parameter. The pressure rise per wavelength  $\Delta p$  and the flow rate  $F_2$  are

$$\Delta p = \int_0^1 \frac{dp}{dx} dx, \quad F_2 = \int_0^h v dz. \quad (6.29)$$

Equations (6.16) and (6.17) give

$$\frac{\partial}{\partial z} \left[ \frac{\partial S_{xz}}{\partial z} + 2T'v \right] = 0, \quad (6.30)$$

$$\frac{\partial S_{yz}}{\partial z} - 2T' \left( \frac{\partial \psi}{\partial z} + 1 \right) = 0. \quad (6.31)$$

Here we neglect secondary flow pressure due to rotational effect.

### 6.3 Solution methodology

Eqs. (6.30), (6.31) and (6.22) with boundary conditions (6.25) – (6.27) have the exact solutions:

$$\begin{aligned} \psi(z) = & \left( \sin \frac{2h\sqrt{T'}}{\sqrt{1+\alpha_3}} - \sinh \frac{2h\sqrt{T'}}{\sqrt{1+\alpha_3}} \right)^{-1} \left[ -z \sin \frac{2h\sqrt{T'}}{\sqrt{1+\alpha_3}} - A_1 \left\{ (F_1 + h) \cosh \frac{z\sqrt{T'}}{\sqrt{1+\alpha_3}} \sin \frac{z\sqrt{T'}}{\sqrt{1+\alpha_3}} \right. \right. \\ & \left. \left. - F_1 \cos \frac{z\sqrt{T'}}{\sqrt{1+\alpha_3}} \sinh \frac{z\sqrt{T'}}{\sqrt{1+\alpha_3}} - h \cos \frac{z\sqrt{T'}}{\sqrt{1+\alpha_3}} \sinh \frac{z\sqrt{T'}}{\sqrt{1+\alpha_3}} \right\} + z \sinh 2h\sqrt{T'} \right. \\ & \left. + (1+i)(F_1 + h)A_2 \left\{ \sin(1+i) \frac{z\sqrt{T'}}{\sqrt{1+\alpha_3}} - \sinh(1+i) \frac{z\sqrt{T'}}{\sqrt{1+\alpha_3}} \right\} \right], \quad (6.32) \end{aligned}$$

$$\begin{aligned} v(z) = & \left\{ (\sqrt{1+\alpha}) \sin \frac{2h\sqrt{T'}}{\sqrt{1+\alpha_3}} - \sinh \frac{2h\sqrt{T'}}{\sqrt{1+\alpha_3}} \right\}^{-1} \left[ A_3 + A_4 \cos \frac{z\sqrt{T'}}{\sqrt{1+\alpha_3}} \cosh \frac{z\sqrt{T'}}{\sqrt{1+\alpha_3}} \right. \\ & \left. - A_5 \sin \frac{z\sqrt{T'}}{\sqrt{1+\alpha_3}} \sin \frac{z\sqrt{T'}}{\sqrt{1+\alpha_3}} \right], \quad (6.33) \end{aligned}$$

$$\begin{aligned}\theta(z) = & C_1 \cos \sqrt{S}z + C_2 \sin \sqrt{S}z - C_3 B_{lm} \{(\cos D_{lm}z + \cosh D_{lm}z \\ & + \sin D_{lm}z + \sinh D_{lm}z)(\sin \sqrt{S}z + \cos \sqrt{S}z)\}\end{aligned}\quad (6.34)$$

$$\Delta p = \left\{(\sqrt{1 + \alpha_3}) \sin \frac{2h\sqrt{T'}}{\sqrt{1 + \alpha_3}} - \sinh \frac{2h\sqrt{T'}}{\sqrt{1 + \alpha_3}}\right\}^{-1} [4(F_1 + h)T^{\frac{3}{2}} \left\{\cos \frac{2h\sqrt{T'}}{\sqrt{1 + \alpha_3}} + \cosh \frac{2h\sqrt{T'}}{\sqrt{1 + \alpha_3}}\right\}], \quad (6.35)$$

$$\begin{aligned}F_2 = & -\left\{(\sqrt{1 + \alpha_3}) \sin \frac{2h\sqrt{T'}}{\sqrt{1 + \alpha_3}} - \sinh \frac{2h\sqrt{T'}}{\sqrt{1 + \alpha_3}}\right\}^{-1} [(F_1 + h) \left\{-2h\sqrt{T'} \left(\cos \frac{2h\sqrt{T'}}{\sqrt{1 + \alpha_3}}\right. \right. \\ & \left. \left. + \cosh \frac{2h\sqrt{T'}}{\sqrt{1 + \alpha_3}}\right) + \sqrt{1 + \alpha_3} \left(\sin \frac{2h\sqrt{T'}}{\sqrt{1 + \alpha_3}} + \sinh \frac{2h\sqrt{T'}}{\sqrt{1 + \alpha_3}}\right)\right\}],\end{aligned}\quad (6.36)$$

where  $A_i$  ( $i = 1 - 5$ ),  $C_j$  ( $j = 1 - 3$ ),  $B_{lm}$  and  $D_{lm}$ 's have been computed algebraically.

## 6.4 Discussion

Figs. (6.2 – 6.6(a, b)) are plotted to observe the effects of fluid parameter  $\alpha_3$  and Taylor number  $T'$  on axial  $u$  and secondary  $v$  velocities, pressure per rise wavelength  $\Delta p$  and flow rate due to secondary velocity  $F_2$ . Fig. 6.2(a) depicts that velocity is enhanced near centre of channel whereas it decays near channel boundaries when  $\alpha_3$  increases. Since fluid parameter is inversely proportional to viscosity therefore for larger  $\alpha_3$  the viscosity decreases and hence velocity decays near walls. Opposite outcome is achieved for Taylor number  $T'$  (see Fig. 6.2(b)). In fact the secondary flow is responsible for decrease in velocity near centre of channel. Secondary velocity via  $\alpha_3$  is shown in Fig. 6.3(a). Here  $v$  decreases for increasing values of  $\alpha_3$ . The motion of fluid particles becomes faster when we increase the rotation parameter  $T'$  and thus secondary velocity is enhanced (see Fig. 6.3(b)). It can be visualized from Figs. 6.4(a) and 6.4(b) that pressure  $\Delta p$  rises for fluid parameter  $\alpha_3$  and Taylor number  $T'$  in retrograde pumping region while it decays in augmented pumping region. It is because of the fact that for larger angular velocity, the pressure does not rise in direction of peristaltic wave.. Further the Coriolis force is responsible for fluid drag outwards in  $y$ -direction and consequently  $\Delta p$  reduces. Figs. 6.5(a, b) plot variation of fluid parameter  $\alpha_3$  on secondary velocity. In Fig. 6.5(a) when  $F_1 = -1$ , the flow rate of the fluid is enhanced in wider portion of channel. However when  $F_1 = -0.5$  the flow due to secondary velocity becomes positive for larger values of fluid parameter over the whole

length of the channel (see Fig. 6.5(b)). Opposite results of  $F_2$  is observed in Figs. 6.6(a, b) for larger values of Taylor number  $T'$  when  $F_1 = -1$  and  $-0.5$ .

Figs. 6.7(a – e) show temperature  $\theta$  variation versus different parameters. Fig. 6.7(a) is plotted for fluid parameter against  $\theta$ . It is noticed from this Fig. that temperature distribution tends to rise when the fluid parameter enhances. It can be observed from Fig. 6.7(b) that for larger rotation parameter  $T'$  the temperature profile diminishes. In fact with the increase in rotation, the motion of the fluid particles enhances which causes resistance to flow and ultimate there is decrease in temperature profile. Fig. 6.7(c) is portrayed to analyze the variation of  $\theta$  for heat source/sink parameter  $S$ . It can be observed from Fig. that with the increase in  $S$  the temperature profile is enhanced. Behavior of Biot number  $Bi_1$  can be visualized through Fig. 6.7(d). Temperature rapidly decays as we increase  $Bi_1$ . It is due to enhancement in strength of convecting heating which causes decrease in temperature. Temperature via Brinkman number  $Br$  in Fig. 6.7(e). Here for larger values of  $Br$  the temperature increases. It is through argument that less heat conduction occurs for viscous dissipation.

Now  $Z$  for different variable is demonstrated through Figs. 6.8(a – e). In Fig. 6.8(a) we observed that heat transfer rate  $Z$  rises by increasing fluid parameter  $\alpha$ . The magnitude of heat transfer coefficient  $Z$  near centerline decreases for Taylor number  $T'$  whereas it enhances near the channel boundaries (see Fig. 6.8(b)). Variation in heat transfer rate  $Z$  for heat generation/absorption  $S$  is portrayed in Fig. 6.8(c). Rate of heat transfer of fluid increases when we take larger values of  $S$ . Opposite result for  $Z$  via Biot number is observed in Fig. 6.8(d). Here Fig. 6.8(e) is plotted for viscous dissipation parameter  $Br$  on heat transfer rate  $Z$ . It is noticed that larger values of Brinkman number  $Br$  increases  $Z$  for a small range.

The next interesting part of this section is trapping. Figs. 6.9(a – c) and 6.10(a – c) are plotted for this purpose with the help of contours. It can be seen in Fig. 6.9 that when the fluid parameter  $\alpha_3$  increases then the size of bolus enhances. Also for viscous fluid ( $\alpha_3 = 0$ ) the trapped bolus vanishes. It depicts from Fig. 6.10 that due to the influence of rotation the size of the bolus decreases slowly. It can also be observed from Fig. that the bolus disappears when the rotation of the fluid particles increases.

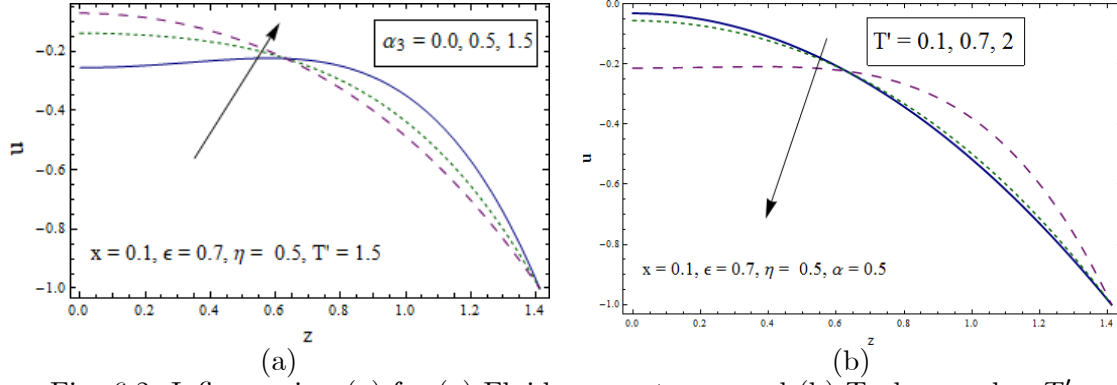


Fig. 6.2: Influence in  $u(z)$  for (a) Fluid parameter  $\alpha_3$  and (b) Taylor number  $T'$ .

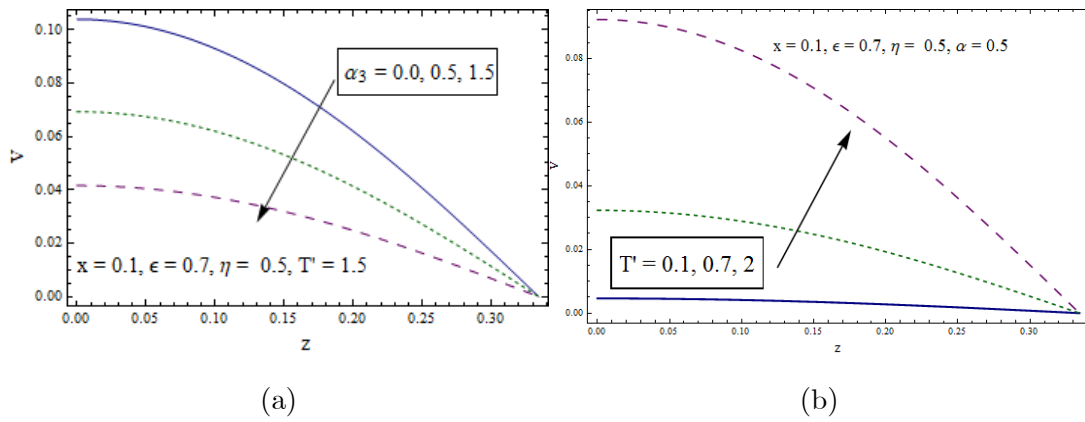


Fig. 6.3: Influence in secondary velocity  $v(z)$  for (a) Fluid parameter  $\alpha_3$  and (b) Taylor number  $T'$ .

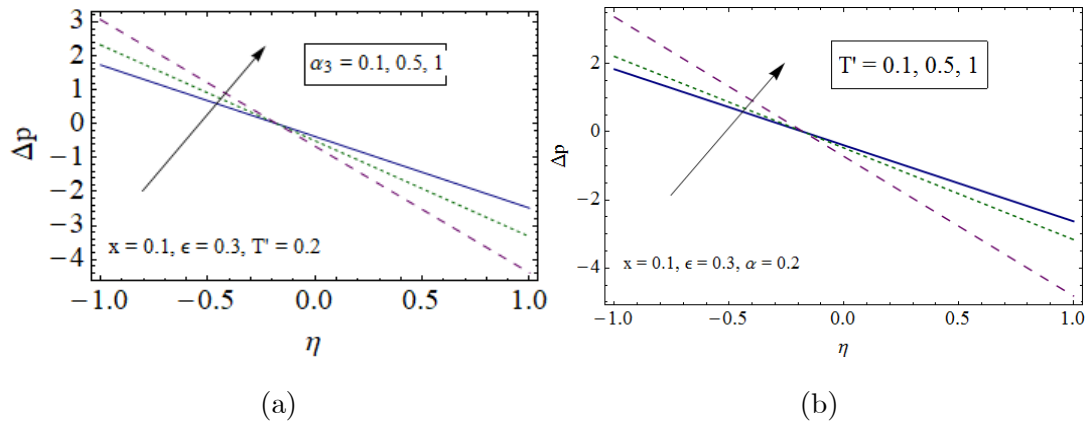


Fig. 6.4: Variation in pressure rise per wavelength  $\Delta p$  for (a) Fluid parameter  $\alpha_3$  and (b)

Taylor number  $T'$ .

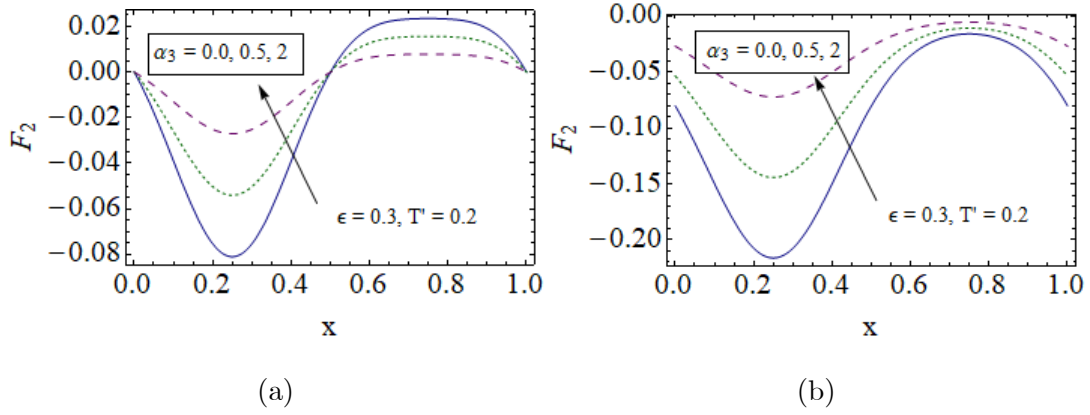


Fig. 6.5: Variation in dimensionless flow rate due to secondary velocity  $F_2$  for fluid parameter when (a)  $F_1 = -1$  and (b)  $F_1 = -0.5$ .

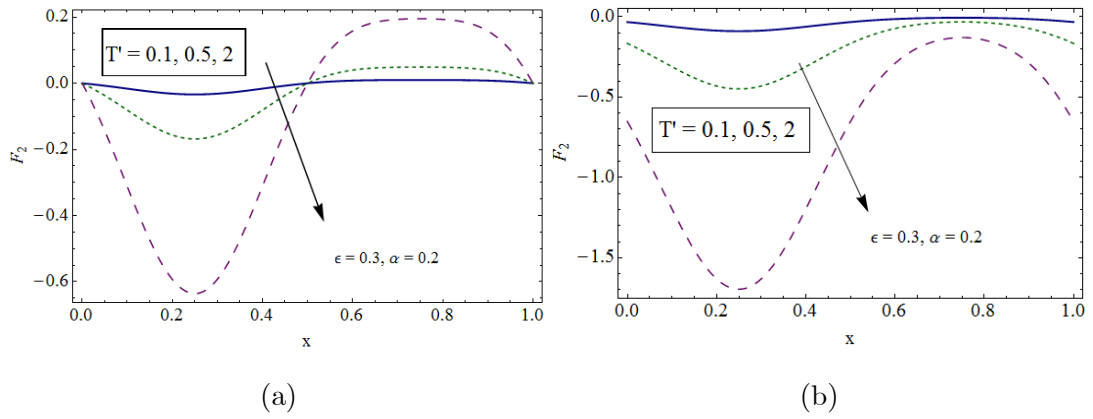
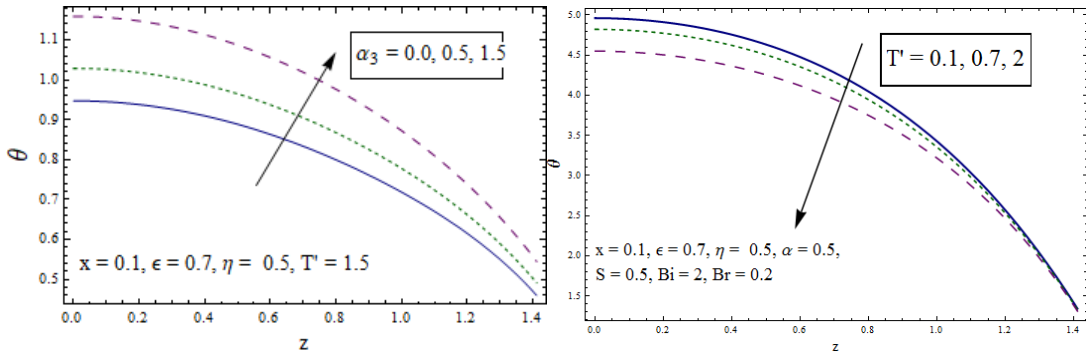


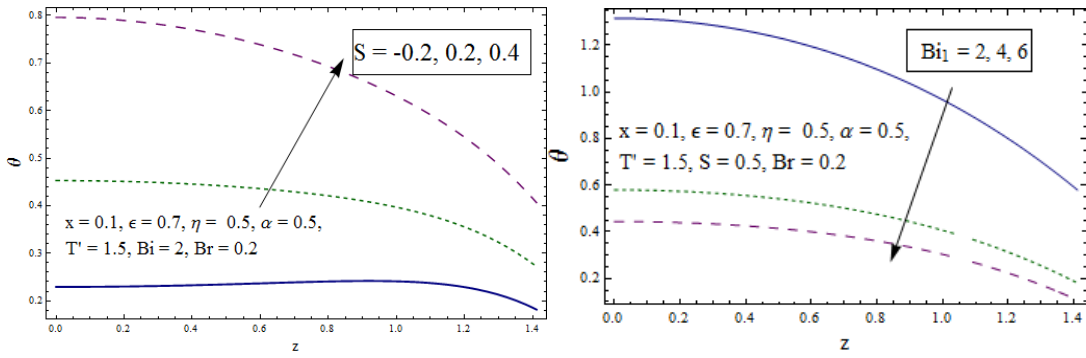
Fig. 6.6: Variation in flow rate due to secondary velocity  $F_2$  for Taylor number  $T'$  when (a)

$F_1 = -1$  and (b)  $F_1 = -0.5$ .



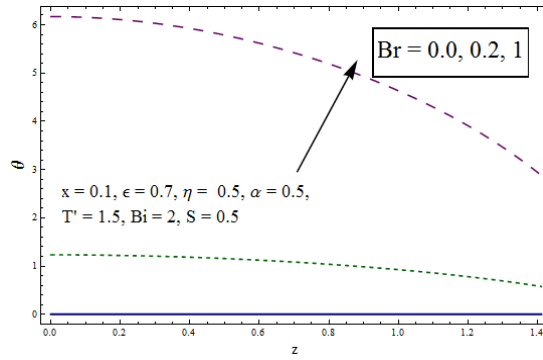
(a)

(b)



(c)

(d)



(e)

Fig. 6.7: Influence in  $\theta(z)$  for (a) Fluid parameter  $\alpha_3$ , (b) Taylor number  $T'$ , (c) non-uniform source/sink parameter  $S$ , (d) Biot number  $Bi_1$  and (e) Brinkman number  $Br$ .



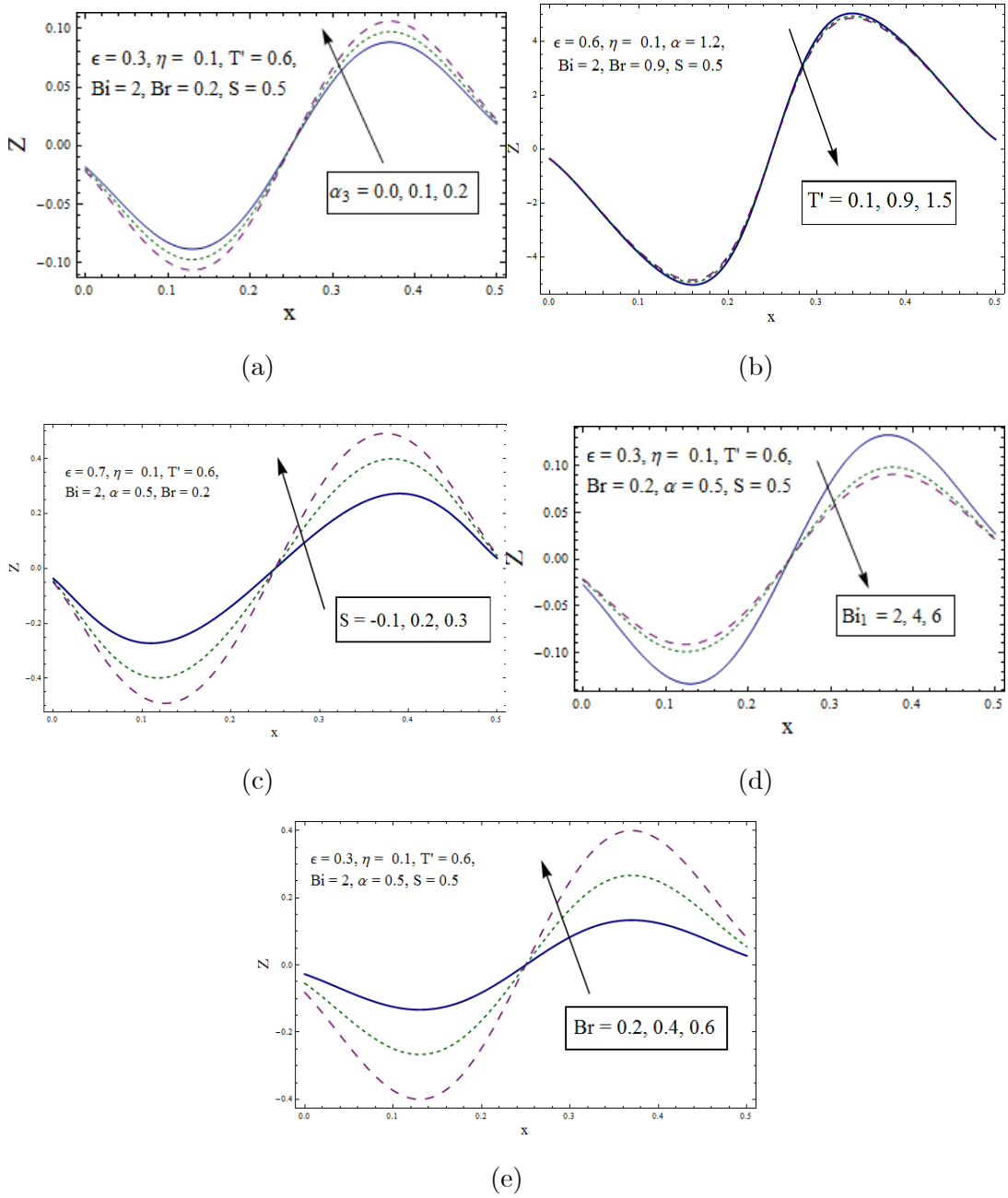


Fig. 6.8: Influence in  $Z(x)$  for (a) Fluid parameter  $\alpha_3$ , (b) Taylor number  $T'$ , (c) non-uniform

source/sink parameter  $S$ , (d) Biot number  $Bi_1$  and (e) Brinkman number  $Br$ .

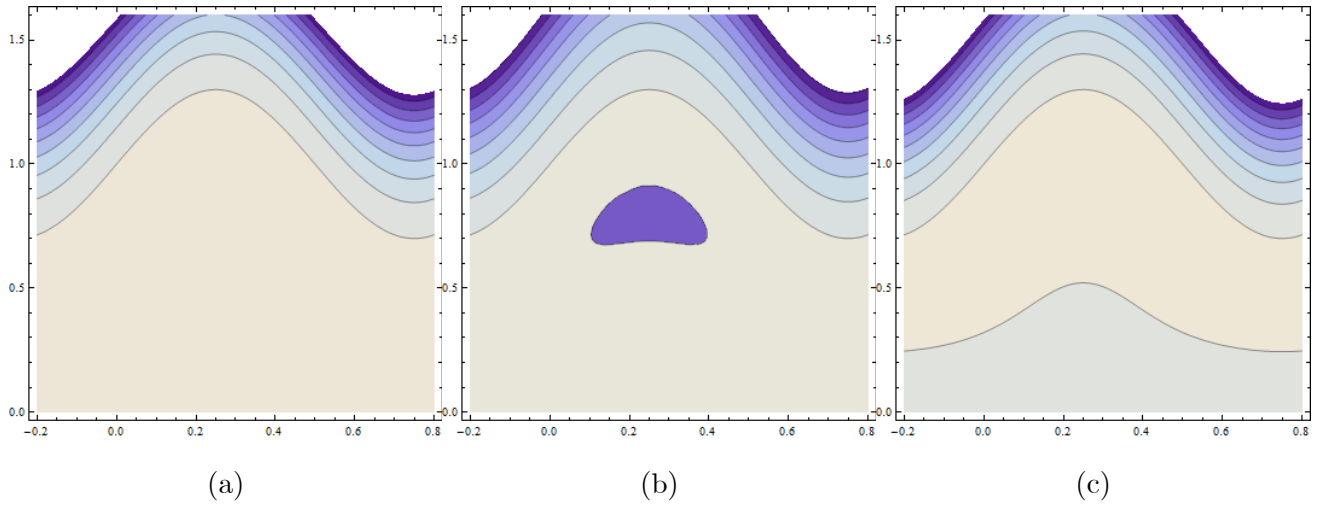


Fig. 6.9: Variation in streamlines for fluid parameter  $\alpha_3$  when (a)  $\alpha_3 = 0$  (b)  $\alpha_3 = 0.9$  and (c)  $\alpha_3 = 2$ .

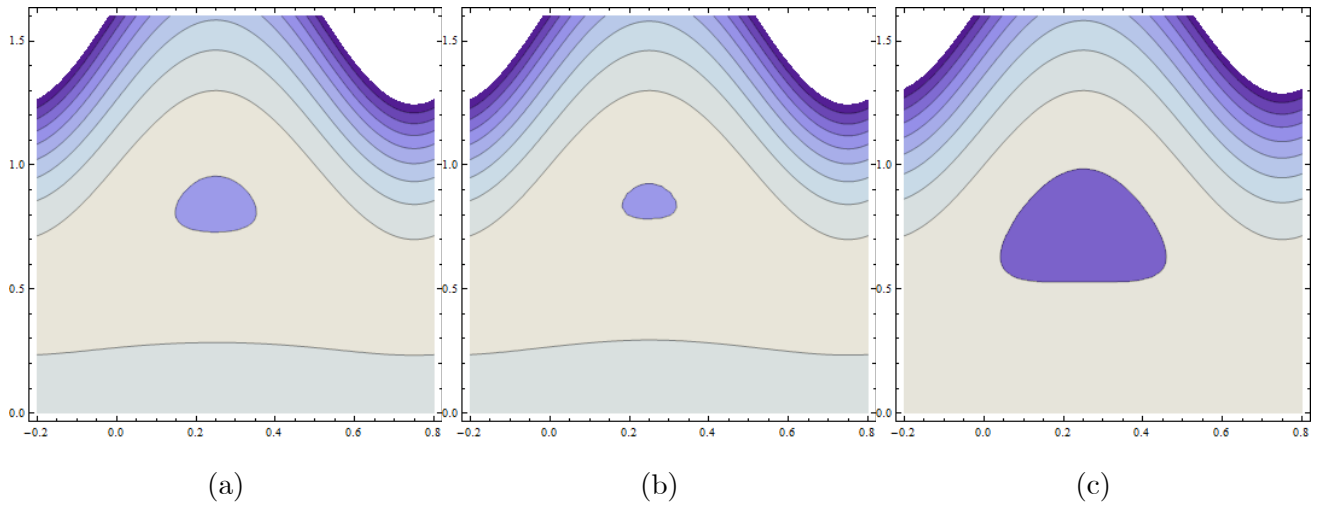


Fig. 6.10: Variation in streamlines for Taylor number  $T'$  when (a)  $T' = 0$  (b)  $T' = 0.5$  and (c)  $T' = 2$ .

## 6.5 Conclusions

Here simultaneous outcome of rotation and heat generation/absorption on peristalsis of Ree-Eyring fluid have been pointed out. Major observations include:

- Dual behavior of fluid parameter  $\alpha_3$  and Taylor number  $T'$  on the axial velocity is noticed.
- Opposite effect is observed on secondary velocity for fluid parameter  $\alpha_3$  and Taylor number  $T'$ .
- Similar behavior of pressure rise  $\Delta p$  is observed for fluid  $\alpha_3$  and rotation  $T'$  parameters.
- Variation in dimensionless flow rate due to secondary velocity  $F_2$  for fluid  $\alpha_3$  and rotation parameters  $T'$  is quite opposite.
- Temperature is an increasing function of fluid parameter  $\alpha_3$ , heat generation/absorption  $S$  and Brinkman number whereas it is decreasing function of rotation parameter  $T'$  and Biot number  $Bi_{11}$ .
- Rate of heat transfer decreases for increasing  $T'$  and  $Bi_{11}$  but it enhances for  $\alpha_3$ ,  $S$  and  $Br$ .
- Fluid and rotational parameters on trapped bolus have opposite contributions.
- For viscous fluid, the present problem is reduced by taking  $\alpha_3 \rightarrow 0$ .

## Chapter 7

# Numerical analysis for ionslip and Hall current on peristaltic transport of rotating Ree-Eyring fluid

### 7.1 Introduction

Ion-slip and Hall current in peristalsis of Ree-Eyring liquid are analyzed. In addition energy equation contains Ohmic dissipation. Whole system is in rotating frame. Governing equations representing flow of a fluid are reduced into ordinary differential equations. Problem formulation is developed by small Reynolds number and long wavelength approximation. Shooting method is applied to find numerical results. Variation of emerging dimensionless parameters of present problem is illustrated through graphs. We observed that velocity and temperature distributions in Ree-Eyring fluid are more than viscous fluid. Rotation and fluid parameters have opposite effects on velocity. It is also found that influence of ionslip in momentum equation causes an enhancement in velocity.

### 7.2 Problem development

Here we consider an incompressible Ree-Eyring fluid in a channel with width  $(d_1 + d_2)$ . Both channel and fluid rotate with uniform angular velocity  $\bar{\Omega}$  about the  $\hat{z}$  - axis. Travelling waves

of speed  $c$ , amplitudes  $(a_1, a_2)$  and wavelength  $\lambda$  propagate along the channel walls  $(\bar{H}_1, \bar{H}_2)$ . Mathematically we represent such waves in the form

$$\bar{H}_1(\hat{x}, \hat{t}) = d_1 + a_1 \sin \frac{2\pi}{\lambda}(\hat{x} - c\hat{t}), \quad (7.1)$$

$$\bar{H}_2(\hat{x}, \hat{t}) = -d_2 - a_2 \sin \frac{2\pi}{\lambda}(\hat{x} - c\hat{t}), \quad (7.2)$$

in which  $\hat{t}$  is the time. The governing equations for rotating flow are:

$$\nabla \cdot \mathbf{V} = 0, \quad (7.3)$$

$$\rho \frac{d\mathbf{V}}{dt} + \rho [\bar{\Omega} \times (\bar{\Omega} \times \mathbf{V}) + 2\bar{\Omega} \times \mathbf{V}] = -\nabla P + \text{div } \mathbf{S} + \mathbf{J} \times \mathbf{B}, \quad (7.4)$$

$$\rho c_p \frac{dT}{dt} = k_T \nabla^2 T + \mathbf{L} \cdot \mathbf{S} + \frac{1}{\sigma_f} \mathbf{J} \cdot \mathbf{J}, \quad (7.5)$$

where

$$\mathbf{J} = \sigma(\mathbf{V} \times \mathbf{B}) - \frac{w_e t_e}{B_0} (\mathbf{J} \times \mathbf{B}) + \frac{w_e t_e \beta_i}{B_0^2} ((\mathbf{J} \times \mathbf{B}) \times \mathbf{B}), \quad (7.6)$$

$$\mathbf{B} = (0, 0, B_0) \quad (7.7)$$

and extra stress tensor for Ree-Eyring fluid [28, 29] is

$$\begin{aligned} \mathbf{S} &= \mu \text{grad } \mathbf{V} + \frac{1}{\dot{A}_3} \left( \frac{1}{\dot{A}_4} \text{grad } \mathbf{V} \right), \\ \mathbf{L} &= \text{grad } \mathbf{V}, \end{aligned}$$

in which  $\mathbf{V} = (\hat{u}, \hat{v}, \hat{w})$  denotes fluid velocity,  $\mathbf{J}$  the current density [86, 87],  $\sigma$  fluid electric conductivity,  $w_e$  the cyclotron frequency,  $t_e$  electron collision time,  $\beta_i$  ionslip parameter,  $\mathbf{L} \cdot \mathbf{S}$  the viscous dissipation term,  $\frac{1}{\sigma} \mathbf{J} \cdot \mathbf{J}$  Ohmic dissipation term and  $\mathbf{J} \times \mathbf{B}$  the Lorentz force. Eq. (6) can be solved in  $\mathbf{J}$  to yield

$$\mathbf{J} \times \mathbf{B} = -\frac{\sigma_f B_0^2}{\alpha^2 + \beta^2} [(\beta \hat{u} - m \hat{v}), (\beta \hat{v} + m \hat{u}), 0], \quad (7.8)$$

$$\mathbf{J} \cdot \mathbf{J} = \frac{\sigma_f^2 B_0^2}{m^2 + \beta^2} (\hat{u}^2 + \hat{w}^2), \quad (7.9)$$

where  $m(= w_e t_e)$  the Hall parameter and  $\beta = 1 + \beta_i \alpha$ .

Now using wave frame transformations and dimensionless variables

$$\begin{aligned} x &= \hat{x} - ct, \quad y = \hat{y}, \quad z = \hat{z}, \quad p = \hat{p}(\hat{x}, \hat{y}, \hat{z}), \\ u(x, y, z) &= \hat{u}(\hat{x}, \hat{y}, \hat{z}) - c, \quad v(\hat{x}, \hat{y}, \hat{z}) = \hat{v}(\hat{x}, \hat{y}, \hat{z}), \quad w(\hat{x}, \hat{y}, \hat{z}) = \hat{w}(\hat{x}, \hat{y}, \hat{z}), \end{aligned} \quad (7.10)$$

$$\begin{aligned} x^* &= \frac{x}{\lambda}, \quad y^* = \frac{y}{\lambda}, \quad z^* = \frac{z}{b_1}, \quad t^* = \frac{ct}{\lambda}, \quad p^* = \frac{d_1^2 p}{\mu c \lambda}, \\ u^* &= \frac{u}{c}, \quad v^* = \frac{v}{c}, \quad w^* = \frac{w}{c}, \quad \zeta = \frac{d_2}{d_1}, \quad h_1 = \frac{\bar{H}_1}{d_1}, \quad h_2 = \frac{\bar{H}_2}{d_1}, \\ \theta &= \frac{T - T_0}{T_0}, \quad \mathbf{S}^* = \frac{d_1 \mathbf{S}}{\mu c}, \quad \delta = \frac{d_1}{\lambda}, \quad \text{Re} = \frac{\rho c d_1}{\nu}. \end{aligned} \quad (7.11)$$

Eqs. (7.3) – (7.5) become

$$\delta \frac{\partial u}{\partial x} + \delta \frac{\partial v}{\partial y} + \frac{\partial w}{\partial z} = 0,$$

$$\delta \text{Re} \left[ u \frac{\partial u}{\partial x} + w \frac{\partial u}{\partial z} \right] - 2T'v = -\frac{\partial \tilde{p}}{\partial x} + \delta \frac{\partial S_{xx}}{\partial \bar{x}} + \delta \frac{\partial S_{xy}}{\partial \bar{y}} + \frac{\partial S_{xz}}{\partial \bar{z}} - \frac{H^2}{\alpha^2 + \beta^2} [\beta(u+1) - mv], \quad (7.12)$$

$$\delta \text{Re} \left[ u \frac{\partial v}{\partial x} + w \frac{\partial v}{\partial z} \right] + 2T'u = -\frac{\partial \tilde{p}}{\partial y} + \delta \frac{\partial S_{yx}}{\partial \bar{x}} + \delta \frac{\partial S_{yy}}{\partial \bar{y}} + \frac{\partial S_{yz}}{\partial \bar{z}} - \frac{H^2}{\alpha^2 + \beta^2} [\beta v + m(u+1)], \quad (7.13)$$

$$\delta \text{Re} \left[ u \frac{\partial w}{\partial x} + w \frac{\partial w}{\partial z} \right] = -\frac{\partial \tilde{p}}{\partial \bar{z}} + \delta \frac{\partial S_{zx}}{\partial \bar{x}} + \delta \frac{\partial S_{zy}}{\partial \bar{y}} + \frac{\partial S_{zz}}{\partial \bar{z}}, \quad (7.14)$$

$$\begin{aligned} \text{Pr} \delta \text{Re} \left[ \frac{\partial T}{\partial \bar{x}} + u \delta \frac{\partial^2 T}{\partial \bar{y}^2} + \frac{\partial^2 T}{\partial \bar{z}^2} \right] &= \left[ \delta^2 \frac{\partial^2 \theta}{\partial x^2} + \delta^2 \frac{\partial^2 \theta}{\partial y^2} + \frac{\partial^2 \theta}{\partial z^2} \right] + \delta S_{xx} \frac{\partial u}{\partial x} + Br S_{xz} \left( \frac{\partial u}{\partial z} + \frac{\partial w}{\partial x} \right) \\ &+ \delta S_{zz} \frac{\partial w}{\partial z} + \frac{Br H^2}{m^2 + \beta^2} [(u+1)^2 + w^2], \end{aligned} \quad (7.15)$$

in which bars have been suppressed. Defining stream function

$$u = \psi_z, \quad w = -\delta \psi_x \quad (7.16)$$

and applying long wavelength and small Reynolds approximation, the Eqs. (14) – (17) become

$$\frac{\partial p}{\partial x} - \frac{\partial S_{xz}}{\partial z} - 2T'v + \frac{H^2}{\alpha^2 + \beta^2} \left[ \beta \left( \frac{\partial \psi}{\partial z} + 1 \right) - \alpha v \right] = 0, \quad (7.17)$$

$$\frac{\partial p}{\partial y} - \frac{\partial S_{yz}}{\partial z} + 2T' \left( \frac{\partial \psi}{\partial z} + 1 \right) + \frac{H^2}{m^2 + \beta^2} \left[ \beta v + m \left( \frac{\partial \psi}{\partial z} + 1 \right) \right] = 0, \quad (7.18)$$

$$\frac{\partial p}{\partial z} = 0, \quad (7.19)$$

$$\frac{\partial^2 \theta}{\partial z^2} + Br S_{xz} \psi_{zz} + \frac{Br H^2}{m^2 + \beta^2} \left( \frac{\partial \psi}{\partial z} + 1 \right)^2 = 0, \quad (7.20)$$

$$S_{xz} = (1 + \alpha_3) \psi_{zz}, \quad (7.21)$$

$$S_{yz} = (1 + \alpha_3) v_z, \quad (7.22)$$

in which incompressibility condition is trivially satisfied. The appropriate boundary conditions are

$$h_1 = 1 + \epsilon_1 \cos 2\pi x, \quad h_2 = -\zeta - \epsilon_2 \cos(2\pi x + \varphi) \quad (7.23)$$

$$\psi = \frac{F_1}{2}, \quad \psi_z = -1, \quad v = 0, \quad \frac{\partial \theta}{\partial z} + Bi_1 \theta = 0 \quad \text{at } z = h_1, \quad (7.24)$$

$$\psi = -\frac{F_1}{2}, \quad \psi_z = -1, \quad v = 0, \quad \frac{\partial \theta}{\partial z} - Bi_1 \theta = 0 \quad \text{at } z = h_2, \quad (7.25)$$

where  $F_1 = \int_0^h \psi_z dz$ ,  $\alpha_3 = \frac{1}{\mu A_3 A_4}$  the fluid parameter,  $\epsilon_1 = \frac{a_1}{d_1}$  and  $\epsilon_2 = \frac{a_2}{d_2}$ .

Eqs. (7.19) and (7.20) give

$$\frac{\partial}{\partial z} \left[ \frac{\partial S_{xz}}{\partial z} + 2T' v + \frac{H^2}{m^2 + \beta^2} \left( \beta \left( \frac{\partial \psi}{\partial z} + 1 \right) - \alpha v \right) \right] = 0, \quad (7.26)$$

$$\frac{\partial S_{yz}}{\partial z} - 2T' \left( \frac{\partial \psi}{\partial z} + 1 \right) + \frac{H^2}{m^2 + \beta^2} \left[ \beta v + m \left( \frac{\partial \psi}{\partial z} + 1 \right) \right] = 0. \quad (7.27)$$

Here we neglect secondary flow pressure due to rotational effect.

### 7.3 Solution methodology

Analytical solution of the system of nonlinear partial differential Eqs. (7.28), (7.29) and (7.22) seems difficult. Thus appropriate numerical method is employed to compute the solution. Numerical technique via shooting method is applied to solve these equations with corresponding boundary conditions (Eqs. (7.25) – (7.27)).

## 7.4 Discussion

Effect of Ree-Eyring fluid parameter  $\alpha_3$  on  $u$ ,  $v$ ,  $\theta$  and  $Z$  are sketched in Figs. 7.1(a – d). Fig. 7.1(a) depicts that axial velocity  $u$  is enhanced for increasing fluid parameter  $\alpha_3$ . In fact viscosity of the fluid decreases as  $\alpha_3$  increases. It is also noteworthy to mention that in non-Newtonian case velocity is greater when compared to viscous fluid ( $\alpha_3 = 0$ ). Opposite behavior of secondary flow  $v$  is captured in Fig. 7.1(b) for larger values of  $\alpha_3$ . In fact due to rotation the fluid particles motion in secondary direction becomes faster and hence  $v$  rapidly decays. Temperature  $\theta$  rises when fluid parameter is enhanced (see Fig. 7.1(c)). Similar result of  $\alpha_3$  is observed in Fig. 7.1(d) for heat transfer rate.

Figs. 7.2(a – d) are demonstrated to see the effects of rotation parameter  $T'$  on  $u$ ,  $v$ ,  $\theta$  and  $Z$  respectively. Fig. 7.2(a) shows dual behavior of axial velocity for  $T'$ . This Fig depicts that rotation parameter decays the axial velocity at centre of channel and near the channel walls it enhances  $u$ . At centre of channel, due to faster rotation the secondary flow is induced which minimizes  $u$ . Impact of rotation parameter  $T'$  on  $v$  is observed through Fig. 7.2(b). In fact an increase in rotation enhances the motion of fluid particles and thus  $v$  has been increased. Fig. 7.2(c) presents the influence of increasing  $T'$  on  $\theta$ . It is because of Coriolis force which is responsible to drag the fluid outwards in the  $y$ -direction and subsequently it reduces the temperature. Heat transfer rate decays for larger values of Taylor number (see Fig. 7.2(d)).

Effect of Hall parameter  $m$  through Figs. 7.3(a – d) can be visualized for  $u$ ,  $v$ ,  $\theta$  and  $Z$  respectively. It is observed from Fig. 7.3(a) that  $u$  tends to rise when  $\alpha$  enhances. It is because of the fact that electrical conductivity of fluid particles reduced as we increase  $m$ . Hence magnetic damping force diminishes and thus axial velocity is enhanced. For larger  $m$  secondary velocity is enhanced (see Fig. 7.3(b)). Similar variation for  $m$  is noticed in study of Hayat et. al [156]. Behavior of  $m$  on temperature  $\theta$  is observed through Fig. 7.3(c). The application of magnetic field offers resistance to flow so kinetic energy decreases and hence there is reduction in temperature. Fluctuation in heat transfer rate  $Z$  for Hall current  $m$  is portrayed in Fig. 7.3(d). Rate of heat transfer decays as we increase Hall parameter  $m$ .

Impact of ionslip parameter  $\beta_i$  on  $u$ ,  $v$ ,  $\theta$  and  $Z$  is portrayed in Figs. 7.4(a – d). Addition of ionslip effect decreases the resistive force imposed by magnetic field and thus effective conductivity decays. Thus decrease in conduction rate enhances the axial velocity (see Fig.



7.4(a)). Fig. 7.4(b) shows increasing behavior of  $v$  for larger values of ionslip parameter. It can be noticed from Fig. 7.4(c) that temperature profile decays with increase in  $\beta$ . Physically it means that kinetic energy of fluid particles decreases for smaller magnetic field. Such decrease in energy implies decay in Joule heating and hence temperature falls. Similar behavior has been reported in [86, 87]. They solved the nonlinear governing equations by employing the perturbation and numerical technique respectively when the system is non-rotating frame. In Fig. 7.4(d) we noticed that near the centerline, the magnitude of heat transfer rate  $Z$  for  $\beta$  decreases whereas near boundaries it enhances.

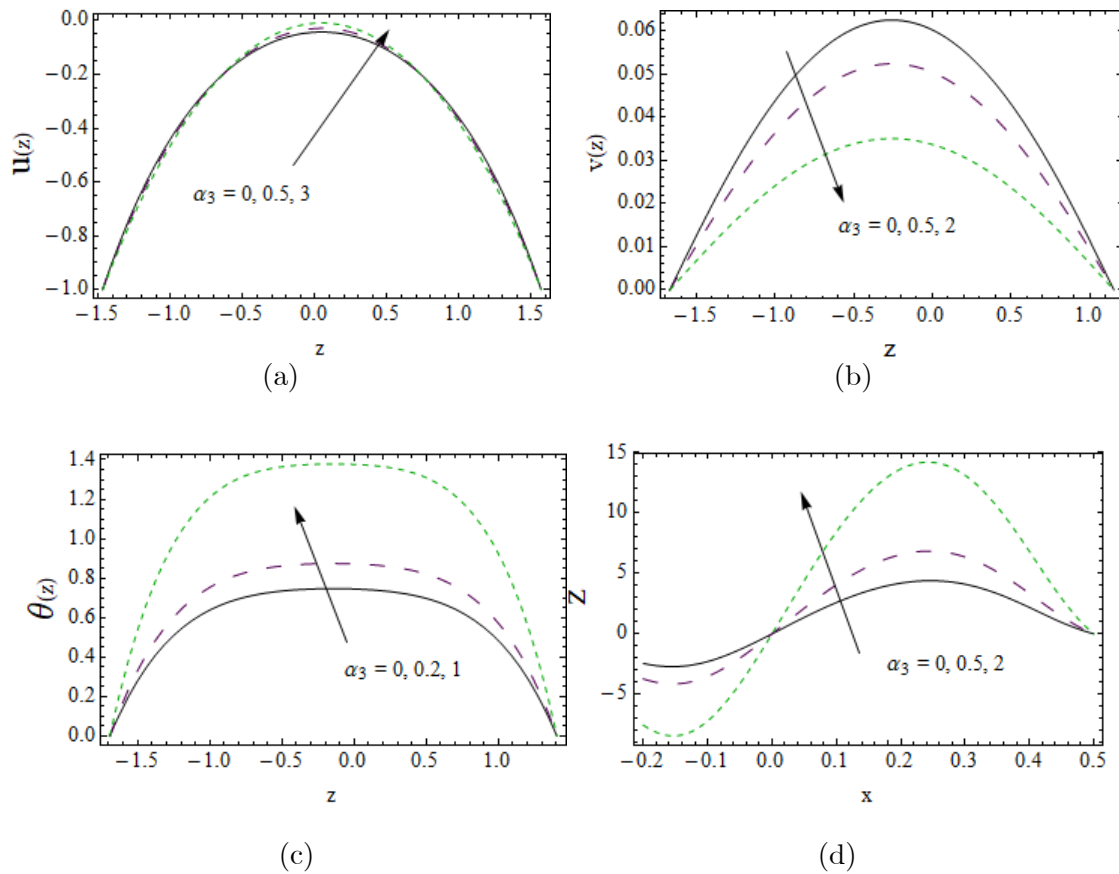


Fig. 7.1: Influence of fluid parameter  $\alpha_3$  on (a)  $u(z)$  (b)  $v(z)$  (c)  $\theta(z)$  (d)  $Z(x)$ .

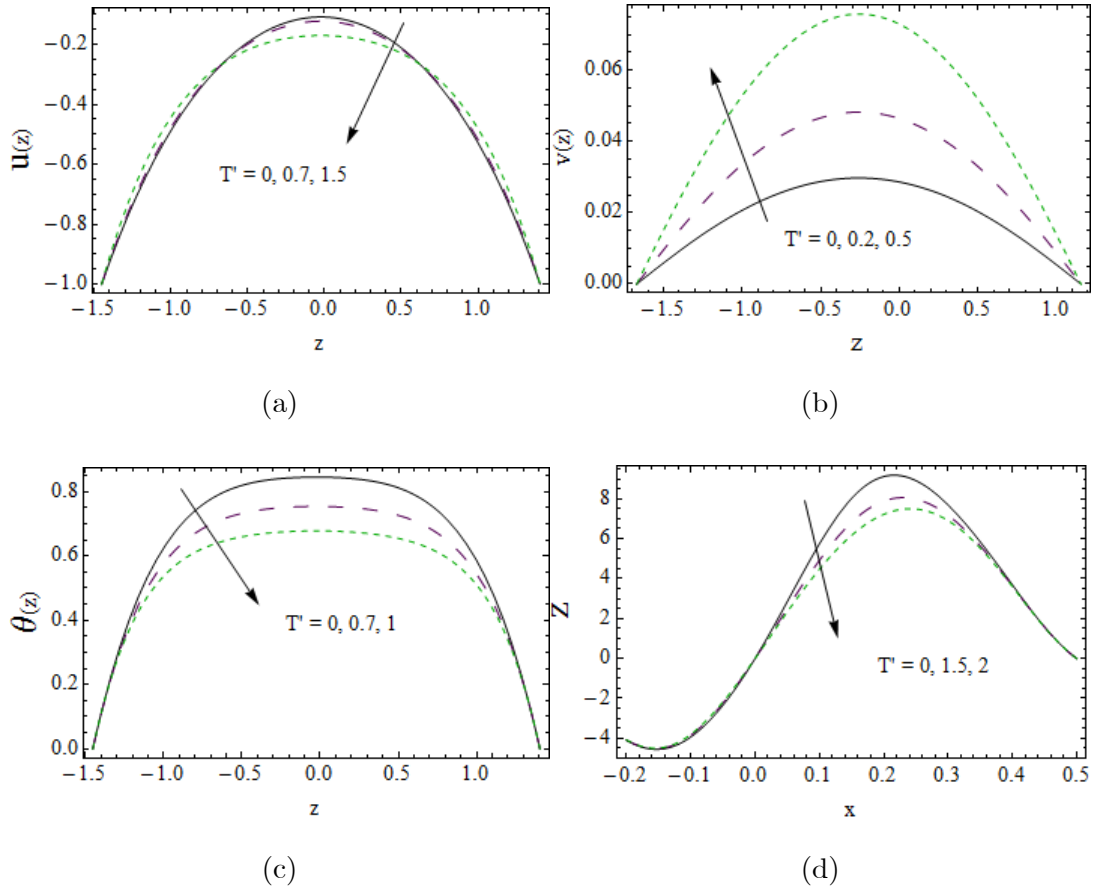
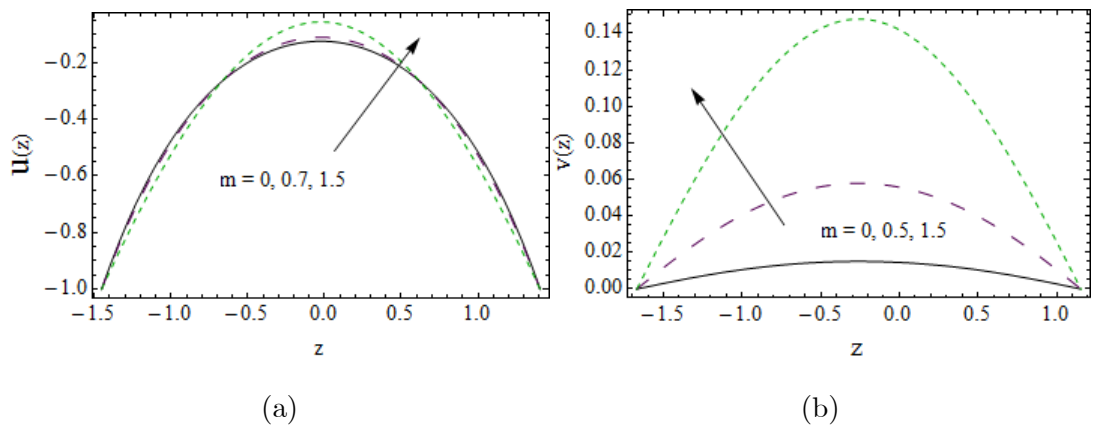


Fig. 7.2: Influence of Taylor number  $T'$  on (a)  $u(z)$  (b)  $v(z)$  (c)  $\theta(z)$  (d)  $Z(x)$ .



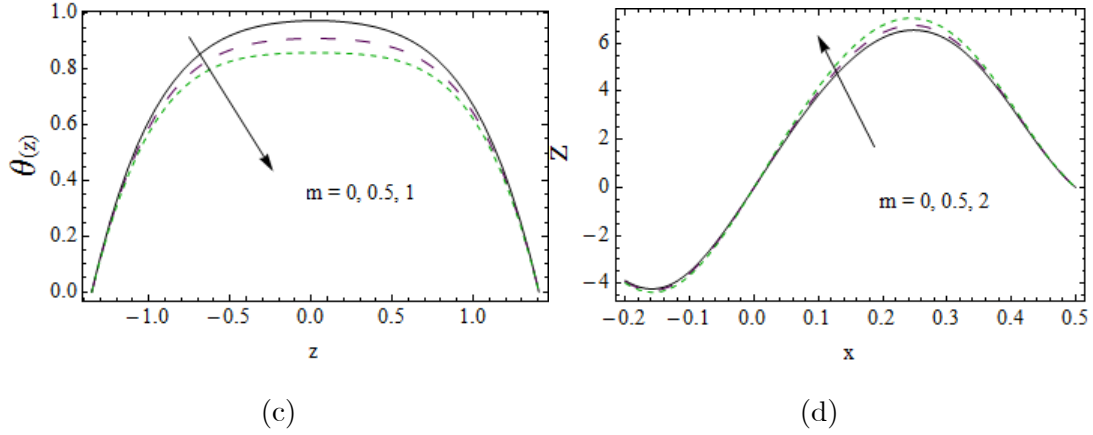


Fig. 7.3: Influence of Hall parameter  $\alpha$  on (a)  $u(z)$  (b)  $v(z)$  (c)  $\theta(z)$  (d)  $Z(x)$ .

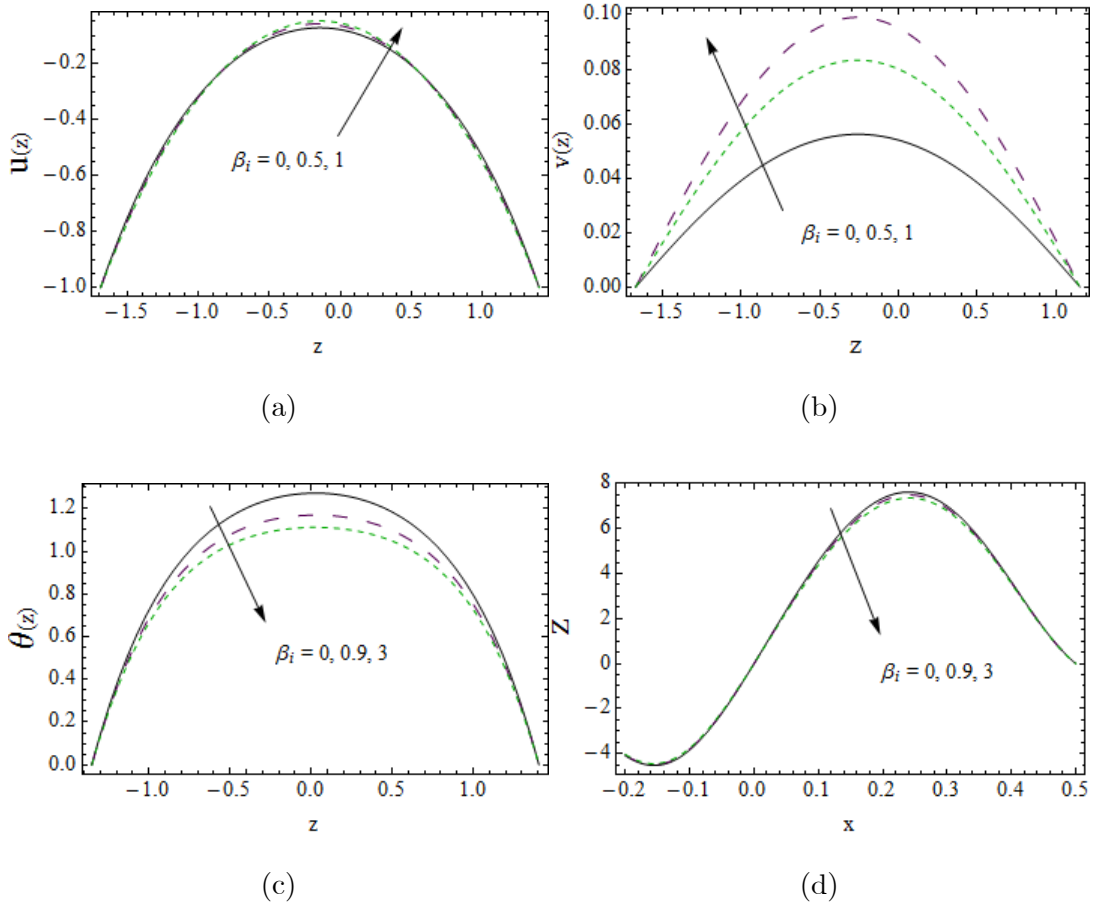


Fig. 7.4: Influence of ionslip parameter  $\beta_i$  on (a)  $u(z)$  (b)  $v(z)$  (c)  $\theta(z)$  (d)  $Z(x)$ .

## 7.5 Conclusions

The present study here investigated the influences of Hall current, Joule heating and ionslip on MHD peristaltic motion of rotating Ree-Eyring fluid. Main salient features are listed below:

- Magnitude of axial velocity  $u$  for Ree-Eyring fluid ( $\alpha_3 \neq 0$ ) is higher than viscous fluid ( $\alpha_3 = 0$ ).
- Effects of  $T'$  on  $u$  and  $v$  are opposite.
- Secondary flow for Ree-Eyring fluid is lower than viscous fluid.
- Variation of  $m$  on  $u$  and  $v$  are similar to that of  $\beta_i$ .
- Temperature is an increasing function of  $\alpha_3$  whereas it decreases for  $T'$ ,  $m$  and  $\beta_i$ .
- Heat transfer rate from walls to the fluid increases when fluid parameter  $\alpha_3$  is enhanced. However it decreases by increasing rotation parameters  $T'$ , Hall parameter  $m$  and ionslip parameter  $\beta_i$ .

## Chapter 8

# Peristalsis of couple stress liquid in a non-uniform rotating geometry

### 8.1 Introduction

Thermal radiation in peristaltic rotating flow of couple stress liquid in a non-uniform channel is addressed. Slip boundary conditions for velocity and temperature are satisfied by channel boundaries. Impact of non-uniform heat source/sink in heat transfer phenomena is also accounted here. Complexity in mathematical formulation of problem is reduced by employing assumptions of long wavelength and low Reynolds number. Resulting non-linear system of equations is solved through numerical technique. The behavior of velocities and temperature for different physical parameters has been displayed through graphs and interpreted physically.

### 8.2 Problem development

Here peristaltic pumping of incompressible couple stress liquid through a nonuniform channel of width  $(d_1 + d_2)$  is examined. Peristaltic transport is engendered by propagation of sinusoidal wavetrains with constant speed  $c$  along channel walls. A solid body rotation is observed in both liquid and channel. The coordinates are chosen in such a way that  $x - axis$  is along centerline and  $z - axis$  is normal to it. Geometrical representation of wall surface is given as

$$\bar{H}_1(\hat{x}, \hat{t}) = d_1 + K\hat{x} + a_1 \cos \left[ \frac{2\pi}{\lambda}(\hat{x} - c\hat{t}) \right], \quad (8.1)$$

$$\bar{H}_2(\hat{x}, \hat{t}) = -d_2 - K\hat{x} - a_2 \cos \left[ \frac{2\pi}{\lambda}(\hat{x} - c\hat{t}) + \varphi \right]. \quad (8.2)$$

The geometry of problem is presented in Fig. 8.1.

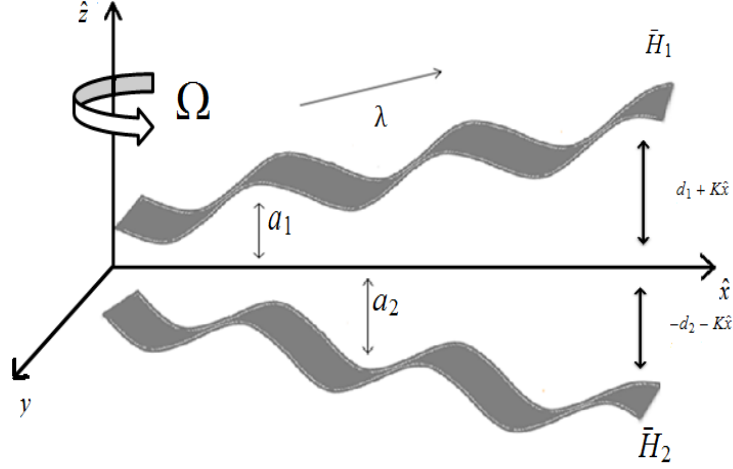


Fig. 8.1: Geometry of problem.

In which  $\hat{t}$  designates the time,  $\varphi$  is the phase difference,  $(a_1, a_2)$  are the amplitudes,  $(\bar{H}_1, \bar{H}_2)$  represent walls of channel and  $\lambda$  is the wavelength.

Mathematical formulation is given as:

$$\nabla \cdot \mathbf{V} = 0, \quad (8.3)$$

$$\rho \left[ \frac{d\mathbf{V}}{d\hat{t}} \right] + \rho [\bar{\Omega} \times (\bar{\Omega} \times \mathbf{V}) + 2\bar{\Omega} \times \mathbf{V}] = -\nabla P + \mu \nabla^2 \mathbf{V} - \mu_1 \nabla^4 \mathbf{V}, \quad (8.4)$$

$$\rho c_p \frac{dT}{d\hat{t}} = k_T \nabla^2 T + \nabla \cdot \mathbf{q}_r + Q_0(T - T_0), \quad (8.5)$$

where

$$\mathbf{q}_r = -\frac{4\sigma^*}{3k^*} \nabla T^4, \quad (8.6)$$

here  $\mu$  is the dynamic viscosity,  $\mu_1$  is couple stress constant,  $Q_0$  is the coefficient non-uniform heat source/sink,  $k^*$  the mean absorption coefficient,  $\sigma^*$  is the Stefan- Boltzmann constant and  $\nabla^2 = \frac{\partial}{\partial x^2} + \frac{\partial}{\partial y^2} + \frac{\partial}{\partial z^2}$  with  $\nabla^4 = \nabla^2 \nabla^2$ .

Laboratory and waves frames are related as:

$$\begin{aligned} x &= \hat{x} - ct, \quad y = \hat{y}, \quad z = \hat{z}, \quad p = \hat{p}(\hat{x}, \hat{y}, \hat{z}), \\ u(x, y, z) &= \hat{u}(\hat{x}, \hat{y}, \hat{z}) - c, \quad v(\hat{x}, \hat{y}, \hat{z}) = \hat{v}(\hat{x}, \hat{y}, \hat{z}), \quad w(\hat{x}, \hat{y}, \hat{z}) = \hat{w}(\hat{x}, \hat{y}, \hat{z}). \end{aligned} \quad (8.7)$$

Invoking above transformations, Eqs. (8.3 – 8.5) take the form:

$$u_x + w_z = 0, \quad (8.8)$$

$$\rho[(u + c)u_x + vu_y + wu_z - 2\Omega v] = -p_x + \mu \nabla^2(u + c) - \mu_1 \nabla^4(u + c), \quad (8.9)$$

$$\rho[(u + c)v_x + vv_y + wv_z + 2\Omega(u + c)] = -p_y + \mu \nabla^2 v - \mu_1 \nabla^4 v, \quad (8.10)$$

$$\rho[(u + c)w_x + vw_y + ww_z] = -p_z + \mu \nabla^2 w - \mu_1 \nabla^4 w, \quad (8.11)$$

$$\rho c_p [T_x + vT_y + wT_z] = k_T [T_{xx} + T_{yy} + T_{zz}] - (q_r)_z + Q_0(T - T_0). \quad (8.12)$$

Dimensionless quantities involved in problem are listed below:

$$\begin{aligned} x^* &= \frac{x}{\lambda}, \quad y^* = \frac{y}{\lambda}, \quad z^* = \frac{z}{d_1}, \quad t^* = \frac{ct}{\lambda}, \quad p^* = \frac{l_1^2 \bar{p}}{\mu_0 c \lambda}, \quad h_1 = \frac{\bar{H}_1}{d_1}, \quad h_2 = \frac{\bar{H}_2}{d_2}, \\ \epsilon_1 &= \frac{a_1}{d_1}, \quad \epsilon_2 = \frac{a_2}{d_1}, \quad d = \frac{d_2}{d_1}, \quad u^* = \frac{u}{c}, \quad v^* = \frac{v}{c}, \quad w^* = \frac{w}{c}, \quad \eta^* = \frac{\eta}{d_1}, \quad \nu = \frac{\mu}{\rho}, \\ \theta &= \frac{T - T_0}{T_1 - T_0}, \quad \delta = \frac{d}{\lambda}, \quad \text{Re} = \frac{cd_1}{\mu}, \quad \alpha_4 = \sqrt{\frac{\mu}{\eta}} d_1, \quad T' = \frac{\text{Re} \bar{\Omega} d}{c}, \\ Pr &= \frac{\mu c_p}{k_T}, \quad R_n = \frac{16\sigma^*}{3k_T k^{**}} T_0^3, \quad S = \frac{Q_0 d^2}{k_T}, \quad Bi_1 = \frac{\hat{h}_1 d}{k_T}, \quad k = \frac{K}{d_1}, \quad \beta^* = \frac{\beta}{d_1}, \\ \beta_1^* &= \frac{\beta_1}{d_1}, \quad \beta_2^* = \frac{\beta_2}{d_1}, \quad u = \psi_z, \quad w = -\delta \psi_x. \end{aligned} \quad (8.13)$$

Adopting lubrication approach, Eqs. (8.8) – (8.11) are reduced to

$$p_x = \psi_{zzz} - \frac{1}{\alpha_4^2} \psi_{zzzzz} + 2T' v, \quad (8.14)$$

$$p_y = v_{zz} - \frac{1}{\alpha_4^2} v_{zzzz} + 2T'(\psi_z + 1), \quad (8.15)$$

$$p_z = 0, \quad (8.16)$$

$$(1 + \text{Pr } R_n)\theta_{zz} + S\theta = 0. \quad (8.17)$$

Defining

$$F_1 = \eta - 1 - d, \quad (8.18)$$

with

$$F_1 = \int_{h_1}^{h_2} \psi_z dz,$$

and the dimensionless conditions

$$h_1 = 1 + kx + \epsilon_1 \cos(2\pi x), \quad h_2 = -d - kx - \epsilon_2 \cos(2\pi x + \varphi), \quad (8.19)$$

$$\begin{aligned} \psi &= \frac{F_1}{2}, \quad \psi_{zzz} = 0, \quad \psi_z + \beta\psi_{zz} = -1, \quad v_{zz} = 0, \\ v_z + \beta_1 v_{zz} &= -1, \quad \theta + \beta_2 \theta_z = 1, \quad \text{at } z = h_1, \end{aligned} \quad (8.20)$$

$$\begin{aligned} \psi &= -\frac{F_1}{2}, \quad \psi_{zzz} = 0, \quad \psi_z - \beta\psi_{zz} = -1, \quad v_{zz} = 0, \\ v_z - \beta_1 v_{zz} &= -1, \quad \theta - \beta_2 \theta_z = 0, \quad \text{at } z = h_2, \end{aligned} \quad (8.21)$$

where  $\psi$  denotes stream function,  $\beta$  axial velocity slip,  $\beta_1$  secondary velocity slip and  $\beta_2$  temperature slip parameters.

Eq. (8.15) indicates that  $p \neq p(z)$  and thus compatibility equation satisfies

$$\psi_{zzzzzz} - \alpha_4^2 \psi_{zzzz} - 2T' \alpha_4^2 v = 0 \quad (8.22)$$

and Eq. (8.14) becomes

$$v_{zzzz} - \alpha_4^2 v_{zz} + 2T' \alpha_4^2 (\psi_z + 1) = 0. \quad (8.23)$$

### 8.3 Solution methodology

Built-in routine NDSolve in Mathematica is utilized to get numerical solution for reduced system of equations. In this section graphical results are drawn to observe the impact of pertinent



parameters on velocities and temperature.

## 8.4 Discussion

### 8.4.1 Axial velocity

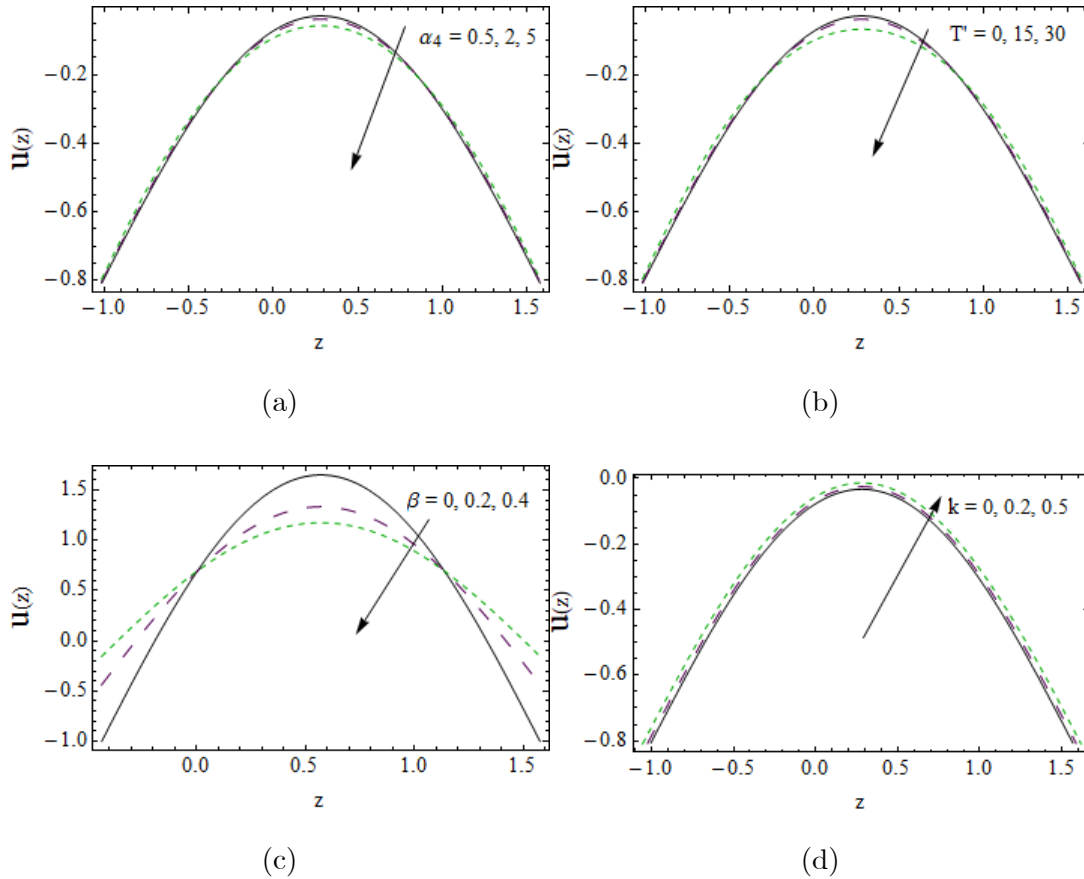
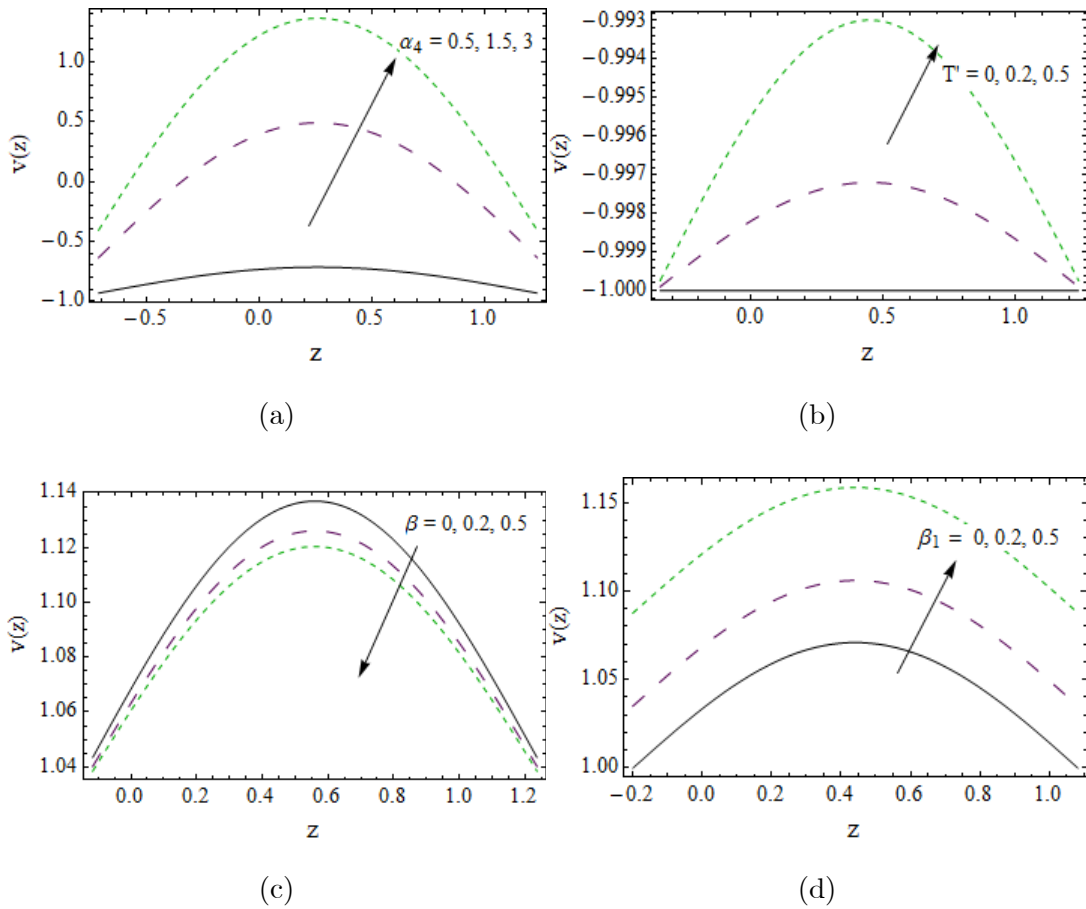


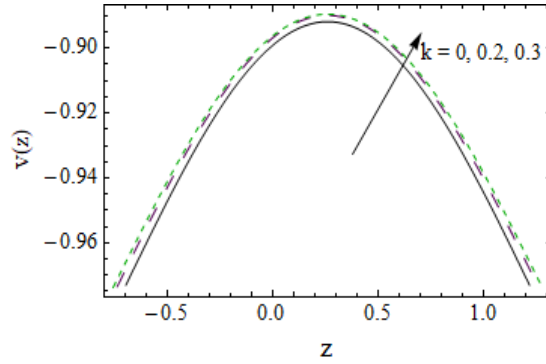
Fig. 8.2: Graph of  $u(z)$  for (a)  $\alpha_4$  (b)  $T'$  (c)  $\beta$  (d)  $k^*$ .

The axial velocity  $u$  against sundry variables are shown in Figs. 8.2(a – d). Fig. 8.2(a) manifests the impact of couple stress parameter  $\alpha_4$  on axial velocity. It is obvious that velocity declines at the center of channel whereas it grows near channel walls. Physically for rising values of  $\alpha_4$  stress among fluid particles increases which in turn produces a decay in velocity. It can be seen through Fig. 8.2(b) that there is a decrease in velocity at center of channel for increase in Taylor number  $T'$ . In fact secondary flow along  $y$  – axis produced by rotation resists

the flow and hence velocity declines. Variation in  $u$  for larger slip parameter  $\beta$  is manifested in Fig. 8.2(c). Velocity decreases via increasing  $\beta$  because fluid experiences more slip at the channel walls which in turn reduces  $u$ . Inverse relation between velocity and non-uniformity parameter is illustrated in Fig. 8.2(d). A gradual increase in velocity is observed for increasing values of  $k$ . It is due to decrease in frictional force offered by channel walls.

### 8.4.2 Secondary velocity





(e)

Fig. 8.3: Graph of  $v$  for (a)  $\alpha_4$  (b)  $T'$  (c)  $\beta$  (d)  $\beta_1$  (e)  $k^*$ .

In this section, variation in secondary velocity for involved parameters is investigated through Figs. 8.3(a – e). Fig. 8.3(a) indicates that secondary velocity grows for enhancing values of fluid parameter  $\alpha_4$ . Influence of Taylor number on velocity profile is displayed in Fig. 8.3(b). It is obvious that velocity increases via  $T'$  because of enhancement in rotation of fluid and channel. Effect of axial velocity slip parameter of secondary velocity is manifested through Fig. 8.3(c). The resulting panel exhibit an increment in  $v$  for larger  $\beta$ . Fig. 8.3(d) reveals that velocity is an increasing function of secondary velocity slip parameter  $\beta_1$ . A very small rise in secondary velocity is noticed for growing values of  $k$  as seen through Fig. 8.3(e).

### 8.4.3 Temperature profile

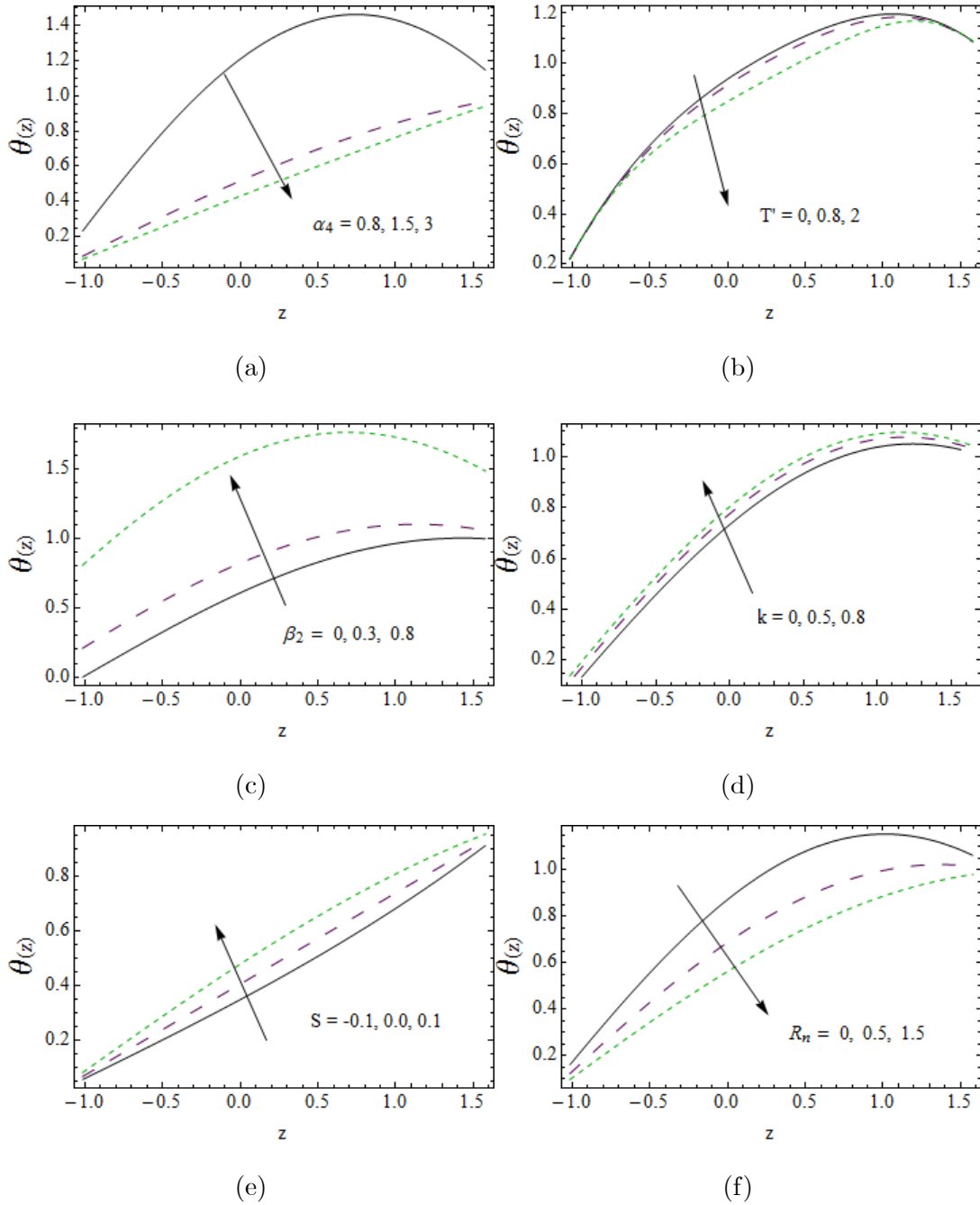
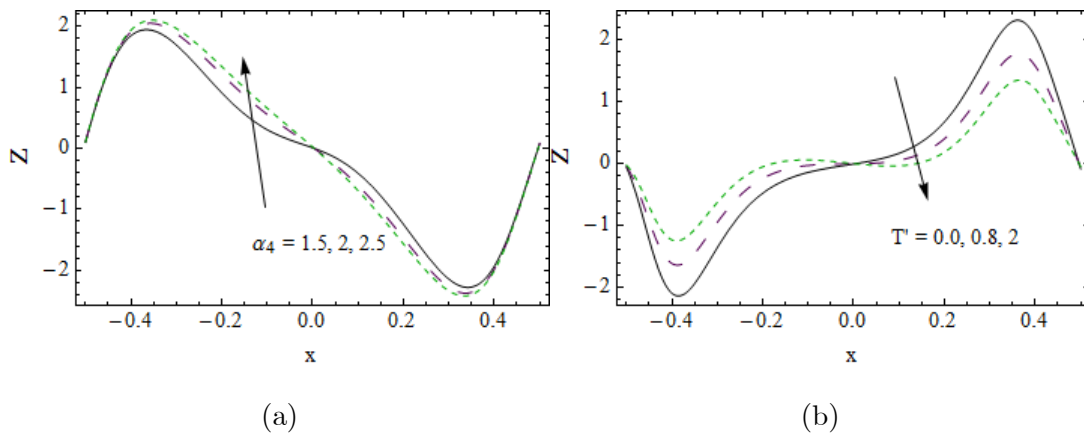


Fig. 8.4: Graph of  $\theta$  for (a)  $\alpha_4$  (b)  $T'$  (c)  $\beta_2$  (d)  $k^*$  (e)  $S$  (f)  $R_n$ .

This subsection is devoted to illustrate the behavior of pertinent parameters on temperature profile through Figs. 8.4(*a – f*). Decreasing response of temperature towards growing fluid parameter is depicted in Fig. 8.4(*a*). As viscosity of fluid enhances via larger values of  $\gamma$  which provides retardation to flow therefore temperature drops. Motion of fluid particles is related with rotation of channel. When Taylor number is increased, fluid particle move rapidly without experiencing any retardation. As a result, temperature decreases (see Fig. 8.4(*b*)). Fig. 8.4(*c*) is plotted to observe the impact of temperature slip parameter on  $\theta$ . For growing values of  $\beta$  kinetic energy of fluid particle increases which produces a rise in temperature. Increasing impression of  $k$  on temperature profile is disclosed in Fig. 8.4(*d*). It is obvious from Fig. 8.4(*e*) that temperature declines for negative values of heat generation/absorption coefficient ( $S < 0$ ) whereas a rise in temperature is noticed for its positive values ( $S > 0$ ). In fact for  $S < 0$ , a heat sink is produced which absorbs heat and for ( $S > 0$ ) more heat is added to the system. A decline in temperature for enhancing values of radiation parameter  $Rd$  is evident from Fig. 8.4 (*f*). As effect of natural convection is reduced by adding more radiations therefore temperature declines.

#### 8.4.4 Heat transfer rate



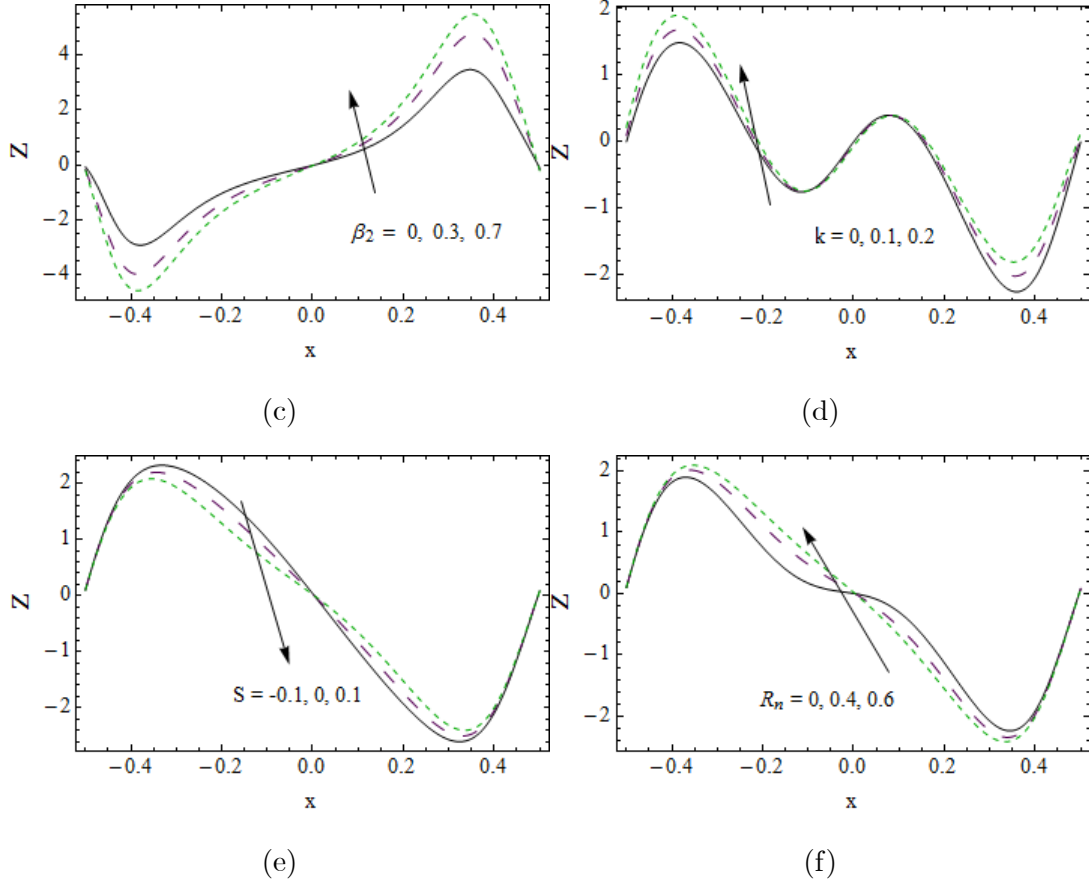


Fig. 8.5: Graph of  $Z$  for (a)  $\alpha_4$  (b)  $T'$  (c)  $\beta_2$  (d)  $k^*$  (e)  $S$  (f)  $R_n$ .

Figs. 8.5(a – f) are prepared to interpret the variation in heat transfer coefficient  $Z$  for multiple values of various physical parameters. Fig. 8.5(a) characterizes increasing influence of fluid parameter  $\alpha_4$  on  $Z$ . It is evident from resulting sketch that magnitude of heat transfer grows for larger  $\alpha_4$ . It is noteworthy that heat transfer coefficient. Fig. 8.5(b) is portrayed for observing the influence of Taylor number  $T'$  on heat transfer coefficient. Result clarifies that heat transfer rate grows via  $T'$ . Fig. 8.5(c) indicates that there is an enhancement in heat transfer coefficient for rising values of slip parameter  $\beta_2$ . An increment in  $Z$  for growing values of non-uniformity parameter  $k$  is reported in Fig. 8.5(d). Magnitude of heat transfer coefficient decays for rise in heat generation/absorption coefficient as depicted in Fig. 8.5(e). Fig. 8.5(f) depicts a decline in  $Z$  for rise in radiation parameter  $R_n$ . A heat loss is generated for stronger thermal radiations and hence  $Z$  decreases.

### 8.4.5 Streamlines

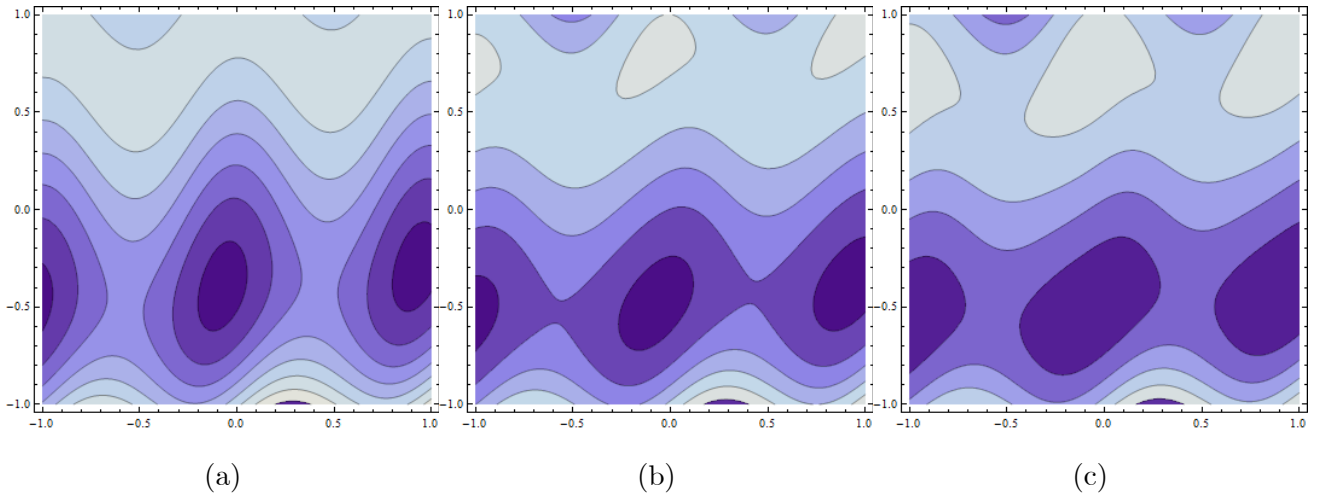


Fig. 8.6: Streamlines for  $T'$  with fixed values of  $k = 0.01$ ,  $\eta = 1.5$ ,  $a = 0.2$ ,  $b = 0.1$ ,  $d = 1.2$ ,  $\phi = \frac{\pi}{2}$ ,  $\beta = \beta_1 = 0.2$ ,  $\gamma = 2$  for (a)  $T' = 0.0$  (b)  $T' = 0.5$  (c)  $T' = 2$ .

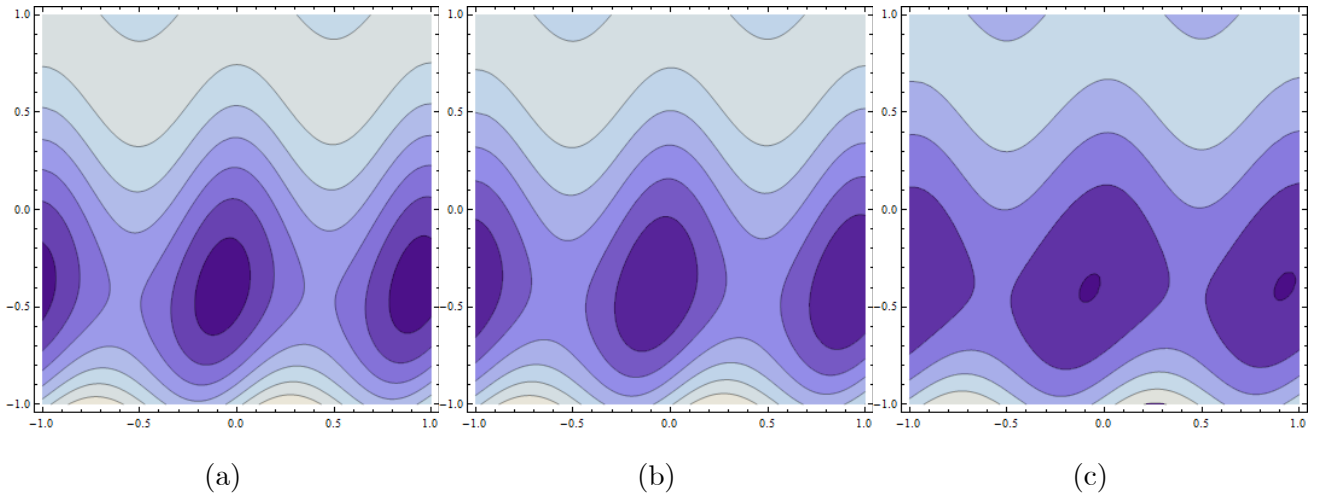


Fig. 8.7: Streamlines for  $\alpha_4$  for (a)  $\alpha_4 = 0.0$  (b)  $\alpha_4 = 2.5$  (c)  $\alpha_4 = 5$ .

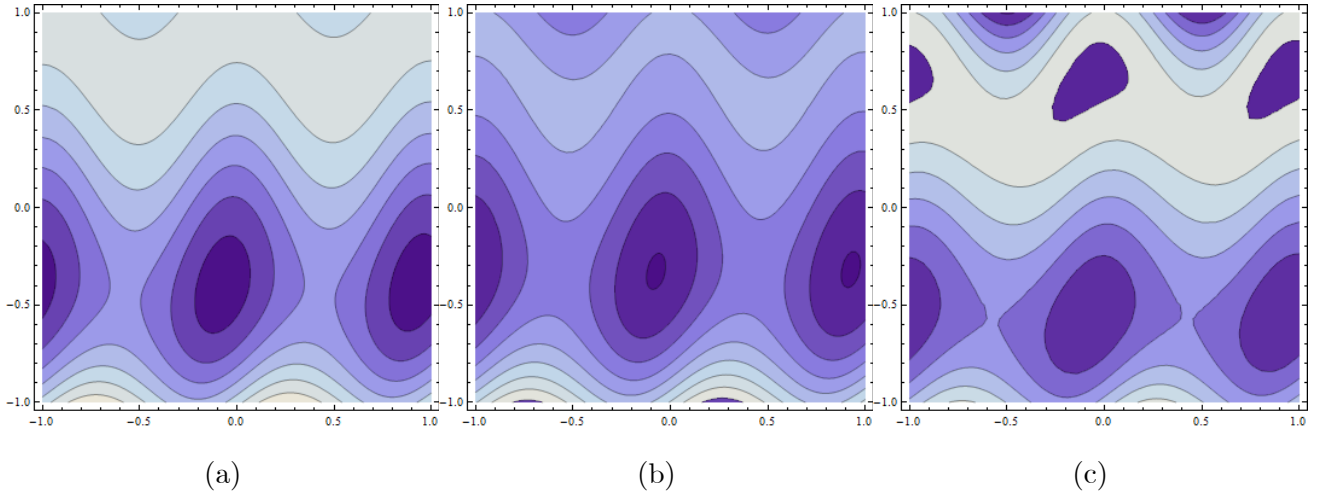


Fig. 8.8: Streamlines for  $\beta$  for (a)  $\beta = 0.2$  (b)  $\beta = 0.4$  (c)  $\beta = 0.6$ .

Figs. 8.6(a – c) are sketched to notice the effect of Taylor number on trapping phenomenon. The size of trapping bolus decreases at lower channel for increase in rotation. It is also clear that trapping bolus disappears for further rise in  $T'$ . A similar impact is observed for fluid parameter and velocity slip parameter as seen through Figs. 8.7 and 8.8.

## 8.5 Conclusions

Peristaltic pumping of couple stress fluid under the influences of heat source/sink, thermal radiation and slip conditions is examined. Key findings of investigation are given by:

- A decline in axial velocity distribution is observed for increasing values of velocity slip parameter  $\beta$ , fluid parameter  $\alpha_4$  and rotation  $T'$  however velocity increases via non-uniformity parameter  $k$ .
- Similar outcomes of  $\alpha_4$ ,  $T'$ ,  $\beta_1$  and  $k$  on secondary velocity are observed whereas  $\beta$  affects  $v$  oppositely.
- Temperature is increasing function of  $S$ ,  $\beta_2$  and  $k$ .
- There is an inverse relationship between temperature and rising values of  $\alpha_4$ ,  $T'$ ,  $R_n$ .



- Decaying response is depicted by heat transfer coefficient for growing values of  $S$  and  $T'$ .
- Heat transfer coefficient increases via  $R_n$ ,  $\beta_2$ ,  $\alpha_4$  and  $k$ .

## Chapter 9

# Peristaltic motion of third grade fluid subject to nonlinear radiation

### 9.1 Introduction

This chapter addressed nonlinear radiation effect on peristaltic motion of third grade liquid in a tapered asymmetric geometry. System in rotating frame is entertained. Relevant problems have been numerically solved. The velocity, temperature and heat transfer rate are physically stressed.

### 9.2 Problem statement

An incompressible third grade liquid in a tapered channel is considered. The waves with amplitudes  $(a_1, a_2)$  and phase  $\varphi$  are taken. A case of rigid body rotation for channel and fluid is considered. System rotates about  $\hat{z}$ -axis. Nonlinear version of radiation is considered. The waves shapes are described by

$$\bar{H}_1(\hat{x}, \hat{t}) = d_1 + K\hat{x} + a_1 \cos \left[ \frac{2\pi}{\lambda}(\hat{x} - c\hat{t}) \right], \quad (9.1)$$

$$\bar{H}_2(\hat{x}, \hat{t}) = -d_2 - K\hat{x} - a_2 \cos \left[ \frac{2\pi}{\lambda}(\hat{x} - c\hat{t}) + \varphi \right]. \quad (9.2)$$

The constitutive equations for third order fluid are

$$\mathbf{T} = -p\mathbf{I} + \mathbf{S}, \quad (9.3)$$

$$\mathbf{S} = \mu\mathbf{A}_1 + \alpha'_1\mathbf{A}_2 + \alpha'_2\mathbf{A}_1^2 + \beta'_1\mathbf{A}_3 + \beta'_2(\mathbf{A}_1\mathbf{A}_2 + \mathbf{A}_2\mathbf{A}_1) + \beta'_3(\text{tra}\mathbf{A}_2)\mathbf{A}_1. \quad (9.4)$$

According to Fosdick and Rajagopal [67]:

$$\mu \geq 0, \alpha'_1 \geq 0, \beta'_1 = \beta'_2 = 0, \beta'_3 \geq 0, |\alpha'_1 + \alpha'_2| \leq \sqrt{24\mu\beta'_3}.$$

Eq. (9.4) becomes

$$\mathbf{S} = \mu\mathbf{A}_1 + \alpha'_1\mathbf{A}_2 + \alpha'_2\mathbf{A}_1^2 + \beta'_3(\text{tra}\mathbf{A}_2)\mathbf{A}_1. \quad (9.5)$$

Rotating flow is described by the equations

$$\text{div } \mathbf{V} = 0, \quad (9.6)$$

$$\rho \left[ \frac{\partial \mathbf{V}}{\partial \bar{t}} + (\mathbf{V} \cdot \nabla) \mathbf{V} \right] + \rho [\bar{\Omega} \times (\bar{\Omega} \times \bar{\mathbf{r}}) + 2\bar{\Omega} \times \mathbf{V}] = \text{div } \mathbf{T}, \quad (9.7)$$

$$\rho c_p \frac{dT}{dt} = k_T \nabla^2 T + \nabla \cdot \mathbf{q}_r + \mathbf{T} \cdot \mathbf{L}. \quad (9.8)$$

In above equations  $\alpha'_i (i = 1, 2)$  and  $\beta'_j (j = 1 - 3)$  are material parameters,  $\mathbf{A}_i = (\mathbf{V} \cdot \nabla) \mathbf{A}_{i-1} + \mathbf{A}_{i-1} \mathbf{L} + \mathbf{L}^t \mathbf{A}_{i-1}$ ,  $\mathbf{A}_1 = \mathbf{L} + \mathbf{L}^t$ ,  $\mathbf{L} = \nabla \mathbf{V}$ ,  $\mathbf{V}$  the velocity and  $\bar{\mathbf{r}}$  the position vector. Nonlinear thermal radiation after using Rosseland approximation is given by

$$\mathbf{q}_r = -\frac{4\sigma^*}{3k^*} \frac{\partial T^4}{\partial z} = -\frac{16\sigma^*}{3k^*} T^3 \frac{\partial T}{\partial z}, \quad (9.9)$$

in which  $\sigma^*$  and  $k^*$  represents the Stefan- Boltzmann constant and the mean absorption coefficient respectively.

Applying below transformations

$$\begin{aligned} x &= \hat{x} - ct, \quad y = \hat{y}, \quad z = \hat{z}, \quad p = \hat{p}(\hat{x}, \hat{y}, \hat{z}), \\ u(x, y, z) &= \hat{u}(\hat{x}, \hat{y}, \hat{z}) - c, \quad v(\hat{x}, \hat{y}, \hat{z}) = \hat{v}(\hat{x}, \hat{y}, \hat{z}), \quad w(\hat{x}, \hat{y}, \hat{z}) = \hat{w}(\hat{x}, \hat{y}, \hat{z}), \end{aligned} \quad (9.10)$$

Eqs. (9.6 – 9.8) become

$$(u)_x + (v)_y + (w)_z = 0, \quad (9.11)$$

$$\rho \left\{ (u+c)(u)_x + v(u)_y + w(u)_z - 2\Omega v \right\} = -(p)_x + (S_{xx})_x + (S_{xy})_y + (S_{xz})_z, \quad (9.12)$$

$$\rho \left\{ (u+c)(v)_x + v(v)_y + w(v)_z + 2\Omega(u+c) \right\} = -(p)_y + (S_{yx})_x + (S_{yy})_y + (S_{yz})_z, \quad (9.13)$$

$$\rho \left\{ (u+c)(w)_x + v(w)_y + w(w)_z \right\} = -(p)_z + (S_{zx})_x + (S_{zy})_y + (S_{zz})_z, \quad (9.14)$$

$$\rho c_p \left\{ (T)_x + v(T)_y + w(T)_z \right\} = k_T \left\{ (T)_{xx} + (T)_{yy} + (T)_{zz} \right\} \quad (9.15)$$

$$-(q_r)_z + S_{xx}(u)_x + S_{xz}((u)_z + (w)_x) + S_{zz}(w)_z \quad (9.16)$$

Consider dimensionless variables and stream function as

$$\begin{aligned} x^* &= \frac{x}{\lambda}, \quad y^* = \frac{y}{\lambda}, \quad z^* = \frac{z}{d}, \quad t^* = \frac{ct}{\lambda}, \quad p^* = \frac{d_1 p}{\mu c \lambda}, \quad h_1 = \frac{\bar{H}_1}{d_1}, \quad h_2 = \frac{\bar{H}_2}{d_1}, \\ \epsilon_1 &= \frac{a_1}{d_1}, \quad \epsilon_2 = \frac{a_2}{d_2}, \quad u^* = \frac{u}{c}, \quad v^* = \frac{v}{c}, \quad w^* = \frac{w}{c}, \quad \eta^* = \frac{\eta}{b_1}, \quad \nu = \frac{\mu}{\rho}, \\ \theta &= \frac{T - T_0}{T_1 - T_0}, \quad \delta = \frac{d_1}{\lambda}, \quad \text{Re} = \frac{\rho c d_1}{\mu}, \quad T' = \frac{\text{Re} \bar{\Omega} d}{c}, \quad \theta_m = \frac{T_1}{T_0}, \\ Pr &= \frac{\mu C_p}{k_T}, \quad R_n = \frac{4\sigma^*}{k_T k^*} T_0^3, \quad Bi_1 = \frac{\dot{h}_1 d}{k_T}, \quad Bi_2 = \frac{\dot{h}_2 d}{k_T}, \quad k = \frac{K}{d_1}, \\ \alpha_5 &= \frac{c^2 \beta'_3}{\mu d_1^2}, \quad u = \psi_z, \quad w = -\delta \psi_x. \end{aligned} \quad (9.17)$$

Now applying lubrication approach, Eqs. (9.10) – (9.14) can be reduced as follows:

$$p_x = (S_{xz})_z + 2T'v, \quad (9.18)$$

$$p_y = (S_{yz})_z - 2T'((\psi)_z + 1), \quad (9.19)$$

$$p_z = 0, \quad (9.20)$$

$$\left[ 1 + R_n \text{Pr} (\theta(\theta_m - 1) + 1)^3 \right] (\theta)_{zz} + \left[ 3R_n \text{Pr} (\theta(\theta_m - 1) + 1)^2 (\theta_m - 1) \right] (\theta^2)_z = 0, \quad (9.21)$$

$$\begin{aligned}
S_{xz} &= (\psi)_{zz} + 2\alpha_5((\psi^2)_{zz} + (v^2)_z)(\psi)_{zz}, \\
S_{yz} &= (v)_z + 2\alpha_5((\psi^2)_{zz} + (v^2)_z)(v)_z,
\end{aligned}$$

with dimensionless conditions

$$h_1 = 1 + kx + \epsilon_1 \cos(2\pi x), \quad h_2 = -1 - kx - \epsilon_2 \cos(2\pi x + \varphi), \quad (9.22)$$

$$\psi = \frac{F_1}{2}, \quad (\psi)_z = -1, \quad v = 0, \quad (\theta)_z - Bi_1(1 - \theta) = 0, \quad \text{at } z = h_1, \quad (9.23)$$

$$\psi = -\frac{F_1}{2}, \quad (\psi)_z = -1, \quad v = 0, \quad (\theta)_z - Bi_2(1 + \theta) = 0, \quad \text{at } z = h_2, \quad (9.24)$$

where

$$\begin{aligned}
F_1 &= \eta - 1 - d, \\
F_1 &= \int_{h_1}^{h_2} (\psi)_z dz.
\end{aligned} \quad (9.25)$$

Eqs. (9.16) and (9.17) take the forms:

$$\left( (S_{xz})_z + 2T'v \right)_z = 0, \quad (9.26)$$

$$(S_{yz})_z - 2T'((\psi)_z + 1) = 0. \quad (9.27)$$

## 9.3 Solution methodology

The Eqs. (9.16) – (9.19) and conditions (9.20) – (9.22) have been numerically solved for  $(u, v)$ ,  $\theta$  and  $Z$ .

## 9.4 Discussion

### 9.4.1 Velocity profile

Figs. 9.1(a – c) are displayed for velocity against  $\alpha_5$ ,  $k$  and  $T'$ . The velocity is generally parabolic. It has maximum value at channel centre. Velocity has dual behavior for  $\alpha_5$ . In upper portion of channel, the axial velocity increases. Physical such increase corresponds to

decay in fluid viscosity. In lower portion of channel, the situation is different (Fig. 9.1(a)). In Fig. 9.1(b),  $u$  at channel centre is an increasing function of  $k$ . Fig. 9.1(c) represents effect of  $T'$  on axial velocity. There is generation of secondary velocity for rotation. It increases  $u$ . Effects of  $\alpha_5$ ,  $k$  and  $T'$  on secondary velocity are shown in Figs. 9.2(a – c). There is decay in  $v$  for  $\alpha_5$  (Fig. 9.2(a)). Also secondary velocity decays for  $k$  (Fig. 9.2(b)). The reason behind this fact is that fluid rapidly compressed in narrow portion and induced frictional force at wall is reduced. Fig. 9.2(c) indicates  $v$  against  $T'$ . Gradual increase in  $v$  is observed for  $T'$ . This happens due to faster rotation of liquid particles.

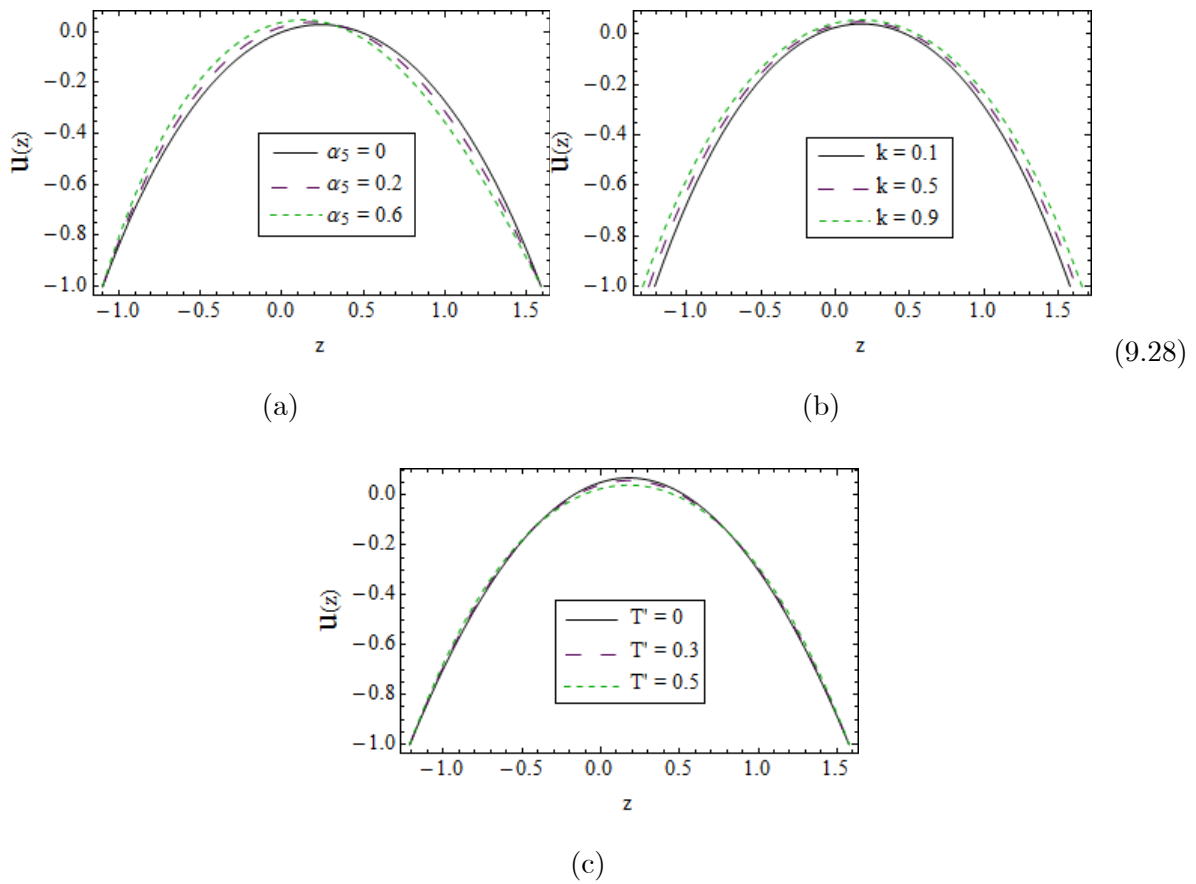


Fig. 9.1: Influence of (a)  $\alpha_5$  (b)  $k$  (c)  $T'$  on  $u(z)$  when  $k = 0.2$ ,  $x = 0.1$ ,  $\eta = 1$ ,  $\epsilon_1 = 0.7$ ,  $\epsilon_2 = 0.5$ ,  $d = 0.8$ ,  $\varphi = \frac{\pi}{4}$ ,  $\alpha_5 = 0.01$  and  $T' = 0.5$ .

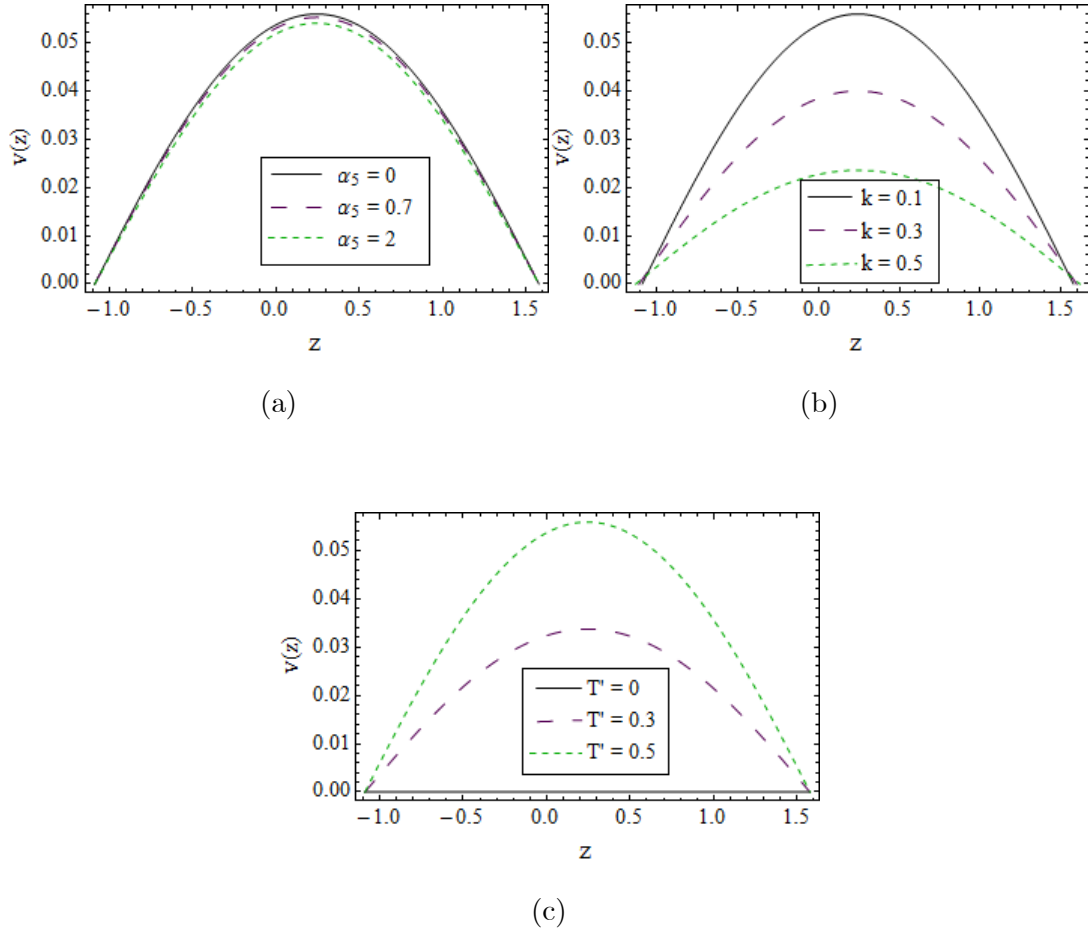
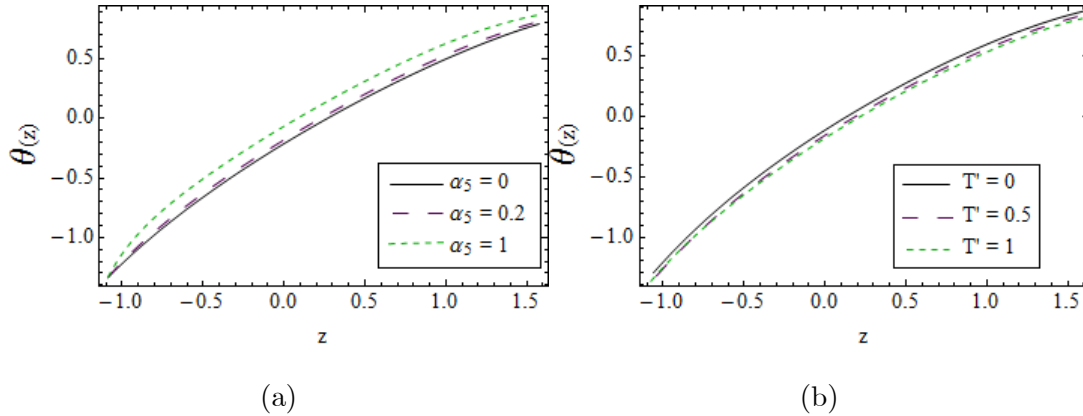


Fig. 9.2: Effect of (a)  $\alpha_5$  (b)  $k$  (c)  $T'$  on  $v(z)$  when  $k = 0.1$ ,  $x = 0.1$ ,  $\eta = -1$ ,  $\epsilon_1 = 0.7$ ,  $\epsilon_2 = 0.5$ ,  $d = 0.8$ ,  $\varphi = \frac{\pi}{4}$ ,  $\alpha_5 = 0.01$  and  $T' = 0.5$ .

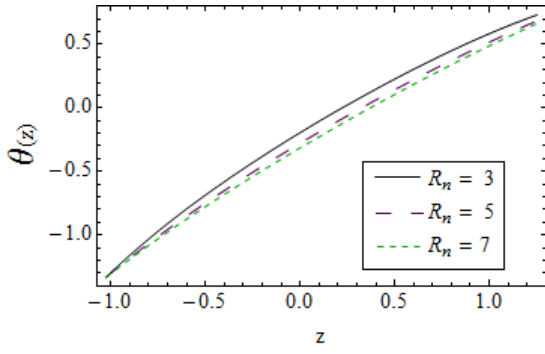
### 9.4.2 Heat transfer

Figs. 9.3(a – h) are sketched for temperature against  $\alpha_5$ ,  $T'$ ,  $R_n$ ,  $\theta_m$ ,  $Bi_1$ ,  $Bi_2$ ,  $Br$  and  $Pr$ . Fluctuation in  $\theta$  for greater  $\alpha_5$  is captured in Fig. 9.3(a). In fact viscosity of fluid decreases. Decrease in  $\theta$  for larger  $T'$  is shown in Fig. 9.3(b). Physically such decrease in  $\theta$  corresponds to faster motion of fluid particles. In Fig. 9.3(c),  $\theta$  is decreasing function of  $R_n$ . There is less energy is absorbed by fluid for greater  $R_n$ , therefore temperature decays. Opposite behavior of temperature ratio parameter  $\theta_m$  on temperature distribution is noticed in Fig. 9.3(d). In fact thermal state of fluid is enhanced with  $\theta_m$  which is responsible for rise in  $\theta$ . Also in the

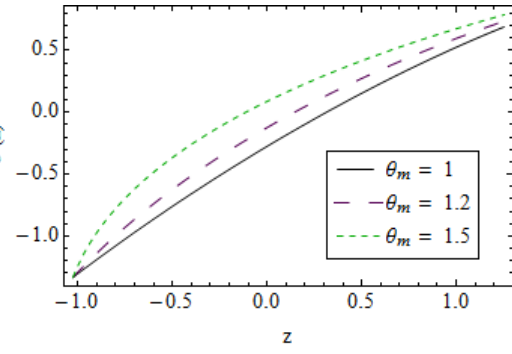
Fig. 9.3(d) solid line obtained for linear radiation problem ( $\theta_m = 1$ ) and dotted lines are computed through Eq. (9.19) with the variation in  $\theta_m$  for nonlinear radiation. It is worth pointing here that when  $\theta_m \approx 1$ , temperature profiles are close to corresponding profiles for the case of linear radiative heat flux. Figs. 9.3(e) and 9.3(f) compare the results of linear and non-linear radiation for different values of radiation when  $\theta_m = 1.1$  and  $\theta_m = 3$  respectively. It is seen that linear and non-linear results match each other better at  $\theta_m = 1.1$  when compared with  $\theta_m = 3$ . The profiles show a significant decrease as the radiation parameter is gradually increased. Similar response of Biot numbers ( $Bi_1, Bi_2$ ) on  $\theta$  at both upper and lower walls are demonstrated through Figs. 9.3(g) and 9.3(h). There is more convection generated with higher values of ( $Bi_1, Bi_2$ ) and consequently temperature is enhanced. Variation for larger  $Br$  on  $\theta$  is sketched in Fig. 9.3(i). In fact viscous dissipation is responsible for enhancement in temperature. Fig. 9.3(j) reveals that  $\theta$  decreases for different values of  $Pr$ . Thermal diffusivity of fluid is reduced with an increase in  $Pr$  and consequently  $\theta$  decays. Figs. 9.4(a–c) are plotted for  $Z$  against different flow physical parameters. We noticed from Fig. 9.4(a) that because of heat loss,  $Z$  decays in magnitude when  $R_n$  increases. For larger  $\theta_m$  and  $Br$ , the reversed trend is followed (see Figs. 9.4(b) and (c)).



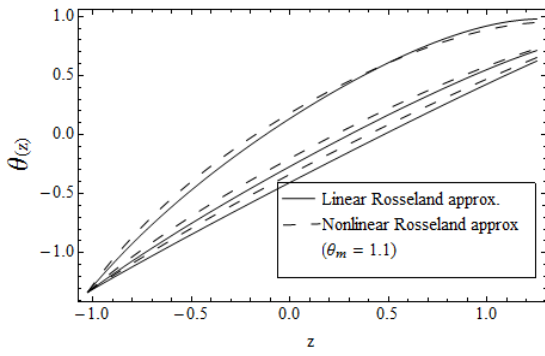




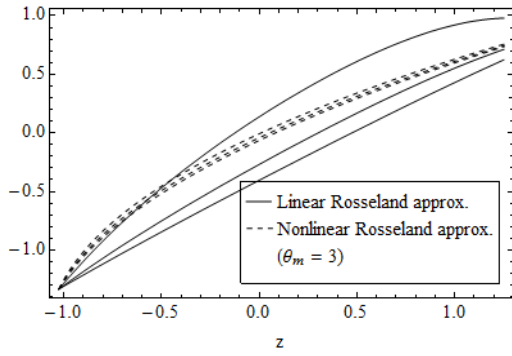
(c)



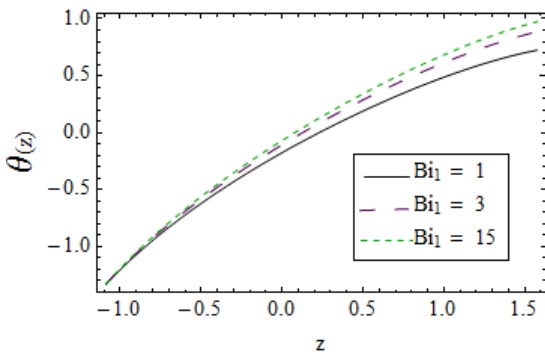
(d)



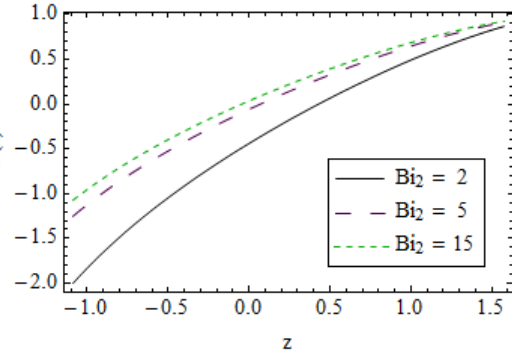
(e)



(f)



(g)



(h)

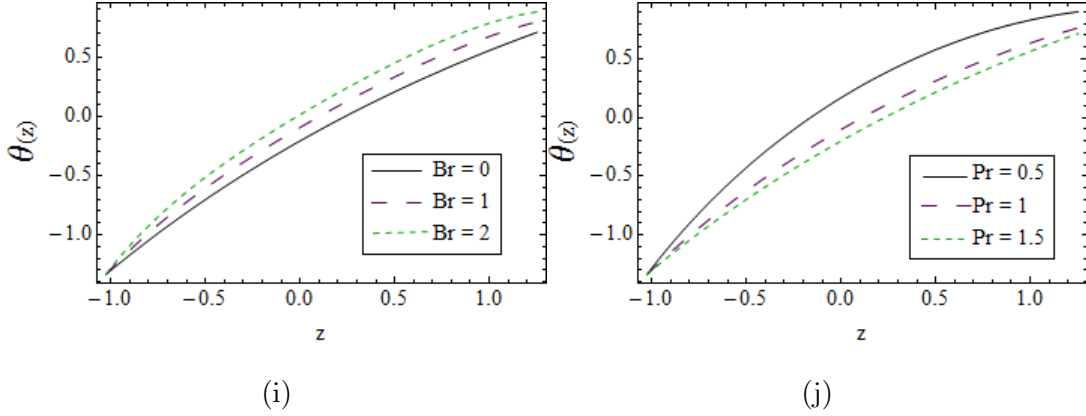


Fig. 9.3: Effect of (a)  $\alpha_5$  (b)  $T'$  (c)  $R_n$  (d)  $\theta_m$  (e) comparison between linear and nonlinear radiation when  $\theta_m = 1.1$  (f) comparison between linear and nonlinear radiation  $\theta_m = 3$  (g)  $Bi_1$  (h)  $Bi_2$  (i)  $Br$  (j)  $Pr$  on  $\theta(z)$  when  $k = 0.1$ ,  $x = 0.1$ ,  $\eta = 1$ ,  $\epsilon_1 = 0.7$ ,  $\epsilon_2 = 0.5$ ,  $d = 0.8$ ,  $\varphi = \frac{\pi}{4}$ ,  $\alpha_5 = 0.01$ ,  $Bi_1 = 2$ ,  $Bi_2 = 4$ ,  $Br = 0.7$ ,  $Pr = 1.5$ ,  $R_n = 3$ ,  $\theta_m = 1.1$  and  $T' = 0.5$ .

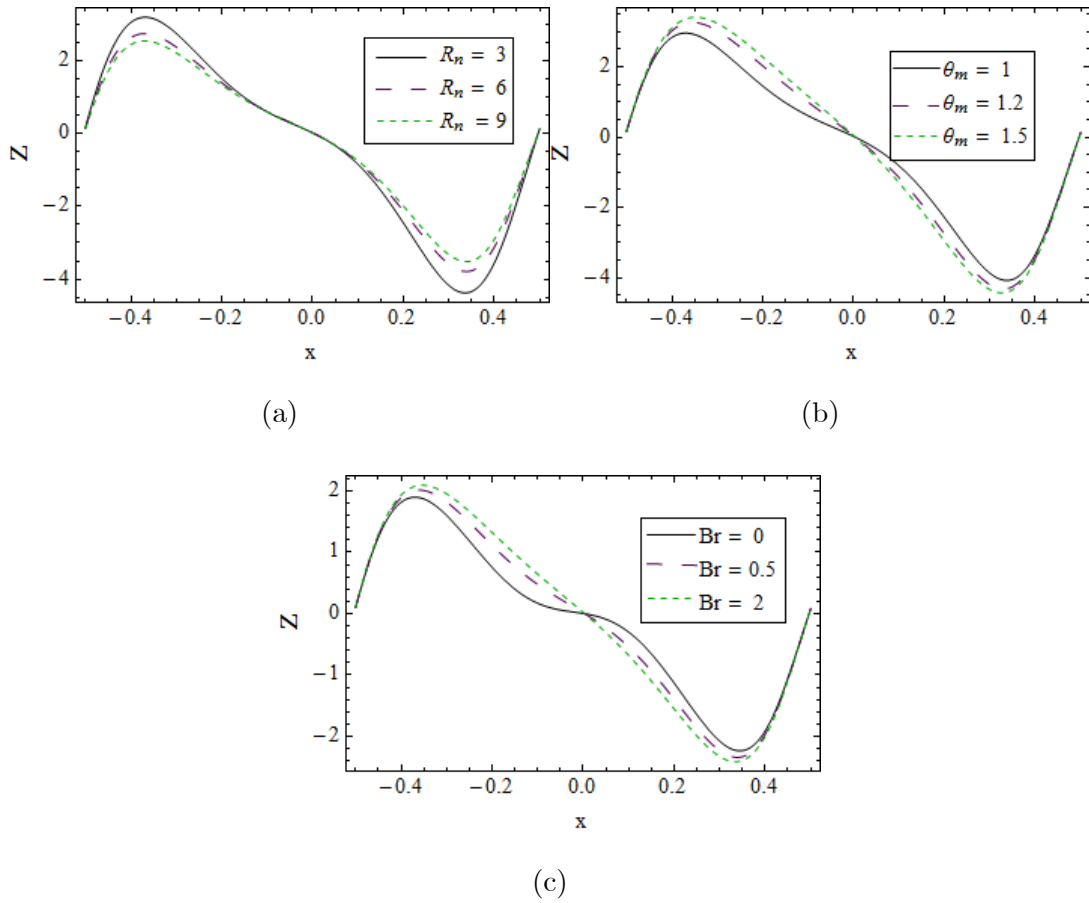


Fig. 9.4: Effect of (a)  $R_n$  (b)  $\theta_m$  (c)  $Br$  on  $Z(x)$  when  $k = 0.1$ ,  $\eta = 1$ ,  $\epsilon_1 = 0.7$ ,  $\epsilon_2 = 0.5$ ,

$$d = 0.8, \varphi = \frac{\pi}{4}, \alpha_5 = 0.01, Bi_1 = 2, Bi_2 = 4, Br = 0.7, Pr = 1.5, R_n = 3, \theta_m = 1.1 \text{ and } T' = 0.5.$$

## 9.5 Conclusions

Main points here are

- There is dual behavior of  $\alpha_5$  velocity.
- Behaviors of  $k$  and  $T'$  on  $u$  are opposite.
- Effect of  $T'$  on  $v$  is reverse to that of  $k$  and  $\alpha_5$ .
- There is decrease in temperature for  $T', R_n$  and  $Pr$ .
- Larger values of  $\alpha_5, \theta_m$  and  $Br$  give rise to temperature.
- Heat transfer rate  $Z$  is enhanced for  $\theta_m$  and  $Br$ .
- $Z$  is decreasing function of  $R_n$ .

## Chapter 10

# Entropy generation impact on peristaltic motion in a rotating frame

### 10.1 Introduction

This chapter intends to investigate the peristalsis of Casson fluid in rotating frame and entropy generation. Constitutive equations are formulated by invoking thermal radiation and viscous dissipation. Slip conditions for temperature and velocity are satisfied. Lubrication approach is employed for reducing the system of equation in simplified form. Exact solutions for resulting systems are obtained. Graphical results are prepared to observe the outcomes of fluid parameter, Brinkman number, compliant wall parameters, Taylor, Bejan number and radiation parameter. Entropy generation is also examined. It is noticed that slip effects can control entropy generation.

### 10.2 Problem definition

Consider an incompressible flow of Casson fluid in channel with width  $2d$ . Compliant properties of channel are studied. Rigid body rotation for fluid and channel through constant  $\Omega$  is discussed. Flow is generated due to travelling waves by wavelength  $\lambda$  and amplitude  $a$ .

Mathematically one has

$$z = \pm\eta(x, t) = \pm \left[ d + a \cos \left\{ \frac{2\pi}{\lambda}(x - ct) \right\} \right]. \quad (10.1)$$

Here we also consider entropy generation through radiation and viscous dissipation effects. The radiative term  $q_r$  is defined as

$$\mathbf{q}_r = -\frac{4\sigma^*}{3k^*} \frac{\partial T^4}{\partial z},$$

in which  $\sigma^*$  and  $k^*$  represent the Stefan-Boltzmann constant and Rosseland's mean absorption coefficient respectively. After expanding  $T_4$  about  $T_0$  and ignoring higher-order terms  $\mathbf{q}_r$  one has

$$\mathbf{q}_r = -\frac{16\sigma^*}{3k^*} T_0^3 \frac{\partial T}{\partial z}. \quad (10.2)$$

For Casson fluid the stress tensor is

$$\begin{aligned} \mathbf{T} &= -p\mathbf{I} + \mathbf{S}, \\ \mathbf{S} &= \left( \mu_B + \sqrt{\frac{2\pi_c}{p_y}} \right) 2e_{ij}, \end{aligned} \quad (10.3)$$

where  $p_y$  is yield stress and  $\pi = e_{ij}$ ,  $e_{ij}$  is the  $(i, j)$  component of deformation rate and  $\mu_B$  a plastic viscosity of fluid. Here

$$e_{ij} = \frac{1}{2} \left( \frac{\partial v_i}{\partial x_j} + \frac{\partial v_j}{\partial y_i} \right).$$

Continuity equation for the flow consideration is

$$\frac{\partial u}{\partial x} + \frac{\partial w}{\partial z} = 0. \quad (10.4)$$

Components of momentum equation in rotating frame are

$$\rho \left[ \frac{\partial u}{\partial t} + u \frac{\partial u}{\partial x} + v \frac{\partial u}{\partial y} + w \frac{\partial u}{\partial z} - 2\Omega v \right] = -\frac{\partial \tilde{p}}{\partial x} + \frac{\partial S_{xx}}{\partial x} + \frac{\partial S_{xy}}{\partial y} + \frac{\partial S_{xz}}{\partial z}, \quad (10.5)$$

$$\rho \left[ \frac{\partial v}{\partial t} + u \frac{\partial v}{\partial x} + v \frac{\partial v}{\partial y} + w \frac{\partial v}{\partial z} + 2\Omega u \right] = -\frac{\partial \tilde{p}}{\partial y} + \frac{\partial S_{yx}}{\partial x} + \frac{\partial S_{yy}}{\partial y} + \frac{\partial S_{yz}}{\partial z}, \quad (10.6)$$

$$\rho \left[ \frac{\partial w}{\partial t} + u \frac{\partial w}{\partial x} + v \frac{\partial w}{\partial y} + w \frac{\partial w}{\partial z} \right] = -\frac{\partial \tilde{p}}{\partial z} + \frac{\partial S_{zx}}{\partial x} + \frac{\partial S_{zy}}{\partial y} + \frac{\partial S_{zz}}{\partial z}, \quad (10.7)$$

Energy equation give

$$\begin{aligned} \rho c_p \left[ \frac{\partial T}{\partial t} + u \frac{\partial T}{\partial x} + v \frac{\partial T}{\partial y} + w \frac{\partial T}{\partial z} \right] &= k_T \left[ \frac{\partial^2 T}{\partial x^2} + \frac{\partial^2 T}{\partial y^2} + \frac{\partial^2 T}{\partial z^2} \right] + \frac{\partial q_r}{\partial z} \\ &+ S_{xx} \frac{\partial u}{\partial x} + S_{xz} \left( \frac{\partial u}{\partial z} + \frac{\partial w}{\partial x} \right) + S_{zz} \frac{\partial w}{\partial z}. \end{aligned} \quad (10.8)$$

Complaint walls equation can be expressed as

$$G(\eta) = p - p_0,$$

with

$$G = -\tau \frac{\partial^2}{\partial x^2} + m \frac{\partial^2}{\partial t^2} + d' \frac{\partial}{\partial t}, \quad (10.9)$$

$$\frac{\partial}{\partial x} G(\eta) = \frac{\partial p}{\partial x} = \frac{\partial S_{xx}}{\partial x} + \frac{\partial S_{xy}}{\partial y} + \frac{\partial S_{xz}}{\partial z} - \rho \left[ \frac{\partial u}{\partial t} + u \frac{\partial u}{\partial x} + v \frac{\partial u}{\partial y} + w \frac{\partial u}{\partial z} - 2\Omega v \right] \quad (10.10)$$

Defining non-dimensional variables and stream function as

$$\begin{aligned} x^* &= \frac{x}{\lambda}, \quad y^* = \frac{y}{\lambda}, \quad z^* = \frac{z}{d}, \quad t^* = \frac{ct}{\lambda}, \quad p^* = \frac{d\tilde{p}}{\mu c \lambda}, \\ u^* &= \frac{u}{c}, \quad v^* = \frac{v}{c}, \quad w^* = \frac{w}{c}, \quad \bar{\eta} = \frac{\eta}{d}, \quad \nu = \frac{\mu}{\rho}, \\ \theta &= \frac{T - T_0}{T_1 - T_0}, \quad \delta = \frac{a}{d}, \quad Re = \frac{\rho c d}{\mu}, \quad T' = \frac{Re \bar{\Omega} d}{c}, \\ Pr &= \frac{\mu C_p}{k_T}, \quad Rd = \frac{4\sigma^*}{k_T k^*} T_0^3, \quad Br = Ec Pr, \quad \alpha_6 = \mu \frac{\sqrt{2\pi c}}{p_y} \\ E_1 &= -\frac{\tau d^3}{\lambda^3 \mu c}, \quad E_2 = \frac{m_1^* c d^3}{\lambda^3 \mu}, \quad E_3 = \frac{d^3 d'}{\mu \lambda^2}, \\ \mathbf{S}_{ij} &= \frac{\mu c}{d} \bar{\mathbf{S}}_{ij}, \quad \bar{\beta}_1 = \frac{\beta_1}{d}, \quad \bar{\beta}_2 = \frac{\beta_2}{d}, \quad \bar{\beta}_3 = \frac{\beta_3}{d}, \end{aligned} \quad (10.11)$$

$$u = \psi_z, \quad w = -\delta \psi_x. \quad (10.12)$$

Eqs. (10.3 – 10.8) in view of large wavelength and small Reynolds are

$$p_x = \frac{\partial}{\partial z} S_{xz} + 2T'v, \quad (10.13)$$

$$p_y = \frac{\partial}{\partial z} S_{yz} - 2T'\psi_z, \quad (10.14)$$

$$p_z = 0, \quad (10.15)$$

$$(1 + RdPr) \frac{\partial^2 \theta}{\partial z^2} + Br S_{xz} = 0, \quad (10.16)$$

$$\begin{aligned} S_{xz} &= \left(1 + \frac{1}{\alpha_6}\right) \frac{\partial^2 \psi}{\partial z^2}, \\ S_{yz} &= \left(1 + \frac{1}{\alpha_6}\right) \frac{\partial v}{\partial z}. \end{aligned} \quad (10.17)$$

Boundary conditions in dimensionless form

$$\frac{\partial \psi}{\partial z} \pm \beta_1 \left(1 + \frac{1}{\alpha_6}\right) \frac{\partial^2 \psi}{\partial z^2} = 0, \quad \text{at } z = \pm \eta, \quad (10.18)$$

$$\left[ E_1 \frac{\partial^3}{\partial x^3} + E_2 \frac{\partial^3}{\partial x \partial t^2} + E_3 \frac{\partial^2}{\partial x \partial t} \right] \eta = \frac{\partial S_{xz}}{\partial z} - 2T'v$$

$$v \pm \beta_2 \left(1 + \frac{1}{\alpha_6}\right) \frac{\partial v}{\partial z} = 0, \quad \text{at } z = \pm \eta, \quad (10.19)$$

$$\left\{ \begin{array}{l} \theta + \beta_3 \frac{\partial \theta}{\partial z} = 1, \\ \theta - \beta_3 \frac{\partial \theta}{\partial z} = 0 \end{array} \right\}, \quad \text{at } z = -\eta, \quad (10.20)$$

where

$$\eta = 1 + \epsilon \sin 2\pi(x - t), \quad (10.21)$$

here  $\alpha$  the fluid parameter. From Eqs. (10.13) to (10.15), we have:

$$\left(1 + \frac{1}{\alpha_6}\right) \frac{\partial^4 \psi}{\partial z^4} + 2T' \frac{\partial v}{\partial z} = 0, \quad (10.22)$$

$$\left(1 + \frac{1}{\alpha_6}\right) \frac{\partial^2 v}{\partial z^2} - 2T' \frac{\partial \psi}{\partial z} = 0. \quad (10.23)$$

### 10.3 Entropy generation

Dimensional form of the entropy generation is given as

$$N_{gen}''' = \frac{k_T}{\theta_0^2} \left[ \left\{ \left( \frac{\partial T}{\partial x} \right)^2 + \left( \frac{\partial T}{\partial z} \right)^2 + \frac{16\sigma^* T_0^3}{3k^*} \left( \frac{\partial T}{\partial z} \right)^2 \right\} \right. \\ \left. + \frac{\mu}{\theta_0} \left[ S_{xx} \frac{\partial u}{\partial x} + S_{xz} \left( \frac{\partial u}{\partial z} + \frac{\partial w}{\partial x} \right) + S_{zz} \frac{\partial w}{\partial z} \right] \right]. \quad (10.24)$$

In dimensionless form, entropy generation can be written as follows:

$$N_{gen} = \frac{N_{gen}'''}{N_g''} = (1 + RdPr) \left( \frac{\partial \theta}{\partial z} \right)^2 + \dot{\lambda} Br \left( 1 + \frac{1}{\alpha} \right) \frac{\partial^2 \psi}{\partial z^2}, \quad (10.25)$$

where  $\dot{\lambda} = \frac{\theta_0}{(T_1 - T_0)}$  and  $N_g'' = \frac{k_T(T_1 - T_0)^2}{\theta_0^2 d^2}$  represents the temperature difference parameter and entropy generation characteristics. In Eq. (10.24) first and second terms corresponds to entropy generation due to heat transfer ( $HT$ ) and fluid friction ( $FF$ ) respectively. Now defining Bejan number  $Be$

$$Be = \frac{HT}{HT + FF}. \quad (10.26)$$

### 10.4 Solution methodology

The exact solutions of equations (10.16, 10.22, 10.23 and 10.25) corresponding to boundary conditions (10.18 – 10.21) are as follows

$$\psi = \left( 6 + 24T'^2 \beta_1 \beta_2 \eta^2 + \alpha_6 (6 + 8T'^2 \beta_2 \eta^2 (3\beta_1 + \eta)) \right)^{-1} \\ Lz [z^2 \alpha_6 - 3\eta (2(1 + \alpha_6) \beta_1 + \alpha_6 \eta)], \quad (10.27)$$

$$v = \left( 4(1 + \alpha_6) (3 + 12T'^2 \beta_1 \beta_2 \eta^2 + \alpha_6 (3 + 4T'^2 \beta_2 \eta^2 (3\beta_1 + \eta))) \right)^{-1} \\ LT' [z^4 \alpha_6^2 - 6z^2 \alpha_6 \eta (2(1 + \alpha_6) \beta_1 + \alpha_6 \eta) + \eta^2 (12(1 + \alpha_6) \beta_1 (2(1 + \alpha_6) \beta_2 \\ + \alpha_6 \eta) + \alpha_6 \eta (8(1 + \alpha_6) \beta_2 + 5\alpha_6 \eta))], \quad (10.28)$$



$$\begin{aligned}
\theta = & \frac{1}{4}[2z(\beta_3 + \eta)^{-1} - ((1 + \text{Pr } Rd)(3(1 + \alpha_6) + 12T'^2(1 + \alpha_6)\beta_1\beta_2\eta^2 \\
& + 4T'^2\alpha_6\beta_2\eta^3)^2)^{-1}3BrL^2z^4\alpha_6(1 + \alpha_6) - 2(\beta_3 + \eta)^{-1}[3BrL^2\eta^3\alpha_6(1 + \alpha_6)(\beta_3 + \eta)(4\beta_3 \\
& + \eta)((1 + \text{Pr } Rd)(3(1 + \alpha_6) + 12T'^2(1 + \alpha_6)\beta_1\beta_2\eta^2 + 4T'^2\alpha_6\beta_2\eta^3)^2)^{-1} \\
& - (-\beta_1 - \eta)(-1 - 3BrL^2\eta^3\alpha_6(1 + \alpha_6)(\beta_3 + \eta)(4\beta_3 + \eta)((1 + \text{Pr } Rd) \\
& (3(1 + \alpha_6) + 12T'^2(1 + \alpha_6)\beta_1\beta_2\eta^2 + 4T'^2\alpha_6\beta_2\eta^3)^2)^{-1}]], \tag{10.29}
\end{aligned}$$

$$\begin{aligned}
N_{gen} = & \frac{1}{4}(1 + \text{Pr } Rd)[(\beta_3 + \eta)^{-1} - ((1 + \text{Pr } Rd)(3(1 + \alpha_6) + 12T'^2(1 + \alpha_6)\beta_1\beta_2\eta^2 \\
& + 4T'^2\alpha_6\beta_2\eta^3)^2)^{-1}6BrL^2z^3\alpha(1 + \alpha) + 9\dot{A}BrL^2z^2\alpha_6(1 + \alpha_6) \\
& ((3 + 12T'^2\beta_1\beta_2\eta^2 + \alpha_6(3 + 4T'^2\alpha_6\beta_2\eta^2(3\beta_1 + \eta)))^2)^{-1}]. \tag{10.30}
\end{aligned}$$

## 10.5 Discussion

Impact of various involved parameters on axial velocity is demonstrated in Figs. (10.1 – 10.5). Fig. 10.1 depicts the variation in  $u$  for multiple values of Taylor's number. It is obvious that velocity declines via  $T'$  since a secondary flow is induced by increase in rotation which decreases velocity of fluid in axial direction. Fig. 10.2 clarifies an enhancement in velocity for growing values of fluid parameter  $\alpha_6$ . It is due to reduction in viscosity of fluid. Fig. 10.3 is plotted to observe the impact of slip parameter  $\beta_1$  on axial velocity. Resulting sketch shows an increment in velocity for larger  $\beta_1$ . In fact for larger slip parameter, less resistance is offered to the fluid which tend to rise the velocity. It can be seen through Fig. 10.4 that axial velocity is a decreasing function of secondary slip parameter  $\beta_2$ . Impact of wall parameters ( $E_1, E_2, E_3$ ) on velocity profile is illustrated through Fig. 10.5. Wall elasticity parameters ( $E_1, E_2$ ) accelerates the flow of fluid however a reduction in velocity is observed for increasing damping parameter  $E_3$ .

Variation in secondary velocity for embedded parameters is analyzed through Figs. (10.6 – 10.9). It is found from Fig. 10.6 that secondary velocity grows for larger fluid parameter  $\alpha_6$ . Secondary velocity  $v$  is an increasing function of Taylor's number as demonstrated in Fig. 10.7. The reason lies behind the fact the fluid moves faster in secondary direction for increase in rotation. Fig. 10.8 serves to manifest the impact of slip parameter  $\beta_2$  on  $v$ . Here velocity grows

via  $\beta_2$ . Impact of wall parameters on secondary velocity is similar as observed for axial velocity (see Fig. 10.9).

Figs. (10.10 – 10.15) characterize the effect of physical parameters on temperature profile. A decline in temperature is obtained for rise in Taylor's number  $T'$  as demonstrated in Fig. 10.10. Fig. 10.11 discloses that temperature of fluid decreases as fluid parameter grows. It due to decrease in viscosity of fluid. Variation in  $\theta$  for larger  $\beta_3$  is portrayed in Fig. 10.12. It is obvious from resulting graph that there is in increment in temperature for enhancing slip parameter. Wall elasticity parameters  $E_i (i = 1, 2)$  tend to rise the temperature however an opposite behavior is noticed for wall damping parameter  $E_3$  (see Fig. 10.13). Fig. 10.14 highlights the decaying outcomes of radiation parameter on temperature profile. Since for higher  $R_n$ , absorbing power of fluid particle tend to reduce and hence temperature drops. Fig. 10.15 determines the behavior of temperature for rising values of Brinkman number  $Br$ . As more heat is generated for stronger viscous dissipation therefore temperature rises.

Figs. (10.16 – 10.21) are captured to investigate the behavior of heat transfer coefficient for variation in pertinent parameters. Decaying response of heat transfer coefficient towards growing Taylor number is recorded in Fig. 10.16. Fluid parameter produces an increment in magnitude heat transfer coefficient as depicted in Fig. 10.17. Physically for larger  $\alpha_6$ , the strength of viscous forces increase. As a result,  $Z$  grows. Fig. 10.18 clarifies that heat transfer coefficient is an increasing function of thermal slip parameter  $\beta_3$ . Since heat transfer coefficient and temperature are in direct relation with each other therefore wall parameters  $E_1, E_2$  and  $E_3$  affect  $Z$  is same manner as that of temperature profile (see Fig. 10.19). Upon increasing radiation parameter, heat transfer coefficient declines as shown in Fig. 10.20. Fig. 10.21 characterizes an inverse relationship between  $Z$  and Brinkman number  $Br$ .

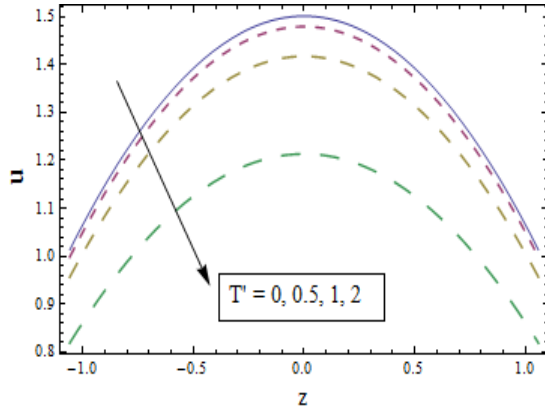


Fig. 10.1

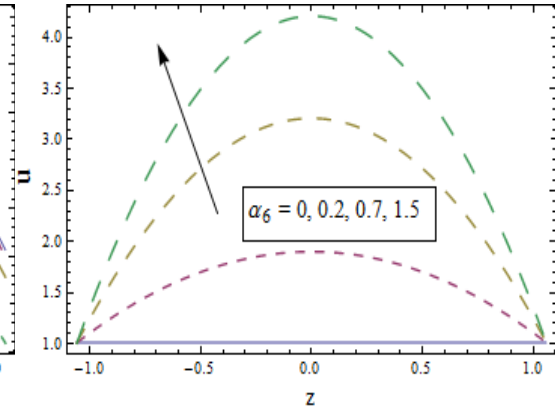


Fig. 10.2

Fig. 10.1: Effect of  $T'$  on  $u(z)$

Fig. 10.2: Effect of  $\alpha_6$  on  $u(z)$ .

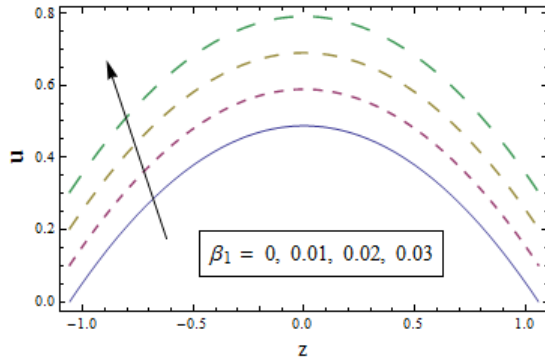


Fig. 10.3

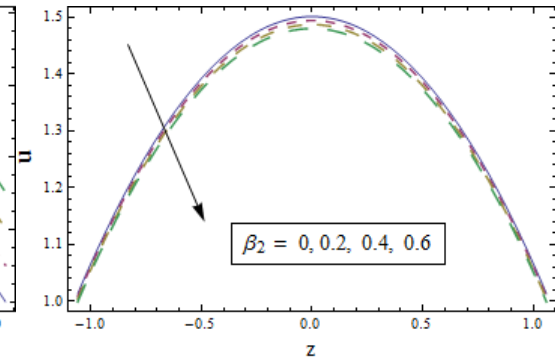


Fig. 10.4

Fig. 10.3: Effect of  $\beta_1$  on  $u(z)$

Fig. 10.4: Effect of  $\beta_2$  on  $u(z)$ .

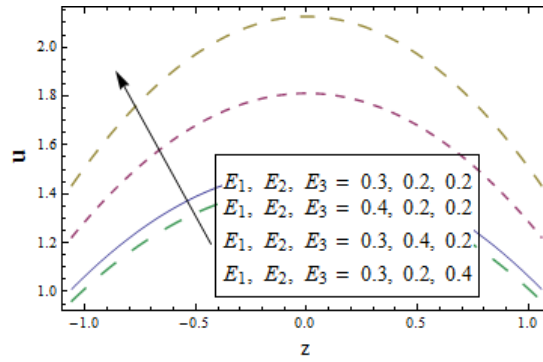


Fig. 10.5

Fig. 10.5: Effect of  $E_1, E_2, E_3$  on  $u(z)$ .

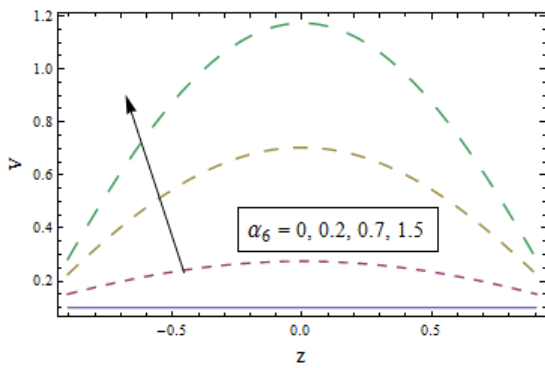


Fig. 10.6

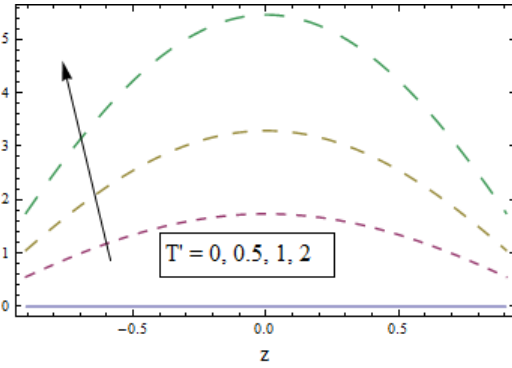


Fig. 10.7

Fig. 10.6: Effect of  $\alpha_6$  on  $v(z)$ .

Fig. 10.7: Effect of  $T'$  on  $v(z)$ .

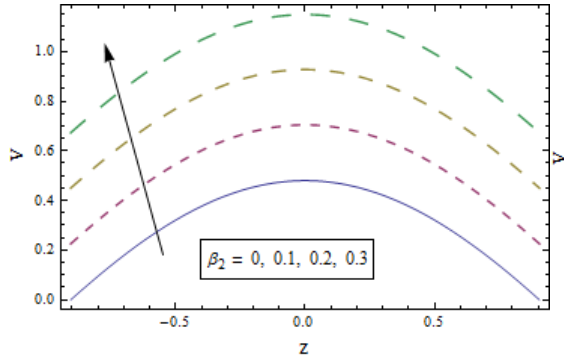


Fig. 10.8

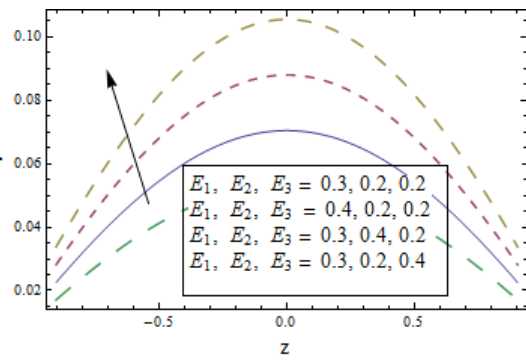


Fig. 10.9

Fig. 10.8: Effect of  $\beta_2$  on  $v(z)$ .

Fig. 10.9: Effect of  $E_1, E_2, E_3$  on  $v(z)$ .

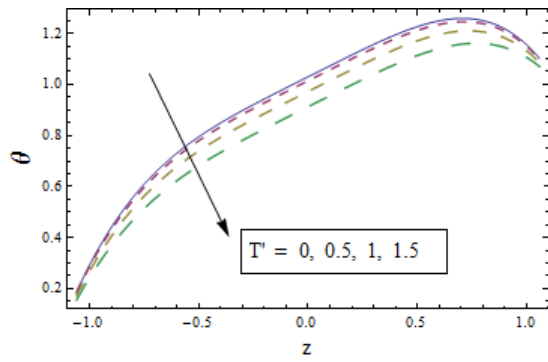


Fig. 10.10

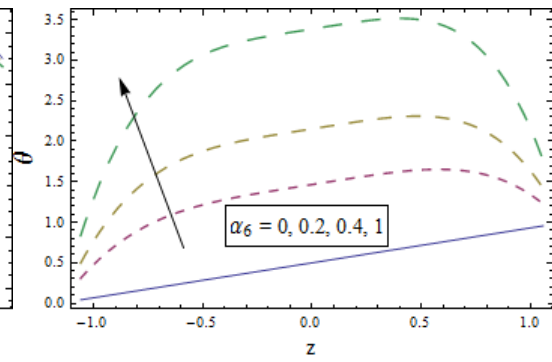


Fig. 10.11

Fig. 10.10: Effect of  $T'$  on  $\theta(z)$ .

Fig. 10.11: Effect of  $\alpha_6$  on  $\theta(z)$ .

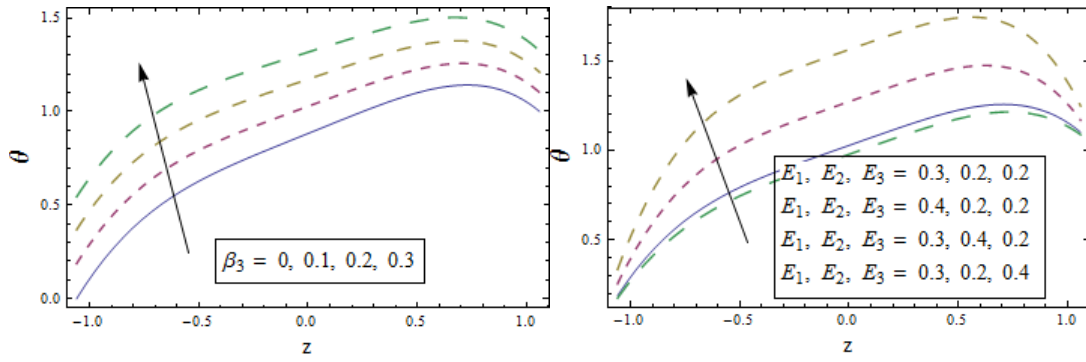


Fig. 10.12

Fig. 10.13

Fig. 10.12: Effect of  $\beta_3$  on  $\theta(z)$ .

Fig. 10.13: Effect of  $E_1, E_2, E_3$  on  $\theta(z)$ .

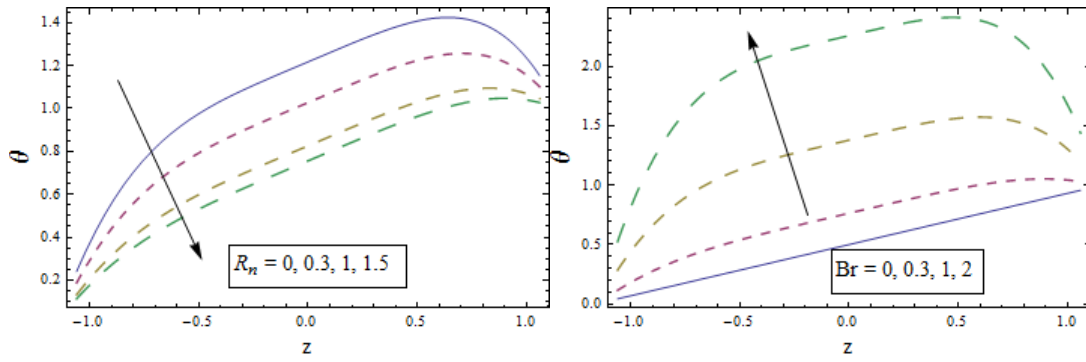


Fig. 10.14

Fig. 10.15

Fig. 10.14: Effect of  $R_n$  on  $\theta(z)$ .

Fig. 10.15: Effect of  $Br$  on  $\theta(z)$ .

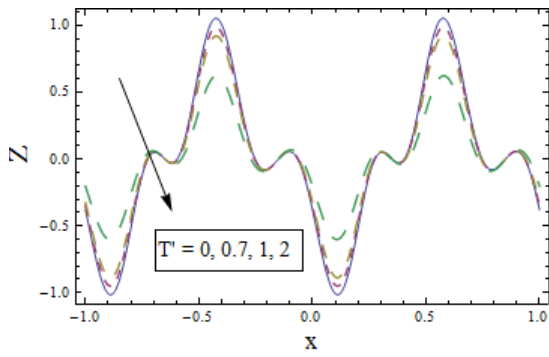


Fig. 10.16

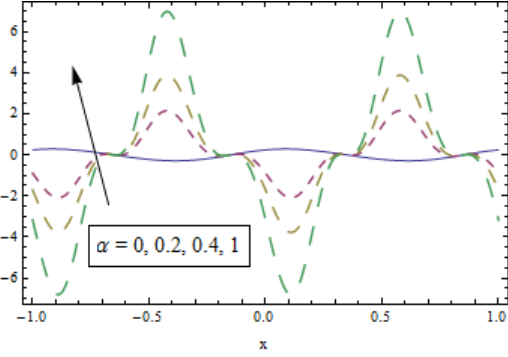


Fig. 10.17

Fig. 10.16: Effect of  $T'$  on  $Z(x)$ .

Fig. 10.17: Effect of  $\alpha_6$  on  $Z(x)$ .

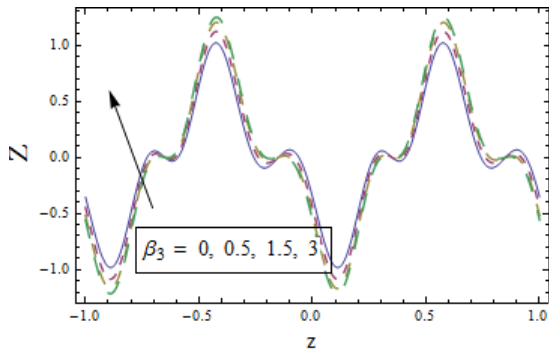


Fig. 10.18

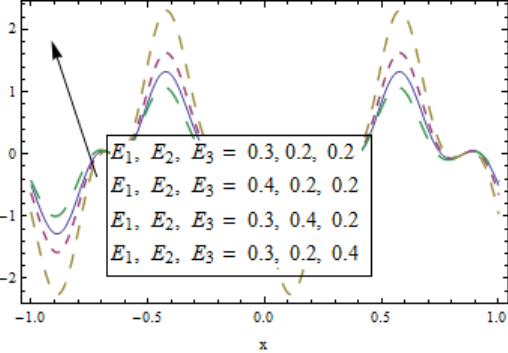


Fig. 10.19

Fig. 10.18: Effect of  $\beta_3$  on  $Z(x)$ .

Fig. 10.19: Effect of  $E_1, E_2, E_3$  on  $Z(x)$ .

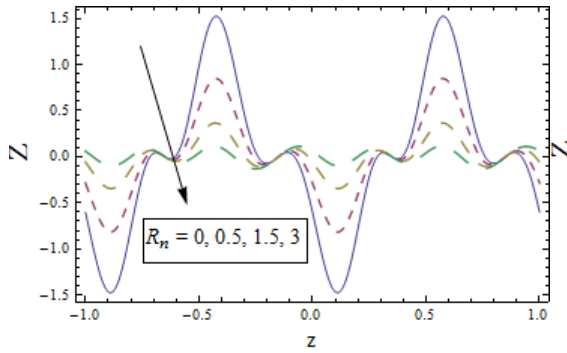


Fig. 10.20

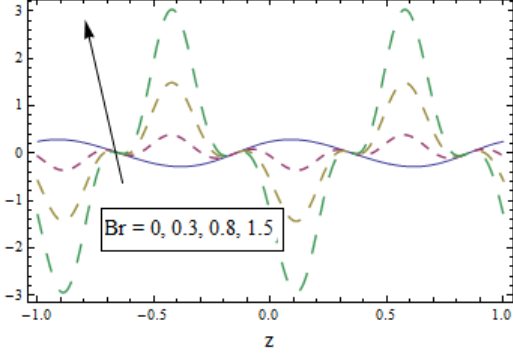


Fig. 10.21

Fig. 10.20: Effect of  $R_n$  on  $Z(x)$ .

Fig. 10.21: Effect of  $Br$  on  $Z(x)$ .

### 10.5.1 Entropy generation

Figs. (10.22 – 10.26) reveal the impression of sundry parameters on entropy generation. Fig. 10.22 displays a growing outcome of fluid parameter on entropy generation. A less entropy is produced at center of channel as compared to channel walls. A reverse relationship is noticed with the larger values of thermal slip, rotation and thermal radiation and can be viewed through Figs. 10.23 – 10.25. When channel is rotated at high speed, more heat is generated and hence entropy declines. Fig. 10.26 indicates a rise in entropy generation via larger values of Brinkman parameter  $BrA^{-1}$ . It is obvious that more disturbance in fluid is generated through larger Brinkman parameter which tend to enhance  $N_s$ .

Figs. 10.27 and 10.28 show that for larger Taylor number and thermal radiation parameter the heat transfer irreversibility is high when compared with total irreversibility for heat transfer and fluid friction. A reduction is demonstrated by  $Be$  for increasing values of fluid and thermal slip parameter (see Figs. 10.29 and 10.30). Figs. 10.29 and 10.30 reveal a development in magnitude of Bejan number for growth in Taylor number and radiation parameter. Kinetic energy of fluid rises via  $T'$  and  $Rd$  which produces an enhancement in  $Be$ . A growing impression of Brinkman number on Bejan number is portrayed in Fig. 10.31.



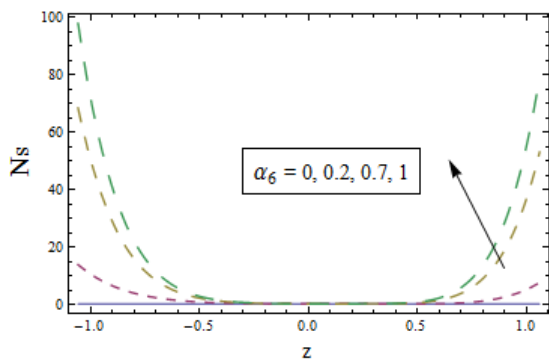


Fig. 10.22

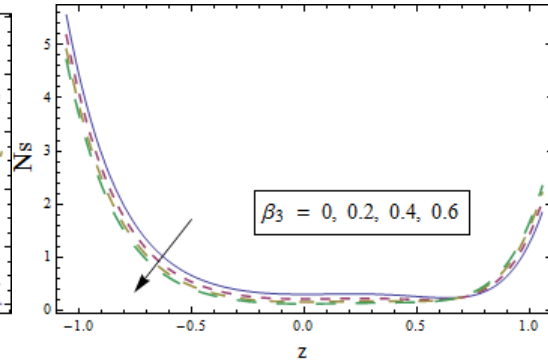


Fig. 10.23

Fig. 10.22: Effect of  $\alpha_6$  on  $N_s$ .

Fig. 10.23: Effect of  $\beta_3$  on  $N_s$ .

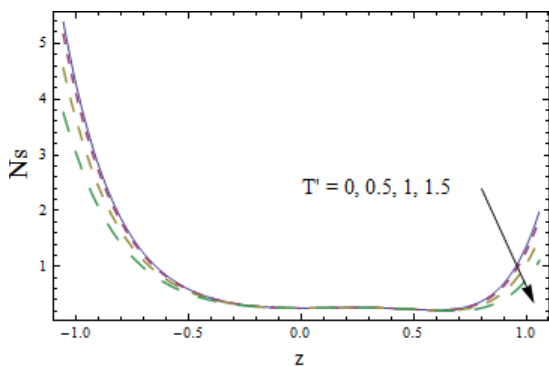


Fig. 10.24

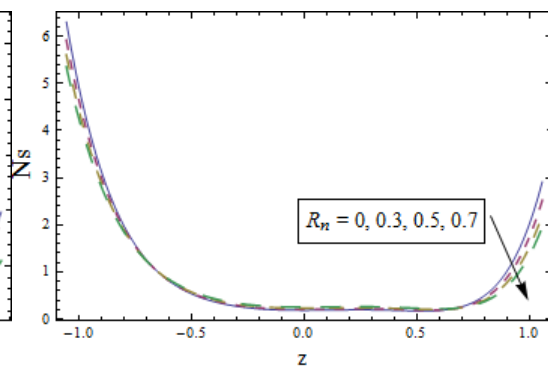


Fig. 10.25

Fig. 10.24: Effect of  $T'$  on  $N_s$ .

Fig. 10.25: Effect of  $R_n$  on  $N_s$ .

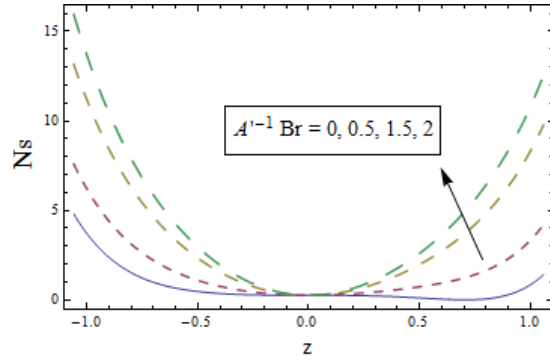


Fig. 10.26

Fig. 10.26: Effect of  $BrA^{-1}$  on  $N_s$ .

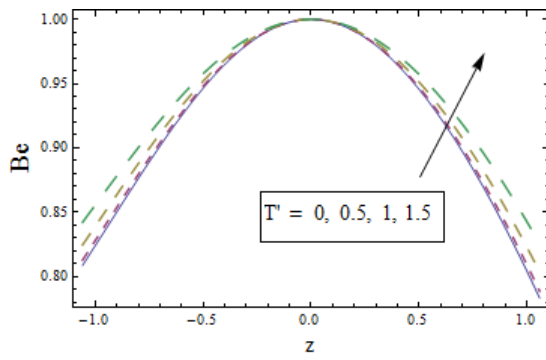


Fig. 10.27

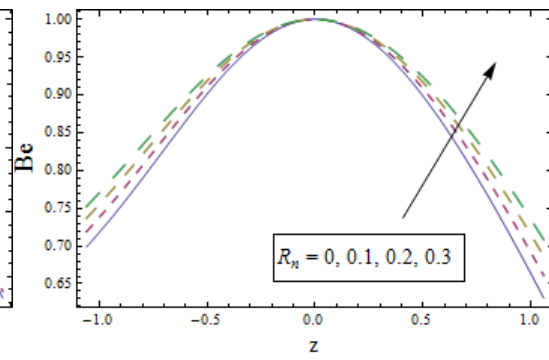


Fig. 10.28

Fig. 10.27: Effect of  $T'$  on  $Be$ .

Fig. 10.28: Effect of  $R_n$  on  $Be$ .

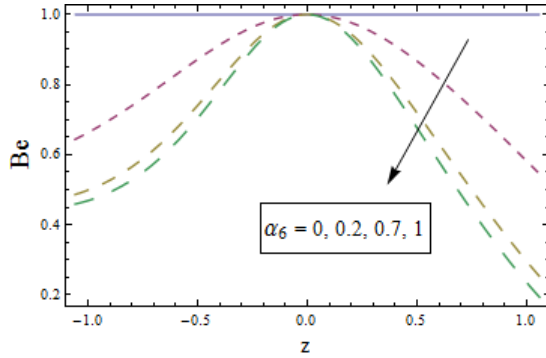


Fig. 10.29

Fig. 10.29: Effect of  $\alpha_6$  on  $Be$ .

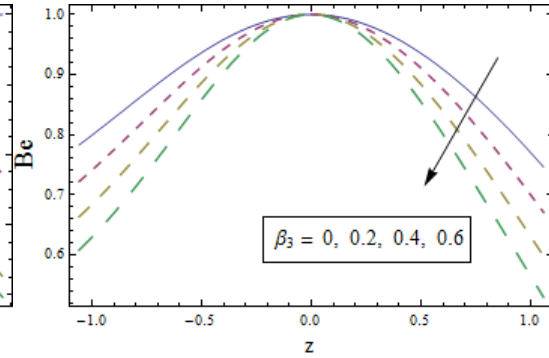


Fig. 10.30

Fig. 10.30: Effect of  $\beta_3$  on  $Be$ .

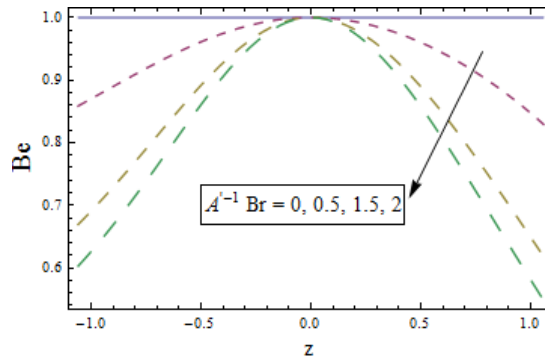


Fig. 10.31

Fig. 10.31: Effect of  $BrA^{-1}$  on  $Be$ .

### 10.5.2 Trapping

In Figs. 10.32 and 10.33, trapping phenomenon is observed for various involved parameters. Fig. 10.32 elucidates that size and number of trapping bolus reduces for larger values of Casson parameter  $\alpha_6$ . It is due to decrease in kinetic energy of fluid particles. It is clear from Fig. 10.33 that size of trapped bolus decreases for rising values of rotation parameter  $T'$ .

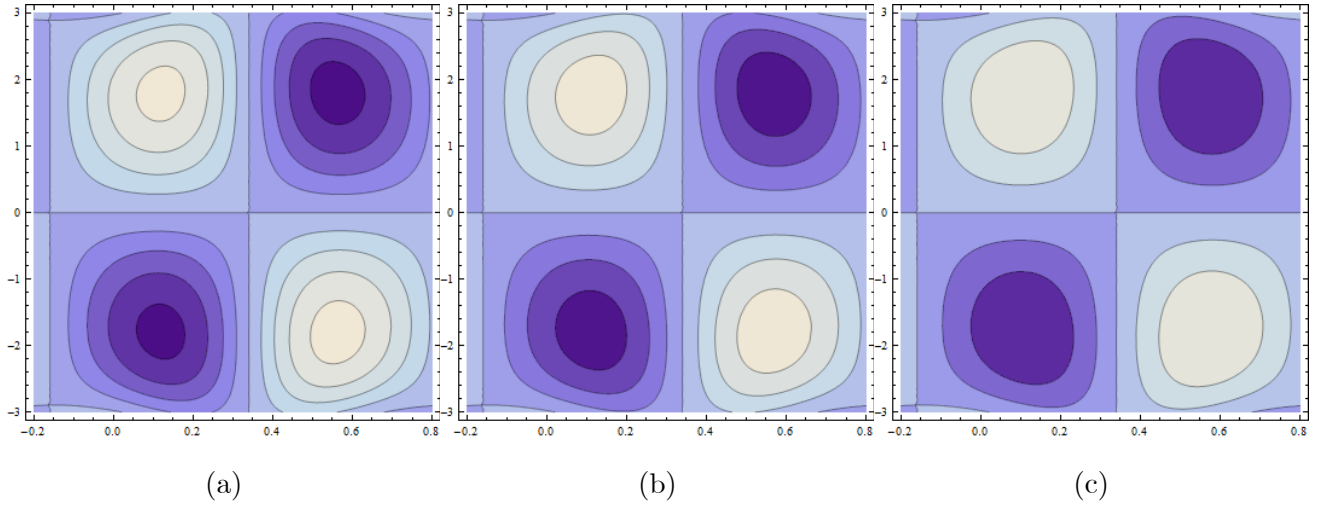


Fig. 10.32: Stream lines for (a)  $T' = 0$  (b)  $T' = 0.5$  (c)  $T' = 5$ .

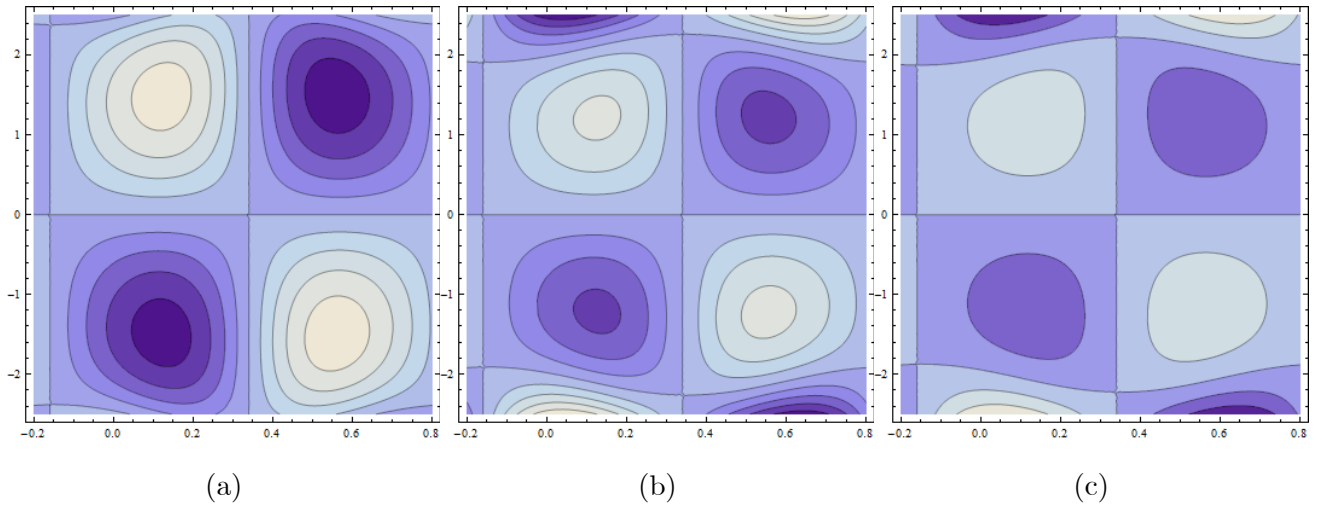


Fig. 10.33: Streamlines for  $\alpha_6$  (a)  $\alpha = 0$  (b)  $\alpha = 0.2$  (c)  $\alpha = 1$ .

## 10.6 Conclusions

Here peristaltic transport Casson fluid under the influence of entropy generation through a rotating channel in examined. The key findings of investigation are

- There is a reduction in axial velocity for growing Taylor number  $T'$ .
- Impact of fluid parameter  $\alpha_6$  on  $u$ ,  $\theta$ ,  $Z$ ,  $Ns$  is opposite when compared with Bejan number  $Be$ .
- A significant rise in secondary velocity via larger wall parameter,  $T'$ ,  $\alpha_6$  and  $\beta_2$  is observed.
- There is an inverse relationship between axial velocity and the slip parameters.
- Increasing outcomes of elastic parameters ( $E_1, E_2$ ) towards  $u$  are noticed however impact of  $E_3$  on  $u$  is quite opposite.
- Temperature distribution is decreasing function of  $T'$  and  $Rd$  however it is directly related with  $\alpha_6$ ,  $\beta_3$  and  $Br$ .
- Multiple values of  $A^{-1}Br$ ,  $\beta_3$  and  $\alpha_6$  tend to raise entropy generation.
- Decaying impression of  $T'$  and  $R_n$  is observed on entropy generation.
- Increasing values of  $\alpha_6$  and  $\beta_3$  have tendency to reduce Bejan number. However  $T'$  and  $R_n$  have a growing impact on  $Be$ .
- Heat transfer coefficient is directly related with  $\alpha_6$ ,  $\beta_3$  and  $Br$ . However  $Z$  declines via  $T'$  and  $R_n$ .

# Bibliography

- [1] T.W. Engelmann, Zur Physiologie des Ureter, Pflug. Arch. Ges. Physiol., 2 (1869) 243-293.
- [2] J. Lapedes, The physiology of the intact human ureter., J. Urol., 59 (1948) 501-537.
- [3] F. Kiil, Function of the ureter and renal pelvis, Annals. Sur., 148 (1958) 280-291.
- [4] S. Boyarsky, Surgical physiology of the renal pelvis and ureter, Monogr. Sur. Sci., 1 (1964) 173-213.
- [5] T.W. Latham, Fluid motion in a peristaltic pump, M.I.T Camdridge MA, (1966).
- [6] A.H. Shapiro, Pumping and retrograde diffusion in peristaltic waves, In "Proceedings of the Workshop on ureteral reflux in children". Nat. Acad. Sci., Washington, D. C., (1967) 109-126.
- [7] E.C. Eckstein, Experimental and theoretical pressure studies of peristaltic pumping, M. S. Thesis, Dep. Mech. Eng., M.I.T., Cambridge, MA (1970).
- [8] S.L. Weinberg, A theoretical and experimetal treatment of peristaltic pumping and its relation to uretal function, PhD Thesis, Dep. Mech. Eng., M.I.T., Cambridge, MA (1970).
- [9] S.L. Weinberg, M. Y. Jaffrin and A. H. Shapiro, A hydrodynamical model of ureteral function. In "Proceedings Workshop Hydrodynam. Upper urinary tract"., Nat. Acad. Sci., Washington, D. C. (1971).
- [10] P.S. Lykoudis, Peristaltic pumping: a bioengineering model. In "Proceedings Workshop Hydrodynam. Upper urinary tract"., Nat. Acad. Sci., Washington, D. C. (1971).

- [11] T.F. Zien and S. Ostrach, A long wave approximation to peristaltic motion, *J. Biomech.*, 3 (1970) 63-75
- [12] Y.C. Fung, Peristaltic pumping, a bioengineering model, In: S. Boyarsky (Ed.) *Urodynamic.: Hydrodynam. Ureter renal pelvis*, Acad. Press, New York, (1971*a*).
- [13] Y.C. Fung, Muscle controlled flow, Proc. 12th Midwestern Mech. Conf. Univ. Notre Dame, South Bend, Indiana, (1971*b*).
- [14] J.C. Burns and T. Parkes, Peristaltic motion, *J. Fluid Mech.*, 29 (1967) 731-743.
- [15] M. Hanin, The flow through a channel due to transversely oscillating walls, *Israel J. Technol.*, 6 (1968) 67-71.
- [16] J.R. Meginniss, An analytical investigation of flow and hemolysis in peristaltic type blood pumps, M.S. Thesis, Dep. Mech. Eng., M.I.T., Cambridge, MA (1970).
- [17] C.C. Yin and Y.C. Fung, Peristaltic wave in circular cylindrical tubes, *J. Appl. Mech.*, 36 (1969) 579-587.
- [18] H.S. Lew, Y.C. Fung and C. B. Lowenstein, Peristaltic carrying and mixing of chyme in the small intestine (An analysis of a mathematical model of peristalsis of the small intestine), *J. Biomech.*, 4 (1971) 297-315.
- [19] H.S. Lew and Y.C. Fung, A study on the low Reynolds number in a valved vessel, *J. Biomech.*, 4 (1971) 85-94.
- [20] C. Barton and S. Raynor, Peristaltic flow in tubes, *Bull. Math. Bio.*, 30 (1968) 663-680.
- [21] M.Y. Jaffrin, Inertia and streamline curvature effects on peristaltic pumping, *Int. J. Eng. Sci.*, 11 (1973) 681-699.
- [22] P.Tong and D. Vawter, An analysis of peristaltic pumping, *J. Appl. Mech.*, 39 (1972) 857-862.
- [23] R.E. Semleser, W.J. Shack and T.J. Lardner, The swimming of spermatozoa in an active channel, *J. Biomech.*, 7 (1974) 349-355.

- [24] T.K. Mitra and S.N. Prasad. Interaction of peristaltic motion with Poiseuille flow, *Bull. Math. Biol.*, 36 (1974) 127-141.
- [25] N. Liron, On peristaltic flow and its efficiency, *Bull. Math. Biol.*, 38 (1976) 573-596.
- [26] T.D. Brown and T.K.Hung, Computational and experimental investigations of two-dimensional nonlinear peristaltic flows, *J. Fluid Mech.*, 83 (1977) 249-272.
- [27] L.M. Srivastava and V.P. Srivastava, Peristaltic transport of a two-layered model of physiological fluid, *J. Biomech.*, 15 (1982) 257-265.
- [28] S. Nakanishi and M. Kawaguti, Numerical study on peristaltic flow of viscous fluid, *J. Phys. Soc. Jpn.* 52, (1983) 848-855.
- [29] S. Takabatake, K. Ayukawa and A. Mori, Peristaltic pumping in circular cylindrical tubes: a numerical study of fluid transport and its efficiency, *J. Fluid Mech.*, 193 (1988) 267-283.
- [30] Kh.S. Mekheimer, Peristaltic transport of a Newtonian fluid through a uniform and non-uniform annulus, *Arab. J. Sci. Eng.*, 30 (2005) 69-83.
- [31] A.R. Rao and M. Mishra, Nonlinear and curvature effects on peristaltic flow of a viscous fluid in an asymmetric channel, *Acta. Mech.*, 168 (2004) 35-59.
- [32] T. Hayat, M. Javed, and A.A. Hendi, Peristaltic transport of viscous fluid in a curved channel with compliant walls, *Int. J. Heat Mass Transf.*, 54 (2011) 1615-1621.
- [33] H.S. Lew, Peristaltic carrying and mixing of chyme in the small intestine (An analysis of a mathematical model of peristalsis of the small intestine), *J. Biomech.*, 4(1971) 297-315.
- [34] J.C. Misra and B.K. Sahu, Forced contraction and expansion of a valved blood vessel: A mathematical model, *Math. Comput. Model.*, 12 (1989) 761-776.
- [35] M. Patel and M.G. Timol, The stress strain relationship for viscoelastic non Newtonian fluids, *Int. J. Appl. Math. Mech.* 6 (2010) 79-93.
- [36] N.S. Akbar, S. Nadeem and Z.H. Khan, Numerical simulation of peristaltic flow of a Carreau nanofluid in an asymmetric channel, *Alexand. Eng. J.*, 53 (2014) 191-197.



- [37] R. Ellahi and F. Hussain, Simultaneous effects of MHD and partial slip on peristaltic flow of Jeffery fluid in a rectangular duct, *J. Mag. Magn. Mater.*, 393 (2015) 284-292.
- [38] M.M. Bhatti and M.A. Abbas, Simultaneous effects of slip and MHD on peristaltic blood flow of Jeffrey fluid model through a porous medium, *Alexand. Eng. J.*, 55 (2016) 1017-1023.
- [39] R.G. Devi and R. Devanathan, Peristaltic transport of micropolar fluid, *Proc. Indian Acad. Sci.*, 81(A) (1975) 149-163.
- [40] M. Sheikholeslami, D.D. Ganji, R. Ashorynejad and H.B. Rokni, Analytical investigation of Jeffery-Hamel flow with high magnetic field and nanoparticle by Adomian decomposition method, *Appl. Math. Mech. -Engl. Ed.*, 33 (2012) 25-36.
- [41] G. Radhakrishnamacharya and V.R. Murthy, Heat transfer to peristaltic transport in a non-uniform channel, *Defence Sci. J.*, 43 (1993) 275-280.
- [42] V.P. Srivastava and M. Saxena, A two-fluid model of non-Newtonian blood flow induced by peristaltic waves, *Rheol. Acta.*, 34 (1995) 406-414.
- [43] E.F. Elshehawey, A. M. El Misery and A. E. H. Abd El Naby, Peristaltic motion of generalized Newtonian fluid in a non-uniform channel, *J. Phys. Soc. Jpn.*, 67 (1998) 434-440.
- [44] A. Riaz, R. Ellahi and S. Nadeem, Peristaltic transport of a Carreau fluid in a compliant rectangular duct, *Alexand. Eng. J.*, 53 (2014) 475-484.
- [45] T. Hayat, R.J. Moitsheki and S. Abelman, Stokes' first problem for Sisko fluid over a porous wall, *Appl. Math. Comput.*, 217 (2010) 622-628.
- [46] T. Hayat, T. Muhammad, B. Ahmad and S.A. Shehzad, Impact of magnetic field in three dimensional flow of Sisko nanofluid with convective condition, *J. Mag. Magn. Mater.*, 413 (2016) 1-8.
- [47] A. Zaman, N. Ali and O.A. Bég, Numerical study of unsteady blood flow through a vessel using Sisko model, *Eng. Scien. Techn., an Int. J.*, 19 (2016) 538-547.

- [48] T. Hayat, F.M. Abbasi and A. Alsaedi, Numerical analysis for MHD peristaltic transport of Carreau-Yasuda fluid in a curved channel with Hall effects, *J. Mag. Magn. Mater.*, 382 (2015) 104-110.
- [49] A. V. Mernone, J. N. Mazumdar and S. K. Lucas, A mathematical study of peristaltic transport of Casson fluid, *Math. Comput. Model.*, 35 (2002) 894-912.
- [50] O. Eytan and D. Elad, Analysis of intrauterine fluid motion induced by uterine contractions, *Bull. Math. Bio.*, 61 (1999) 221-238.
- [51] S. Nadeem and S. Akram, Peristaltic transport of a hyperbolic tangent fluid model in an asymmetric channel, *Z. Naturforsch.*, 64a (2009) 559-567.
- [52] S. Hina, M. Mustafa, T. Hayat and Naif D. Alotaibi, On peristaltic motion of pseudo-plastic fluid in a curved channel with heat/mass transfer and wall properties, *App. Math. Comp.*, 263 (2015) 378-391.
- [53] N. S. Akbar, S. Nadeem, C. Lee, Z. H. Khan and Rizwan Ul Haq, Numerical study of Williamson nano fluid flow in an asymmetric channel, *Res. Physics*, 3 (2013) 161-166.
- [54] A. Riaz, S. Nadeem, R. Ellahi and N. S. Akbar, The influence of wall flexibility on unsteady peristaltic flow of Prandtl fluid in a three dimensional rectangular duct, *Appl. Math. Comp.*, 241 (2014) 389-400.
- [55] T. Hayat, H. Zahir, A. Tanveer and A. Alsaedi, Influences of Hall current and chemical reaction in mixed convective peristaltic flow of Prandtl fluid, *J. Mag. Magn. Mater.*, 407 (2016) 321-327.
- [56] H.M. Shawky, Pulsatile flow with heat transfer of dusty magnetohydrodynamic Ree-Eyring fluid through a channel, *Heat/mass Tran.*, 45 (2009) 1261-1269.
- [57] M.M. Bhatti, M. Ali Abbas and M.M. Rashidi, Combine effects of Magnetohydrodynamics (MHD) and partial slip on peristaltic Blood flow of Ree-Eyring fluid with wall properties, *Eng. Sci. Tech. Int. J.*, 19 (2016) 1497-1502.
- [58] F.M. Abbasi, A. Alsaedi and T. Hayat, Peristaltic transport of Eyring-Powell fluid in a curved channel, *J. Aerosp. Eng.*, (2014) DOI: 10.1061/(ASCE)AS.1943-5525.0000354.

- [59] S. Hina, M. Mustafa and T. Hayat and A. Alsaedi, Peristaltic transport of Powell-Eyring fluid in a curved channel with heat/mass transfer and wall properties, *Int. J. Heat Mass Transf.*, 101 (2016) 156-165.
- [60] A. C. Eringen, Nonlinear theory of simple micro-elastic solids-I, *Int. J. Eng. Sci.*, 2 (1964) 189-203.
- [61] M. W. Johnson and D. Segalman, A model for viscoelastic fluid behavior which allows non-affine deformation, *J. Non-Newtonian Fluid Mech.*, 2 (1977) 255-270.
- [62] P. Chaturani and R.P. Samy, A study of non-Newtonian aspects of blood flow through stenosed arteries and its application in arterial diseases, *J. Biorheol.*, 22 (1985) 521-531.
- [63] G. Bohme and R. Friedrich, Peristaltic flow of viscoelastic liquids, *J. Fluid Mech.*, 128 (1983) 109-122.
- [64] T. Hayat, A. Tanveer, H. Yasmin and A. Alsaedi, Effects of convective conditions and chemical reaction on peristaltic flow of Eyring-Powell fluid, *Appl. Bion. Biomech.*, 11 (2014) 221-233.
- [65] N. Alvi, T. Latif, Q. Hussain and S. Asghar, Peristalsis of nonconstant viscosity Jeffrey fluid with nanoparticles, *Results in Physics*, 6 (2016) 1109-1125.
- [66] T. Latif, N. Alvi, Q. Hussain and S. Asghar Variable properties of MHD third order fluid with peristalsis, *Results in Physics*, 6 (2016) 963-972.
- [67] R.L. Fosdick and K.R. Rajagopal, Thermodynamics and stability of fluids of third grade, *Proc. R. Soc. Lond. Ser. A*, 339 (1980) 351-377.
- [68] D. Tripathi, S.K. Pandey and S. Das, Peristaltic flow of viscoelastic fluid with fractional Maxwell model through a channel, *Applied Mathematics and Computation*, 215 (2010) 3645-3654.
- [69] K.S. Mekheimer and Y. Abd Elmaboud, Peristaltic flow of a couple stress fluid in an annulus: Application of an endoscope, *Physica A*, 387 (2008) 2403-2415.

- [70] G.C. Shit and M. Roy, Hydromagnetic effect on inclined peristaltic flow of a couple stress fluid, *Alex. Eng. J.* 53 (2014) 949-958.
- [71] K. Ramesh, Influence of heat and mass transfer on peristaltic flow of a couple stress fluid through porous medium in the presence of inclined magnetic field in an inclined asymmetric channel, *J. Mol. Liquids*, 219 (2016) 256-270.
- [72] D. C. Sanyal and N. K. Maji, Thermoregulation through skin under variable atmospheric and physiological conditions, *J. Theor. Biol.*, 208 (2001) 451-456.
- [73] M. D. Shera, A. S. Gladman, S. R. Davidson, J. Trachtenberg and M. R. Gertner, Helical antenna arrays for interstitial microwave thermal therapy for prostate cancer: tissue phantom testing and simulations for treatment, 46 (2001) 1905-1918.
- [74] G. Radhakrishnamacharya and V.R. Murthy, Heat transfer to peristaltic transport in a non-uniform channel, *defence Sci. J.*, 43 (1993) 275-280.
- [75] K. Vajravelu, G. Radhakrishnamacharya and V. Radhakrishnamurthy, Peristaltic flow and heat transfer in a vertical porous medium with long wave approximation, *Int. J. Nonlinear Mech.*, 42 (2007) 754-759.
- [76] J.R. Oleson, Hyperthermia by magnetic induction: I. Physical characteristics of the technique, *Int. J. Radiation Oncology (Biology and Physics)*, 8 (2001) 1747-1756.
- [77] P.A. Voltairas, D.I. Fotiadis and M.K. Michalis, Hydrodynamics of magnetic drug targeting, *J. Biomech.*, 35 (2002) 813-820.
- [78] A. Ogulu, Hydromagnetic heat transfer to blood flow in the microcirculation, *J. Fizik Malaysia*, 17 (1996) 135-140
- [79] J. M. R. Carlton, C. A. Yowell, K. A. Sturrock and J. B. Dame, Biomagnetic separation of contaminating host leukocytes from plasmodium infected erythrocytes, *Exp. Parasitol.*, 97 (2001) 111-115.
- [80] V. K. Sud, G. S. Sekhon and R. K. Mishra, Pumping action on blood by a magnetic field, *Bull. Math. Biol.*, 39 (1977) 385-390.

- [81] H. L. Agarwal and B. Anwaruddin, Peristaltic flow of blood in a branch, Ranchi Univ. Math. J., 15 (1984) 111-121.
- [82] G. Radhakrishnamacharya and V. R. Murty, Heat transfer to peristaltic transport in a non-uniform channel, Defence Sci. J. 43 (1993) 275-280.
- [83] Y. Wang, T. Hayat, N. Ali and M. Oberlack, Magnetohydrodynamic peristaltic motion of a Sisko fluid in a symmetric or asymmetric channel, Physica A: Stat. Mech. Appl., 387 (2008) 347-36.
- [84] T. Hayat, M. Shafique, A. Tanveer and A. Alsaedi, Magnetohydrodynamic effects on peristaltic flow of hyperbolic tangent nanofluid with slip conditions and Joule heating in an inclined channel, Int. J. Heat Mass Transf., 102 (2016) 54-63.
- [85] M. Awais, S. Farooq, H. Yasmin, T. Hayat and A. Alsaedi, Convective heat transfer analysis for MHD peristaltic flow in an asymmetric channel, Int. J. Biomath., 7 (2014) DOI: 10.1142/S1793524514500235 (15 pages).
- [86] F.M. Abbasi, Saba and S.A. Shehzad, Heat transfer analysis for peristaltic flow of Carreau-Yasuda fluid through a curved channel with radial magnetic field, Int. J. Heat Mass Transf., 115 (2017) 777-783.
- [87] R. Ellahi, M.M. Bhatti and C.M. Khalique, Three-dimensional flow analysis of Carreau fluid model induced by peristaltic wave in the presence of magnetic field, J. Mol. Liquids, 241 (2017) 1059-1068.
- [88] S. Asghar, Q. Hussain, T. Hayat and F. Alsaadi, Hall and ion slip effects on peristaltic flow and heat transfer analysis with Ohmic heating, Appl. Math. Mech., 35 (2014) 1509-1524.
- [89] T. Hayat, M. Shafique, A. Tanveer and A. Alsaedi, Hall and ion slip effects on peristaltic flow of Jeffrey nanofluid with Joule heating, J. Magn. Mag. Materials, 407 (2016) 51-59.
- [90] K. Nowar, Peristaltic flow of a nanofluid under the effect of Hall current and porous medium, Math. Prob. Eng., DOI: 10.1155/2014/389581.

- [91] R. Ellahi, M. M. Bhatti and I. Pop, Effects of Hall and ion slip on MHD peristaltic flow of Jeffrey fluid in a non-uniform rectangular duct, *Int. J. Num. Meth. Heat and Fluid Flow*, 26 (2016) 1802 - 1820.
- [92] M. M. Bhatti, M. Ali Abbas and M. M. Rashidi, Effect of Hall and ion slip on peristaltic blood flow of Eyring Powell fluid in a non-uniform porous channel, *World J. Model. Simul.*, 12 (2016) 268-279.
- [93] S. Noreen and M. Qasim, Influence of Hall current and viscous dissipation on pressure driven flow of pseudoplastic fluid with heat generation: A mathematical study, *Plosone*, DOI: 10.1371/journal.pone.0129588.
- [94] M. Gnanaswara Reddy, K. Venugopal Reddy and O.D. Makinde, Hydromagnetic peristaltic motion of a reacting and radiating couple stress fluid in an inclined asymmetric channel filled with a porous medium, *Alex. Eng. J.*, 55 (2016) 1841-1853.
- [95] A.A. Dar and K. Elangovan, Impact of an inclined magnetic field, heat generation/absorption and radiation on the peristaltic flow of a Micropolar fluid through a porous non-uniform channel with slip velocity, *NTMSCI*, 5 (2017), 227-244.
- [96] Y. A. Elmaboud , K. S. Mekheimer and M. S. Mohamed , Series solution of a natural convection flow for a Carreau fluid in a vertical channel with peristalsis, *J. Hydrodynamics, Ser. B*, 27 (2015) 969—979.
- [97] T. Hayat, S. Farooq and B. Ahmad, A. Alsaedi, Homogeneous-heterogeneous reactions and heat source/sink effects in MHD peristaltic flow of micropolar fluid with Newtonian heating in a curved channel, *J. Mol. Liq.*, 223 (2016) 469-488.
- [98] M. Rehman, S. Noreen, A. Haider and H. Azam, Effect of heat sink/source on peristaltic flow of Jeffrey fluid through a symmetric channel, *Alex. Eng. J.*, 54 (2015) 733-743.
- [99] E.P. Siva and A. Govindarajan, Thermal radiation and Soret effect on MHD peristaltic transport through a tapered asymmetric with convective boundary conditions, *Glob. J. Appl. Math.*, 12 (2016) 213-221.

- [100] T. Hayat, F. Shah, M.I. Khan and A. Alsaedi, Framing the performance of heat absorption/generation and thermal radiation in chemically reactive Darcy-Forchheimer flow, *Res.Physics*, 7 (2017) 3390-3395.
- [101] M.M. Bhatti, A.Zeeshan, N.Ijaz, O.Anwar Bég and A. Kadir, Mathematical modelling of nonlinear thermal radiation effects on EMHD peristaltic pumping of viscoelastic dusty fluid through a porous medium duct, *Eng. Sci. Tech. Int. J.*, 20 (2017) 1129-1139.
- [102] T. Hayat, S. Asad and A. Alsaedi, Non-uniform heat source/sink and thermal radiation effects on the stretched flow of cylinder in a thermally stratified medium, *J. Appl. Fluid Mech.*, 10 (2016) 915-924.
- [103] L. Lecoq, D. Flick, E. Derens, H.M. Hoang and O. Laguerre, Simplified heat and mass transfer modeling in a food processing plant, *J. Food Eng.*, 171 (2016) 1-13.
- [104] F. Gavelli, Computational fluid dynamics simulation of fog clouds due to ambient air vaporizers, *J. Loss Prevention Process Indust.*, 23 (2010) 773-780.
- [105] Z.G. Ariyan, V.M. Sadesh and B. Mojtaba, Numerical analysis of complicated heat and mass transfer inside a Wustite Pellet during reducing to sponge iron by H<sub>2</sub> and CO gaseous mixture, *J. Iron Steel Research, Int.*, 23 (2016) 1142-1150.
- [106] A.R. Goerke, J. Leung and S.R. Wickramasinghe, Mass and momentum transfer in blood oxygenators, *Chem. Eng. Scien.*, 57 (2002) 2035-2046.
- [107] S.G. Agrawal and R.N. Methekar, Mathematical model for heat and mass transfer during convective drying of pumpkin, *Food Bioprod. Proces.*, 101 (2017) 68-73.
- [108] A.R. Budu, G.L. Pavel and D.E. Moraru, Heat and mass transfer aspects in nuclear power generation, *Energy Proced.*, 112 (2017) 571-578.
- [109] A. Ogulu, Effect of heat generation on low Reynolds number fluid and mass transport in a single lymphatic blood vessel with uniform magnetic field, *Int. Commun. Heat Mass Transfer*, 33 (2006) 790-799.
- [110] S. Nadeem and N. S. Akbar, Influence of heat and mass transfer on a peristaltic motion of a Jeffrey-six constant fluid in an annulus, *Heat Mass Transfer*, 46 (2010) 485-493.

- [111] T. Hayat, S. Noreen, M. S. Alhothuali, S. Asghar and A. Alhomaïdan, Peristaltic flow under the effects of an induced magnetic field and heat and mass transfer, *Int. J. Heat Mass Transfer*, 55 (2012) 443-452.
- [112] A. A. Shaaban and M. Y. Abou-zeid, Effects of heat and mass transfer on MHD peristaltic flow of a non-Newtonian fluid through a porous medium between two coaxial cylinders, *Math. Prob. Eng.*, 2013 (2013) 11 pages.
- [113] T. Hayat, F.M. Abbasi, M. Al-Yami and S. Monaqueel, Slip and Joule heating effects in mixed convection peristaltic transport of nanofluid with Soret and Dufour effects, *J. Mol. Liq.*, 194 (2014) 93-99.
- [114] M. Mustafa, S. Abbasbandy, S. Hina and T. Hayat, Numerical investigation on mixed convective peristaltic flow of fourth grade fluid with Dufour and Soret effects, *J. Taiwan Inst. Chem. Eng.*, 45 (2014) 308-316.
- [115] T. Hayat, R. Iqbal, A. Tanveer and A. Alsaed, Soret and Dufour effects in MHD peristalsis of pseudoplastic nanofluid with chemical reaction, *J. Mol. Liq.*, 220 (2016) 693-706.
- [116] S. Farooq, M. Awais, M. Naseem, T. Hayat and B. Ahmad, Magneto-hydrodynamic peristalsis of variable viscosity Jeffrey liquid with heat and mass transfer, *Nucl. Eng. Technol.*, 49 (2017) 1396-1404.
- [117] T. Hayat, S. Farooq, M. Mustafa and B. Ahmad, Peristaltic transport of Bingham plastic fluid considering magnetic field, Soret and Dufour effects, *Res. Phys.*, 7 (2017) 2000-2011.
- [118] M. Mustafa, S. Abbasbandy, S. Hina and T. Hayat, Numerical investigation on mixed convective peristaltic flow of fourth grade fluid with Dufour and Soret effects, *J. Taiwan Inst. Chem. Eng.*, 45 (2014) 308-316.
- [119] T. Hayat, H. Yasmin and M. Al-Yami, Soret and Dufour effects in peristaltic transport of physiological fluids with chemical reaction: a mathematical analysis, *Comput. Fluids*, 89 (2015), 242-253.



- [120] G. Sankad and M. Dchange, Peristaltic pumping of an incompressible viscous fluid in a porous medium with wall effects and chemical reactions, *Alex. Eng. J.*, 55 (2016) 2015-2021.
- [121] R. Muthuraj, K. Nirmala and S. Srinivas, Influences of chemical reaction and wall properties on MHD Peristaltic transport of a Dusty fluid with Heat and Mass transfer, *Alex. Eng. J.*, 55 (2016) 597-611.
- [122] T. Hayat, A. Tanveer and A. Alsaedi, Mixed convective peristaltic flow of Carreau–Yasuda fluid with thermal deposition and chemical reaction, *Int. J. Heat Mass Trans.*, 96 (2016) 474-481.
- [123] G. R. Machireddy and V. R. Kattamreddy, Impact of velocity slip and joule heating on MHD peristaltic flow through a porous medium with chemical reaction, *J. Nigerian Math. Soc.*, 35 (2016) 227-244.
- [124] M. G. Reddy, K. V. Reddy and O.D. Makinde, Hydro magnetic peristaltic motion of a reacting and radiating couple stress fluid in an inclined asymmetric channel filled with a porous medium, *Alex. Eng. J.*, 55 (2016) 1841-1853.
- [125] J. C. Misra, B. Mallick and A. Sinha, Heat and mass transfer in asymmetric channels during peristaltic transport of an MHD fluid having temperature-dependent properties, *Alex. Eng. J.*, <https://doi.org/10.1016/j.aej.2016.09.021>.
- [126] S. A. Shehzad, F. M. Abbasi, T. Hayat and F. Alsaadi, MHD mixed convective peristaltic motion of nanofluid with Joule heating and thermophoresis effects, *Plos One*, DOI: <https://doi.org/10.1371/journal.pone.0111417>.
- [127] T. Hayat, M. Rafiq and B. Ahmad, Influences of rotation and thermophoresis on MHD peristaltic transport of Jeffrey fluid with convective conditions and wall properties, *J. Magn. Mater.*, 410 (2016) 89-99.
- [128] A. Ali, S. Asghar and M. Awais, Thermophoresis and concentration effects in a fourth grade peristaltic flow with convective walls, *J. Central South Univ.*, 24 (2017) 1654-1662.

- [129] A. Aziz, A similarity solution for laminar thermal boundary layer over a flat plate with a convective surface boundary condition, *Commun. Nonlin. Sci. Numer. Simulat.*, 14 (2009) 1064-1068.
- [130] O. D. Makinde, Thermal stability of a reactive viscous flow through a porous saturated channel with convective boundary conditions, *Appl. therm. Eng.*, 29 (2009) 1773-1777.
- [131] T. Hayat, H. Yasmin and M. Al-Yami, Soret and Dufour effects in peristaltic transport of physiological fluids with chemical reaction: A mathematical analysis, *Comput. Fluids*, 89 (2014) 242-253.
- [132] T. Hayat, A. Tanveer, H. Yasmin and A. Alsaedi, Effects of convective conditions and chemical reaction on peristaltic flow of Eyring-Powell fluid, *Appl. Bionics Biomech.*, 11 (2014) 221-233.
- [133] F. M. Abbasi, T. Hayat and B. Ahmad, Peristaltic flow in an asymmetric channel with convective boundary conditions and Joule heating, *J. Cent. South Univ.*, 21 (2014) 1411-1416.
- [134] N. S. Akbar, Natural convective MHD peristaltic flow of a nanofluid with convective surface boundary conditions, *J. Comput. Theor. Nanosci.*, 12 (2015) 257-262.
- [135] T. Hayat, M. Iqbal, H. Yasmin, F. E. Alsaadi and H. Gao, Simultaneous effects of Hall and convective conditions on peristaltic flow of couple-stress fluid in an inclined asymmetric channel, *Pranama J. Phys.*, 85 (2015) 125-148.
- [136] N. Ali, Q. Hussain, T. Hayat and S. Asghar, Slip effects on the peristaltic transport of MHD fluid with variable viscosity, *Physics Lett. A*, 372 (2008) 1477-1489.
- [137] T. Hayat, A. Tanveer and A. Alsaedi, Numerical analysis of partial slip on peristalsis of MHD Jeffery nanofluid in curved channel with porous space, *J. Mol. Liquids*, 224 (2016) 944-953.
- [138] T. Hayat, S. Hina and N. Ali, Simultaneous effects of slip and heat transfer on the peristaltic flow, *Commun. Nonlin. Sci. Numer. Simul.*, 15 (2010) 1526-1537.

- [139] K. Ramesh, Effects of slip and convective conditions on the peristaltic flow of couple stress fluid in an asymmetric channel through porous medium, *Comp. Methods Prog. Biomed.*, 135 (2016) 1-14.
- [140] S. Hina, M. Mustafa and T. Hayat, Peristaltic motion of Johnson-Segalman fluid in a curved channel with slip conditions, *Plos One*, 9 (2014) e114168.
- [141] A. Yildirim and S.A. Sezer, Effects of partial slip on the peristaltic flow of a MHD Newtonian fluid in an asymmetric channel, *Math. Comput. Model.*, 52 (2010) 618-625.
- [142] Y.V.K.R. Kumar, S.V.H.N.K. Kumari, M.V.R.Murthy and S. Sreenadh, Peristaltic transport of a power-law fluid in an asymmetric channel bounded by permeable walls, *Adv. Appl. Sci. Res.*, 2 (2011) 396-406.
- [143] R. Ellahi and F. Hussain, Simultaneous effects of MHD and partial slip on peristaltic flow of Jeffrey fluid in a rectangular duct, *J. Mag. Magn. Materials*, 393 (2015) 284-292.
- [144] R. Saravana, R.H. Reddy, S. Sreenadh, S. Vekataramana and A. Kavitha, Influence of slip, heat and mass transfer on the peristaltic transport of a third order fluid in an inclined asymmetric channel, *Int. J. Appl. Math. Mech.*, 9 (2013) 51-86.
- [145] K. Das, Slip effects on heat transfer and peristaltic pumping of a Johnson-Segalman fluid in an inclined asymmetric channel, *Arab. J. Math.*, 1 (2012) 159-174.
- [146] B. Jyothi and P. K. Rao, Slip effects on MHD peristaltic transport of a Williamson fluid through a porous medium in a symmetric channel, *J. Math. Comput.*, 3 (2013) 1306-1324.
- [147] A. Sinha, G.C. Shit and N.K. Ranjit, Peristaltic transport of MHD flow and heat transfer in an asymmetric channel: Effects of variable viscosity, velocity-slip and temperature jump, *Alex. Eng. J.*, 54 (2015) 691-704.
- [148] S.I. Abdelsalam and K. Vafai, Combined effects of magnetic field and rheological properties on the peristaltic flow of a compressible fluid in a microfluidic channel, *European J. Mech. B/Fluids*, <https://doi.org/10.1016/j.euromechflu.2017.02.002>.

- [149] T. Hayat, M. Shafique, A. Tanveer and A. Alsaedi, Slip and Joule heating effects on radiative peristaltic flow of hyperbolic tangent nanofluid, *Int. J. Heat Mass Trans.*, 112 (2017) 559-567.
- [150] A. M. Abd-Alla, S. M. Abo-Dahab and H. D. El-Shahrany, Effects of rotation and initial stress on peristaltic transport of fourth grade fluid with heat transfer and induced magnetic field, *J. Mag. Magn. Mater.*, 349 (2014) 268–280.
- [151] A. M. Abd-Alla, S. M. Abo-Dahab and H. D. El-Shahrany, Effect of rotation on peristaltic flow of a micropolar fluid through a porous medium with an external magnetic field, *J. Mag. Magn. Mater.*, 348 (2013) 33–43.
- [152] A. M. Abd-Alla and S. M. Abo-Dahab, Magnetic field and rotation effects on peristaltic transport of a Jeffrey fluid in an asymmetric channel, *J. Mag. Magn. Mater.*, 374 (2015) 680–689.
- [153] N. Ali, M. Sajid, T. Javed and Z. Abbas, Peristalsis in a rotating fluid, *Scien. Essays*, 32 (2012) 2891-2897.
- [154] S.R. Mahmoud, Effect of rotation and magnetic field through porous medium on peristaltic transport of a Jeffrey fluid in tube, *Math. Prob. Eng.*, 2011 (2011)
- [155] T. Hayat, M. Rafiq and B. Ahmad, Soret and Dufour effects on MHD peristaltic flow of Jeffrey fluid in a rotating system with porous medium, *Plos One.*, DOI: 10.1371/journal.pone.0145525.
- [156] T. Hayat, M. Rafiq and A. Alsaedi, Investigation of Hall current and slip conditions on peristaltic transport of Cu-water nanofluid in a rotating medium, *Int. J. Thermal Sci.*, 112 (2017) 129-141.

## Turnitin Originality Report

On Peristaltic transfert with he .... ranfer and rotation aspects

by Hina Zahir



From Theses (QAU theses)

- Processed on 27-Aug-2018 19:09 PKT
- ID: 993693712
- Word Count: 26043

## Similarity Index

13%

## Similarity by Source

## Internet Sources:

7%

## Publications:

5%

## Student Papers:

5%

**sources:**

1

1% match (student papers from 31-Jul-2018)

[Submitted to Higher Education Commission Pakistan on 2018-07-31](#)

2

1% match (Internet from 29-Aug-2008)

<http://hal.physast.uga.edu/~jss/1120L/data/CCJD/Lab%20%233/19LYN%205s%20B%20filter.fit>

3

1% match (Internet from 20-Jul-2018)

<https://vdocuments.mx/documents/kurita-handbook-55c80e4d6bfd4.html>

4

1% match (Internet from 09-Jul-2018)

<https://doaj.org/article/76214b03fa4c44d69577c0537e4afba5>

5

1% match (student papers from 12-Jan-2018)

[Submitted to Higher Education Commission Pakistan on 2018-01-12](#)

6

&lt; 1% match (Internet from 09-Jul-2018)

<https://doaj.org/article/038391852cb34866a5367c111e2e7be0>

7

&lt; 1% match (student papers from 05-Oct-2016)

[Submitted to Higher Education Commission Pakistan on 2016-10-05](#)

8

&lt; 1% match (Internet from 29-Aug-2008)

<http://hal.physast.uga.edu/~jss/1120L/data/CCJD/Lab%20%232/Jupiter25sempty.fit>

&lt; 1% match (publications)

9

[Hayat, T., Quratulain, M. Rafiq, Fuad Alsaadi, and M. Ayub. "Soret and Dufour effects on peristaltic transport in curved channel with radial magnetic field and convective conditions", Journal of Magnetism and Magnetic Materials, 2016.](#)

---

10

< 1% match (publications)

[Hayat, T., M. Rafiq, and B. Ahmad. "Influences of rotation and thermophoresis on MHD peristaltic transport of Jeffrey fluid with convective conditions and wall properties", Journal of Magnetism and Magnetic Materials, 2016.](#)

---

11

< 1% match (Internet from 12-Feb-2018)

<http://article.sciencepublishinggroup.com/html/10.11648.j.ajma.20150305.12.html>

---

12

< 1% match (Internet from 25-Aug-2018)

<https://www.mechanics-industry.org/articles/meca/pdf/2017/03/mi160095.pdf>

---

13

< 1% match (publications)

[Hayat, T., Rija Iqbal, A. Tanveer, and A. Alsaedi. "Soret and Dufour effects in MHD peristalsis of pseudoplastic nanofluid with chemical reaction", Journal of Molecular Liquids, 2016.](#)

---

14

< 1% match (Internet from 05-Oct-2017)

<http://pr.hec.gov.pk/Thesis/3010S.pdf>

---

15

< 1% match (publications)

[Tasawar Hayat, Javaria Akram, Ahmed Alsaedi, Hina Zahir. "Endoscopy and homogeneous-heterogeneous reactions in MHD radiative peristaltic activity of Ree-Eyring fluid", Results in Physics, 2018](#)

---

16

< 1% match (Internet from 24-Mar-2016)

<http://www.aki.che.tohoku.ac.jp/prev/htm6/chutia-48thBatteries.files/oledata.mso>

---

17

< 1% match (student papers from 10-Nov-2016)

[Submitted to Myongji University Graduate School on 2016-11-10](#)

---

18

< 1% match (student papers from 10-Nov-2016)

[Submitted to Higher Education Commission Pakistan on 2016-11-10](#)

---

19

< 1% match (student papers from 22-Jul-2014)

[Submitted to Higher Education Commission Pakistan on 2014-07-22](#)

---

20

< 1% match (publications)

[Anum Tanveer, T. Hayat, A. Alsaedi, B. Ahmad. "Mixed convective peristaltic flow of Sisko fluid in curved channel with homogeneous-heterogeneous reaction effects", Journal of Molecular Liquids, 2017](#)

---

21

< 1% match (publications)

[Hayat, T., Maimona Rafiq, and B. Ahmad. "Combined effects of rotation and thermal radiation on peristaltic transport of Jeffrey fluid", International Journal of Biomathematics, 2015.](#)

---

22 < 1% match (Internet from 08-Apr-2009)  
<http://tods.acm.org/accepted/2008/KarrasHierarchical.pdf>

---

23 < 1% match (publications)  
[Hina, S., M. Mustafa, T. Hayat, and A. Alsaedi. "Peristaltic transport of Powell–Eyring fluid in a curved channel with heat/mass transfer and wall properties", International Journal of Heat and Mass Transfer, 2016.](#)

---

24 < 1% match (student papers from 13-Oct-2017)  
[Submitted to Higher Education Commission Pakistan on 2017-10-13](#)

---

25 < 1% match (student papers from 19-Sep-2015)  
[Submitted to Higher Education Commission Pakistan on 2015-09-19](#)

---

26 < 1% match (Internet from 22-Sep-2003)  
<http://cinemah.com/videosofia/tesi-cristo-immagine-cinematografica/tesi-cristo-immagine-cinematografica.pdf>

---

27 < 1% match (student papers from 21-Jul-2018)  
[Submitted to Higher Education Commission Pakistan on 2018-07-21](#)

---

28 < 1% match (publications)  
[Maryam Javed, Ruqia Arif. "Magneto hydrodynamic \(MHD\) peristaltic blood flow of Ree-Eyring fluid in a compliant channel with influence of heat and mass transfer", 2017 14th International Bhurban Conference on Applied Sciences and Technology \(IBCAST\), 2017](#)

---

29 < 1% match (Internet from 22-Feb-2014)  
[http://iisonline.org/files/uploads/2012/06/222\\_OLAOSEBIKAN-ola-olaosebikanversion1\\_v2.pptx](http://iisonline.org/files/uploads/2012/06/222_OLAOSEBIKAN-ola-olaosebikanversion1_v2.pptx)

---

30 < 1% match (publications)  
[Hayat, T., Z. Nisar, H. Yasmin, and A. Alsaedi. "Peristaltic transport of nanofluid in a compliant wall channel with convective conditions and thermal radiation", Journal of Molecular Liquids, 2016.](#)

---

31 < 1% match (student papers from 09-Nov-2015)  
[Submitted to University of Sheffield on 2015-11-09](#)

---

32 < 1% match (Internet from 11-Mar-2016)  
[https://afni.nimh.nih.gov/pub/dist/bin/NIH.openSUSE.11.4\\_64/3dFriedman](https://afni.nimh.nih.gov/pub/dist/bin/NIH.openSUSE.11.4_64/3dFriedman)

---

33 < 1% match (student papers from 17-Jan-2016)  
[Submitted to Cranfield University on 2016-01-17](#)

---

- 34 < 1% match (Internet from 07-Jun-2018)  
<https://www.thieme-connect.de/products/ebooks/html/10.1055/b-0038-161015>
- 35 < 1% match (Internet from 03-Oct-2011)  
<http://www.scribd.com/doc/6315897/Atlas-of-Anaomical-Pahology>
- 36 < 1% match (publications)  
[Tasawar Hayat, Aqsa Saleem, Anum Tanveer, Fuad Alsaadi. "Numerical analysis for peristalsis of Williamson nanofluid in presence of an endoscope", International Journal of Heat and Mass Transfer, 2017](#)
- 37 < 1% match (publications)  
[T. Hayat, Rija Iqbal, A. Tanveer, A. Alsaedi. "Soret and Dufour effects in MHD peristalsis of pseudoplastic nanofluid with chemical reaction", Journal of Molecular Liquids, 2016](#)
- 38 < 1% match (student papers from 20-Nov-2007)  
[Submitted to University of Greenwich on 2007-11-20](#)
- 39 < 1% match (Internet from 28-Dec-2017)  
[https://www.scipedia.com/public/Bhatti\\_Abbas\\_2016a](https://www.scipedia.com/public/Bhatti_Abbas_2016a)
- 40 < 1% match (Internet from 02-Jun-2018)  
[https://www.scitechnol.com/peer-review/peristaltic-flow-in-a-nonuniform-channel-with-heat-and-mass-transfer-TIWD.php?article\\_id=6830](https://www.scitechnol.com/peer-review/peristaltic-flow-in-a-nonuniform-channel-with-heat-and-mass-transfer-TIWD.php?article_id=6830)
- 41 < 1% match (Internet from 27-Nov-2017)  
<https://link.springer.com/content/pdf/10.1134%2FS0021894417010072.pdf>
- 42 < 1% match (publications)  
[Hayat, T., M. Rafiq, and A. Alsaedi. "Investigation of Hall current and slip conditions on peristaltic transport of Cu-water nanofluid in a rotating medium", International Journal of Thermal Sciences, 2017.](#)
- 43 < 1% match (publications)  
[Hayat, T., S. Farooq, B. Ahmad, and A. Alsaedi. "Effectiveness of entropy generation and energy transfer on peristaltic flow of Jeffrey material with Darcy resistance", International Journal of Heat and Mass Transfer, 2017.](#)
- 44 < 1% match (publications)  
[Tasawar Hayat, Shahid Farooq, Bashir Ahmad, Ahmed Alsaedi. "Peristalsis of Eyring-Powell magneto nanomaterial considering Darcy-Forchheimer relation", International Journal of Heat and Mass Transfer, 2017](#)
- 45 < 1% match (Internet from 12-May-2018)



<http://oxcon.ouplaw.com/view/10.1093/ocw/law-ocw-cd1088.regGroup.1/law-ocw-cd1088?print=>

46 < 1% match (Internet from 23-Aug-2007)  
[http://www.ilc.tsukuba.ac.jp/rehp/jp/hp/survey\\_h15/vbreportH15.pdf](http://www.ilc.tsukuba.ac.jp/rehp/jp/hp/survey_h15/vbreportH15.pdf)

47 < 1% match (Internet from 17-Mar-2009)  
<http://www.nordtech.ubm.ro/issues/2007/2007.02.33.pdf>

48 < 1% match (publications)  
[Simon Hsu-Sheng, Chi-Cheng Cheng. "Chapter 30 On Direct Adaptive Control for Uncertain Dynamical Systems - Synthesis and Applications", InTech, 2006](#)

49 < 1% match (publications)  
[T. Hayat, Sadia Ayub, Ahmed Alsaedi, Bashir Ahmad. "Numerical simulation of buoyancy peristaltic flow of Johnson-Segalman nanofluid in an inclined channel", Results in Physics, 2018](#)

50 < 1% match (publications)  
[Afify, Ahmed A.. "The Influence of Slip Boundary Condition on Casson Nanofluid Flow over a Stretching Sheet in the Presence of Viscous Dissipation and Chemical Reaction.\(Research Article\)\(Report\)", Mathematical Problems in Engineering](#)

51 < 1% match (Internet from 16-Mar-2014)  
[http://game.perm.ru/files/cstrike/maps/zm\\_house\\_s.bsp](http://game.perm.ru/files/cstrike/maps/zm_house_s.bsp)

52 < 1% match (publications)  
[Hayat, T., S. Farooq, A. Alsaedi, and B. Ahmad. "Numerical study for Soret and Dufour effects on mixed convective peristalsis of Oldroyd 8-constants fluid", International Journal of Thermal Sciences, 2017.](#)

53 < 1% match (publications)  
[Nowar, Khalid. "Peristaltic flow of a nanofluid under the effect of hall current and porous medium.\(Research Article\)", Mathematical Problems in Engineering, Annual 2014 Issue](#)

54 < 1% match (publications)  
[Sadia Ayub, T. Hayat, S. Asghar, B. Ahmad. "Thermal radiation impact in mixed convective peristaltic flow of third grade nanofluid", Results in Physics, 2017](#)

55 < 1% match (publications)  
[T. Hayat, Sadia Ayub, Anum Tanveer, Ahmed Alsaedi. "Numerical simulation for MHD Williamson fluid utilizing modified Darcy's law", Results in Physics, 2018](#)

56 < 1% match (publications)  
[T. Hayat, S. Farooq, A. Alsaedi, B. Ahmad. "Hall and radial magnetic field effects on radiative peristaltic flow of Carreau-Yasuda fluid in a channel with convective heat and mass transfer", Journal of Magnetism and Magnetic Materials, 2016](#)

57

&lt; 1% match (Internet from 15-Feb-2012)

<http://ijens.org/Vol%2011%20%2001/101306-1101-4949%20IJET-IJENS.pdf>

58

&lt; 1% match (student papers from 09-Apr-2018)

[Submitted to Higher Education Commission Pakistan on 2018-04-09](#)

59

&lt; 1% match (student papers from 21-Dec-2013)

[Submitted to Higher Education Commission Pakistan on 2013-12-21](#)

60

&lt; 1% match (publications)

[Mekheimer, Kh.S. Abd elmaboud, Y.. "Simultaneous effects of variable viscosity and thermal conductivity on peristaltic flow in a vertica", Canadian Journal of Physics, Dec 2014 Issue](#)

61

&lt; 1% match (student papers from 14-May-2018)

[Submitted to Higher Education Commission Pakistan on 2018-05-14](#)

62

&lt; 1% match (student papers from 16-Aug-2017)

[Submitted to University of Dayton on 2017-08-16](#)

63

&lt; 1% match (student papers from 06-Aug-2018)

[Submitted to Higher Education Commission Pakistan on 2018-08-06](#)

64

&lt; 1% match (student papers from 27-Jun-2017)

[Submitted to International School of Management and Technology on 2017-06-27](#)

65

&lt; 1% match ()

[http://www.ee.ust.hk/~analog/thesis/900M\\_cmos\\_wireless\\_transceiver.pdf](http://www.ee.ust.hk/~analog/thesis/900M_cmos_wireless_transceiver.pdf)

66

&lt; 1% match (publications)

[T. Hayat, S. Farooq, B. Ahmad, A. Alsaedi. "Homogeneous-heterogeneous reactions and heat source/sink effects in MHD peristaltic flow of micropolar fluid with Newtonian heating in a curved channel", Journal of Molecular Liquids, 2016](#)

67

&lt; 1% match (student papers from 26-May-2017)

[Submitted to Higher Education Commission Pakistan on 2017-05-26](#)

68

&lt; 1% match (Internet from 03-Sep-2010)

<http://www.seas.gwu.edu/~simhaweb/cs173/classwork/module4/module4.html>

69

&lt; 1% match (Internet from 27-May-2014)

<http://scik.org/index.php/jmcs/article/download/209/109>

70

&lt; 1% match (Internet from 03-Aug-2018)

<http://www.mdpi.com/2071-1050/10/8/2671/htm>

- 71 < 1% match (Internet from 09-Sep-2010)  
[http://courses.engr.illinois.edu/ece445/projects/fall2000/project30\\_final\\_paper.doc](http://courses.engr.illinois.edu/ece445/projects/fall2000/project30_final_paper.doc)
- 72 < 1% match (Internet from 07-Aug-2018)  
<https://epdf.tips/curves-and-surfaces-for-computer-graphics.html>
- 73 < 1% match ()  
[http://syd.falundafa.org.au/book/eng/pdf/dymf\\_en.pdf](http://syd.falundafa.org.au/book/eng/pdf/dymf_en.pdf)
- 74 < 1% match (Internet from 25-May-2018)  
<https://upcommons.upc.edu/bitstream/handle/2117/96362/TLT1de1.pdf>
- 75 < 1% match (Internet from 30-Mar-2015)  
[http://103.23.100.141/dokumen/astrodb/exe/SolarEclipse/AS\\_CIL.CBD](http://103.23.100.141/dokumen/astrodb/exe/SolarEclipse/AS_CIL.CBD)
- 76 < 1% match (Internet from 06-Mar-2017)  
<http://wah.comsats.edu.pk/Research/publications.aspx>
- 77 < 1% match (Internet from 22-May-2018)  
<http://usir.salford.ac.uk/40763/7/1-s2.0-S2215098616308138-main.pdf>
- 78 < 1% match ()  
<http://www.computerinnovation.com/ProjectAJMM40.htm>
- 79 < 1% match (Internet from 05-Jun-2008)  
<http://www.chemweb.com/journals?type=issue&jid=07351933&iid=00330006>
- 80 < 1% match (Internet from 12-Oct-2008)  
<http://www.agbios.com/cstudies.php?book=FSA&ev=GTS&chapter=Molecular&lang=>
- 81 < 1% match (Internet from 08-Jun-2011)  
[http://www-cdslab.ece.umn.edu/cdslab/library/theses/toenning\\_ms.pdf](http://www-cdslab.ece.umn.edu/cdslab/library/theses/toenning_ms.pdf)
- 82 < 1% match (Internet from 18-May-2014)  
<http://www.icm2010.in/wp-content/icmfiles/abstracts/Contributed-Abstracts-5July2010.pdf>
- 83 < 1% match (Internet from 07-Jul-2014)  
<http://www.hood-online.co.uk/shinkansen/book1/5-10.php>
- 84 < 1% match (Internet from 05-Jun-2018)  
<http://shura.shu.ac.uk/20365/1/10701011.pdf>

- 85 < 1% match (Internet from 09-Jul-2018)  
<https://doaj.org/article/e3974ef1bd65404f9f46099b11b51bea>
- 
- 86 < 1% match (Internet from 19-Aug-2018)  
[http://jafmonline.net/JournalArchive/download?file\\_ID=37193&issue\\_ID=222](http://jafmonline.net/JournalArchive/download?file_ID=37193&issue_ID=222)
- 
- 87 < 1% match (Internet from 15-Aug-2014)  
[http://tastyspleen.net/~quake2/baseq2/maps/q1edge\\_x7.bsp](http://tastyspleen.net/~quake2/baseq2/maps/q1edge_x7.bsp)
- 
- 88 < 1% match ()  
[http://www2.eng.cam.ac.uk/~ypc21/YPCheng\\_MPhil.pdf](http://www2.eng.cam.ac.uk/~ypc21/YPCheng_MPhil.pdf)
- 
- 89 < 1% match (Internet from 27-Aug-2011)  
<http://www.coursehero.com/file/2732635/beltranj76411/>
- 
- 90 < 1% match (Internet from 24-Nov-2017)  
<http://journals.plos.org/plosone/article?id=10.1371%2Fjournal.pone.0129588>
- 
- 91 < 1% match (Internet from 08-Feb-2014)  
<http://cosmodroid.ru/uploads/files/audio/DogTeaserSoundBox.apk>
- 
- 92 < 1% match (Internet from 29-Nov-2010)  
[http://ajse.kfupm.edu.sa/articles/301A\\_06P.pdf](http://ajse.kfupm.edu.sa/articles/301A_06P.pdf)
- 
- 93 < 1% match (Internet from 19-Aug-2018)  
[http://jafmonline.net/JournalArchive/download?file\\_ID=40237&issue\\_ID=235](http://jafmonline.net/JournalArchive/download?file_ID=40237&issue_ID=235)
- 
- 94 < 1% match (Internet from 15-Feb-2017)  
[http://www.medjchem.com/public/journals/3/cv/cv\\_rashidi17.pdf](http://www.medjchem.com/public/journals/3/cv/cv_rashidi17.pdf)
- 
- 95 < 1% match (Internet from 08-Sep-2011)  
<http://tarksheel.com/admin/books/Chamkda%20Stara.pdf>
- 
- 96 < 1% match (Internet from 26-Aug-2018)  
<http://textroad.com/pdf/JBASR/J.%20Basic.%20Appl.%20Sci.%20Res.,%201%287%29751-758,%202011.pdf>
- 
- 97 < 1% match (publications)  
[International Journal of Numerical Methods for Heat & Fluid Flow, Volume 24, Issue 5 \(2014-09-16\)](http://www.ijnumerical.com/International-Journal-of-Numerical-Methods-for-Heat-&-Fluid-Flow-Volume-24-Issue-5-(2014-09-16))
- 
- 98 < 1% match (publications)  
[Hayat, T., S. Farooq, A. Alsaedi, and B. Ahmad. "Hall and radial magnetic field effects on radiative peristaltic flow of Carreau–Yasuda fluid in a channel with convective heat and mass](http://www.ijnumerical.com/Hayat-T-S-Farooq-A-Alsaedi-and-B-Ahmad-Hall-and-radial-magnetic-field-effects-on-radiative-peristaltic-flow-of-Carreau-Yasuda-fluid-in-a-channel-with-convective-heat-and-mass)

[transfer", Journal of Magnetism and Magnetic Materials, 2016.](#)

99

< 1% match (publications)

[Liu, Hongzhi and Nagano, Katsunori. "Numerical simulation of an open sorption thermal energy storage system using composite sorbents built into a honeycomb structure", Elsevier, 2014.](#)

100

< 1% match (publications)

[Rashidi, Mohammad Mehdi Ali, Mohamed Ros. "Heat and mass transfer for MHD viscoelastic fluid flow over a vertical stretching sheet with consider", Mathematical Problems in Engineering, Annual 2015 Issue](#)

101

< 1% match (student papers from 18-Dec-2017)

[Submitted to Higher Education Commission Pakistan on 2017-12-18](#)

102

< 1% match (publications)

[Hayat, T., S. Farooq, B. Ahmad, and A. Alsaedi. "Homogeneous-heterogeneous reactions and heat source/sink effects in MHD peristaltic flow of micropolar fluid with Newtonian heating in a curved channel", Journal of Molecular Liquids, 2016.](#)

103

< 1% match (publications)

[Hayat, T., Rija Iqbal, Anum Tanveer, and A. Alsaedi. "Influence of convective conditions in radiative peristaltic flow of pseudoplastic nanofluid in a tapered asymmetric channel", Journal of Magnetism and Magnetic Materials, 2016.](#)

104

< 1% match (publications)

[Hayat, T., Anum Tanveer, and A. Alsaedi. "Numerical analysis of partial slip on peristalsis of MHD Jeffery nanofluid in curved channel with porous space", Journal of Molecular Liquids, 2016.](#)

105

< 1% match (publications)

[Hina, S., M. Mustafa, T. Hayat, and A. Alsaedi. "Peristaltic flow of Powell-Eyring fluid in curved channel with heat transfer: A useful application in biomedicine", Computer Methods and Programs in Biomedicine, 2016.](#)

#### paper text:

Contents 1 Literature review and basic laws 5 1.1 Literature survey . . . . . 5

331.2 Basic **equations** . . . . . 14 **1.2.1 Mass conservation** . . . . . 14 **1.2.2 Momentum conservation** . . . . . 15 **1.2.3 Energy conservation** . . . . . 15 **1.**

2.4 Concentration conservation . . . . . 15 1.2.5 Transformations and volume flow rate . . . . . 16 1.2.6 Dimensionless parameters . . . . . 17 2

Hall current and Joule heating impacts in peristaltic transport of rotating liquid 19  
 19 2.1 Introduction .....  
 ..... 19 2.2 Problem development .....  
 19 2.3 Solution methodology ..... 22 2.4 Discussion .....  
 ..... 22 2.4.1 Axial velocity ..... 22 2.4.2  
 Secondary velocity ..... 24 2.4.3 Temperature .....  
 ..... 25 2.4.4 Heat transfer coefficient ..... 27 2.5 Conclusions .....  
 ..... 28 3 Impact of thermal radiation and thermophoresis on  
 peristalsis in rotating frame 30

**143.1 Introduction ..... 30**  
**3.2 Problem development ..... 31**  
**3.3**

Solution methodology ..... 34 3.4 Discussion .....  
 ..... 34 3.5 Conclusions ..... 40 4 Peristaltic  
 activity of rotating Prandtl fluid 42 4.1 Introduction ..... 42 4.2  
 Definition ..... 42 4.3 Analysis .....  
 ..... 45 4.4 Conclusions ..... 53 5

**9MHD peristaltic flow of rotating Prandtl fluid with Soret and**

Dufour effects 54 5.1 5.2 5.3 5.4 5.4.1 5.4.2 5.4.3 5.4.4 5.4.5 Introduction .....  
 ..... 54 Problem development ..... 54 Solution methodology .  
 ..... 58 Discussion ..... 58  
 Axial velocity ..... 58 Secondary velocity .....  
 ..... 60 Temperature ..... 62 Concentration .....  
 ..... 65 Heat transfer coefficient ..... 68 5.5 Conclusions .....  
 ..... 70 6 Heat transfer analysis on peristalsis of Ree-Eyring fluid 71

**146.1 Introduction ..... 71**  
**6.2 Problem development ..... 71**  
**6.3 Solution**

methodology ..... 75 6.4 Discussion .....  
 ..... 76 6.5 Conclusions ..... 82 7 Numerical analysis  
 for ionslip and Hall current on peristaltic transport of rotating Ree-Eyring fluid 84

**147.1 Introduction ..... 84**  
**7.2 Problem development ..... 84**  
**7.3 Solution**

methodology ..... 87 7.4 Discussion .....  
 ..... 88 7.5 Conclusions ..... 92 8 Peristalsis of  
 couple stress liquid in a non-uniform rotating geometry

64	<b>93 8.1 Introduction</b>	93	<b>8.2</b>
	<b>Problem</b> development	93	<b>8.3 Solution</b>

methodology	96	8.4 Discussion	
97	8.4.1 Axial velocity	97	8.4.2 Secondary velocity
	98	8.4.3 Temperature profile	
100	8.4.4 Heat transfer rate	101	8.4.5 Streamlines
	103	8.5 Conclusions	104
	106	9.1 Introduction	9
	106	9.2 Problem statement	106
	109	9.3 Solution methodology	9.3
	109	9.4 Discussion	
	109	9.4.1 Velocity profile	109
	109	9.4.2 Heat transfer	
	111	9.5 Conclusions	
	115	10 Entropy generation impact on peristaltic motion in a rotating frame	116
	116	10.1 Introduction	
	116	10.2 Problem definition	
	116	10.3 Entropy generation	120
	120	10.4 Solution methodology	
	120	10.5 Discussion	
	121	10.5.1 Entropy generation	128
	121	10.5.2 Trapping	
	131	10.6 Conclusions	

132 Chapter 1 Literature review and basic laws This chapter deals with literature review related to peristalsis and transfer of heat with different effects in a rotating frame. Some fundamental equations for fluids flow are also presented in this chapter. 1.1 Literature survey Peristalsis in human physiological systems has gained much attention of the researchers. Engelmann [1] was the first to investigate the existence of peristaltic waves in ureter. After his initial work, several other researchers like Lapidus [2], Kiil [3] and Boyarsky [4] put their efforts to extend this study. The phenomenon of peristaltic pumping was discussed by Latham [5]. Shapiro et al. [6] presented experimental work by considering the inertia free flow in a flexible tube.

#### 54 The pioneer work of Latham [5] and Shapiro et al.

[6] opened new ways for further advancements in peristaltic transport. After the confirmation of Shapiro's theory based on

#### 98 long wavelength and low Reynolds number approximation by Eckstein [7] and

Weinberg [8], a number of attempts have been made for advancements in this direction. Further the ureteral system as peristaltic pump by imposing different waves on ureteral walls was analyzed by Weinberg et al. [9] and Lykoudis [10]. Zein and Ostrach [11] investigated significance of peristalsis in ureteral system. Afterwards, Fung [12? 13] discussed the effect of biomechanical forces on dynamics of urethral muscles. Peristalsis of viscous liquid in both symmetric and asymmetric configurations is explored by Burns and Parkes [14]. Lubrication approach was adopted by Hanin [15] along with consideration of small amplitude ratio. An investigation on studying the impact of low Reynolds number on peristalsis in a tube of roller pump is carried out by Meghiniss [16].

**5 Peristaltic flow of viscous fluid through circular tube is addressed by Yin and Fung**

[17]. Lew and Fung [18? 19] explored asymmetric flow of viscous fluid in a cylindrical tube. Their investigation presents the importance of fluid motion inside vessels of living organisms. Barton et al. [20] discussed the peristaltic motion in tubes. An analysis on peristalsis of viscous fluid subject to inertial and streamline curvature is conducted by Jaffrin [21]. Tong and Vawter [22] adopted finite element method to analyze the peristaltic transport through a tube.

**1 Movement of spermatozoa in tube is mathematically investigated by Semleser et al.**

[23]. Mitra and Parsad managed to determine

**43 the impact of Poiseuille flow on peristalsis in a two dimensional channel**

[24]. Liron [25] developed the series solution by double expansion about long wavelength and Reynolds number for peristalsis in pipe and channel. He studied the efficiency of biological functions in terms of peristaltic flow. Assumption of small wave number is invoked in his analysis. Impacts of wave amplitude and wavelength on flow field was first presented by Brown and Hung [26]? He observed that reflux occurs on the axis of the tube for short wavelengths. However reflux occurs off the axis for longer wavelengths. A detailed examination of peristaltic flow through pipe and channel is carried out by Srivastava and Srivastava [27]. Nakanishi [28] numerically investigated a two-dimensional model of peristalsis of viscous fluid through a channel with pro- gressive waves of wall contraction. Takabatake et al. [29] adopted finite difference scheme for analyzing the peristaltic pumping through a tube. Peristalsis of incompressible viscous

**92 fluid through uniform and non-uniform annulus is**

elaborated by Makheimer [30]. Inertia and curva- ture effects on peristalsis in asymmetric geometry is explored by Rao and Mishra

**1 [31]. Viscous fluid flow subject to complaint walls has been analyzed by Hayat et al. [32].**

There is no doubt that many realistic liquids are different then viscous fluids. Non-Newtonian characteristics have been exhibited by peristalsis transport of chyme in [33] and contraction and expansion of blood vessels in [34].

**25 The classical Navier Stokes relations are unable to describe the nature of rheological complex**



liquids such as lubricants, hydrocarbons, industrial oils, shampoo, muds, petroleum and blood etc. Non-Newtonian fluids have wide utility in many phenomena. In order to investigate the non-Newtonian behavior of fluids, many models have been formulated by the investigators. Patel and Timol [35] mentioned the stress strain relation- ship for non-Newtonian fluids. Akbar et al. [36] performed an analysis for

105 **flow of Carreau fluid through** asymmetric channel. **A**

study on peristaltic transport of Jeffrey fluid through rectangu- lar duct is commenced by Ellahi and Hussain [37]. Jeffrey fluid flow with simplest mathematical form is capable of relating the retardation and relaxation times effects. Bhatti and Abbas [38] investigated peristaltic blood flow by considering Jeffrey model saturating porous medium. Ap- plication of low Reynolds number on peristaltic motion of micropolar fluid was discussed by Devi and Devanathan [39]. Adomian decomposition method was adopted by Sheikholeslami et al. [40] in order to investigate Jeffrey-Hamel flow analytically. Long wavelength assumption is employed on two-dimensional peristalsis of non-Newtonian fluid by Rahakrishnamacharya [41].

5 **Srivastava and Saxena** [42] observed **the peristaltic** transport **of blood** through a tube of **uniform diameter**. **They** employed **constitutive relation of Casson fluid for blood**.

5 **Elshehawey et al.** [43] scrutinized **the peristaltic motion of Carreau fluid** by invoking the **lubrication approach** and employing the **perturbation technique for small Weissenberg number**.

An analytical discussion on flow properties

30 **of Carreau fluid in a compliant rectangular duct**

is commenced by Riaz et al. [44]? Sisko fluid is one of the most important non-Newtonian fluids comprised of shear thinning as well as shear thickening attributes. Sisko fluid model has tendency to represent the proper- ties of Newtonian and non-Newtonian fluids for suitable choice of material fluid parameter. An analysis for porosity and

53 **magnetic field** effects **on flow of** Sisko **fluid**

is

23 **provided by Hayat et al.** [45? 46]. Zaman **et al.**

[47] managed to study blood flow through vessel by assuming the blood as Sisko fluid. Hayat et al. [48] reported a numerical investigation of peristalsis of non-Newtonian Carreau-Yasuda fluid under the influence of Hall effect. Mernone and Mazumdar [49] provided a detailed theoretical investigation of Casson fluid through an axisymmetric channel. Eytan and Elad [50] inspected the motion of intrauterine fluid motion due to myometric contraction as peristaltic transport. Nadeem and Akram [51] scrutinized two-dimensional peristaltic flow of hyperbolic tangent fluid and simplified the problem under lubrication approach.

1 Hina et al. [52] examined the wall properties on peristalsis in a curved channel

by considering pseudo-plastic fluid and

1 heat and mass transfer. They discussed the shear-thinning/thickening effects followed by lubrication approach. Akbar et al. [53] employed non-Newtonian Williamson fluid for numerical study of peristalsis

in an axisymmetric channel. Peristalsis of Prandtl

1 fluid under long wavelength assumption has been reported by Riaz et al.

[54]? This work is extended by Hayat et al. [55] with Hall and chemical reaction effects. Viscoelastic non-Newtonian fluids have tremendous applications in physiology and industry.

17 Ree-Eyring can be reduced to Newtonian fluid model for both high and low shear rates. Also its constitutive equation can be obtained from kinetic theory of fluids instead of empirical relation.

Ketchup, polymer solutions, ketchup, nail polish and wiped cream are some of the relevant examples. Physiological fluids movement like blood also contains such characteristics. Pulsatile flow of Ree-Eyring

102 fluid in a channel is discussed by Shawky et al.

[56]. Bhatti et al. [57] discussed blood flow in a vessel by considering Ree-Eyring fluid. Abbasi et al. [58] worked out

54 flow of Eyring Power liquid in curved channel.

This work was extended by Hina et al. [59] in

14 presence of heat and mass transfer. Theory of micropolar fluid

was explained by Eringen [60] and characteristics like body couples, microinertial effects, couple stresses and microrotation are illustrated in details. Johnson and Segalman [61] introduced the theory for viscoelastic fluids expressing non-affine deformation. Chaturani and samy [62] analyzed the blood flow through arteries. Bohme and Friedrich [63] modeled a problem for investigating attributes of an incompressible viscoelastic fluid in a planar channel without any inertial force. Chaturani and Samy performed an analysis for peristalsis of blood through stenosed artery [64].

23 **Flow of Eyring Powell fluid** model through straight **channel**

is demonstrated

23 **by Hayat et al.** [64]. Alvi **et al.**

[65] examined impact of non-constant viscosity on peristaltic activity of Jeffrey fluid containing nanoparticles. Latif et al. [66] discussed the peristalsis of third order liquid with variable properties. Also Fosdick and Rajagopal [67] presented thermodynamics analysis for third grade fluid. Tripathi et al. [68] explored the peristalsis of fractional Maxwell fluid in a channel. Couple stress fluid model is intended for the body couples and couple stresses in the medium of fluid. It has applications to understand many physical problems as it possesses the rheological convoluted fluid phenomena. Coating of paper, plasma, nuclear fuel slurries, polymers, fossil fuels, lubrication with heavy oils and greases carry such rheological characteristics. From industry point of view, many applications e.g., colloidal fluids, extrusion of polymer fluids, exotic lubricants, metallic plate cooling in bath and solidification of liquid crystals are related to this fluid. In the lubrication of engine rod bearings and tribology of thrust bearings, this fluid is also important. Couple stress model has been used to discuss biomedical phenomena such as infected urine from a diseased kidney and human and animal blood. Peristalsis of couple stress liquid in an endoscope was investigated by Mekheimer and Abd elaboud [69]. Then his work is extended by Shit and Roy [70] through inclined

24 **channel. The problem is** solved analytically **by** taking **long wavelength and low Reynolds number assumptions.** Ramesh [71] stated **the** rheology of

couple stresses in transport of fluids. Importance of heat transfer in medical and industrial applications cannot be ignored.

5 **Par- ticularly, the heat transfer** phenomenon **in human body is an important area of research.**

Due to its wide spread significance in human tissues, many biomedical engineers are attracted to- wards human thermoregulation system [72] and thermotherapy [73]. In humans heat transfer take place as conduction in cancer tissues, metabolic heat generation,

10 **dilution technique in examining blood flow,**

10 **perfusion of arterial-venous blood through the pores of the**

tissues and vasodilation. Transfer of heat with the interaction of peristaltic fluid flows is significant in hemodialysis, oxygenation, laser therapy and thermal energy storage. Radhakrishnamacharaya

63 **et al. [74] and Vajravelu et al. [75] analyzed the heat transfer on peristaltic flow of viscous**

fluid in non-uniform channel and tube. Peristaltic flows of

9 **viscous and non-Newtonian fluids in the presence of magnetic field**

is significant in physiological processes such as medicine and bio- engineering. Many phenomena are based on MHD principles such as

36 **design of heat exchangers, flow meters, radar systems, MHD compressor operation etc. Such**

effects is useful in the de- velopment of magnetic devices, hyperthermia [76], blood reduction during surgeries and cancer tumor treatment, MHD drug targeting [77], micro-circulation flows [78] and biomedical flow control, separation devices [79], in treatment of the pathologies e.g., gastroenric pathologies, rheumatisms, constipation and hypertension. Another important aspect of MHD is related to Hall and ionslip effects. Hall current is much more significant for higher externally applied magnetic field. Further when the electron-atom-collision frequency is high then ionslip effect cannot be ignored. Some applications which basically lie on Hall and ionslip currents include MHD generators, electric transformers, power generators, Hall accelerators, heating elements, refrigeration coils and flight MHD. In addition flow of fluid is much affected by the presence of Joule heating.

21 **The study of heat transfer with Joule heating effects has immense applications in**

biomedical engineering and food industries. Effect of Joule heating arises from the fluid elec- trical resistivity and applied electric field.

19 **One of the applications of electro osmosis is the fluid delivery in lab-on-a-chip devices, where one deals with thermally labile samples. Temperature rise due to Joule heating can result in low column separation efficiency, reduction of analysis resolution and even loss of injected samples.**

Therefore several investigations regarding these effects in peristalsis are performed. Sud et al. [80] discussed the magnetic field effect for blood flow. Peristaltic activity of blood flow in equally branched channel is investigated by Agrawal et al. [81]. Their study concludes that during cardiac surgeries the magnetic field may be used in blood pump. Radhakrishnamacharya and Murty [82] examined the MHD aspects of

9 **peristaltic flow in a non-uniform**

channel. Wang et al. [83] discussed magnetohydrodynamics effects on

57 **peristaltic motion of Sisko fluid in symmetric channel.** Hayat et al. [84] convassed the **peristaltic flow of MHD hyperbolic tangent fluid**

55 **with Joule heating and slip conditions.**

Awais et al. [85] examined convective

40 **heat transfer on MHD peristaltic flow in a**

symmetric channel. Abbasi et al. [86] observed MHD

24 **peristaltic flow of Carreau fluid in curved channel under long wavelength and low Reynolds number**

assumptions. Further his work was extended by Ellahi et al. [87] by employing a uniform duct of rectangular cross section. Analytical solutions are obtained by employing a perturbation method. They also compared their results by numerical solutions. Heat transfer phenomenon with Ohmic heating is discussed by Asghar et al. [88]. They also considered the Hall and ionslip effects in their analysis. Hayat et al. [89] extended the work of Asghar et al. [88] for Jeffrey nanofluid. Nowar [90] investigated peristaltic flow of nanofluid saturating porous space inside the channel with Hall effect.

9 **In a non-uniform rectangular duct**

Pop et al. [91] observed

12 **the peristaltic flow of non-Newtonian fluid with**

magnetic and ionslip effects.

94 **Blood flow of Powell Eyring fluid in a porous**

medium with ionslip effect

11 **is studied by Bhatti et al. [92]. Noreen and Qasim [93] analyzed the flow of**

pseudoplastic fluid in presence of Hall current. In many environmental and scientific processes,

20 **thermal radiation plays a significant role. Radiative heat transfer**

occurs when electromagnetic waves propagate across pore-air spaces. Heating and cooling of chambers, astrophysical flows, solar power technology and water evaporation from open reservoirs are useful applications of this effect. Thermal insulation, cooling of nuclear reactors, combustion, fluidized bed heat exchanger, biological tissues, turbid water bodies, furnace design, gas turbines, power generation systems, high temperature plasmas, fire spreads, solar fans, solar collectors, cancer therapy are such significant examples of thermal radiation. In addition heat generation/absorption effect is quite useful in thermal performance of working fluids.

20 **Radiation can control the excess heat generation inside the body since high temperatures pose serious stresses for the human body placing it in serious danger of injury or even death.**

Further the involvement of heat generation/absorption effect in heat transfer is encountered frequently in many fields such as engineering, aerosol technology and industrial sector. It is also quite useful in the manufacture of plastic and rubber sheets, food stuff storage, disposal of radioactive waste material and dislocating of fluids in packed bed reactors.

1 **Having all such in mind the representative studies for**

non-uniform heat source/sink and

1 **radiation of nonlinear fluids have been addressed by number of researchers**

[94 – 102]. Mass transfer mechanism involves transfer of mass from one location to another. Mass transfer occurs in variety of engineering process. Specifically in chemical industry, mass transfer has widespread applications such as diffusion of chemical impurities, distillation process, reverse osmosis and membrane separation process. The rate of mass transfer rely on diffusivity and flow pattern of fluid. Investigation of combined heat and mass transfer species is important in seeking better understanding of various physical phenomena. Heat and mass transfer is not only responsible for energy distribution in the system but these

also influence the system mechanics. Peristalsis with heat and mass transfer has vital position in biomedical sciences and industry. Few relevant applications are food processing [103], fog dispersion [104], metal purification [105], vasodilation, perspiration in hot weather, blood transfusions [106], heat convection occurring due to blood flow through pores of tissues, food drying [107], nuclear power generation [108], underground disposal of nuclear waste and extraction of geothermal energy. Energy flux induced by

13 **concentration gradient is** referred **as Dufour effect** whereas **mass flux** produced **by temperature gradient is** known **as Soret effect**.

Importance of Soret-Dufour effect cannot be neglected in isotopes separation, catalytical reactor, reservoir engineering and paper industry. Ogulu [109] put forward his efforts in investigating

79 **fluid and mass transfer flow of blood** through **single vessel**.

Nadeem and Akbar [110] discussed peristalsis of Jeffrey-six constant fluid filled

11 **with heat and mass transfer** simultaneously. **Hayat et al.**

[111] scrutinized

12 **heat and mass transfer** effects **on peristaltic** transport **of** pseudoplastic **in the presence of** induced **magnetic field**. Shaaban **and**

Abou-zeid [112] performed a comprehensive study on MHD

23 **peristaltic flow of Eyring-Powell fluid**. **Hayat et al.**

[113] examined Joule heating aspects

9 **on mixed convective peristaltic flow of** viscous nano **fluid with** Soret **-Dufour effects**.

Mustafa et al. [114] focused their attention on study of peristalsis of

13 **fourth grade fluid under** the influence of **Dufour and Soret effects**.

They adopted Keller-box method for numerical solution of non-linear boundary value problem. Hayat et al. [115] discussed

13 **Soret and Dufour effects on** peristalsis **of pseudoplastic** fluid through **a tapered channel.**

Farooq et al. [116] considered the mathematical aspects of

52 **Soret and Dufour** phenomena **on MHD peristalsis of**

Jeffrey fluid. He performed his analysis subject to variable viscosity.

13 **Hayat et al.** [117] accounted **the Soret-Dufour**

impacts on peristalsis of Bingham plastic fluid by regular perturbation technique for series solution of problem. Chemical reaction is another phase of mass transfer. Investigation of heat and mass transfer problems with chemical reaction has promising applications in industry such as burning of fuels, making cheese, solar collector, combustion system, smelting iron and brewing beer. Chemical reactions are integral part of many complicated processes of living organisms. Mustafa et al. [118] addressed

40 **heat and mass transfer on** mixed convective peristalsis **of fourth grade fluid.**

Hayat et al. [119] attempted to investigate

85 **the peristaltic transport of** Casson **fluid under the influence of**

chemical reaction and Soret-Dufour effect. Sankad and Dhange [120] modeled

30 **peristaltic transport of incompressible viscous fluid** with flexible walls **and**

chemical reaction. He computed the mean effective coefficient of dispersion through Taylor's limit and long wavelength hypothesis. Muthuraj et al. [121] performed a comprehensive examination

39 **on peristaltic** pumping **of dusty fluid in the presence of**

chemical reaction and wall properties. Impact of thermal deposition and chemical reaction on peristalsis of Carreau-Yasuda fluid is reported by Hayat et al. [122]. Machireddy and Kattamreddy [123] commenced a study for Joule heating and chemical reaction effects on

104 **peristaltic flow through porous medium.** Influence of **chemical reaction**



on hydromagnetic peristaltic pumping of radiating and reacting couple stress fluid passing through an inclined

52channel is explored by Reddy et al. [124]. Mishra et al.

[125] explained impact of chemical reactions on peristalsis of physiological fluids with temperature dependent properties. Thermophoresis is a kind of mass transfer that occurs due to movement of colloidal particles due to macroscopic temperature. Small suspended particles are more likely to travel in the direction of decreasing

10temperature when temperature gradient is maintained in the gas.

10This phenomenon arises due to difference of average velocities of particles. The most common

applications of thermophoresis are stone statue erosion, eliminate the particles from gas stream, silicon thin film deposition and

10blackening of glass of kerosene lantern. The

novel features of Joule heating

10and thermophoresis on MHD peristaltic pumping of

viscous nanofluid are elaborated by Shehzad

53et al. [126]. Hayat et al. [127] scrutinized the effects of thermophoresis and

rotations on MHD peristalsis of Jeffrey fluid with non-uniform heat source/sink and flexible wall channel. Ali et al. [128] considered fourth grade for peristaltic transport through asymmetric channel of convective walls with concentration and thermophoresis effects. Analytic solution of problem is approximated through perturbation technique. Analysis of heat transfer in fluid flow by movement of particles is known as convection. In many physical processes such as gas turbines, thermal storage and nuclear fluid transport, macroscopic fluid transportation produces development in heat transfer. Transfer of heat between static fluid and solid boundary through physical contact is referred as conduction. In case of moving fluids, heat transfer occurs through conduction as well as convection. For such problems boundary conditions can be modified by

5Fourier law of heat conduction and the Newton's law of cooling. These conditions are referred as convective

boundary conditions [129? 130]. Hemodialysis and oxygenation, hypothermia treatment,

60 **sanitary fluid transport, blood pump in heart-lung machines, transport of corrosive fluids,**

laser therapy and coldness cryosurgery are some practical applications. In view of such importance various researchers studied the peristaltic flow subject to convective boundary condition [131 – 135]? Flow pattern with

18 **slip boundary characteristics has special significance in many applications.**  
Undoubtedly due to **the** wetted wall, **a loss of adhesion**

by fluid is presented

18 **which compels it to slide along the wall.**

In fluid-solid interaction situations, slip effect is meaningful in describing the macroscopic effects of certain molecular phenomena. Some daily life applications of slip are rarefied fluid, polishing of internal cavities and artificial heart valves,

42 **fluid motion within human body, flow on multitudinal interfaces**

and thin film.

1 **However less devotion towards slip relative to peristalsis is shown in the literature.**

18 **Ali et al.** [136] examined **the slip effects on MHD peristaltic flow of viscous fluid with variable viscosity.** Hayat **et al.** [137? 138] captured **the** effect of **slip** under **peristaltic flow of** Jeffrey **and**

viscous materials respectively. Couple stress fluid flow with peristalsis through porous medium comprising slip effects has been reported by Ramesh [139]. Hina et al. [140] studied peristalsis of Johnson-Segalman fluid in curved geometry subject to slip conditions. Yildirim and Sezer [141] discussed

76 **partial slip on MHD peristalsis of viscous fluid in an asymmetric channel.**  
Peristaltic motion **of**

power-law model is analyzed by Kumar et al. [142]. Ellahi and Hussain [143] discussed peristaltic flow in a rectangular duct with slip effects. Some more investigations for slip effect are reported via studies [144 – 149]. Existing literature on peristaltic mechanism were done in straight or curved channels. However literature peristalsis of viscous and non-Newtonian fluids in rotating channel is scarce. Flow of fluid in rotating frame has gained much importance amongst the researchers. It is because of its vast applications in ocean circulation, gas turbines, medical equipment, galaxies formation, aircraft, rotational spectroscopy, rotational air cleaner and geophysical flows. This phenomenon through rigid body rotation give rise to effects of centrifugal and Coriolis force in addition of inertial forces. Few aspects for peristalsis with rotating frame are discussed in the attempts [150 – 156].

1.2 Basic equations Here the basic laws for mass, momentum, energy and concentration are presented.

1.2.1 Mass conservation The mass conservation equation in differential form is  $\rho \nabla \cdot \mathbf{V} = 0$  (1.1) Here  $\rho$  denotes the density,  $\mathbf{V}$  the velocity and  $\nabla$  represents gradient operator. For incompressible material  $\nabla \cdot \mathbf{V} = 0$  (1.2)

1.2.2 Momentum conservation Generalized equation of motion is  $\rho \frac{D\mathbf{V}}{Dt} = \nabla \cdot \boldsymbol{\tau} + \mathbf{f} - \nabla p + \mathbf{S}$  (1.3) (1.4) where  $\boldsymbol{\tau}$  represents Cauchy-stress tensor,  $\mathbf{f}$  body force,  $\mathbf{I}$  identity tensor,  $\mathbf{S}$  extra stress tensor,  $\frac{D}{Dt}$  the material time differentiation, and  $p$  the pressure. Equation of momentum in rotating is written as:  $\rho \frac{D\mathbf{V}}{Dt} + \rho [2(\boldsymbol{\Omega} \times \mathbf{V}) + \boldsymbol{\Omega} \times (\boldsymbol{\Omega} \times \mathbf{r})] = \nabla \cdot \boldsymbol{\tau} + \mathbf{f}$  (1.5) where on left hand side second and third terms present the Coriolis and centrifugal force respectively. Here  $\boldsymbol{\Omega}$  denotes angular velocity.

1.2.3 Energy conservation The energy equation is  $\rho \frac{D\theta}{Dt} = -\nabla \cdot \mathbf{q} + \dot{q}$  (1.6) where  $\theta$  shows temperature,  $\dot{q}$  specific heat and  $\mathbf{q}$  fluid's thermal conductivity. First and second term on right side stands for energy flux and source term related to transport of energy. For the modification of heat transport characteristics the source term is responsible for consideration of velocity components, radiative heat flux, surface heating cooling, and viscous dissipation. Moreover, it also stands for other physical phenomena such as Joule heating and Dufour effects.

1.2.4 Concentration conservation Suppose  $c$  be the mass concentration of fluid per unit volume, then equation of mass can be given as:  $\frac{Dc}{Dt} + \nabla \cdot \mathbf{J} = 0$  (1.7) in which  $\frac{D}{Dt}$  presents the thermal-diffusion ratio,  $\mathbf{J}$  stands for mass diffusion coefficient and  $\theta$  is the mean temperature.

1.2.5 Transformations and volume flow rate In present thesis we use Galilean transformations for flow analysis from laboratory to wave frames of reference. The variables are designed as  $\mathbf{r}^* = \mathbf{r} - \mathbf{U}t$

$$\frac{Dc}{Dt} + \nabla \cdot \mathbf{J} = 0 \quad (1.7)$$

8) where  $p^*$  and  $\mathbf{V}^*$  are the pressure and velocity components with respect to wave frame.

**69 The dimensionless volume flow rate** for asymmetric channel in fixed and wave frames is given by

$$Q^* = \int_{-1}^1 u^* dz \quad (1.9)$$

8), the volume flow rate can be related by  $Q^* = Q + U$

**11 The time mean flow at a fixed position over a period** (say  $T$ ) is

Putting Eq. (1.10) into Eq. (1.11) and then evaluating the integral we get  $\Theta^- = \bar{\theta} + \theta_1 + \theta_2$ . Now defining nondimensional mean time flow in fixed and wave frames respectively  $\Theta^- \bar{\theta} = \theta_1 \theta_2 = \theta_1 \theta_2$  finally we obtain  $\theta = \theta_1 + \theta_2$  (1.10) (1.11) (1.12) (1.13) (1.14) in which  $\theta_1(\theta) \theta_2 = \theta_1(\theta) \theta_2$  (1.15) Similarly for symmetric channel the flow rate is given by  $\theta(\theta) \theta_1 = \theta_1(\theta) \theta_2$  (1.16)

**1.2.6 Dimensionless parameters** The non-dimensionless parameters occurring in whole thesis are defined as  $\theta_0 = \theta = \theta_2 = \theta_2 = \text{Re} \Omega^- \theta_1 \theta_2 = \theta_1 \theta_2 \theta_3 = \theta_1 \theta_2 \theta_3 \theta_4 \theta_5 \theta_6 \theta_7 \theta_8 \theta_9 \theta_{10} \theta_{11} \theta_{12} \theta_{13} \theta_{14} \theta_{15} \theta_{16} \theta_{17} \theta_{18} \theta_{19} \theta_{20} \theta_{21} \theta_{22} \theta_{23} \theta_{24} \theta_{25} \theta_{26} \theta_{27} \theta_{28} \theta_{29} \theta_{30} \theta_{31} \theta_{32} \theta_{33} \theta_{34} \theta_{35} \theta_{36} \theta_{37} \theta_{38} \theta_{39} \theta_{40} \theta_{41} \theta_{42} \theta_{43} \theta_{44} \theta_{45} \theta_{46} \theta_{47} \theta_{48} \theta_{49} \theta_{50} \theta_{51} \theta_{52} \theta_{53} \theta_{54} \theta_{55} \theta_{56} \theta_{57} \theta_{58} \theta_{59} \theta_{60} \theta_{61} \theta_{62} \theta_{63} \theta_{64} \theta_{65} \theta_{66} \theta_{67} \theta_{68} \theta_{69} \theta_{70} \theta_{71} \theta_{72} \theta_{73} \theta_{74} \theta_{75} \theta_{76} \theta_{77} \theta_{78} \theta_{79} \theta_{80} \theta_{81} \theta_{82} \theta_{83} \theta_{84} \theta_{85} \theta_{86} \theta_{87} \theta_{88} \theta_{89} \theta_{90} \theta_{91} \theta_{92} \theta_{93} \theta_{94} \theta_{95} \theta_{96} \theta_{97} \theta_{98} \theta_{99} \theta_{100}$  (1.17) Here Re denotes the Reynolds number,  $\Omega^-$  the angular velocity,  $\theta$  the displacement,  $\theta$  the wave speed,  $\theta$  the wavelength,  $\theta$  the fluid density,  $\theta$  the kinematic viscosity,  $\theta$  the electrical conductivity,  $\theta_0$  the magnetic field strength,  $\theta$  the electron,  $\theta$  the cyclotron frequency,  $\theta$  the dynamic viscosity,  $\theta_0$  concentration at walls,  $\theta_0$  temperature at walls,  $\theta$  the specific heat,  $\theta$  thermal conductivity,  $\theta$  the amplitudes,  $\theta_1$ ,  $\theta_2$  heat and mass transfer coefficient,  $\theta$

**5 the elastic tension,  $\theta_1$  the mass per unit area,  $\theta_0$  the damping coefficient,  $\theta_*$  the**

Stephen Boltzman constant,  $\theta_*$  the mean absorption coefficient,  $\theta_0$

**101 non-uniform heat source/sink coefficient,  $\theta_{**}$  the thermophoretic coefficient,  $\theta_*$  the**

reference temperature,  $\theta$  the mass diffusivity coefficient,  $\theta_*$  concentration susceptibility,  $\theta_*$  mean fluid temperature,  $\theta_0$  thermal diffusion ratio,  $\theta_1$  the chemical reaction coefficient,  $\theta$  non-uniform channel coefficient,  $\theta_0$  denotes

**7 the Taylor number,  $\theta$  the Hall parameter,  $\theta$  the Hartman number,  $\theta_*$  Brinkman number,  $\theta$  Eckert number, Pr Prandtl number,**

$\theta_*$  amplitude ratio variable,  $\theta_1$

**99 heat transfer Biot number,  $\theta_*$  mass transfer Biot number,**

$\theta_*(\theta) =$

**361  $\theta_*$  the wall parameters,  $\theta_*$  the radiation variable,  $\theta$  the non-**

uniform heat source/sink parameter,  $\theta_0$  thermophoretic parameter,  $\theta$  wavelength, Re Reynolds number,  $\theta_*$  Schmidt number,  $\theta$  non-uniform channel parameter,  $\theta_*$  Dufour number,  $\theta$  chemical reaction parameter and  $\theta_*$  Soret number. Chapter 2 Hall current and Joule heating impacts in peristaltic transport of rotating liquid

2.1 Introduction The present chapter is

**6arranged to study the Hall current and Joule heating effects on peristaltic flow of viscous fluid. Channel with flexible**

boundaries is considered. System consisting of liquid and channel behaves like a rigid body.

**6Convective conditions for heat transfer in the formulation are adopted. Viscous dissipation in energy expression is taken into account. Resulting differential systems after invoking small Reynolds number and long wavelength considerations are numerically solved. Runge-Kutta scheme of order four is implemented**

temperature, axial and

**6secondary velocities and heat transfer coefficient. Comparison with previous limiting studies is shown. Outcome of new parameters of interest is analyzed.**

2.2 Problem development We choose channel with compliant boundaries. Viscous liquid is electrically conducted. Electric field effect is not considered. However the Hall and Joule heating effects are accounted. Both the channel and

**82fluid rotates with a uniform angular velocity  $\Omega$  about the z-axis. The**

channel walls are convectively heated. Viscous dissipation impact is accounted. The sinusoidal waves propagating along the channel walls (at  $y = \pm a$ ) are  $y = \pm a + b \sin 2\pi(x - ct)$  (2.1), Fig. 2.1: Geometry of problem. where  $b$ ,  $\lambda$  and  $c$  represent the wave amplitude, wavelength, wave speed and time respectively. The equations in rotating frame can be put as follows:  $\nabla^2 \psi = 0$  + (2.2)  $\nabla^2 \theta = -2\Omega \psi$  (2.3),  $1 + \frac{2\Omega}{\nu} \psi = -\frac{2\Omega}{\nu} \theta$  (2.4)  $\frac{d\psi}{dx} = -\frac{2\Omega}{\nu} \theta$  (2.5),  $\frac{d\theta}{dx} = \frac{2\Omega}{\nu} \psi$  (2.6)  $\mu \frac{d\psi}{dx} = \mu \frac{d\theta}{dx}$  The conditions for present problem are  $\psi = 0$  at  $y = 0$  (2.7)  $\theta = 0$  at  $y = 0$  (2.8)  $\psi = 0$  at  $y = \pm a$  (2.9) and compliant wall condition is  $\frac{d\psi}{dy} + \frac{d\theta}{dy} = 0$  at  $y = \pm a$  (2.10)  $\psi = -\frac{2\Omega}{\nu} \theta$  at  $y = \pm a$  (2.11) where  $\psi = \frac{1}{2} \Omega^2 (a^2 - y^2)$  If  $\psi$  is the stream function then  $\psi = \frac{1}{2} \Omega^2 (a^2 - y^2)$  (2.14)  $\psi = 0$  (2.15) Define the dimensionless variables as:  $x^* = \frac{x}{\lambda}$ ,  $y^* = \frac{y}{a}$ ,  $t^* = \frac{ct}{\lambda}$ ,  $\psi^* = \frac{\psi}{\Omega a^2}$ ,  $\theta^* = \frac{\theta}{\Omega a^2}$  (2.12) The problems

**44subject to long wavelength and small Reynolds number become  $\psi = \frac{1}{2} \Omega^2 (a^2 - y^2)$**

**1**

$\mu (2.13) \frac{\partial}{\partial r} \left( \frac{\partial \psi}{\partial r} + \frac{\partial^2 \psi}{\partial r^2} - \frac{\partial \psi}{\partial z} + \frac{\partial^2 \psi}{\partial z^2} \right) = 0$  (2.16)  $\psi = 1 + \sin 2\theta$  ( $\theta = ?$ ) (2.17)  $\psi + \frac{\partial \psi}{\partial r} = 0$  at  $r = 1$   $\frac{\partial \psi}{\partial r} = 0$  at  $r = -1$  (2.18)  $\psi = 0$   $\frac{\partial \psi}{\partial z} = 0$  at  $z = \pm 1$  (2.19)  $\frac{\partial \psi}{\partial r} + \frac{\partial^2 \psi}{\partial r^2} + \frac{\partial \psi}{\partial z} = 0$  at  $r = 1$   $\frac{\partial \psi}{\partial r} = 0$  at  $r = -1$  (2.20)  $\mu \frac{\partial}{\partial r} \left( \frac{\partial \psi}{\partial r} + \frac{\partial^2 \psi}{\partial r^2} \right) = 6 \psi$  (2.21)  $\mu \frac{\partial \psi}{\partial r} - 1 + \frac{\partial \psi}{\partial z} = 0$   $\frac{\partial \psi}{\partial z} - 1 + \frac{\partial^2 \psi}{\partial z^2} (\theta + \frac{\partial \psi}{\partial z}) - 2 \frac{\partial \psi}{\partial r} = 0$  (2.22) Here the pressure term is neglected because of secondary flow which is produced due to rotation. 2.3 Solution methodology Now our interest is to solve equations (2.16), (2.21) and (2.22) subject to the conditions (2.17)– (2.20). Therefore we apply a numerical technique (shooting technique

50with fourth order Runge- Kutta integration) built in command of Mathematica. The

graphical outcomes of velocities ( $\psi$ ), temperature ( $\theta$ ) and

96heat transfer coefficient ( $h$ ) have been discussed in detail for the sundry parameters. 2.

#### 4 Discussion 2.4

27.1 Axial velocity Figs. (2.22 – 2.25) are plotted to see the effects of

$\theta$  and  $\frac{\partial \psi}{\partial r}$  on axial velocity ( $\psi$ ).

56The impact of Hartman number  $H$  on

velocity profile ?

37is sketched in Fig. 2.27. Result in Fig. shows decaying behavior of  $\psi$  via larger

?. It is due to the resistive nature of Lorentz force. Impact of Taylor number  $T$  on velocity profile

5is displayed in Fig. 2.23. It is evident from Fig. that velocity is enhanced by increasing rotation. The

5reason behind this fact is that the rotation of fluid

induced the secondary flow which causes decrease in velocity. The result matches with the study [155]. On the other hand Fig. 2.24 shows the increasing impact of axial velocity for increasing Hall parameter  $\beta$ . In fact

for larger values of  $\eta$

49 **the effective conductivity decreases.** It causes **decrease in magnetic damping force**

and hence axial velocity enhances. Variation in  $\eta$  for wall parameters is depicted in Fig. 2.25. The velocity increases for larger  $\eta_1$  and  $\eta_2$  while it decays for increasing damping parameter  $\eta_3$ .

26 **Fig. 2.2 Fig. 2.3 Fig. 2.2:**

Axial velocity  $\eta$  for  $\eta$  with  $\eta = 0.22$   $\eta = 0.22$   $\eta = 0.1$   $\eta_1 = 0.3$   $\eta_2 = 0.1$   $\eta_3 = 0.1$   $\eta = 0.5$   $\eta_0 = 0.22$   $\eta_1 = 2$   $\eta_2 = 0.3$  Fig. 2.3: Axial velocity  $\eta$  for  $\eta_0$  with  $\eta = 0.22$   $\eta = 0.22$   $\eta = 0.1$   $\eta_1 = 0.3$   $\eta_2 = 0.1$   $\eta_3 = 0.1$   $\eta = 0.5$   $\eta_0 = 0.22$   $\eta_1 = 2$   $\eta_2 = 0.3$

26 **Fig. 2.4 Fig. 2.5 Fig. 2.4:**

Axial velocity  $\eta$  for  $\eta$  with  $\eta = 0.22$   $\eta = 0.22$   $\eta = 0.1$   $\eta_1 = 0.3$   $\eta_2 = 0.1$   $\eta_3 = 0.1$   $\eta = 0.22$   $\eta_0 = 0.22$   $\eta_1 = 2$   $\eta_2 = 0.3$  Fig. 2.5: Axial velocity  $\eta$  for  $\eta_1$   $\eta_2$   $\eta_3$  with  $\eta = 0.22$   $\eta = 0.22$   $\eta = 0.1$   $\eta = 0.5$   $\eta = 0.22$   $\eta_0 = 0.22$   $\eta_1 = 2$   $\eta_2 = 0.3$  2.4.2 Secondary velocity Figs. (2.6 – 2.9) are sketched for the outcome of emerging parameters on secondary velocity  $\eta(\eta)$ . In Fig. 2.6 secondary velocity decreases for increasing Hartman number  $\eta$ . Fig. 2.7 depicts that for larger Taylor number  $\eta_0$  the secondary velocity increases. It is because of the fact that secondary velocity is enhanced due to an increase in rotation. This result also agrees with previous studies of Hayat et al. [155] and Mahmoud [154]. Also Fig. 2.7 shows no variation when  $\eta_0 = 0$ . In Fig. 2.8 the effect of Hall current parameter  $\eta$  on  $\eta(\eta)$  is depicted. Larger  $\eta$  lead to secondary velocity enhancement. The result shows that  $\eta$  resists the change in fluid caused by

41 **an increase in the applied magnetic field strength. Fig.**

2.9 witnesses that  $\eta$  is enhanced for greater values of  $\eta_1$  and  $\eta_2$  whereas it has reversed behavior for  $\eta_3$ .

26 **Fig. 2.6 Fig. 2.7 Fig. 2.6:**

Secondary velocity  $\eta$  for  $\eta$  with  $\eta = 0.5$   $\eta = 0.1$   $\eta = 0.1$   $\eta_1 = 0.3$   $\eta_2 = 0.1$   $\eta_3 = 0.1$   $\eta = 0.4$   $\eta_0 = 0.22$   $\eta_1 = 2$   $\eta_2 = 0.3$  Fig. 2.7: Secondary velocity  $\eta$  for  $\eta_0$  with  $\eta = 0.5$   $\eta = 0.1$   $\eta = 0.1$   $\eta_1 = 0.3$   $\eta_2 = 0.1$   $\eta_3 = 0.1$   $\eta = 0.5$   $\eta = 0.5$   $\eta_1 = 2$   $\eta_2 = 0.3$

3 **Fig. 2.8 Fig. 2.9 Fig. 2.**

8: Secondary velocity  $\eta$  for  $\eta$  with  $\eta = 0.5$   $\eta = 0.1$   $\eta = 0.1$   $\eta_1 = 0.3$   $\eta_2 = 0.1$   $\eta_3 = 0.1$   $\eta = 0.5$   $\eta_0 = 0.22$   $\eta_1 = 2$   $\eta_2 = 0.3$  Fig. 2.9: Secondary velocity  $\eta$  for  $\eta_1$   $\eta_2$   $\eta_3$  with  $\eta = 0.5$   $\eta = 0.22$   $\eta = 0.1$   $\eta = 0.4$   $\eta = 0.5$   $\eta_0 = 0.22$   $\eta_1 = 2$   $\eta_2 = 0.3$  2.4.3 Temperature Variations of temperature distribution  $\eta$

plotted against  $\gamma$  for several interesting parameters are observed through Figs. 2.10– 2.14. Temperature decays as we increase Hartman number  $\gamma$  and rotation parameter  $\Omega$  (see Figs. 2.10 and 2.11). In Fig. 2.12 the temperature reduces when heat transfer Biot number  $Bi$  increases. The obtained result indicates that

the thermal conductivity of the fluid reduces with the

increase in  $Bi$  and thus temperature decreases. Fig. 2.13 reveals that temperature increases for larger Brinkman number  $Br$ . In fact minimum heat conduction is produced by viscous dissipation. The increasing behaviors of temperature for elastic parameters  $\beta_1$  and  $\beta_2$  and decreasing behavior for damping parameter  $\beta_3$  are shown in

Fig. 2.10 Fig. 2.11 Fig. 2.12 Fig. 2.13 Fig. 2.14

Fig. 2.10: Temperature  $\theta$  for  $\gamma$  with  $\Omega = 0.2$ ,  $\beta_1 = 0.1$ ,  $\beta_2 = 0.1$ ,  $\beta_3 = 0.1$ ,  $Bi = 0.4$ ,  $\Omega = 0.2$ ,  $\beta_1 = 0.2$ ,  $\beta_2 = 0.3$  Fig. 2.11: Temperature  $\theta$  for  $\Omega$  with  $\gamma = 0.2$ ,  $\beta_1 = 0.1$ ,  $\beta_2 = 0.1$ ,  $\beta_3 = 0.1$ ,  $Bi = 0.4$ ,  $\Omega = 0.5$ ,  $\beta_1 = 0.2$ ,  $\beta_2 = 0.3$

Fig. 2.12 Fig. 2.13 Fig. 2.14

Fig. 2.12: Temperature  $\theta$  for  $Bi$  with  $\gamma = 0.2$ ,  $\Omega = 0.1$ ,  $\beta_1 = 0.3$ ,  $\beta_2 = 0.1$ ,  $\beta_3 = 0.1$ ,  $\Omega = 0.2$ ,  $\beta_1 = 0.4$ ,  $\beta_2 = 0.2$  Fig. 2.13: Temperature  $\theta$  for  $Br$  with  $\gamma = 0.2$ ,  $\Omega = 0.1$ ,  $\beta_1 = 0.3$ ,  $\beta_2 = 0.1$ ,  $\beta_3 = 0.1$ ,  $\Omega = 0.5$ ,  $\beta_1 = 0.2$ ,  $\beta_2 = 0.4$ ,  $\beta_3 = 0.3$  Fig. 2.14 Fig. 2.14: Temperature  $\theta$  for  $\beta_1$ ,  $\beta_2$ ,  $\beta_3$  with  $\gamma = 0.2$ ,  $\Omega = 0.1$ ,  $\beta_1 = 0.1$ ,  $\beta_2 = 0.4$ ,  $\beta_3 = 0.1$ ,  $\Omega = 0.2$ ,  $\beta_1 = 0.2$ ,  $\beta_2 = 0.3$

2.4.4 Heat transfer coefficient The impacts of  $\beta_1$ ,  $\beta_2$  and  $\beta_3$  on rate of heat transfer at channel walls are portrayed in Figs. 2.15 – 2.18. Fig. 2.15 shows oscillatory behavior for increasing Hartman number  $\gamma$ . Here  $\gamma$  shows decreasing behavior for increasing Taylor number (see Fig. 2.16). In Fig. 2.17 the rate of heat transfer coefficient  $h$  is enhanced for larger Brinkman number  $Br$  due to stronger viscous dissipation effect. The magnitude of heat transfer coefficient  $h$  near centerline increases for wall parameters whereas it decreases near the boundaries of the channel (see

Fig. 2.15 Fig. 2.16 Fig. 2.17 Fig. 2.18

15:

Heat transfer coefficient  $h$  for  $\gamma$  with  $\Omega = 0.2$ ,  $\beta_1 = 0.1$ ,  $\beta_2 = 0.1$ ,  $\beta_3 = 0.1$ ,  $Bi = 0.4$ ,  $\Omega = 0.2$ ,  $\beta_1 = 0.2$ ,  $\beta_2 = 0.3$ ,  $\beta_3 = 0.1$ ,  $\Omega = 0.5$

$\Omega = 0.2$ ,  $\beta_1 = 0.2$ ,  $\beta_2 = 0.3$  Fig. 2.16:



**1 Heat transfer coefficient  $\gamma$  for  $\theta = 0$  with  $\theta = 0$   $\gamma = 0.1$   $\gamma_1 = 0$   $\gamma_2 = 0$   
 $\gamma_3 = 0$**

$\gamma = 0.5$   $\gamma = 0.2$   $\gamma_1 = 2$   $\gamma = 0.3$  Fig. 2.17 Fig. 2.18

**1 Fig. 2.17: Heat transfer coefficient  $\gamma$  for  $\theta = 0$   $\gamma = 0.1$   $\gamma_1 = 0$   $\gamma_2 = 0$   
 $\gamma_3 = 0$   $\gamma = 0$   $\gamma_5$**

$\theta = 0.2$   $\theta = 0.4$   $\gamma_1 = 2$  Fig. 2.18: Heat transfer coefficient  $\gamma$  for  $\theta = 0.2$   $\theta = 0.1$   $\theta = 0.4$   $\theta = 0.5$   $\theta = 0.2$   $\gamma_1 = 2$   $\gamma = 0.3$  2.5 Conclusions

**6 Hall current and Ohmic heating effects on peristaltic flow in a rotating**

frame are analyzed. The major key findings are: • Impact of Hartman and Taylor numbers on the axial velocity are found similar. • Both axial and secondary velocities are increasing functions of Hall parameter. • Opposite behavior of Taylor number on axial and secondary velocities is observed. • The axial and secondary velocities show similar behavior for wall parameters. • Rotation parameter leads to an enhancement of temperature. • Temperature decays for increasing  $\gamma_1$  while it enhances for Brinkman number, Hartman number and wall parameters. • Hartman and Taylor numbers outcomes on heat transfer rates are opposite to that of Brinkman number and wall parameters. Chapter 3 Impact of thermal radiation and thermophoresis on peristalsis in rotating frame 3.1 Introduction

**4 Thermal radiation effect on peristaltic activity of rotating flow in a channel**

is addressed in this chapter.

**4 The influences of thermophoresis and chemical reaction are taken into account. Convective heat and mass transfer conditions in formulation are adopted. In addition, the non-uniform heat source/sink effect is included in heat transfer analysis. Exact solutions for stream function and temperature are obtained. Numerical solution for concentration of developed mathematical model are obtained by considering low Reynolds number and long wavelength. The effects of emerging physical parameters are analyzed through graphical illustrations. It is found that influences of thermophoretic and thermal radiation parameters on temperature and concentration are quite opposite. Further heat transfer coefficient decays when rotation is increased.**

3.2 Problem development Consider an incompressible

6 viscous fluid in a channel with width  $2l$ . Both the channel and

fluid rotates with a uniform angular velocity  $\Omega$  about the  $z$ -axis. Mathematical expression for wave propagation along the channel walls at  $y = \pm l$

is given by  $\psi(\eta, \tau) = \psi_0 + \psi_1 \sin 2\eta(\eta - \tau)$

(3.1) In a rotating frame the governing equations are given by

$$16\eta^2 \psi'' + \eta \psi' = 0 \quad (3.2) \quad \psi'' - 2\Omega \psi' = -\eta^2 + \eta \psi'' \quad \eta \psi'' + \eta^2 \psi' + \eta \psi'' = 0 \quad (3.3) \quad \psi'' + 2\Omega \psi' = -\eta^2 + \eta \psi''$$

$\eta$

$$29\eta^2 \psi'' + \eta \psi' = 0 \quad (3.4) \quad \psi'' - 2\Omega \psi' = -\eta^2 + \eta \psi'' \quad \eta \psi'' + \eta^2 \psi' + \eta \psi'' = 0 \quad (3.5) \quad \psi'' + 2\Omega \psi' = -\eta^2 + \eta \psi''$$

$+ \mu$

$$91\eta^2 \psi'' + \eta \psi' = 0 \quad (3.6) \quad \psi'' - 2\Omega \psi' = -\eta^2 + \eta \psi''$$

$\eta = \eta \cdot \eta^2 \eta^2 \eta^2$ ,  $+$   $-\eta(\eta(\eta - \eta_0)) \eta - \eta_1(\eta - \eta_0)$  (3.7) Using Rosseland heat flux approximation we have  $\eta = -43\eta\eta\eta\eta$  (3.8) where  $\eta_*$  and  $\eta_{**}$  represent the Rosseland mean absorption coefficient and Stefan-Boltzmann respectively. Expanding  $\eta$  about  $\eta_0$  and ignoring higher order terms of  $(\eta - \eta_0)$ . Then  $\eta = -\eta\eta\eta\eta_{**}\eta$  (3.9) where  $\eta_{**}$  and  $\eta$  denote the kinematic viscosity, thermophoretic coefficient and reference temperature respectively. The conditions for present problem are

$$32\eta^2 \psi'' = 0 \quad \eta \psi' = 0 \quad \psi'' - 2\Omega \psi' = 0 \quad \eta \psi'' = 0 \quad \text{at } \eta = 0 \quad \eta \psi'' = 0 \quad \eta \psi' = 0 \quad \eta \psi'' = -\eta_1(\eta_0 - \eta) \quad \eta \psi'' = -\eta_2(\eta_0 - \eta) \quad \text{at } \eta = \eta_0$$

(3.10) (3.11) in which  $\eta_1$  and  $\eta_2$  indicate the heat and mass transfer coefficients respectively. Putting Eqs. (3.8) and (3.9) in Eqs. (3.6) and (3.7) and then using the wave frame transformations  $\eta =$

$$2\eta - \eta\eta\eta\eta = \eta\eta\eta\eta = \eta(\eta\eta\eta\eta) \quad \eta(\eta\eta\eta\eta) = \eta(\eta\eta\eta\eta) - \eta\eta\eta\eta \quad (\eta\eta\eta\eta) = \eta(\eta\eta\eta\eta) \quad \eta(\eta\eta\eta\eta) = \eta(\eta\eta\eta\eta) \quad \text{Eqs. (3.2) - (3.7)} \quad \text{become } \eta\eta\eta\eta = 0$$

+ (??)??+??+??-2Ω? =-??+? ??2 ??2 ??2 ?? ?? ?? ?? ??2 ??2 ??2 + + ? · , , ?? ?? ?? ?? ?? ??2 ??2 · (??)??+??+??+2Ω? =-??+? ??2 ??2 ??2 + + ? , , · (??)?? +??+???, ?? ?? ?? = - + ? ?? ?? ??2 ? 2? · ??2 ??2 ??2 + + ? ?? , ?? ?? 2 2 2 + + ?? ?? 2 ??? ?? = ? ??2 ??2 ??2 ? + ? · , "μ ?? + ?? ¶ # + 136?? \*\* ?03 ??2 + ?0(? - ?0)? 2? ?? 2? 2? 2? \*\*? ? ?? ?? = ? ??2 ??2 + + · ??2 ?+ , ? ? · ?? ?? (? - ?0) - ?1(? - ?0)? μ ¶, (3.12) (3.13) (3.14) (3.15) (3.16) (3.17) (3.18) Using

**7 dimensionless variables  $u^* = \frac{u}{U_0}$ ,  $v^* = \frac{v}{U_0}$ ,  $w^* = \frac{w}{U_0}$ ,  $\theta^* = \frac{T - T_0}{T_1 - T_0}$ ,  $\phi^* = \frac{\phi}{U_0 R}$ ,  $\psi^* = \frac{\psi}{U_0 R^2}$  and applying lubrication approach, the Eqs.**

(3.14) - (3.18) give  $\frac{\partial \theta}{\partial x} - \frac{\partial \theta}{\partial z} - 2 \theta = 0$  at  $z = 0$  and the conditions in non-dimensional form are (3.19) (3.20) (3.21) (3.22) (3.23) (3.24) (3.25)  $\theta(0) = 1 + \sin 2z$  at  $z = 0$  and  $\theta = -1$  at  $z = 1$  where the stream function  $\psi$  gives  $\psi = 0$  at  $z = 0$  and  $\psi = 1$  at  $z = 1$ . From Eq. (3.23)  $\psi = 6 \theta$  thus Eq. (3.21) becomes  $\frac{\partial \theta}{\partial x} + 2 \theta = 0$  (3.26) (3.27) (3.28) (3.29) and due to rotational effect, we neglect pressure term caused by secondary flow. Therefore Eq. (3.22) becomes  $\frac{\partial \theta}{\partial x} - 2 \theta = 0$  (3.30) 3.3 Solution methodology The closed form solutions of Eqs. (3.29) (3.30) and (3.24) and boundary conditions (3.26) - (3.27) are  $\theta(x,z) = \sin 2z \cdot 0 - \sinh 2z \cdot 0 [-\sin 2z \cdot 0 - \frac{1}{2}(1 + z) \cosh 2z \cdot 0 \sin 2z \cdot 0 \sqrt{-1} \sqrt{\sqrt{-2}} \cos 2z \cdot 0 \sinh 2z \cdot 0 - 2 \cos 2z \cdot 0 \sinh 2z \cdot 0 + \sinh 2z \cdot 0 \sqrt{-1} \sqrt{\sqrt{-2}} + (1 + z)(1 + z)^2 (\sin(1 + z) \cdot 0 - \sinh(1 + z) \cdot 0)] \sqrt{0}$  (3.31)  $\theta(x,z) = \sin 2z \cdot 0 - \sinh 2z \cdot 0 [2(1 + z)(\cos 2z \cdot 0 - \cosh 2z \cdot 0 \sqrt{-1} \sqrt{\sqrt{-2}} \cos 2z \cdot 0 \cosh 2z \cdot 0) + \sinh 2z \cdot 0 + 4 \sin 2z \cdot 0 \sinh 2z \cdot 0] \sqrt{0}$  (3.32)  $\theta(x,z) = (1 + z) \cosh 2z \cdot 0 + (1 - z) \sinh 2z \cdot 0 + 4[(\cosh 2z \cdot 0 - \sinh 2z \cdot 0) \cos 2z \cdot 0 + \cosh 2z \cdot 0 + \sin 2z \cdot 0 + \sinh 2z \cdot 0]$  (3.33) where  $\theta(1) = 1 - 4$ ,  $\theta(0) = 1 - 5$   $\theta(1) = 1 - 32$ ,  $\theta(0) = 1 - 32$ ,  $\theta(1) = 1 - 32$  and  $\theta(0) = 1 - 32$  have been computed algebraically. Eq. (25) is solved numerically using NDSolve built in MATHEMATICA. 3.4 Discussion The Taylor number  $Ta$  effect on

**11 axial velocity is sketched in Fig. 3.1. It is noticed from Fig. that**

velocity is decreasing function of  $z$  in the upper half of the channel whereas it shows an increasing behavior in lower half of channel. It is because of the fact that the secondary flow is produced by rotation which causes decay of velocity. Fig. 3.2 depicts that for increasing Taylor number  $Ta$  the secondary velocity increases. In fact secondary velocity is enhanced due to an increase in rotation. Figs. 3.3- 3.7 are plotted to observe the effect of temperature distribution  $\theta$  for several parameters. Temperature rapidly decays as we increase rotation parameter  $Ta$  (see Fig. 3.3). The reason behind this fact is that as we increase  $Ta$  the motion of the fluid particles increases which causes decrease in  $\theta$ . Effect of increasing non-uniform source/sink parameter  $\phi$  on  $\theta$  is observed in Fig. 3.4. We noticed that temperature distribution rises for larger  $\phi$ . The distribution of temperature is portrayed

**6 for different values of  $\phi$  in Fig. 3.5. It is noticed that**

for larger radiation parameter  $\beta$  the temperature decreases. It is in fact due to the loss of heat. Effect of Brinkman number  $Br$  is shown in Fig. 3.6. Here temperature enhances for increasing Brinkman number  $Br$ .

Involvement of viscous dissipation effect in ?? produced minimum heat conduction which results rise in ?. In Fig. 3?7 the temperature reduces when heat transfer Biot number ??1 increases. The obtained result indicates that the thermal conductivity of fluid reduces with an increase in ??1 and so decay in ? is noticed. The impacts of ? 0? ?? ?? ?? and ??1 on heat transfer rate ? at channel walls are portrayed in Figs. 3?8 – 3?12? Fig. 3?8 predicts that ? increases for larger ? 0 when rotation increases. Opposite behavior for heat generation/absorption ? is shown in Fig. 3?9. This indicates that ? is higher for ?  $\hat{A}$  0. In Fig. 3?10 the magnitude of heat transfer coefficient ? near centerline enhances for radiation parameter whereas it decreases near the channel boundaries. In Fig. 3?11 due to stronger viscous dissipation effect the rate of heat transfer coefficient ? rises for larger Brinkman number ?. Influence of ??1 on heat transfer rate ? is illustrated in Fig. 3?12. Decrease in ? is seen for larger values of ??1? Effect of different emerging parameters on dimensionless concentration ? are demonstrated through Figs. 3?13 – 3?17. As temperature and concentration have inverse relation so concentration shows opposite behavior for sundry parameters. In Fig. 3?13 we observed that concentration ? increases for larger Taylor number ? 0. An enhancement of ? is shown in Fig. 3?14 for increasing values of heat generation/absorption ?. Similar graphical result of concentration field ? is obtained in Fig. 3?15 for growing values of chemical reaction parameter ?. Since chemical effect increases the rate of interfacial mass transfer and thus reduces the local concentration which in turn increases concentration flux when we have constructive chemical reaction. Here Fig. 3?16 is plotted to analyze the behavior of thermophoretic parameter ? on concentration ?? It is noticed that larger values of thermophoresis parameter increases the concentration for a small range? In fact larger temperature gradient increases ? 0 which causes an enhancement in concentration profile. Fluctuation in ? for mass transfer Biot number ??2 is portrayed in Fig. 3?17. Concentration of fluid increases when we take larger values of

73???. Fig. 3.1 Fig. 3.2 Fig. 3.

1: Plot of ? via ? 0 when ? = 0?7? ? = 0?1? ? = 0?5? Fig. 3.2: Plot of ? via ? 0 when ? = 0?7? ? = 0?5? ? = 0?5?

71Fig. 3.3 Fig. 3.4 Fig. 3.3: Plot of

? via ? 0 when ? = 0?7? ? = 0?1? ? = 0?7? Pr = 0?5? ??1 = 5? ?? = 2? ?? = 0?3? ? = 0?5? Fig. 3.4: Plot of ? via ? when ? = 0?7? ? = 0?1? ? = 0?7? Pr = 0?5? ??1 = 5? ?? = 2? ?? = 0?3? ? 0 = 0?2?

3Fig. 3.5 Fig. 3.6 Fig. 3.

5: Plot of ? via ?? when ? = 0?7? ? = 0?1? ? = 0?7? Pr = 0?5? ??1 = 5? ?? = 2? ? = 0?5? ? 0 = 0?2? Fig. 3.6: Plot of ? via ?? when ? = 0?7? ? = 0?1? ? = 0?7? Pr = 0?5? ??1 = 5? ?? = 0?3? ? = 0?5? ? 0 = 0?2? Fig. 3.7 Fig. 3.7: Plot of ? via ??1 when ? = 0?7? ? = 0?1? ? = 0?7? Pr = 0?5? ?? = 0?2? ?? = 0?3? ? = 0?5? ? 0 = 0?2?

3Fig. 3.8 Fig. 3.9 Fig. 3. 8: Plot of

? via ? 0 when ? = 0?3? ? = 0?1? Pr = 1?5? ??1 = 5? ?? = 2? ? = 1?4? ?? = 0?3? Fig. 3.9: Plot of ? via ? when ? = 0?3? ? = 0?1? Pr = 1?5? ??1 = 5? ?? = 2? ?? = 0?3? ? 0 = 0?2?

**3Fig. 3.10 Fig. 3.11 Fig. 3.10: Plot of**

? via ?? when ? = 0?3? ? = 0?1? Pr = 1?5? ??1 = 5? ?? = 2? ? 0 = 0?2? ? = 0?5? Fig. 3.11: Plot of ? for via ?? when ? = 0?3? ? = 0?1? Pr = 1?5? ??1 = 5? ?? = 0?3? ? 0 = 0?2? ? = 0?5? Fig. 3.12 Fig. 3.12: Plot of ? via ??1 when ? = 0?3? ? = 0?1? Pr = 1?5? ?? = 2? ?? = 0?3? ? 0 = 0?2? ? = 0?5?

**3Fig. 3.13 Fig. 3.14 Fig. 3.**

13: Plot of ? via ?0 when ? = 0?3? ? = 0?2? ? = 0?7? ??1 = 10? ??2 = 10? Pr = 0?7? ?? = 2? ?? = 1? ? = 0?8? ?0 = 0?7? ?? = 0?2? ? = 0?3? Fig. 3.14: Plot of ? via ? when ? = 0?3? ? = 0?2? ? = 0?7? ??1 = 10? ??2 = 10? Pr = 0?7? ?? = 2? ?? = 1? ?0 = 0?7? ?? = 0?2? ? = 0?3? ?0 = 0?2?

**3Fig. 3.15 Fig. 3.16 Fig. 3.**

15: Plot of ? via ? when ? = 0?3? ? = 0?2? ? = 1?5? ??1 = 10? ??2 = 10? Pr = 0?7? ?? = 2? ?? = 1? ?0 = 0?7? ?? = 0?2? ? = 0?5? ?0 = 0?2? Fig. 3.16: Plot of ? via ?0 when ? = 0?3? ? = 0?2? ? = 0?7? ??1 = 10? ??2 = 10? Pr = 0?7? ?? = 2? ?? = 0?8? ? = 0?3? ?? = 0?2? ? = 0?5? ?0 = 2? Fig. 3.17 Fig. 3.17: Plot of ? via ??2 when ? = 0?3? ? = 0?2? ? = 0?7? ??1 = 10? ? = 0?1? Pr = 0?7? ?? = 2? ?? = 0?8? ? = 0?3? ?? = 0?2? ? = 0?5? ? 0 = 2? 3.5 Conclusions Influences of thermal radiation and thermophoresis on peristaltic rotating flow are focused. Key findings of present analysis are: • Dual effect of Taylor number on ? is observed. • Secondary velocity is an increasing function of Taylor number. • Similar behavior of temperature is noticed for rotation and radiation parameters. • Temperature is an increasing function of heat generation/absorption and Brinkman number. • Opposite behavior of temperature and concentration is noticed for emerging parameters. • Heat transfer rate decreases by increasing ? 0, ?? and ??1 whereas it enhances for ? and ??.

Chapter 4 Peristaltic activity of rotating Prandtl fluid 4.1 Introduction Peristaltic motion of MHD rotating

**21flow of Prandtl fluid in channel with flexible characteristics is discussed.**

Constant angular velocity is adopted. Channel is convectively heated. Numerical results are obtained.

**6Axial and secondary velocities, temperature and heat transfer coefficient**

are examined. 4.2 Definition Consider

**12peristaltic motion of MHD Prandtl fluid in a uniform channel**

of thickness 2?. Uniform magnetic field ?0 is applied. Effect of electric field is not retained. Convectively heated channel has flexible walls. The wall surface satisfies ? = ±?(??) = ± ? + ? sin 2? ? (? - ??) ? (4.1)

For Prandtl fluid, the general constitutive equations are represented as:  $\tau = -\eta \dot{\gamma} + S \dot{\gamma}$  (4.2)

$\left[ \sin^{-1}(\frac{1}{2}) \frac{1}{3} \frac{1}{3} \frac{1}{3} \frac{1}{3} \frac{1}{3} \frac{1}{3} \right] \frac{1}{3} \frac{1}{3} \frac{1}{3} \frac{1}{3} \frac{1}{3} \frac{1}{3} \left[ \frac{1}{2} \frac{1}{2} \frac{1}{2} \frac{1}{2} \right] \frac{1}{3} \frac{1}{3} \frac{1}{3} \frac{1}{3} = 1 ?$  (4.3)

Using Patel et. al. [35] we have  $\psi = \psi_1 \sin^{-1}[\psi_2^2 + (\psi_3^2)^2]^{1/2}$  where  $\psi_1$  and  $\psi_2$  are material constants relating to Prandtl fluid. Considering velocity components  $u, v, w$  in  $x, y, z$  directions, we have  $V = [u^2 + v^2 + w^2]^{1/2}$  (4.4) Mass, momentum and energy conservation equations in rotating frame are  $\rho \frac{D\rho}{Dt} = 0$ ,  $\rho \frac{D\mathbf{v}}{Dt} = -\nabla p - 2\boldsymbol{\Omega} \times \mathbf{v}$ ,  $\rho \frac{Dh}{Dt} = \nabla \cdot \mathbf{q} + \dot{q}$  (4.5) (4.6) (4.7) (4.8) (4.9) with conditions  $\psi = -\psi_1(\psi_2 - \psi_3)$  at  $\psi = \psi_1$ ,  $\psi = -\psi_1(\psi_2 - \psi_3)$  at  $\psi = -\psi_1$ ,  $\psi = 0$  at  $\psi = \pm\psi_1$ ,  $\psi = 0$  at  $\psi = \pm\psi_1$  where  $\psi = -\psi_1^2 \psi_2^2 + \psi_3^2$  (4.10) (4.11) (4.12) (4.13) Consider  $\psi^* = \psi_1 \psi_2^2 + \psi_3^2$ ,  $S^* = S \psi_1 \psi_2^2 + \psi_3^2$ ,  $Re = \frac{\rho \psi_1 \psi_2^2}{\mu}$  (4.14) Defining the stream function ( $\psi$ ) by  $\psi = -\psi_1 \psi_2^2$  (4.15) and invoking lubrication technique one obtains from (4.5) - (4.9) as  $-\psi_1^2 \psi_2^2 = -\psi_1^2 \psi_2^2 - \psi_3^2 + (4.16)$   $2\psi_1 \psi_2^2 = -\psi_1^2 \psi_2^2 - \psi_3^2 + (4.17)$   $\psi_1 \psi_2^2 = -\psi_1^2 \psi_2^2 + \psi_3^2$  (4.18)  $\psi_1 \psi_2^2 + \psi_3^2 = 0$  (4.19) Through Eq. (4.3) we can write  $\psi = \psi_1^2 \psi_2^2 + \psi_3^2$  (4.20) (4.21) (4.22) with the dimensionless conditions  $\psi = 1 + \psi_1 \sin 2\psi$  ( $\psi - \psi_1$ ) (4.23)  $\psi_1 \psi_2^2 + \psi_3^2 = 0$  at  $\psi = \psi_1$ ,  $\psi_1 \psi_2^2 = 0$  at  $\psi = -\psi_1$  (4.24)  $\psi = 0$  at  $\psi = \pm\psi_1$  (4.25) (4.26)  $\psi_1 \psi_2^2 + \psi_3^2 = 0$  at  $\psi = \psi_1$ ,  $\psi_1 \psi_2^2 = 0$  at  $\psi = -\psi_1$  (4.27) (4.28) Our interest is now to find numerical solution by shooting technique with

50fourth order Runge- Kutta scheme. 4.3 Analysis Various pertinent parameters

effects on  $\psi(\psi)$  are concluded via Figs. 4?1 ( $\psi - \psi_1$ ). Figs. 4?1( $\psi$ ) and ( $\psi$ ) depict a visible reduction in velocity profile with the increase in  $\psi_1$  and  $\psi_2$  respectively. Higher Prandtl fluid parameters  $\psi_1$  and  $\psi_2$  characterize an increase in viscosity. Consequently a decreasing velocity profile is captured. Same results are reported by Riaz et al. [54] and Hayat et al. [55]. Externally applied magnetic field helps in aligning the fluid particles. Fluid velocity is decreased. This effect of magnetic field makes it valuable in biomedical applications like GMR (see Fig. 4?1( $\psi$ )). A numerical study

100using Runge-Kutta Fehlberg method presented by Akbar et al. [52] approves the

present finding via larger Hartman number. Velocity against wall parameters is presented via Fig. 4?1( $\psi$ ). The obtained result illustrates velocity enhancement against  $\psi_1$  and  $\psi_2$ . However velocity is decreased by  $\psi_3$ . Larger  $\psi_1$  and  $\psi_2$  give less resistance to flow and so velocity decreases for  $\psi_3$ . Results of [53] also confirm these outcomes. Rotation in system induces a secondary flow. This secondary flow is perceived to yield decrease in axial velocity (shown by Fig. 4?1( $\psi$ )). Accordingly the

10axial velocity is quite high in the absence of rotation

parameter  $\psi_3 = 0$ . The

31 Taylor number ( $T_0$ ) is a dimensionless quantity which characterizes the importance of centrifugal forces due to rotation of fluid relative to viscous forces.

Figs. 4.2(a) – (e) indicate secondary velocity  $v$  by rotation about  $z$ -axis. Secondary velocity for  $T_1$  and  $T_2$  has similar behavior to that of axial velocity (see Figs. 4.2(a) and 4.2(b)). Fig. 4.2(c) depicts decay in secondary for larger Hartman number  $h$ . Externally applied magnetic field acts as drag force and so resists the fluid flow. In Fig. 4.2(d) the wall parameters have similar impact on secondary velocity when compared to that of axial velocity. Impact of Taylor number  $T_0$  on  $v$  is shown via Fig. 4.2(e). An interesting fact worth mentioning here is the opposite behavior of secondary velocity in response to rotation. Secondary velocity, in contrast to axial velocity, enhances in the presence of rotation. For authenticity the results of  $T_0$  can be compared with Mahmoud [154] and Hayat et al. [155]. However secondary velocity vanishes for  $T_0 = 0$ . Figs. 4.3(a) – (e) are included to elaborate the behavior of temperature distribution  $T$ . From Figs. 4.3(a) and (b) it is observed that fluid cools down for fluid parameters  $T_1$  and  $T_2$ . Parabolic temperature profile is observed in these figures, referring to the fact that fluid has the highest velocity and temperature, at centre of channel. Fig. 4.3(c) concludes a decreasing behavior when  $h$  is enhanced. Fig. 4.3(d) illustrates the impact of wall parameters. Variation of wall parameter leads to temperature enhancement. Average kinetic energy is known as temperature. The velocity and temperature have similar effects. Temperature is decreased for larger  $T_1$  (see Fig. 4.3(e)). Note that dissipation effect leads to Brinkman number. Clearly such dissipation generates heat in channel. There is temperature enhancement when  $Br$  enhances (see Fig. 4.3(f)). Temperature is decreased via  $T_0$  (see Fig. 4.3(g)). Behavior of heat transfer coefficient  $h$  for parameters  $T_1$ ,  $T_2$ ,  $h$ ,  $Br$  and wall parameters  $Br$  are shown through Figs. 4.4(a) – (e). Heat transfer coefficient defined by  $h = \frac{q_w}{T_w - T_f}$  involves temperature of the fluid as well as position of channel walls. It is found from Figs. 4.4(a) and (b) that larger fluid parameters  $T_1$  and  $T_2$  ensure lower heat transfer rate. Hartman number  $h$  decays magnitude of heat transfer coefficient  $h$  near channel centre whereas it increases near the boundaries (see Fig. 4.4(c)). From Fig. 4.4(d) it is noticed that  $h$  increases for  $T_1$  and  $T_2$ . Effects of  $h$  on  $h$  is different to that of  $T_1$  and  $T_2$ . Fig. 4.4(e) depicts no absolute value of heat transfer coefficient when  $T_1$  varies. The obtained result from Fig. 4.4(e) shows increasing behavior of  $h$ . Heat transfer rate between wall and fluid decays for larger rotation (see in Fig.

874.2(a) – (e) Fig. 4.

1: Axial velocity  $v$  for (a) Prandtl fluid parameter  $T_1$  when  $T_1 = 0.03$ ,  $T_2 = 0.02$ ,  $T_3 = 0.01$ ,  $T_4 = 0.02$ ,  $T_5 = 0.01$ ,  $T_6 = 0.02$ ,  $T_7 = 0.05$ ,  $T_8 = 0.03$ ,  $T_9 = 2$ ,  $T_{10} = 0.02$ ,  $T_{11} = 0.03$  (b) Prandtl fluid parameter  $T_2$  when  $T_1 = 0.03$ ,  $T_2 = 0.02$ ,  $T_3 = 0.01$ ,  $T_4 = 0.02$ ,  $T_5 = 0.01$ ,  $T_6 = 0.02$ ,  $T_7 = 0.05$ ,  $T_8 = 0.03$ ,  $T_9 = 2$ ,  $T_{10} = 0.02$ ,  $T_{11} = 0.03$  (c) Hartman number  $h$  when  $T_1 = 0.03$ ,  $T_2 = 0.02$ ,  $T_3 = 0.01$ ,  $T_4 = 0.02$ ,  $T_5 = 0.01$ ,  $T_6 = 0.02$ ,  $T_7 = 0.05$ ,  $T_8 = 0.03$ ,  $T_9 = 2$ ,  $T_{10} = 0.02$ ,  $T_{11} = 2$  (d) wall parameters  $Br_1$ ,  $Br_2$ ,  $Br_3$  when  $T_1 = 2$ ,  $T_2 = 0.01$ ,  $T_3 = 0.02$ ,  $T_4 = 0.05$ ,  $T_5 = 0.03$ ,  $T_6 = 2$ ,  $T_7 = 0.02$ ,  $T_8 = 0.03$  (e) Taylor number  $T_0$  when  $T_1 = 0.03$ ,  $T_2 = 0.02$ ,  $T_3 = 0.01$ ,  $T_4 = 0.02$ ,  $T_5 = 0.01$ ,  $T_6 = 0.02$ ,  $T_7 = 0.05$ ,  $T_8 = 0.03$ ,  $T_9 = 2$ ,  $T_{10} = 0.02$ ,  $T_{11} = 2$  (a) (b) (c) (d) (e) Fig. 4.2: Secondary velocity  $v$  for (a) Prandtl fluid parameter  $T_1$  when  $T_1 = 0.05$ ,  $T_2 = 0.04$ ,  $T_3 = 0.03$ ,  $T_4 = 0.02$ ,  $T_5 = 0.01$ ,  $T_6 = -0.02$ ,  $T_7 = 0.05$ ,  $T_8 = 0.03$ ,  $T_9 = 2$ ,  $T_{10} = 0.02$ ,  $T_{11} = 0.03$  (b) Prandtl fluid parameter  $T_2$  when  $T_1 = 0.05$ ,  $T_2 = 0.04$ ,  $T_3 = 0.03$ ,  $T_4 = 0.02$ ,  $T_5 = 0.01$ ,  $T_6 = -0.02$ ,  $T_7 = 0.05$ ,  $T_8 = 0.03$ ,  $T_9 = 2$ ,  $T_{10} = 0.02$ ,  $T_{11} = 2$  (c) Hartman number  $h$  when  $T_1 = 0.05$ ,  $T_2 = 0.04$ ,  $T_3 = 0.03$ ,  $T_4 = 0.02$ ,  $T_5 = 0.01$ ,  $T_6 = -0.02$ ,  $T_7 = 0.05$ ,  $T_8 = 0.03$ ,  $T_9 = 2$ ,  $T_{10} = 0.02$ ,  $T_{11} = 2$  (d) wall parameters  $Br_1$ ,  $Br_2$ ,  $Br_3$  when  $T_1 = 2$ ,  $T_2 = 0.01$ ,  $T_3 = -0.02$ ,  $T_4 = 0.05$ ,  $T_5 = 0.03$ ,  $T_6 = 2$ ,  $T_7 = 0.02$ ,  $T_8 = 0.03$ ,  $T_9 = 2$

= 2? ? 0 = 0?2? ? = 0?3 (e) Taylor number ? 0 when ?1 = 0?5? ?2 = 0?4? ?3 = 0?3? ? = 0?2? ? = 0?1, ? = -0?2, ?2 = 0?5? ?? = 0?3? ??1 = 2? ? = 0?3? ?1 = 2?

45(a) (b) (c) (d) (e) (f) (g) Fig. 4.

3: Temperature ? for (a) Prandtl fluid parameter ?1 when ?1 = 0?3? ?2 = 0?2? ?3 = 0?1? ? = 0?2? ? = 0?1, ? = 0?2, ?2 = 0?5? ?? = 0?3? ??1 = 2? ?0 = 0?2, ? = 0?3 (b) Prandtl fluid parameter ?2 when ?1 = 0?3? ?2 = 0?2 ?3 = 0?1? ? = 0?2? ? = 0?1, ? = 0?2, ?1 = 2? ?? = 0?3? ??1 = 2? ?0 = 0?2? ? = 0?3 (c) Hartman number ? when ?1 = 0?3? ?2 = 0?2? ?3 = 0?1? ? = 0?2? ? = 0?1, ? = 0?2, ?2 = 0?5? ?? = 0?3? ??1 = 2? ? 0 = 0?2, ?1 = 2 (d) wall parameters ?1? ?2? ?3 when ?1 = 2? ? = 0?1, ? = 0?2, ?2 = 0?5? ?? = 0?3? ??1 = 2? ?0 = 0?2? ? = 0?3 (e) Biot number ??1 when ?1 = 0?3? ?2 = 0?2? ?3 = 0?1? ? = 0?2? ? = 0?1, ? = 0?2, ?2 = 0?5? ?? = 0?3? ? = 0?3? ?0 = 0?2, ?1 = 2 (f) Brinkman ?? when ?1 = 0?3? ?2 = 0?2? ?3 = 0?1? ? = 0?2? ? = 0?1, ? = 0?2, ?2 = 0?5? ??1 = 2? ? = 0?3? ?0 = 0?2, ?1 = 2 (g) Taylor number ?0 when ?1 = 0?3? ?2 = 0?2? ?3 = 0?1? ? = 0?2? ? = 0?1, ? = 0?2, ?2 = 0?5? ?? = 0?3? ??1 = 2? ? = 0?3? ?1 = 2?

45(a) (b) (c) (d) (e) (f) (g) Fig. 4.

4: Heat transfer coefficient ? (a) Prandtl fluid parameter ?1 when ?1 = 0?5? ?2 = 0?4? ?3 = 0?3? ? = 0?2? ? = 0?1, ? = 0?2, ?2 = 0?5? ?? = 0?3? ??1 = 2? ?0 = 0?2, ? = 0?3 (b) Prandtl fluid parameter ?2 when ?1 = 0?5? ?2 = 0?4? ?3 = 0?3? ? = 0?2? ? = 0?1, ? = 0?2, ?1 = 2? ?? = 0?3? ??1 = 2? ?0 = 0?2? ? = 0?3 (c) Hartman number ? when ?1 = 0?5? ?2 = 0?4? ?3 = 0?3? ? = 0?2? ? = 0?1, ? = 0?2, ?2 = 0?5? ?? = 0?3? ??1 = 2? ?0 = 0?2, ?1 = 2 (d) wall parameters ?1? ?2? ?3 when ?1 = 2? ? = 0?1, ? = 0?2, ?2 = 0?5? ?? = 0?3? ??1 = 2? ?0 = 0?2? ? = 0?3 (e) Biot number ??1 when ?1 = 0?5? ?2 = 0?4? ?3 = 0?3? ? = 0?2? ? = 0?1, ? = 0?2, ?2 = 0?5? ?? = 0?3? ? = 0?3? ?0 = 0?2, ?1 = 2 (f) Brinkman ?? when ?1 = 0?5? ?2 = 0?4? ?3 = 0?3? ? = 0?2? ? = 0?1, ? = 0?2, ?2 = 0?5? ??1 = 2? ? = 0?3? ?0 = 0?2, ?1 = 2 (g) Taylor number ?0 when ?1 = 0?5? ?2 = 0?4? ?3 = 0?3? ? = 0?2? ? = 0?1, ? = 0?2, ?2 = 0?5? ?? = 0?3? ??1 = 2? ? = 0?3? ?1 = 2? 4.4 Conclusions Important findings here are • Axial and secondary velocities via rotation have opposite effects. • Similar response of Prandtl fluid parameters on ?, ?, ? and ? is seen. • Both velocities are enhanced for flexible characteristics. • Decay in ?, ? and ? is observed for Hartman number. • Brinkman and Biot numbers for temperature and heat transfer coefficient have opposite effects. Chapter 5

9MHD peristaltic flow of rotating Prandtl fluid with Soret and

Dufour effects 5.1 Introduction

9The purpose here is to examine Soret/Dufour effects in MHD peristaltic flows of

rotating Prandtl liquid in a channel with flexible boundaries. Formulation for heat and mass transfer is arranged using convective conditions.



43 **Large wavelength and small Reynolds number are utilized. The numerical solution of**

resulting problems are obtained and analyzed in detail. 5.2 Problem development We examine

5 **peristaltic flow of Prandtl liquid in a rotating system. Channel of width 2? is considered. The channel**

and liquid rotate by constant angular velocity  $\Omega = \Omega \hat{z}$  ( $\hat{z}$  is unit vector parallel to  $z$  - axis). Magnetic field of strength  $H_0$  is applied. The wall surface in mathematical form is  $y = \pm a \sin 2z$  ( $a$  - half channel width). Fig. 5.1: Sketch of problem. For Prandtl fluid, the Cauchy stress tensor  $\tau$  is represented by:  $\tau = -pI + S$  where  $S = \mu \nabla^2 u + \mu' \nabla^2 \nabla u$  and  $\mu, \mu'$  are material constants. For present rotating flow, the governing equations are  $\rho \nabla^2 u = 0$ ,  $\rho \nabla^2 v = -2\Omega v$ ,  $\rho \nabla^2 w = -2\Omega w$ ,  $\rho \nabla^2 \theta = 0$ ,  $\rho \nabla^2 c = 0$  (5.2) (5.3) (5.4) (5.5) (5.6) (5.7) Energy and concentration equations are  $\rho c_p \nabla^2 \theta = \nabla^2 q$ ,  $\rho D \nabla^2 c = \nabla^2 S$  (5.8) (5.9) in which  $\theta, c, q, S$  represent mean fluid temperature, mass diffusivity coefficient, thermal diffusion ratio and concentration susceptibility respectively. The conditions are  $\theta = \theta_w$  at  $y = \pm a$ ,  $c = c_w$  at  $y = \pm a$ ,  $u = v = w = 0$  at  $y = \pm a$  (5.10) (5.11)  $\theta = \theta_w$  at  $y = -a$  (5.12)  $c = c_w$  at  $y = -a$  (5.13)  $\theta = 0, c = 0$  at  $y = \pm a$  (5.14)  $\theta = \theta_w, c = c_w$  at  $y = \pm a$  (5.15)  $\theta = -\theta_w, c = c_w$  at  $y = \pm a$  (5.16)  $\theta = \theta_w, c = c_w$  at  $y = \pm a$  (5.17) Eqs. (5.25) - (5.29) takes the given form after

103 **using long wavelength and low Reynolds number**

considerations,  $\rho \nabla^2 u = 0$ ,  $\rho \nabla^2 v = -2\Omega v$ ,  $\rho \nabla^2 w = -2\Omega w$ ,  $\rho \nabla^2 \theta = 0$ ,  $\rho \nabla^2 c = 0$  Non-dimensional extra stress components through Eq. (5.3) are (5.18) (5.19) (5.20) (5.21) (5.22)  $\tau_{xy} = \mu \nabla^2 u + \mu' \nabla^2 \nabla u$  (5.23)  $\tau_{yz} = \mu \nabla^2 v + \mu' \nabla^2 \nabla v$  (5.24) with  $\mu = \mu' = 1$  and  $\mu = \mu' = 1$  are Prandtl fluid parameters. The corresponding dimensionless conditions are  $\theta = 1 + \sin 2z$  ( $\theta = 0$ ) (5.25)  $\theta = 0$  at  $y = \pm a$  (5.26) (5.27)  $\theta = 0$  at  $y = \pm a$  (5.28)  $\theta = \theta_w, c = c_w$  at  $y = \pm a$  (5.29) From equation (5.20)  $\theta = 6 \theta_w$ , equation (5.18) becomes  $\mu \nabla^2 u + \mu' \nabla^2 \nabla u = 0$  (5.30) and equation (5.19) gives  $\mu \nabla^2 v + \mu' \nabla^2 \nabla v = 0$  (5.31) Here we neglect

7 **the pressure term due to secondary flow which is caused by rotation.**

5.3 Solution methodology We solve equations (5.21), (5.22), (5.30) and (5.31) numerically in Mathematica using built in command ND-Solve. Physical quantities of interest with respect to emerging parameters are

discussed. 5.4 Discussion 5.4.1 Axial velocity First of all axial velocity  $v_z$  is displayed in Figs. 5.2 – 5.6. Impact of  $\Omega$  and  $\tau_w$  on velocity is presented in Figs. 5.2 and 5.3. The obtained results show the decreasing behavior of velocity via larger parameters. Fig. 5.4 is portrayed

**to observe the behavior of Hartman number  $Ha$  on  $v_z$ . It is evident that velocity decreases by increasing**

$\Omega$ . As expected the magnetic field resists the flow. For increasing Taylor number  $Ta$  the axial velocity decays as shown in Fig. 5.5. In fact secondary flow due to rotation decayed the velocity. In absence of rotation, we observed that velocity is maximum. In Fig. 5.6 variation in velocity is depicted for wall parameters. For increment in elastic parameters  $\tau_1$  and  $\tau_2$ ,  $v_z$  increases while for enhancement in damping parameter  $\tau_3$ ,  $v_z$  decays.

**Fig. 5.2 Fig. 5.3 Fig. 5. 2: Sketch of**

$v_z$  versus  $\tau_1$  when  $\Omega = 0.2, 0.4, 0.6, 0.8, 1.0, 1.2, 1.4, 1.6, 1.8, 2.0, 2.2, 2.4, 2.6, 2.8, 3.0, 3.2, 3.4, 3.6, 3.8, 4.0, 4.2, 4.4, 4.6, 4.8, 5.0, 5.2, 5.4, 5.6, 5.8, 6.0, 6.2, 6.4, 6.6, 6.8, 7.0, 7.2, 7.4, 7.6, 7.8, 8.0, 8.2, 8.4, 8.6, 8.8, 9.0, 9.2, 9.4, 9.6, 9.8, 10.0$ . Fig. 5.3: Sketch of  $v_z$  versus  $\tau_2$  when  $\Omega = 0.2, 0.4, 0.6, 0.8, 1.0, 1.2, 1.4, 1.6, 1.8, 2.0, 2.2, 2.4, 2.6, 2.8, 3.0, 3.2, 3.4, 3.6, 3.8, 4.0, 4.2, 4.4, 4.6, 4.8, 5.0, 5.2, 5.4, 5.6, 5.8, 6.0, 6.2, 6.4, 6.6, 6.8, 7.0, 7.2, 7.4, 7.6, 7.8, 8.0, 8.2, 8.4, 8.6, 8.8, 9.0, 9.2, 9.4, 9.6, 9.8, 10.0$

**Fig. 5.4 Fig. 5.5 Fig. 5.**

4: Sketch of  $v_z$  versus  $\tau_3$  when  $\Omega = 0.2, 0.4, 0.6, 0.8, 1.0, 1.2, 1.4, 1.6, 1.8, 2.0, 2.2, 2.4, 2.6, 2.8, 3.0, 3.2, 3.4, 3.6, 3.8, 4.0, 4.2, 4.4, 4.6, 4.8, 5.0, 5.2, 5.4, 5.6, 5.8, 6.0, 6.2, 6.4, 6.6, 6.8, 7.0, 7.2, 7.4, 7.6, 7.8, 8.0, 8.2, 8.4, 8.6, 8.8, 9.0, 9.2, 9.4, 9.6, 9.8, 10.0$ . Fig. 5.5: Sketch of  $v_z$  versus  $\tau_0$  when  $\Omega = 0.2, 0.4, 0.6, 0.8, 1.0, 1.2, 1.4, 1.6, 1.8, 2.0, 2.2, 2.4, 2.6, 2.8, 3.0, 3.2, 3.4, 3.6, 3.8, 4.0, 4.2, 4.4, 4.6, 4.8, 5.0, 5.2, 5.4, 5.6, 5.8, 6.0, 6.2, 6.4, 6.6, 6.8, 7.0, 7.2, 7.4, 7.6, 7.8, 8.0, 8.2, 8.4, 8.6, 8.8, 9.0, 9.2, 9.4, 9.6, 9.8, 10.0$ . Fig. 5.6 Fig. 5.6: Sketch of  $v_z$  versus  $\tau_1, \tau_2, \tau_3$  when  $\Omega = 0.2, 0.4, 0.6, 0.8, 1.0, 1.2, 1.4, 1.6, 1.8, 2.0, 2.2, 2.4, 2.6, 2.8, 3.0, 3.2, 3.4, 3.6, 3.8, 4.0, 4.2, 4.4, 4.6, 4.8, 5.0, 5.2, 5.4, 5.6, 5.8, 6.0, 6.2, 6.4, 6.6, 6.8, 7.0, 7.2, 7.4, 7.6, 7.8, 8.0, 8.2, 8.4, 8.6, 8.8, 9.0, 9.2, 9.4, 9.6, 9.8, 10.0$ . 5.4.2 Secondary velocity Influence of emerging physical parameters on secondary velocity  $v_r$  are sketched in Figs. 5.7 – 5.11. For increasing  $\tau_1$  and  $\tau_2$  axial velocity shows decreasing behavior (see Figs. 5.7 and 5.8). Secondary velocity decreases for increasing Hartman number  $Ha$  as depicted in Fig. 5.9. In Fig. 5.10 the effect of Taylor number  $Ta$  on  $v_r$  is depicted. Increasing rotation enhances secondary velocity. Also we observe that there is no secondary velocity when  $\tau_0 = 0$ . From Fig. 5.11 we see that  $v_r$  is increased by  $\tau_3$  ( $\tau_3 = 1, 2$ ) and reverse effect is noticed for

**Fig. 5.7 Fig. 5.8 Fig. 5.**

7: Secondary velocity  $v_r$  for Prandtl fluid parameter  $\tau_1$  when  $\Omega = -0.2, 0.2, 0.4, 0.6, 0.8, 1.0, 1.2, 1.4, 1.6, 1.8, 2.0, 2.2, 2.4, 2.6, 2.8, 3.0, 3.2, 3.4, 3.6, 3.8, 4.0, 4.2, 4.4, 4.6, 4.8, 5.0, 5.2, 5.4, 5.6, 5.8, 6.0, 6.2, 6.4, 6.6, 6.8, 7.0, 7.2, 7.4, 7.6, 7.8, 8.0, 8.2, 8.4, 8.6, 8.8, 9.0, 9.2, 9.4, 9.6, 9.8, 10.0$ . Fig. 5.8: Secondary velocity  $v_r$  for Prandtl fluid parameter  $\tau_2$  when  $\Omega = -0.2, 0.2, 0.4, 0.6, 0.8, 1.0, 1.2, 1.4, 1.6, 1.8, 2.0, 2.2, 2.4, 2.6, 2.8, 3.0, 3.2, 3.4, 3.6, 3.8, 4.0, 4.2, 4.4, 4.6, 4.8, 5.0, 5.2, 5.4, 5.6, 5.8, 6.0, 6.2, 6.4, 6.6, 6.8, 7.0, 7.2, 7.4, 7.6, 7.8, 8.0, 8.2, 8.4, 8.6, 8.8, 9.0, 9.2, 9.4, 9.6, 9.8, 10.0$

3Fig. 5.9 Fig. 5.10 Fig. 5.

9: Secondary velocity  $w$  for Hartman number  $Ha$  when  $Ha = -0.2$   $w = 0.2$   $w = 0.1$   $w_1 = 0.5$   $w_2 = 0.3$   $w_3 = 0.1$   $w_4 = 0.5$   $w_5 = 0.2$   $w_6 = 2$   $w_7 = 2$   $w_8 = 5$   $w_9 = 0.2$   $w_{10} = 0.4$   $w_{11} = 0.4$   $w_{12} = 0.3$   $w_{13} = 0.2$  Fig. 5.10: Secondary velocity  $w$  for Taylor number  $Ta$  when  $Ta = -0.2$   $w = 0.2$   $w = 0.1$   $w_1 = 0.5$   $w_2 = 0.3$   $w_3 = 0.1$   $w_4 = 0.3$   $w_5 = 0.5$   $w_6 = 2$   $w_7 = 2$   $w_8 = 5$   $w_9 = 0.2$   $w_{10} = 0.4$   $w_{11} = 0.4$   $w_{12} = 0.3$   $w_{13} = 0.2$  Fig. 5.11 Fig. 5.11: Secondary velocity  $w$  for walls parameter  $W$  when  $W = -0.2$   $w = 0.2$   $w = 0.1$   $w_1 = 2$   $w_2 = 0.3$   $w_3 = 0.2$   $w_4 = 0.5$   $w_5 = 2$   $w_6 = 2$   $w_7 = 5$   $w_8 = 0.2$   $w_9 = 0.4$   $w_{10} = 0.4$   $w_{11} = 0.3$   $w_{12} = 0.2$  5.4.3 Temperature The temperature  $T$  with  $Pr$  for  $Bi$   $Bi_1$   $Bi_2$   $Bi_3$   $Bi_4$   $Bi_5$   $Bi_6$   $Bi_7$   $Bi_8$   $Bi_9$   $Bi_{10}$   $Bi_{11}$   $Bi_{12}$   $Bi_{13}$  and  $Pr$  are plotted in Figs. 5?12– 5?22. As we increase fluid parameters  $Bi_1$  and  $Bi_2$   $T$  decays (see Figs. 5? 12 and 5?13). The effects of  $Bi_1$  and  $Bi_2$  on temperature are shown in Figs. 5?14 and 5?15. For increasing heat transfer Biot number  $Bi_1$  temperature decays. In fact thermal conductivity of fluid is reduced. No variation in  $T$  is seen for increasing mass transfer Biot number  $Bi_2$ . Due to fluid resistance, temperature falls for larger  $Bi_1$  (see Fig. 5?16). In Fig. 5?17 temperature decreases for increasing  $Bi_1$ . In Figs. 5?18 and 5?19 temperature rises by increasing Soret  $So$  and Dufour  $Du$  numbers. It is due to increase in thermal diffusion. Impact of Brinkman number  $Br$  on  $T$  is portrayed in Fig. 5?20. Temperature increases due to less heat conduction produced by viscous dissipation. Temperature is increasing function of  $Br$  and  $Pr$  as exhibited in Figs. 5?21 and 5?22. It is because of the fact that for larger  $Pr$  mass diffusivity decays and hence  $T$  enhances. Specific heat of fluid enhances when we increase  $Pr$  which results in rise of temperature.

81Fig. 5.12 Fig. 5.13 Fig. 5.12:

Temperature  $T$  for Prandtl fluid parameter  $Pr$  when  $Pr = 0.2$   $T = 0.2$   $T = 0.1$   $T_1 = 0.3$   $T_2 = 0.1$   $T_3 = 0.1$   $T_4 = 0.3$   $T_5 = 0.2$   $T_6 = 0.2$   $T_7 = 0.5$   $T_8 = 0.2$   $T_9 = 0.4$   $T_{10} = 0.4$   $T_{11} = 0.3$   $T_{12} = 0.2$  Fig. 5.13: Temperature  $T$  for Prandtl fluid parameter  $Pr$  when  $Pr = 0.2$   $T = 0.2$   $T = 0.1$   $T_1 = 0.3$   $T_2 = 0.1$   $T_3 = 0.1$   $T_4 = 0.3$   $T_5 = 0.2$   $T_6 = 0.2$   $T_7 = 0.5$   $T_8 = 0.2$   $T_9 = 0.4$   $T_{10} = 0.4$   $T_{11} = 0.3$   $T_{12} = 0.2$   $T_{13} = 0.2$

80Fig. 5.14 Fig. 5.15 Fig. 5.14:

Temperature  $T$  for heat Biot number  $Bi_1$  when  $Bi_1 = 0.2$   $T = 0.2$   $T = 0.1$   $T_1 = 0.3$   $T_2 = 0.1$   $T_3 = 0.1$   $T_4 = 0.3$   $T_5 = 0.2$   $T_6 = 0.2$   $T_7 = 0.5$   $T_8 = 0.2$   $T_9 = 0.4$   $T_{10} = 0.4$   $T_{11} = 0.3$   $T_{12} = 0.2$  Fig. 5.15: Temperature  $T$  for mass Biot number  $Bi_2$  when  $Bi_2 = 0.2$   $T = 0.2$   $T = 0.1$   $T_1 = 0.3$   $T_2 = 0.1$   $T_3 = 0.1$   $T_4 = 0.3$   $T_5 = 0.2$   $T_6 = 0.2$   $T_7 = 0.5$   $T_8 = 0.2$   $T_9 = 0.4$   $T_{10} = 0.4$   $T_{11} = 0.3$   $T_{12} = 0.2$   $T_{13} = 0.2$

3Fig. 5.16 Fig. 5.17 Fig. 5.

16:

1Temperature  $T$  for Hartman number  $Ha$  when  $Ha = 0.2$   $T = 0.2$   $T = 0.1$   $T_1 = 0.3$   $T_2 = 0.1$   $T_3 = 0.1$   $T_4 = 0.3$   $T_5 = 0.2$   $T_6 = 0.2$   $T_7 = 0.5$   $T_8 = 0.2$   $T_9 = 0.4$   $T_{10} = 0.4$   $T_{11} = 0.3$   $T_{12} = 0.2$

1?  $\eta_2 = 0.75$ ?  $\eta_0 = 0.22$ ?  $\eta_1 = 2$ ?  $\eta_{21} = 2$ ?  $\eta_{22} = 5$ ?  $\eta = 0.22$ ?  $\eta = 0.4$ ?  $\eta = 0.4$ ?  $\eta = 0.3$ ?  $\eta = 0.2$ ?  
 Fig. 5.17: Temperature  $\eta$  for Taylor number  $\eta_0$  when  $\eta = 0.22$ ?  $\eta = 0.22$ ?  $\eta = 0.1$ ?  $\eta_1 = 0.3$ ?  $\eta_2 = 0.1$ ?  $\eta_3 = 0.1$ ?  
 $\eta = 0.3$ ?  $\eta_2 = 0.75$ ?  $\eta_1 = 2$ ?  $\eta_{21} = 2$ ?  $\eta_{22} = 5$ ?  $\eta = 0.22$ ?  $\eta = 0.4$ ?  $\eta = 0.4$ ?  $\eta = 0.3$ ?  $\eta = 0.2$ ?

3Fig. 5.18 Fig. 5.19 Fig. 5.

18: Temperature  $\eta$  for Soret number  $\eta_0$  when  $\eta = 0.22$ ?  $\eta = 0.22$ ?  $\eta = 0.1$ ?  $\eta_1 = 0.3$ ?  $\eta_2 = 0.1$ ?  $\eta_3 = 0.1$ ?  
 $\eta = 0.75$ ?  $\eta_0 = 0.22$ ?  $\eta_1 = 2$ ?  $\eta_{21} = 2$ ?  $\eta_{22} = 5$ ?  $\eta = 0.22$ ?  $\eta = 0.3$ ?  $\eta = 0.4$ ?  $\eta = 0.3$ ?  $\eta = 0.2$ ? Fig.  
 5.19: Temperature  $\eta$  for Dufour number  $\eta_0$  when  $\eta = 0.22$ ?  $\eta = 0.22$ ?  $\eta = 0.1$ ?  $\eta_1 = 0.3$ ?  $\eta_2 = 0.1$ ?  $\eta_3 = 0$ ?  
 $\eta = 0.3$ ?  $\eta_2 = 0.75$ ?  $\eta_1 = 2$ ?  $\eta_{21} = 2$ ?  $\eta_{22} = 5$ ?  $\eta = 0.22$ ?  $\eta = 0.4$ ?  $\eta_0 = 0.22$ ?  $\eta = 0.3$ ?  $\eta = 0.2$ ?

3Fig. 5.20 Fig. 5.21 Fig. 5.

20:

1Temperature  $\eta$  for Brinkman number  $\eta_0$  when  $\eta = 0.22$ ?  $\eta = 0$ ?  $\eta = 0$ ?  $\eta_1 = 0$ ?  
 $\eta = 0$ ?  $\eta_2 = 0$ ?  $\eta_3 = 0$ ?  $\eta = 0$ ?  $\eta = 0$ ?

$\eta = 0.75$ ?  $\eta_0 = 0.22$ ?  $\eta_1 = 2$ ?  $\eta_{21} = 2$ ?  $\eta_{22} = 5$ ?  $\eta = 0.22$ ?  $\eta = 0.3$ ?  $\eta = 0.4$ ?  $\eta = 0.3$ ?  $\eta = 0.4$ ? Fig.  
 5.21: Temperature  $\eta$  for Schmidt number  $\eta_0$  when  $\eta = 0.22$ ?  $\eta = 0.22$ ?  $\eta = 0.1$ ?  $\eta_1 = 0.3$ ?  $\eta_2 = 0.1$ ?  $\eta_3 = 0$ ?  
 $\eta = 0.3$ ?  $\eta_2 = 0.75$ ?  $\eta_1 = 2$ ?  $\eta_{21} = 2$ ?  $\eta_{22} = 5$ ?  $\eta = 0.22$ ?  $\eta = 0.4$ ?  $\eta_0 = 0.22$ ?  $\eta = 0.4$ ?  $\eta = 0.2$ ?  
 Fig. 5.22 Fig. 5.22: Temperature  $\eta$  for Prandtl number  $Pr$  when  $\eta = 0.22$ ?  $\eta = 0.22$ ?  $\eta = 0.1$ ?  $\eta_1 = 0.3$ ?  $\eta_2 = 0.1$ ?  
 $\eta_3 = 0.1$ ?  $\eta = 0.3$ ?  $\eta_2 = 0.75$ ?  $\eta_1 = 2$ ?  $\eta_{21} = 2$ ?  $\eta_{22} = 5$ ?  $\eta = 0.3$ ?  $\eta = 0.4$ ?  $\eta_0 = 0.22$ ?  $\eta = 0.4$ ?  
 $\eta = 0.2$ ? 5.4.4 Concentration This section provides the behavior of involved parameters in the expressions of concentration  $\eta$ . For increasing fluid parameters  $\eta_1$  and  $\eta_2$  decreasing effect in  $\eta$  is noticed (see Figs. 5?23 and 5?24). Fig. 5?25 shows no variation for  $\eta_{21}$  on  $\eta$ . On other hand in Fig. 5?26 the role of  $\eta_{22}$  on the concentration field  $\eta$  is increasing rapidly due to decrease in mass diffusivity. Similar pattern is observed on  $\eta$  for Soret  $\eta_0$  and Dufour  $\eta_0$  numbers on  $\eta$  in Figs. 5?27 and 5?28. Concentration is decreased by  $\eta_0$  and  $\eta_0$ .

35Fig. 5.23 Fig. 5.24 Fig. 5.23:

Concentration  $\eta$  for Prandtl fluid parameter  $\eta_1$  when  $\eta = 0.22$ ?  $\eta = 0.22$ ?  $\eta = 0.1$ ?  $\eta_1 = 0.3$ ?  $\eta_2 = 0.1$ ?  $\eta_3 = 0$ ?  
 $\eta = 0.3$ ?  $\eta_0 = 0.22$ ?  $\eta_2 = 0.75$ ?  $\eta_{21} = 2$ ?  $\eta_{22} = 5$ ?  $\eta = 0.22$ ?  $\eta = 0.4$ ?  $\eta = 0.4$ ?  $\eta = 0.3$ ?  $\eta = 0$ ?  
 2? Fig. 5.24: Concentration  $\eta$  for Prandtl fluid parameter  $\eta_2$  when  $\eta = 0.22$ ?  $\eta = 0.22$ ?  $\eta = 0.1$ ?  $\eta_1 = 0.3$ ?  $\eta_2 = 0.1$ ?  
 $\eta_3 = 0.1$ ?  $\eta = 0.3$ ?  $\eta_0 = 0.22$ ?  $\eta_1 = 2$ ?  $\eta_{21} = 2$ ?  $\eta_{22} = 5$ ?  $\eta = 0.22$ ?  $\eta = 0.4$ ?  $\eta = 0.4$ ?  $\eta = 0$ ?  
 $3$ ?  $\eta = 0.2$

35Fig. 5.25 Fig. 5.26 Fig. 5.25:

Concentration  $\eta$  for heat Biot number  $B_{i,h}$  when  $\eta = 0.2$   $\eta = 0.2$   $\eta = 0.1$   $\eta_1 = 0.3$   $\eta_2 = 0.1$   $\eta_3 = 0.1$   $\eta_2 = 0.5$   $\eta_0 = 0.2$   $\eta_1 = 2$   $\eta_{11} = 2$   $\eta_{22} = 5$   $\eta = 0.2$   $\eta = 0.4$   $\eta = 0.4$   $\eta = 0.3$   $\eta = 0.2$  Fig. 5.26: Concentration  $\eta$  for mass Biot number  $B_{i,m}$  when  $\eta = 0.2$   $\eta = 0.2$   $\eta = 0.1$   $\eta_1 = 0.3$   $\eta_2 = 0.1$   $\eta_3 = 0.1$   $\eta_2 = 0.5$   $\eta_0 = 0.2$   $\eta_1 = 2$   $\eta_{11} = 2$   $\eta_{22} = 5$   $\eta = 0.2$   $\eta = 0.4$   $\eta = 0.4$   $\eta = 0.3$   $\eta = 0.2$

**3 Fig. 5.27 Fig. 5.28 Fig. 5.**

27: Concentration  $\eta$  for Soret number  $S_r$  when  $\eta = 0.2$   $\eta = 0.2$   $\eta = 0.1$   $\eta_1 = 0.3$   $\eta_2 = 0.1$   $\eta_3 = 0.1$   $\eta_2 = 0.5$   $\eta_0 = 0.2$   $\eta_1 = 2$   $\eta_{11} = 2$   $\eta_{22} = 5$   $\eta = 0.2$   $\eta = 0.3$   $\eta = 0.4$   $\eta = 0.3$   $\eta = 0.2$  Fig. 5.28: Concentration  $\eta$  for Dufour number  $D_u$  when  $\eta = 0.2$   $\eta = 0.2$   $\eta = 0.1$   $\eta_1 = 0.3$   $\eta_2 = 0.1$   $\eta_3 = 0.1$   $\eta_2 = 0.5$   $\eta_0 = 0.2$   $\eta_1 = 2$   $\eta_{11} = 2$   $\eta_{22} = 5$   $\eta = 0.2$   $\eta = 0.4$   $\eta_0 = 0.2$   $\eta = 0.3$   $\eta = 0.2$

**3 Fig. 5.29 Fig. 5.30 Fig. 5.**

29: Concentration  $\eta$  for Taylor number  $T_0$  when  $\eta = 0.2$   $\eta = 0.2$   $\eta = 0.1$   $\eta_1 = 0.3$   $\eta_2 = 0.1$   $\eta_3 = 0.1$   $\eta_3 = 0.1$   $\eta = 0.3$   $\eta_2 = 0.5$   $\eta_1 = 2$   $\eta_{11} = 2$   $\eta_{22} = 5$   $\eta = 0.2$   $\eta = 0.4$   $\eta = 0.4$   $\eta = 0.3$   $\eta = 0.2$  Fig. 5.30: Concentration  $\eta$  for Schmidt number  $S_c$  when  $\eta = 0.2$   $\eta = 0.2$   $\eta = 0.1$   $\eta_1 = 0.3$   $\eta_2 = 0.1$   $\eta_3 = 0.1$   $\eta = 0.3$   $\eta_2 = 0.5$   $\eta_1 = 2$   $\eta_{11} = 2$   $\eta_{22} = 5$   $\eta = 0.2$   $\eta = 0.4$   $\eta_0 = 0.2$   $\eta = 0.4$   $\eta = 0.2$  5.4.5 Heat transfer coefficient In Figs. 5.31 – 5.36 the heat transfer coefficient  $h$  is plotted for parameters  $\eta_1$   $\eta_2$   $\eta_3$   $\eta_0$   $\eta$  and  $\eta$ . Heat transfer coefficient has oscillatory character. It is expected in view of waves propagation along channel boundaries.  $h$  shows a decreasing behavior for increasing  $\eta_1$  and  $\eta_2$  (see Figs. 5.31 and 5.32). The oscillatory nature is captured in Figs. 5.33 and 5.34 for Hartman  $\eta$  and Taylor  $T_0$  numbers. Here  $h$  decays for larger  $\eta$  due to strong magnetic strength whereas it increases for larger  $\eta_0$ . In Figs. 5.35 and 5.36,  $h$  increases for  $\eta_1$  and  $\eta_2$  near the centerline whereas it decays near boundaries.

**84 Fig. 5.31 Fig. 5.32 Fig. 5.31:**

Heat transfer coefficient  $h$  for  $\eta_1$  when  $\eta = 0.2$   $\eta = 0.2$   $\eta = 0.1$   $\eta_1 = 0.3$   $\eta_2 = 0.1$   $\eta_3 = 0.1$   $\eta = 0.3$   $\eta_0 = 0.2$   $\eta_2 = 0.5$   $\eta_{11} = 2$   $\eta_{22} = 5$   $\eta = 0.2$   $\eta = 0.4$   $\eta = 0.4$   $\eta = 0.3$   $\eta = 0.2$  Fig. 5.32: Heat transfer coefficient  $h$  for  $\eta_2$  when  $\eta = 0.2$   $\eta = 0.2$   $\eta = 0.1$   $\eta_1 = 0.3$   $\eta_2 = 0.1$   $\eta_3 = 0.1$   $\eta = 0.3$   $\eta_0 = 0.2$   $\eta_1 = 2$   $\eta_{11} = 2$   $\eta_{22} = 5$   $\eta = 0.2$   $\eta = 0.4$   $\eta = 0.4$   $\eta = 0.3$   $\eta = 0.2$

**89 Fig. 5.33 Fig. 5.34 Fig. 5.**

33:

**1 Heat transfer coefficient  $h$  for  $\eta$  when  $\eta = 0.2$   $\eta = 0.2$   $\eta = 0.1$   $\eta_1 = 0.3$   $\eta_2 = 0.1$   $\eta_3 = 0.1$   $\eta = 0.3$   $\eta_0 = 0.2$   $\eta_2 = 0.5$   $\eta_{11} = 2$   $\eta_{22} = 5$   $\eta = 0.2$   $\eta = 0.4$   $\eta = 0.4$   $\eta = 0.3$   $\eta = 0.2$**

1? ?? = 0?5? ? 0 = 0?2? ?1 = 2? ??1 = 2? ??2 = 5? ? ? = 0?2? ?? = 0?4? ?? = 0?4? ?? = 0?3? ?? = 0?2?  
 Fig. 5.34: Heat transfer coefficient ? for ? 0 when ? = 0?2? ? = 0?2? ? = 0?1? ?1 = 0?3? ?2 = 0?1? ?3 = 0?  
 1? ? = 0?3? ?2 = 0?5? ?1 = 2? ??1 = 2? ??2 = 5? ? ? = 0?2? ?? = 0?4? ?? = 0?4? ?? = 0?3? ?? = 0?2?

**3Fig. 5.35 Fig. 5.36 Fig. 5.**

35:

**1Heat transfer coefficient ? for ?? when ? = 0? 2? ? = 0? 2? ? = 0? 1? ?1 = 0? 5?  
 ?2 = 0? 01? ?3 = 0?**

01? ?? = 0?5? ? 0 = 0?2? ?1 = 2? ??1 = 2? ??12 = 5? ? ? = 0?2? ? = 0?3? ?? = 0?4? ?? = 0?3? ?? = 0?2?  
 Fig. 5.36:

**1Heat transfer coefficient ? for ?? when ? = 0? 2? ? = 0? 2? ? = 0? 1? ?1 = 0? 5?  
 ?2 = 0? 01? ?3 = 0?**

01? ? = 0?3? ?2 = 0?5? ?1 = 2? ??1 = 2? ??12 = 5? ? ? = 0?2? ?? = 0?4? ? 0 = 0?2? ?? = 0?3? ?? = 0?2?  
 5.5 Conclusions Influences of

**41Soret and Dufour on peristaltic flow in a rotating channel**

subject to compliant walls are discussed. Main observations are • Decreasing behavior of ?1? ?2 on (?? ?),  
 ? and ? is noticed while for ? increasing effect is observed. • Velocity, temperature and heat transfer  
 coefficient are decreasing functions of Hartman number. However Hartman number leads to an  
 enhancement of concentration. • Both velocities shows opposite behavior for rotation parameter. • Impact of  
 wall parameters on both velocities are identical. • For increasing Taylor parameter ? 0 the temperature  
 decreases . • Temperature increases for ??, ??, ??, ?? and ? ?. • By increasing ??1, ? decays whereas for  
 ??? ? increases. • Heat transfer rate is increasing function of ?? and ?? while it is decreasing function of ?  
 and ? 0. Chapter 6 Heat transfer analysis on peristalsis of Ree-Eyring fluid 6.1

**90Introduction The peristaltic activity of Ree-Eyring fluid in a rotating frame is**

studied. Heat transfer analysis with viscous dissipation and heat source/sink is

**4taken into account. Convective conditions for heat transfer in the  
 formulation are adopted.**

Closed form solutions for axial and secondary velocities, pressure rise per wavelength, flow rate due to  
 secondary flow and temperature

4are obtained by considering small Reynolds number and long wavelength. The variation for different physical parameters are shown through graphical illustrations. This study reveals that influence of

rotation parameter causes significant fluctuations in axial and secondary velocities. It is also found that presence of non-uniform heat source in energy equation causes enhancement in rate of heat transfer coefficient. 6.2 Problem development Here we address an incompressible Ree-Eyring material in a channel of width 2?. Both the channel and fluid rotates with a uniform angular velocity  $\Omega$  about the  $z$  - axis. Mathematical expression for wave propagation along the channel walls at  $(y = \pm 1)$

48is given by  $\psi(r, \theta) = \sum_{n=0}^{\infty} A_n \sin 2n\theta (1 - r^{2n})^2$

? - (6.1) Fig. 6.1: Geometry of the problem. Extra

12stress tensor of Ree- Eyring fluid model is defined as

[56? 57] :  $S_{ij} = \mu \frac{\partial v_i}{\partial x_j} \frac{1}{\sqrt{1 + \frac{1}{2} \sum_{k,l} (\frac{\partial v_k}{\partial x_l})^2}}$  (6.2) Since  $\sinh^{-1} x \approx x - \frac{1}{6} x^3 + \frac{1}{10} x^5 - \dots$

2-1  $\approx x$  for  $|x| \leq 1$  then  $S_{ij} = \mu \frac{\partial v_i}{\partial x_j} (1 - \frac{1}{6} \sum_{k,l} (\frac{\partial v_k}{\partial x_l})^2 + \dots)$

$\mu \frac{\partial v_i}{\partial x_j} + \frac{1}{6} \mu \frac{\partial v_i}{\partial x_j} \sum_{k,l} (\frac{\partial v_k}{\partial x_l})^2$  (6.3) where  $\mu$  is the fluid viscosity,  $\mu_3$  and  $\mu_4$  are material constants and

$2\mu \frac{\partial v_i}{\partial x_j} = (\mu_3 \frac{\partial v_i}{\partial x_j} + \mu_4 \sum_{k,l} (\frac{\partial v_k}{\partial x_l})^2) \frac{\partial v_i}{\partial x_j} = (\mu_3 \frac{\partial v_i}{\partial x_j} + \mu_4 \sum_{k,l} (\frac{\partial v_k}{\partial x_l})^2) \frac{\partial v_i}{\partial x_j}$

77The governing equations of continuity, momentum and energy for incompressible fluid

flow in a rotating frame are

$2\frac{\partial v_r}{\partial r} + \frac{\partial v_\theta}{\partial \theta} = 0$  + (6.4)  $\rho \frac{Dv_r}{Dt} - 2\Omega v_\theta = -\frac{\partial p}{\partial r} + \mu \frac{\partial}{\partial r} (\frac{1}{r} \frac{\partial}{\partial r} (r \frac{\partial v_r}{\partial r})) + \mu \frac{\partial}{\partial r} (\frac{\partial v_\theta}{\partial r})$

$\Omega$

$8\frac{\partial v_\theta}{\partial r} = -\frac{\partial p}{\partial \theta} + \mu \frac{\partial}{\partial r} (\frac{\partial v_r}{\partial r}) + \mu \frac{\partial}{\partial r} (\frac{\partial v_\theta}{\partial r}) + 2\Omega v_r = -\frac{\partial p}{\partial \theta} + \mu \frac{\partial}{\partial r} (\frac{\partial v_r}{\partial r}) + \mu \frac{\partial}{\partial r} (\frac{\partial v_\theta}{\partial r}) + 2\Omega v_r$   
 $\rho \frac{Dv_\theta}{Dt} + 2\Omega v_r = -\frac{\partial p}{\partial \theta} + \mu \frac{\partial}{\partial r} (\frac{\partial v_r}{\partial r}) + \mu \frac{\partial}{\partial r} (\frac{\partial v_\theta}{\partial r}) + 2\Omega v_r$  (6.5) (6.6) (6.7)  $\rho \frac{Dv_r}{Dt} + 2\Omega v_\theta = -\frac{\partial p}{\partial r} + \mu \frac{\partial}{\partial r} (\frac{1}{r} \frac{\partial}{\partial r} (r \frac{\partial v_r}{\partial r})) + \mu \frac{\partial}{\partial r} (\frac{\partial v_\theta}{\partial r})$   
 $\rho \frac{Dv_\theta}{Dt} + 2\Omega v_r = -\frac{\partial p}{\partial \theta} + \mu \frac{\partial}{\partial r} (\frac{\partial v_r}{\partial r}) + \mu \frac{\partial}{\partial r} (\frac{\partial v_\theta}{\partial r}) + 2\Omega v_r$





pressure  $\Delta$  rises for fluid parameter  $\beta$  and Taylor number  $T$  in retrograde pumping region while it decays in augmented pumping region. It is because of the fact that for larger angular velocity, the pressure does not rise in direction of peristaltic wave. Further the Coriolis force is responsible for fluid drag outwards in  $-z$  direction and consequently  $\Delta$  reduces. Figs. 6.25(a, b) plot variation of fluid parameter  $\beta$  on secondary velocity. In Fig. 6.25(a) when  $\beta = -1$  the flow rate of the fluid is enhanced in wider portion of channel. However when  $\beta = -0.5$  the flow due to secondary velocity becomes positive for larger values of fluid parameter over the whole length of the channel (see Fig. 6.25(b)). Opposite results of  $\beta$  is observed in Figs. 6.26(a, b) for larger values of Taylor number  $T$  when  $\beta = -1$  and  $-0.5$ . Figs. 6.27(a, b) show temperature  $\theta$  variation versus different parameters. Fig. 6.27(a) is plotted for fluid parameter against  $\beta$ . It is noticed from this Fig. that temperature distribution tends to rise when the fluid parameter enhances. It can be observed from Fig. 6.27(b) that for larger rotation parameter  $T$  the temperature profile diminishes. In fact with the increase in rotation, the motion of the fluid particles enhances which causes resistance to flow and ultimate there is decrease in temperature profile. Fig. 6.27(c) is portrayed to analyze the variation of  $\theta$  for heat source/sink parameter  $\beta$ . It can be observed from Fig. that with the increase in  $\beta$  the temperature profile is enhanced. Behavior of Biot number  $B$  can be visualized through Fig. 6.27(d). Temperature rapidly decays as we increase  $B$ . It is due to enhancement in strength of convecting heating which causes decrease in temperature. Temperature via Brinkman number  $Br$  in Fig. 6.27(e). Here for larger values of  $Br$  the temperature increases. It is through argument that less heat conduction occurs for viscous dissipation. Now  $\theta$  for different variable is demonstrated through Figs. 6.28(a, b). In Fig. 6.28(a) we observed that heat transfer rate  $q$  rises by increasing fluid parameter  $\beta$ . The magnitude of heat transfer coefficient  $h$  near centerline decreases for Taylor number  $T$  whereas it enhances near the channel boundaries (see Fig. 6.28(b)). Variation in heat transfer rate  $q$  for heat generation/absorption  $\beta$  is portrayed in Fig. 6.28(c). Rate of heat transfer of fluid increases when we take larger values of  $\beta$ . Opposite result for  $q$  via Biot number is observed in Fig. 6.28(d). Here Fig. 6.28(d) is plotted for viscous dissipation parameter  $Br$  on heat transfer rate  $q$ . It is noticed that larger values of Brinkman number  $Br$  increases  $q$  for a small range. The next interesting part of this section is trapping. Figs. 6.9(a, b) and 6.10(a, b) are plotted for this purpose with the help of contours. It can be seen in Fig. 6.9

**12 that when the fluid parameter  $\beta$  increases then the size of bolus**

enhances. Also for viscous fluid ( $\beta = 0$ ) the trapped bolus vanishes.

**17 It depicts from Fig. 6.10 that due to the influence of rotation the size of the bolus decreases slowly.**

It can also be observed from Fig. that the bolus disappears when the rotation of the fluid particles increases.

(a) (b) Fig. 6.2: Influence in  $\theta$  for (a) Fluid parameter  $\beta$  and (b) Taylor number  $T$

(a) (b) Fig. 6.3: Influence in secondary velocity  $v$  for (a) Fluid parameter  $\beta$  and (b) Taylor number  $T$

**14 Fig. 6.4: Variation in pressure rise per wavelength  $\Delta$  for**

(a) Fluid parameter  $\beta$  and (b) Taylor number  $T$

(a) (b) Fig. 6.5: Variation in

7 dimensionless flow rate due to secondary velocity  $\Omega$  for fluid parameter  $\beta$  when (a)  $\beta = -1$  and (b)  $\beta = -0.5$  (a) (b) Fig.

6.6: Variation in

7 flow rate due to secondary velocity  $\Omega$  for

Taylor number  $\Omega = 0$

7 when (a)  $\beta = -1$  and (b)  $\beta = -0.5$  (a) (b) (c) (d) (e) Fig.

6.7: Influence in  $\Omega$  for (a) Fluid parameter  $\beta$ , (b) Taylor number  $\Omega = 0$  (c) non-uniform source/sink parameter  $\beta$ , (d) Biot number  $\beta = 1$  and (e) Brinkman number  $\beta$ . (a) (b) (c) (d) (e) Fig. 6.8: Influence in  $\Omega$  for (a) Fluid parameter  $\beta$ , (b) Taylor number  $\Omega = 0$  (c) non-uniform source/sink parameter  $\beta$ , (d) Biot number  $\beta = 1$  and (e) Brinkman number  $\beta$ . (a) (b) (c) Fig. 6.9: Variation in streamlines for fluid parameter  $\beta$  when (a)  $\beta = 0$  (b)  $\beta = 0.9$  and (c)  $\beta = 2$  (a) (b) (c) Fig. 6.10: Variation in streamlines for Taylor number  $\Omega = 0$  when (a)  $\beta = 0$  (b)  $\beta = 0.5$  and (c)  $\beta = 2$  6.5 Conclusions Here simultaneous outcome of rotation and heat generation/absorption on peristalsis of Ree-Eyring fluid have been pointed out. Major observations include:

- Dual behavior of fluid parameter  $\beta$  and Taylor number  $\Omega = 0$  on the axial velocity is noticed.
- Opposite effect is observed on secondary velocity for fluid parameter  $\beta$  and Taylor number  $\Omega = 0$ .
- Similar behavior of pressure rise  $\Delta P$  is observed for fluid  $\beta$  and rotation  $\Omega = 0$  parameters.
- Variation in dimensionless flow rate due to secondary velocity  $\Omega$  for fluid  $\beta$  and rotation parameters  $\Omega = 0$  is quite opposite.
- Temperature is an increasing function of fluid parameter  $\beta$ , heat generation/absorption  $\beta$  and Brinkman number whereas it is decreasing function of rotation parameter  $\Omega = 0$  and Biot number  $\beta = 1$ .
- Rate of heat transfer decreases for increasing  $\Omega = 0$  and  $\beta = 1$  but it enhances for  $\beta$  and  $\beta$ .
- Fluid and rotational parameters on trapped bolus have opposite contributions.
- For viscous fluid, the present problem is reduced by taking  $\beta \rightarrow 0$

Chapter 7 Numerical analysis for ionslip and Hall current on peristaltic transport of rotating Ree-Eyring fluid 7.1 Introduction Ion-slip and Hall current in peristalsis of Ree-Eyring liquid are analyzed. In addition energy equation contains Ohmic dissipation. Whole system is in rotating frame. Governing equations representing flow of a fluid are reduced into ordinary differential equations. Problem formulation is developed by small Reynolds number and long wavelength approximation. Shooting method is applied to find numerical results. Variation of emerging dimensionless parameters of present problem is illustrated through graphs. We observed that velocity and temperature distributions in Ree-Eyring fluid are more than viscous fluid. Rotation and fluid parameters have opposite effects on velocity. It is also found that influence of ionslip in momentum equation causes an enhancement in velocity. 7.2 Problem development Here we consider an incompressible Ree-Eyring fluid in a channel with width  $(\beta + \beta)$ . Both channel and fluid rotate with uniform angular velocity  $\Omega$  about the  $\beta - \beta$ . Travelling waves of speed  $\beta$ , amplitudes  $(\beta \beta)$  and wavelength  $\beta$  propagate along the channel walls  $(\beta - \beta)$ . Mathematically we represent such waves in the form  $\beta - \beta$

$$2(\beta \beta) = \beta + \beta \sin 2\beta (\beta \beta) - (7.1) \beta - \beta \sin 2\beta (\beta - \beta) \beta$$



Newtonian case velocity is greater when compared to viscous fluid ( $\beta = 0$ )? Opposite behavior of secondary flow  $\beta$  is captured in Fig. 7?1(?) for larger values of  $\beta$ . In fact due to rotation the fluid particles motion in secondary direction becomes faster and hence  $\beta$  rapidly decays. Temperature  $\beta$  rises when fluid parameter is enhanced (see Fig. 7?1(?)). Similar result of  $\beta$  is observed in Fig. 7?1(?) for heat transfer rate. Figs. 7?2(? - ?) are demonstrated to see the effects of rotation parameter  $\beta = 0$  on  $\beta$ ,  $\beta$ ,  $\beta$  and  $\beta$  respectively. Fig. 7?2(?) shows dual behavior of axial velocity for  $\beta = 0$ . This Fig depicts that rotation parameter decays the axial velocity at centre of channel and near the channel walls it enhances  $\beta$ . At centre of channel, due to faster rotation the secondary flow is induced which minimizes  $\beta$ . Impact of rotation parameter  $\beta = 0$  on  $\beta$  is observed through Fig. 7?2(?). In fact an increase in rotation enhances the motion of fluid particles and thus  $\beta$  has been increased. Fig. 7?2(?) presents the influence of increasing  $\beta = 0$  on  $\beta$ . It is because of Coriolis force which is responsible to drag the fluid outwards in the  $\beta$ -direction and subsequently it reduces the temperature.

49 Heat transfer rate decays for larger values of

Taylor number (see Fig. 7?2(?)). Effect of Hall parameter  $\beta$  through Figs. 7?3(? - ?) can be visualized for  $\beta$ ,  $\beta$ ,  $\beta$  and  $\beta$  respectively. It is observed from Fig. 7?3(?) that  $\beta$  tends to rise when  $\beta$  enhances. It is because of the fact that electrical conductivity of fluid particles reduced as we increase  $\beta$ ? Hence magnetic damping force diminishes and thus axial velocity is enhanced. For larger  $\beta$  secondary velocity is enhanced (see Fig. 7?3(?)). Similar variation for  $\beta$  is noticed in study of Hayat et. al [156]. Behavior of  $\beta$  on temperature  $\beta$  is observed through Fig. 7?3(?). The application of magnetic field offers resistance to flow so kinetic energy decreases and hence there is reduction in temperature. Fluctuation in heat transfer rate  $\beta$  for Hall current  $\beta$  is portrayed in Fig. 7?3(?). Rate of heat transfer decays as we increase Hall parameter  $\beta$ . Impact of ionslip parameter  $\beta$  on  $\beta$ ,  $\beta$ ,  $\beta$  and  $\beta$  is portrayed in Figs. 7?4(? - ?). Addition of ionslip effect decreases the resistive force imposed by magnetic field and thus effective conductivity decays. Thus decrease in conduction rate enhances the axial velocity (see Fig. 88 7?4(?)). Fig. 7?4(?) shows increasing behavior of  $\beta$  for larger values of ionslip parameter.

21 It can be noticed from Fig. 7?4(?) that temperature profile decays with increase

in  $\beta$ . Physically it means that kinetic energy of fluid particles decreases for smaller magnetic field. Such decrease in energy implies decay in Joule heating and hence temperature falls. Similar behavior has been reported in [86? 87]. They solved the nonlinear governing equations by employing the perturbation and numerical technique respectively when the system is non-rotating frame. In Fig. 7?4(?) we noticed that near the centerline, the magnitude of heat transfer rate  $\beta$  for  $\beta$  decreases whereas near boundaries it enhances. (a) (b) (c) (d) Fig. 7.1: Influence of fluid parameter  $\beta$  on

22 (a) ?(?) (b) ?(?) (c) ?(?) (d) ?(?)? (a) (b) (c) (d) Fig. 7.

2: Influence of Taylor number  $\beta = 0$  on

22 (a) ?(?) (b) ?(?) (c) ?(?) (d) ?(?)? (a) (b) (c) (d) Fig. 7.

## 3: Influence of Hall parameter ? on

22(a) ?(?) (b) ?(?) (c) ?(?) (d) ?(?)? (a) (b) (c) (d) Fig. 7.

4: Influence of ionslip parameter ?? on (a) ?(?) (b) ?(?) (c) ?(?) (d) ?(?)? 7.5 Conclusions The present study here investigated the influences of Hall current, Joule heating and ionslip on MHD peristaltic motion of rotating Ree-Eyring fluid. Main salient features are listed below: • Magnitude of axial velocity ? for Ree-Eyring fluid ( $\beta = 6$ ) is higher than viscous fluid ( $\beta = 0$ ). • Effects of ? 0 on ? and ? are opposite. • Secondary flow for Ree-Eyring fluid is lower than viscous fluid. • Variation of ? on ? and ? are similar to that of ??? • Temperature is an increasing function of  $\beta$  whereas it decreases for ? 0? ? and ?? . • Heat transfer rate from walls to the fluid increases when fluid parameter  $\beta$  is enhanced. However it decreases by increasing rotation parameters ? 0? Hall parameter ? and ionslip parameter ??. Chapter 8 Peristalsis of couple stress liquid in a non-uniform rotating geometry 8.1 Introduction Thermal radiation in peristaltic rotating

39flow of couple stress liquid in a non-uniform channel

is addressed. Slip boundary conditions for velocity and temperature are satisfied by channel boundaries. Impact of

4non-uniform heat source/sink in heat transfer

phenomena is also accounted here. Complexity in mathematical formulation of problem is reduced

27by employing assumptions of long wavelength and low Reynolds number. Resulting non-linear system of equations is solved through numerical technique. The behavior of velocities and

temperature for different physical parameters has been displayed through graphs and interpreted physically. 8.2 Problem development Here peristaltic pumping of incompressible couple stress liquid through a nonuniform channel of width  $(\beta_1 + \beta_2)$  is examined. Peristaltic transport is engendered by propagation of

56sinusoidal wavetrains with constant speed ? along channel walls.

A solid body rotation is observed in both liquid and channel. The coordinates are

5chosen in such a way that ? - ???? is along centerline and ? - ???? is normal to it. Geometrical representation of

wall surface is given as  $r = 1$



non-uniformity parameter is illustrated in Fig. 8.3. A gradual increase in velocity is observed for increasing values of  $\gamma$ . It is due to decrease in frictional force offered by channel walls. 8.4.2 Secondary velocity

46(a) (b) (c) (d) (e) Fig. 8.3: Graph of  $v$  for (a)

Fig. 8.3(b) (c) (d) (e) In this section, variation in secondary velocity for involved parameters is investigated through Figs. 8.3(a) – (e). Fig. 8.3(b) indicates that secondary velocity grows for enhancing values of fluid parameter  $\gamma$ . Influence of Taylor number

61on velocity profile is displayed in Fig. 8.3(b). It is obvious that velocity increases

via  $\gamma$  because of enhancement in rotation of fluid and channel. Effect of axial velocity slip parameter of secondary velocity is manifested through Fig. 8.3(c). The resulting panel exhibit an increment in  $v$  for larger  $\gamma$ . Fig. 8.3(c) reveals

28that velocity is an increasing function of secondary velocity slip parameter

Fig. 8.3(d). A very small rise in secondary velocity

28is noticed for growing values of  $\gamma$  as seen through Fig.

Fig. 8.3(e). 8.4.3 Temperature profile

47(a) (b) (c) (d) (e) (f) Fig. 8.4: Graph of

$\theta$  for (a) (b) (c) (d) (e) (f) ???

44This subsection is devoted to illustrate the behavior of pertinent parameters on temperature profile

through Figs. 8.4(a) – (f). Decreasing response of temperature towards growing fluid parameter is depicted in Fig. 8.4(a). As viscosity of fluid enhances via larger values of  $\gamma$  which provides retardation to flow therefore temperature drops. Motion of fluid particles is related with rotation of channel. When Taylor number is increased, fluid particle move rapidly without experiencing any retardation. As a result, temperature decreases (see Fig. 8.4(a)). Fig. 8.4(b) is plotted to observe the impact of temperature slip parameter on  $\theta$ . For growing values of  $\gamma$  kinetic energy of fluid particle increases which produces a rise in temperature. Increasing impression of  $\gamma$  on temperature profile is disclosed in Fig. 8.4(c). It is obvious from Fig. 8.4(c) that temperature declines for negative values of heat generation/absorption coefficient ( $\gamma < 0$ ) whereas a rise in temperature is noticed for its positive values ( $\gamma > 0$ ). In fact for  $\gamma = 0$  a heat sink is produced which



absorbs heat and for (??) more heat is added to the system. A decline in temperature for enhancing values of radiation parameter ?? is evident from Fig. 8?4 (?). As effect of natural convection is reduced by adding more radiations therefore temperature declines. 8.4.4 Heat transfer rate

47(a) (b) (c) (d) (e) (f) Fig. 8.5: Graph of

? for (a) ?4 (b) ?0 (c) ?2 (d) ?\* (e) ? (f) ??? Figs. 8?5(? - ?) are prepared to interpret

11the variation in heat transfer coefficient ? for multiple values of various physical parameters.

Fig. 8?5(?) characterizes increasing influence of fluid parameter ?4 on ?? It is evident from resulting sketch that magnitude of heat transfer grows for larger ?4?

9It is noteworthy that heat transfer coefficient. Fig. 8?5(?) is

portrayed for observing

7the influence of Taylor number ?0 on heat transfer coefficient. Result clarifies that heat transfer

rate grows via ?0? Fig. 8?5(?) indicates that there is an enhancement in heat transfer coefficient for rising values of slip parameter ?? An increment in ? for growing values of non-uniformity parameter ? is reported in Fig. 8?5(?). Magnitude of heat transfer coefficient decays for rise in heat generation/absorption coefficient as depicted in Fig. 8?5(?). Fig. 8?5(?) depicts a decline in ? for rise in radiation parameter ??? A heat loss is generated for stronger thermal radiations and hence ? decreases. 8.4.5 Streamlines (a) (b) (c) Fig. 8.6: Streamlines for ?0 with fixed values of ? = 0?01? ? = 1?5? ? = 0?2? ? = 0?1? ? = 1?2? ? = ?2? ? = ?1 = 0? 2? ? = 2 for (a)

68?0 = 0? 0 (b) ?0 = 0? 5 (c) ?0 = 2. (a) (b) (c)

Fig. 8.7: Streamlines for ?4 for (a) ?4 = 0?0 (b) ?4 = 2?5 (c) ?4 = 5. (a) (b) (c) Fig. 8.8: Streamlines for ? for (a) ? = 0?2 (b) ? = 0?4 (c) ? = 0?6. Figs. 8?6(? - ?) are sketched to notice the effect of Taylor number on trapping phenomenon. The size of trapping bolus decreases at lower channel for increase in rotation. It is also clear that trapping bolus disappears for further rise in ? 0 ? A similar impact is observed for fluid parameter and velocity slip parameter as seen through Figs. 8?7 and 8?8. 8.5 Conclusions Peristaltic pumping of couple stress fluid under the influences of heat source/sink, thermal radiation and slip conditions is examined. Key findings of investigation are given by: • A decline in axial velocity distribution

70is observed for increasing values of velocity slip parameter ?, fluid parameter ?4 and



rotation  $\Omega$  however velocity increases via non-uniformity parameter  $\alpha$ . • Similar outcomes of  $\alpha$ ,  $\Omega$ ,  $\beta$  and  $\gamma$  on secondary velocity are observed whereas  $\delta$  affects  $\gamma$  oppositely. • Temperature is increasing function of  $\alpha$ ,  $\beta$  and  $\gamma$ . • There is an inverse relationship between temperature and rising values of  $\alpha$ ,  $\Omega$ ,  $\beta$ . • Decaying response is depicted by heat transfer coefficient for growing values of  $\alpha$  and  $\Omega$ . • Heat transfer coefficient increases via  $\alpha$ ,  $\beta$ ,  $\gamma$  and  $\delta$ . Chapter 9 Peristaltic motion of third grade fluid subject to nonlinear radiation

**9 peristaltic motion of third grade liquid in a**

tapered asymmetric geometry. System in rotating frame is entertained. Relevant problems have been numerically solved. The

**55 velocity, temperature and heat transfer rate are physically**

stressed. 9.2 Problem statement An incompressible third grade liquid

**37 in a tapered channel is considered. The waves**

with amplitudes  $(\alpha, \beta)$  and phase  $\gamma$  are taken. A case of rigid body rotation for channel and fluid is considered. System rotates about  $\Omega$ . Nonlinear version of radiation is considered. The waves shapes are described by

$$8 \bar{r}^{-1}(\alpha, \beta) = \alpha + \beta \cos 2\theta (\alpha - \beta) \quad (9.1) \quad \bar{r}^{-2}(\alpha, \beta) = -\alpha - \beta \cos 2\theta (\alpha + \beta) + \gamma \quad (9.2)$$

The constitutive equations for third order fluid are  $T = -pI + S$ ,  $S = \alpha A_1 + \beta_1 A_2 + \beta_2 A_2 A_1 + \beta_3 A_3 + \beta_4 (A_1 A_2 + A_2 A_1) + \beta_5 (A_1 A_2) A_1$ . According to Fosdick and Rajagopal [67]:  $\alpha \geq 0$ ,  $\beta_1 \geq 0$ ,  $\beta_1 = \beta_2 = 0$ ,  $\beta_3 \geq 0$ ,  $|\beta_1 + \beta_2| \leq 2\beta_3$ . Eq. (9.4) becomes  $S = \alpha A_1 + \beta_1 A_2 + \beta_2 A_2 A_1 + \beta_3 (A_1 A_2) A_1$ . Rotating flow is described by the equations  $\text{div } V = 0$ ,  $\rho \frac{D^2 V}{Dt^2} + (V \cdot \nabla) V + \Omega \times (\Omega \times r) + 2\Omega \times V = \text{div } T$ ,  $\rho \frac{D^2 \theta}{Dt^2} = \nabla^2 \theta + \nabla \cdot q + T \cdot L$ . (9.3) (9.4) (9.5) (9.6) (9.7) (9.8) In above equations  $\beta_1$  ( $\beta_2 = 1 - \beta_1$ ) and  $\beta_3$  ( $\beta_4 = 1 - 3\beta_3$ ) are material parameters,  $A_1 = (V \cdot \nabla)$ ,  $A_2 = -L + L \cdot L$ ,  $A_3 = L + L \cdot L$ ,  $L = \nabla V$ ,  $V$  the velocity and  $r$  the position vector. Nonlinear thermal radiation after using Rosseland approximation is given by  $q = -4\sigma^* \theta = -136\sigma^* \theta^3$  (9.9) in which  $\sigma^*$  and  $\theta$  represents

**11 the Stefan-Boltzmann constant and the mean absorption coefficient respectively.**

Applying below transformations  $\eta =$

2\epsilon - \eta \eta \eta = \eta \eta \eta = \eta \eta \eta = \eta (\eta \eta \eta \eta \eta) \eta (\eta \eta \eta \eta \eta) = \eta (\eta \eta \eta \eta \eta) - \eta \eta \eta

(\eta \eta \eta \eta \eta) = \eta (\eta \eta \eta \eta \eta) \eta (\eta \eta \eta \eta \eta) = \eta (\eta \eta \eta \eta \eta) \eta (9.10)

Eqs. (9?6 - 9?8) become ( ? ) ? + ( ? ) ? + ( ? ) ? = 0 ? (9.11) ? ( ? + ? ) ( ? ) ? + ? ( ? ) ? + ? ( ? ) ? - 2 ? = - ( ? ) ? + ( ? ? ? ) ? + ( ? ? ? ) ? + ( ? ? ? ) ? ? n o ? ( ? + ? ) ( ? ) ? + ? ( ? ) ? + ? ( ? ) ? + 2 ? ( ? + ? ) = - ( ? ) ? + ( ? ? ? ) ? + ( ? ? ? ) ? + ( ? ? ? ) ? ? n o ? ( ? + ? ) ( ? ) ? + ? ( ? ) ? + ? ( ? ) ? = - ( ? ) ? + + ( ? ? ? ) ? + ( ? ? ? ) ? + ( ? ? ? ) ? ? n o ? (9.12) (9.13) (9.14) ??? ( ? ) ? + ? ( ? ) ? + ? ( ? ) ? = ?? ( ? ) ? ? + ( ? ) ? ? + ( ? ) ? ? (9.15) n o - ( ? ? ) ? + ??? ( ? ) ? + ??? ( ( ? ) ? + ( ? ) ? ) + ??? ( ? ) ? (9.16) n o Consider dimensionless variables and stream function as ?\* = ?1 = ?= ??= ?5 = ?? ?\* = ?? ?\* = ?? ?\* = ??? ?\* = ?1?? ?1 = ?-1??2 = ?-2 ? \* = ? ? ? \* = ? ? ? = ? ? ? ? 1 ? ? ? ? 1 ? - ?0 ? 1 ? Re = ? ? ? ? 0 Re ?- ? ? 1 - ?0 ? ? ? = ? ? ? ? ? = ? ? ? ? ? = ?0 ? 1 ? ? ? ? ? ? ? ? = ? 4 ? ? ? \* ?0 3 ? ? ? 1 = ° ? 1 ? ? ? ? ? 2 = ° ? 2 ? ? ? = ? ? ? ? ? 1 ? ? ? ? ? 2 1 0 3 ? ? = ? ? ? ? ? = - ? ? ? ?

(9.17) Now applying lubrication approach, Eqs. (9?10) – (9?14) can be reduced as follows: ?? = (???)? + 2? ?? 0 (9.18) ?? = (???)? - 2? 0 ((?)? + 1) ? (9.19) ?? = 0? (9.20) 1 + ?? Pr (?(? - 1) + 1)3 (??)?? + 3?? Pr (?? - 1) + 1)2 (?? - 1) ?? ? = 0? (9.21)

95 h i h i j \phi ??? = ( ? ) ? ? + 2 ? 5 ( ? 2 ? ? + ? 2 ? ) ( ? ) ? ? ? ? ? ? ? = ( ? ) ? + 2 ?

5( ?;2 ?\phi ? + ?;2 ?\phi ) ( ? ) ? ? j \phi j \phi with dimensionless conditions ?1 = 1 + ?? + ?1 cos (2??) ? ?2 = -1 - ?? - ?2 cos(2?? + ?) ? ? = ?1 2 ? ( ? ) ? = -1? ? = 0? ( ? ) ? - ? ? 1 ( 1 - ? ) = 0? at ? = ?1? ? = - ? 1 2 ? ( ? ) ? = -1? ? = 0? ( ? ) ? - ? ? 2 ( 1 + ? ) = 0? at ? = ? ? ? where (9.22) (9.23) (9.24) ?1 = ? - 1 - ? ? ? ? 2 ? 1 = ( ? ) ? ? ? ? (9.25) Z?1 Eqs. (9?16) and (9?17) take the forms: (???)? + 2? 0 ? = 0? (9.26) 3 ' ? (???)? - 2? ((?)? + 1) = 0? 0 (9.27)

### 9.3 Solution methodology

The Eqs. (9?16)–(9?19) and conditions (9?20)–(9?22) have been numerically solved for (???), ? and ?. **9.4 Discussion**

#### 9.4.1 Velocity profile

Figs. 9.1(? - ?) are displayed for velocity against ?5, ? and ?0. The velocity is generally parabolic. It has maximum value at channel centre. Velocity has dual behavior for ?5. In upper portion of channel, the axial velocity increases. Physical such increase corresponds to decay in fluid viscosity. In lower portion of channel, the situation is different (Fig. 9?1(?)). In Fig. 9?1(? )? ? at channel centre is an increasing function of ?? Fig. 9?1(? ) represents effect of ?0 on axial velocity. There is generation of secondary velocity for rotation. It increases ?. Effects of ?5, ? and ?0 on secondary velocity are shown in Figs. 9?2(?-?)? There is decay in ? for ?5 (Fig. 9?2(?)). Also secondary velocity decays for ? (Fig. 9?2(?)). The reason behind this fact is that fluid rapidly compressed in narrow portion and induced frictional force at wall is reduced. Fig. 9?2(? ) indicates ? against ?0. Gradual increase in ? is observed for ?0. This happens due to faster rotation of liquid particles. (9.28)

46(a) (b) (c) Fig. 9.1: Influence of (a) ?5 (b) ? (c)

? 0 on ??( ? ) when ? = 0?2? ? ? = 0?1? ? ? = 1? ? 1 = 0?7? ? 2 = 0?5? ? ? = 0?8? ? ? = ? 4 ? ? 5 = 0?01 and ? 0 = 0? 5. (a) (b) (c) Fig. 9.2: Effect of (a) ?5 (b) ? (c) ? 0 on ??( ? ) when ? = 0?1? ? ? = 0?1? ? ? = -1? ? 1 = 0?7? ? 2 = 0?5? ? ? = 0?8? ? ? = ? 4 ? ? 5 = 0?01 and ? 0 = 0?5.

#### 9.4.2 Heat transfer

Figs. 9?3(? - ?) are sketched for temperature against ?5, ?0, ??, ??, ??1, ??2, ?? and ??. Fluctuation in ? for greater ?5 is captured in Fig. 9? 3(? ). In fact viscosity of fluid decreases. Decrease in ? for larger ?0 is shown in Fig. 9?3(? ). Physically such decrease in ? corresponds to faster motion of fluid particles. In Fig. 9?3(? )? ? is decreasing function of ??. There is less

15energy is absorbed by fluid for greater ??? therefore temperature

decays. Opposite behavior

15of temperature ratio parameter ?? on temperature distribution is

noticed in Fig. 9?3(?). In fact thermal state of fluid is enhanced with ?? which is responsible for rise in ?. Also in the Fig. 9?3(?) solid line obtained for linear radiation problem ( $?? = 1$ ) and dotted lines are computed through Eq. (9?19) with the variation in ?? for nonlinear radiation. It is worth pointing here that when  $?? \approx 1$ , temperature profiles are close to corresponding profiles for the case of linear radiative heat flux. Figs. 9?3(?) and 9?3(?) compare the results of linear and non-linear radiation for different values of radiation when  $?? = 1?1$  and  $?? = 3$  respectively. It is seen that linear and non-linear results match each other better at  $?? = 1?1$  when compared with  $?? = 3$ . The profiles show a significant decrease as the radiation parameter is gradually increased. Similar response of Biot numbers ( $??1? ??2$ ) on ? at both upper and lower walls are demonstrated through Figs. 9?3(?) and 9?3(?). There is more convection generated with higher values of ( $??1? ??2$ ) and consequently temperature is enhanced. Variation for larger ?? on ? is sketched in Fig. 9? 3(?). In fact viscous dissipation is responsible for enhancement in temperature. Fig. 9?3(?) reveals that ? decreases for different values of ???. Thermal diffusivity of fluid is reduced with an increase in ?? and consequently ? decays. Figs. 9?4(?-?) are plotted for ? against different flow physical parameters. We noticed from Fig. 9?4(?) that because of heat loss, ? decays in magnitude when ?? increases. For larger ?? and ??? the reversed trend is followed (see Figs. 9?4(?) and (?)).

51(a) (b) (c) (d) (e) (f) (g) (h) (i) (j) Fig. 9. 3: Effect of (a) ?5 (b) ?0 (c) ?? (d) ?? (e)

comparison between linear and nonlinear radiation when  $?? = 1?1$  (f) comparison between linear and nonlinear radiation  $?? = 3$  (g) ??1 (h) ??2 (i) ?? (j) ?? on ?(?) when ? = 0?1? ? = 0?1? ? = 1? ?1 = 0?7? ?2 = 0?5? ? = 0?8? ? = ?4? ?5 = 0?01? ??1 = 2? ??2 = 4? ?? = 0?7? Pr = 1?5? ?? = 3? ?? = 1?1 and ?0 = 0?5.

(a) (b) (c) Fig. 9.4: Effect of (a) ?? (b) ?? (c) ?? on ?(?) when ? = 0?1? ? = 1? ?1 = 0?7? ?2 = 0?5? ? = 0?8? ? = ?4 ? ?5 = 0?01? ??1 = 2? ??2 = 4? ?? = 0?7? Pr = 1?5? ?? = 3? ?? = 1?1 and ? 0 = 0?5. 9.5

Conclusions Main points here are • There is dual behavior of ?5 velocity. • Behaviors of ? and ?0 on ? are opposite. • Effect of ?0 on ? is reverse to that of ? and ?5. • There is decrease in temperature for ?0? ?? and ???. • Larger values of ?5, ?? and ?? give rise to temperature. • Heat transfer rate ? is enhanced for ?? and ???. • ? is decreasing function of ??? Chapter 10 Entropy generation impact on peristaltic motion in a rotating frame

10.1 Introduction This chapter intends to investigate the peristalsis of Casson fluid in rotating frame and entropy generation. Constitutive equations are formulated by invoking thermal radiation and viscous dissipation. Slip conditions for temperature and velocity are satisfied. Lubrication approach is employed for reducing the system of equation in simplified form. Exact solutions for re- sulting systems are obtained. Graphical results are prepared to observe the outcomes of fluid parameter, Brinkman number, compliant wall parameters, Taylor, Bejan number and radiation parameter. Entropy generation is also examined. It is noticed that slip effects can control entropy generation.

10.2 Problem definition Consider an incompressible flow of Casson fluid in channel with width 2?. Compliant prop- erties of channel are studied. Rigid body rotation for fluid and channel through constant  $\Omega$  is discussed. Flow is generated due to travelling waves by wavelength ? and amplitude ?. Mathematically one has  $? = \pm?(?? ?) = \pm ? + ? \cos 2? ? (? - ??) ? (10.1) \cdot \frac{1}{2}$   $\frac{3}{4}$ , Here we also consider entropy generation through

**30 radiation and viscous dissipation effects. The**

radiative term  $q_r$  is defined as  $q_r = -3\tau^* \theta \theta''$  in which  $\tau^*$  and  $\theta$  represent

**11 the Stefan-Boltzmann constant and Rosseland's mean absorption coefficient respectively.**

After expanding  $\theta$  about  $\theta_0$  and ignoring higher-order terms  $q_r$  one has  $q_r = -136\tau^* \theta_0 \theta''$  (10.2)

For Casson fluid the stress tensor is  $T = -pI + S$   $S = \tau \dot{\gamma} + s \dot{\gamma}^2$  (10.3) where  $\tau$  is yield stress and  $\dot{\gamma} = \sqrt{2D:D}$ ,  $D$  is the (symmetric) component of deformation rate and  $s$  a plastic viscosity of fluid. Here

$\tau = 1 + \frac{1}{2} \frac{\tau_0}{\tau_0 + \tau_1 \dot{\gamma}}$  Continuity equation for the flow consideration is  $\nabla \cdot u = 0$  + Components of momentum equation in rotating frame are  $\rho \frac{D u}{D t} = -\nabla p + \nabla \cdot S - 2\Omega \times u$  (10.4) (10.5) (10.6) (10.7) Energy equation give  $\rho c_p \frac{D \theta}{D t} = \nabla \cdot (k \nabla \theta) + \Phi$  (10.8)  $\mu \nabla^2 \theta = \Phi$  Complaint walls equation can be expressed as  $\theta(\eta) = \theta_w - \theta_0 \eta^2$  with  $\theta_w = -\frac{1}{2} \frac{q_w}{k} + \theta_0$  (10.9)  $\theta''(\eta) = -\frac{2q_w}{k} + 2\theta_0 \eta$  (10.10)  $\theta'(\eta) = -\frac{2q_w}{k} \eta + \theta_0$  Defining non-dimensional variables and stream function as  $\eta = \frac{r}{R} = \frac{y}{R}$   $u = \frac{U}{U_0} \eta$   $v = \frac{V}{U_0} \eta$   $\theta = \frac{\theta - \theta_w}{\theta_0 - \theta_w}$   $\theta_0 = \frac{1}{2} \frac{q_w}{k}$   $\theta_w = \theta_0 - \frac{1}{2} \frac{q_w}{k}$   $\eta = \frac{r}{R}$   $\eta = \frac{y}{R}$   $\eta = \frac{y}{R}$  (10.11)  $\theta = \frac{\theta - \theta_w}{\theta_0 - \theta_w}$  (10.12) Eqs. (10?3 - 10?8) in view of large wavelength and small Reynolds are  $\frac{D u}{D t} = \frac{\partial u}{\partial t} + u \frac{\partial u}{\partial x} + v \frac{\partial u}{\partial y} = \frac{\partial u}{\partial t} - 2\eta \frac{\partial u}{\partial \eta}$   $0 \frac{\partial u}{\partial \eta} = 0$  (1 + Pr)  $\frac{D \theta}{D t} + \frac{2\eta}{\theta_0 - \theta_w} \frac{\partial \theta}{\partial \eta} = 0$   $\frac{\partial \theta}{\partial \eta} = 1 + \frac{1}{2} \frac{q_w}{k} \frac{\eta}{\theta_0 - \theta_w}$  Boundary conditions in dimensionless form  $\theta(\pm 1) = 1$  (1 + Pr)  $\frac{D \theta}{D t} = 0$  at  $\eta = \pm 1$  (10?9)  $\theta(\pm 1) = 1$  (10?10)  $\theta'(\pm 1) = 0$  (10?11)  $\theta''(\pm 1) = 0$  (10?12)  $\theta''(\pm 1) = 0$  (10?13) to (10?15) we have:  $1 + \frac{1}{2} \frac{q_w}{k} \frac{\eta}{\theta_0 - \theta_w} = 0$   $\mu \frac{D u}{D t} + \frac{2\eta}{\theta_0 - \theta_w} \frac{\partial \theta}{\partial \eta} = 0$   $\mu \frac{D u}{D t} + \frac{2\eta}{\theta_0 - \theta_w} \frac{\partial \theta}{\partial \eta} = 0$  (10.13) (10.14) (10.15) (10.16) (10.17) (10.18) (10.19) (10.20) (10.21) (10.22) (10.23) 10.3 Entropy generation Dimensional form of the entropy generation is given as  $\dot{S}_{gen} = \frac{1}{T^2} (\mu \nabla^2 u)^2 + \frac{1}{T^2} (k \nabla^2 \theta)^2$  + ... in dimensionless form, entropy generation can be written as follows:  $\dot{S}_{gen} = \frac{1}{(T_0 - T_w)^2} (1 + Pr) \mu \frac{D u}{D t}^2 + \frac{1}{(T_0 - T_w)^2} \mu \frac{D u}{D t}^2$  (10.24) (10.25) where  $\theta^* = (\theta - \theta_w)$  and  $\theta_0 = \frac{1}{2} \frac{q_w}{k}$  represents the temperature difference parameter and entropy generation characteristics. In Eq. (10?24) first and second terms corresponds to entropy generation due to heat transfer (??) and fluid friction (??) respectively. Now defining Bejan number  $Be = \frac{\mu \frac{D u}{D t}^2}{\frac{1}{(T_0 - T_w)^2} \mu \frac{D u}{D t}^2}$  (10.26) 10.4 Solution methodology The exact solutions of equations (10?16, 10?22, 10?23 and 10?25) corresponding to boundary conditions (10?18 - 10?21) are as follows  $\theta = 6 + 24\theta_0 \frac{1}{2} \frac{q_w}{k} \frac{\eta}{\theta_0 - \theta_w} + 76(6 + 8\theta_0 \frac{1}{2} \frac{q_w}{k} \frac{\eta}{\theta_0 - \theta_w}) - 1 \frac{1}{2} \frac{q_w}{k} \frac{\eta}{\theta_0 - \theta_w} - 3(2(1 + Pr)\frac{1}{2} \frac{q_w}{k} \frac{\eta}{\theta_0 - \theta_w})^3 - 4(1 + Pr)(3 + 12\theta_0 \frac{1}{2} \frac{q_w}{k} \frac{\eta}{\theta_0 - \theta_w} + 76(3 + 4\theta_0 \frac{1}{2} \frac{q_w}{k} \frac{\eta}{\theta_0 - \theta_w})) - 1 \frac{1}{2} \frac{q_w}{k} \frac{\eta}{\theta_0 - \theta_w} [4\theta_0 \frac{1}{2} \frac{q_w}{k} \frac{\eta}{\theta_0 - \theta_w} - 6\theta_0 \frac{1}{2} \frac{q_w}{k} \frac{\eta}{\theta_0 - \theta_w} (2(1 + Pr)\frac{1}{2} \frac{q_w}{k} \frac{\eta}{\theta_0 - \theta_w} + 76)] + 2(12(1 + Pr)\frac{1}{2} \frac{q_w}{k} \frac{\eta}{\theta_0 - \theta_w} + 76)(8(1 + Pr)\frac{1}{2} \frac{q_w}{k} \frac{\eta}{\theta_0 - \theta_w} + 576))$  (10.27) (10.28)  $\theta = 14 [2(\frac{1}{2} \frac{q_w}{k} \frac{\eta}{\theta_0 - \theta_w} + 76) - 1 - ((1 + Pr)\frac{1}{2} \frac{q_w}{k} \frac{\eta}{\theta_0 - \theta_w}) (3(1 + Pr) + 12\theta_0 \frac{1}{2} \frac{q_w}{k} \frac{\eta}{\theta_0 - \theta_w})^2 - 13\theta_0 \frac{1}{2} \frac{q_w}{k} \frac{\eta}{\theta_0 - \theta_w} (1 + Pr) - 2(\frac{1}{2} \frac{q_w}{k} \frac{\eta}{\theta_0 - \theta_w} + 76) - 1 [3\theta_0 \frac{1}{2} \frac{q_w}{k} \frac{\eta}{\theta_0 - \theta_w} (1 + Pr)(\frac{1}{2} \frac{q_w}{k} \frac{\eta}{\theta_0 - \theta_w} + 76) + ((1 + Pr)\frac{1}{2} \frac{q_w}{k} \frac{\eta}{\theta_0 - \theta_w}) (3(1 + Pr) + 12\theta_0 \frac{1}{2} \frac{q_w}{k} \frac{\eta}{\theta_0 - \theta_w})^2 - 4\theta_0 \frac{1}{2} \frac{q_w}{k} \frac{\eta}{\theta_0 - \theta_w} (1 + Pr) - 2(\frac{1}{2} \frac{q_w}{k} \frac{\eta}{\theta_0 - \theta_w} + 76) - 1] ]$  (10.29)  $\theta = 14 (1 + Pr) [(\frac{1}{2} \frac{q_w}{k} \frac{\eta}{\theta_0 - \theta_w} + 76) - 1 - ((1 + Pr)\frac{1}{2} \frac{q_w}{k} \frac{\eta}{\theta_0 - \theta_w}) (3(1 + Pr) + 12\theta_0 \frac{1}{2} \frac{q_w}{k} \frac{\eta}{\theta_0 - \theta_w})^2 - 13\theta_0 \frac{1}{2} \frac{q_w}{k} \frac{\eta}{\theta_0 - \theta_w} (1 + Pr) - 2(\frac{1}{2} \frac{q_w}{k} \frac{\eta}{\theta_0 - \theta_w} + 76) - 1] ]$

+4? 02?6?2?3)2)-16???2?3?(1 + ?) + 9?'???2?2?6(1 + ?6) ((3 + 12? 02?1?2?2 + ?6(3 + 4? 02?6?2?2(3?1 + ?))2)-1]? (10.30) 10.5 Discussion Impact of various involved parameters on axial velocity is demonstrated

58in Figs. (10? 1 – 10? 5). Fig. 10? 1 depicts the variation in ? for multiple values of

Taylor's number. It is obvious that velocity declines via ? 0 since a secondary flow is induced by increase in rotation which decreases velocity of fluid in axial direction. Fig. 10?2 clarifies an enhancement in velocity for growing values of fluid parameter ?6?

15It is due to reduction in viscosity of fluid. Fig. 10?3 is plotted

to observe the impact of slip parameter ?1 on axial velocity. Resulting sketch

15shows an increment in velocity for larger

?1? In fact for larger slip parameter, less resistance is offered to the fluid which tend to rise the velocity. It can be seen through

66Fig. 10? 4 that axial velocity is a decreasing function of secondary slip parameter

?? Impact of wall parameters (?1? ?? ?3) on velocity profile is illustrated through Fig. 10?5. Wall elasticity parameters (?1? ??) accelerates the flow of fluid however a reduction in velocity is observed for increasing damping parameter ?3? Variation in secondary velocity for embedded parameters is analyzed through Figs. (10?6 – 10?9). It is found from Fig. 10?6 that secondary velocity grows for larger fluid parameter ?6? Secondary velocity ?

28is an increasing function of Taylor's number as demonstrated in Fig.

10?7. The reason lies behind the fact the fluid moves faster in secondary direction for increase in rotation. Fig. 10?8 serves to manifest the impact of slip parameter ?2 on ?? Here velocity grows via ?? Impact of wall parameters on secondary velocity is similar as observed for axial velocity (see Fig. 10?9). Figs. (10?10 – 10?15) characterize the effect of physical parameters on temperature profile. A decline in temperature is obtained for rise in Taylor's number ? 0 as demonstrated in Fig. 10?10? Fig. 10?11 discloses that temperature of fluid decreases as fluid parameter grows. It

15due to decrease in viscosity of fluid. Variation in

? for larger ?3 is portrayed in Fig. 10?12. It is obvious from resulting graph that there is in increment in temperature for enhancing slip parameter. Wall elasticity parameters ??(? = 1? 2) tend to rise the

temperature however an opposite behavior is noticed for wall damping parameter  $\beta$  (see Fig. 10.13). Fig. 10.14 highlights the decaying outcomes of radiation parameter on temperature profile. Since for higher  $\beta$  absorbing power of fluid particle tend to reduce and hence temperature drops. Fig. 10.15 determines the

**15 behavior of temperature for rising values of**

Brinkman number  $Br$ . As more heat is generated for stronger viscous dissipation therefore temperature rises. Figs. (10.16 – 10.21) are captured to investigate the behavior of heat transfer coefficient for variation in pertinent parameters. Decaying response of heat transfer coefficient towards growing Taylor number is recorded in Fig. 10.16. Fluid parameter produces an increment in magnitude heat transfer coefficient as depicted in Fig. 10.17. Physically for larger  $\beta$  the strength of viscous forces increase. As a result,  $h$  grows. Fig. 10.18 clarifies that

**13 heat transfer coefficient is an increasing function of**

thermal slip parameter  $\beta$ . Since heat transfer coefficient and temperature are in direct relation with each other therefore wall parameters  $\beta$ ,  $\gamma$  and  $\delta$  affect  $h$  in same manner as that of temperature profile (see Fig. 10.19). Upon increasing radiation parameter, heat transfer coefficient declines as shown in Fig. 10.20. Fig. 10.21 characterizes an inverse relationship between  $h$  and Brinkman number  $Br$ .

**78 Fig. 10.1 Fig. 10.2 Fig. 10.1:**

Effect of  $\beta$  on  $h$  Fig. 10.2: Effect of  $\gamma$  on  $h$ .

**3 Fig. 10.3 Fig. 10.4 Fig. 10.**

3: Effect of  $\delta$  on  $h$  Fig. 10.5 Fig. 10.5: Effect of  $\beta$ ,  $\gamma$ ,  $\delta$  on  $h$  Fig. 10.6 Fig. 10.7

**59 Fig. 10.6: Effect of  $\gamma$  on  $h$ . Fig. 10.7: Effect of  $\beta$  on  $h$ . Fig. 10.8**

Fig. 10.9 Fig. 10.8: Effect of  $\delta$  on  $h$ . Fig. 10.9: Effect of  $\beta$ ,  $\gamma$ ,  $\delta$  on  $h$ ?

**38 Fig. 10.10 Fig. 10.11 Fig. 10.10:**

Effect of  $\beta$  on  $h$ .

**38 Fig. 10.12 Fig. 10.13 Fig. 10.12:**

Effect of  $\delta$  on  $h$ . Fig. 10.13: Effect of  $\beta$ ,  $\gamma$ ,  $\delta$  on  $h$ .

3Fig. 10. 14 Fig. 10. 15 Fig. 10.14: Effect of ?? on ?(?). Fig. 10. 16 Fig. 10. 17 Fig. 10.

16: Effect of ? 0 on ? (?). Fig. 10.17: Effect of ?6 on ? (?).

34Fig. 10.18 Fig. 10.19 Fig. 10. 18: Effect of

?3 on ?(?).

65Fig. 10. 20 Fig. 10. 21 Fig. 10.20: Effect of ?? on ?(?). Fig. 10.21: Effect of ?? on ? (?). 10.

5.1 Entropy generation Figs. (10?22 – 10?26) reveal the impression of sundry parameters on entropy generation. Fig. 10?22 displays a growing outcome of fluid parameter on entropy generation. A less entropy is produced at center of channel as compared to channel walls. A reverse relationship is noticed with the larger values of thermal slip, rotation and thermal radiation and can be viewed through Figs. 10?23 – 10?25. When channel is rotated at high speed, more heat is generated and hence entropy declines. Fig. 10?26 indicates a rise in entropy generation via larger values of Brinkman parameter ???–1. It is obvious that more disturbance in fluid is generated through larger Brinkman parameter which tend to enhance ??? Figs. 10?27 and 10?28 show that for larger Taylor number and thermal radiation parameter the

62heat transfer irreversibility is high when compared with total irreversibility for heat transfer and fluid friction.

A reduction is demonstrated by ?? for increasing values of fluid and thermal slip parameter (see Figs. 10?29 and 10?30). Figs. 10?29 and 10?30 reveal a development in magnitude of Bejan number for growth in Taylor number and radiation parameter. Kinetic energy of fluid rises via ? 0 and ?? which produces an enhancement in ??? A growing impression of Brinkman number on Bejan number is portrayed in

3Fig. 10? 31? Fig. 10.22 Fig. 10.23 Fig. 10.

22: Effect of ?6 on ?? . Fig. 10.23: Effect of ?3 on ??.

34Fig. 10.24 Fig. 10.25 Fig. 10. 24: Effect of

? 0 on ? ? . Fig. 10.25: Effect of ?? on ? ? . Fig. 10.26 Fig. 10.26: Effect of ???–1 on ??.

3Fig. 10.27 Fig. 10.28 Fig. 10.



27: Effect of  $\beta$  on  $\theta$ . Fig. 10.28: Effect of  $\theta$  on  $\theta$ .

**3 Fig. 10.29 Fig. 10.30 Fig. 10.**

29: Effect of  $\beta$  on  $\theta$ . Fig. 10.30: Effect of  $\theta$  on  $\theta$ . Fig. 10.31 Fig. 10.31: Effect of  $\theta - 1$  on  $\theta$ . 10.5.2 Trapping In Figs. 10.32 and 10.33, trapping phenomenon is observed for various involved parameters. Fig. 10.32 elucidates that

**21 size and number of** trapping bolus reduces **for larger values of**

Casson parameter  $\beta$ ? It is due to decrease in kinetic energy of fluid particles.

**10 It is clear from Fig. 10.33 that size of** trapped bolus decreases **for rising values**

of rotation parameter  $\theta$ . (a) (b) (c) Fig. 10.32: Stream lines for

**72 (a)  $\beta = 0$  (b)  $\beta = 0.5$  (c)  $\beta = 5$ . (a) (b) (c)**

**86 Fig. 10. 33: Streamlines for  $\beta$  (a)  $\beta = 0$  (b)  $\beta = 0.5$  (c)  $\beta = 1$ .**

10.6 Conclusions Here peristaltic transport Casson fluid under the influence of entropy generation through a rotating channel in examined. The key findings of investigation are • There is a reduction in axial velocity for growing Taylor number  $\theta$  • Impact of fluid parameter  $\beta$  on  $\theta$ ,  $\theta$ ,  $\theta$  is opposite when compared with Bejan number  $\theta$  • A significant rise in secondary velocity via larger wall parameter,  $\theta$   $\beta$  and  $\theta$  is observed. • There is an inverse relationship between axial velocity and the slip parameters. • Increasing outcomes of elastic parameters ( $\theta$   $\theta$ ) towards  $\theta$  are noticed however impact of  $\theta$  on  $\theta$  is quite opposite. • Temperature distribution is decreasing function of  $\theta$  and  $\theta$  however it is directly related with  $\beta$   $\theta$  and  $\theta$ . • Multiple values of  $\theta - 1$   $\theta$  and  $\beta$  tend to raise entropy generation. • Decaying impression of  $\theta$  and  $\theta$  is observed on entropy generation. • Increasing values of  $\beta$  and  $\theta$  have tendency to reduce Bejan number. However  $\theta$  and  $\theta$  have a growing impact on  $\theta$  • Heat transfer coefficient is directly related with  $\beta$   $\theta$  and  $\theta$  However  $\theta$  declines via  $\theta$  and  $\theta$  Bibliography [1] T.W. Engelmann, Zur Physiologie des Ureter, Pflug. Arch. Ges. Physiol., 2 (1869) 243- 293. [2] J. Lapedes, The physiology of the intact human ureter., J. Urol., 59 (1948) 501-537. [3] F. Kiil, Function of the ureter and renal pelvis, Annals. Sur., 148 (1958) 280-291. [4] S. Boyarsky, Surgical physiology of the renal pelvis and ureter, Monogr. Sur. Sci., 1 (1964) 173-213. [5] T.W. Latham, Fluid motion in a peristaltic pump, M.I.T Cambridge MA, (1966). [6] A.H. Shapiro, Pumping and retrograde diffusion in peristaltic waves, In "Proceedings of the Workshop on ureteral reflux in children". Nat. Acad. Sci., Washington, D. C., (1967) 109-126. [7] E.C. Eckstein, Experimental and theoretical pressure studies of peristaltic pumping, M. S. Thesis, Dep. Mech. Eng., M.I.T., Cambridge, MA (1970). [8] S.L. Weinberg, A theoretical and experimetal treatment of peristaltic pumping and its relation to uretal function, PhD Thesis, Dep. Mech. Eng., M.I.T., Cambridge, MA (1970)? [9] S.L. Weinberg, M. Y. Jaffrin and A. H. Shapiro, A hydrodynamical model of ureteral function. In "Proceedings Workshop Hydrodynam. Upper urinary tract"., Nat. Acad. Sci., Washington, D. C. (1971) ? [10] P.S. Lykoudis, Peristaltic pumping: a



bioengineering model. In "Proceedings Workshop Hydrodynam. Upper urinary tract", Nat. Acad. Sci., Washington, D. C. (1971) ? [11] T.F. Zien and S. Ostrach, A long wave approximation to peristaltic motion, *J. Biomech.*, 3 (1970) 63-75 [12] Y.C. Fung, Peristaltic pumping, a bioengineering model, In: S. Boyarsky (Ed.) *Urodynamic: Hydrodynam. Ureter renal pelvis*, Acad. Press, New York, (1971?). [13] Y.C. Fung, Muscle controlled flow, *Proc. 12th Midwestern Mech. Conf. Univ. Notre Dame, South Bend, Indiana*, (1971?). [14] J.C. Burns and T. Parkes, Peristaltic motion, *J. Fluid Mech.*, 29 (1967) 731-743. [15] M. Hanin, The flow through a channel due to transversely oscillating walls, *Israel J. Technol.*, 6 (1968) 67-71. [16] J.R. Meginniss, An analytical investigation of flow and hemolysis in peristaltic type blood pumps, M.S. Thesis, Dep. Mech. Eng., M.I.T., Cambridge, MA (1970). [17] C.C. Yin and Y.C. Fung, Peristaltic wave in circular cylindrical tubes, *J. Appl. Mech.*, 36 (1969) 579-587. [18] H.S. Lew, Y.C. Fung and C. B. Lowenstein, Peristaltic carrying and mixing of chyme in the small intestine (An analysis of a mathematical model of peristalsis of the small intestine), *J. Biomech.*, 4 (1971) 297-315. [19] H.S. Lew and Y.C. Fung, A study on the low Reynolds number in a valved vessel, *J. Biomech.*, 4 (1971) 85-94. [20] C. Barton and S. Raynor, Peristaltic flow in tubes, *Bull. Math. Biol.*, 30 (1968) 663-680. [21] M.Y. Jaffrin, Inertia and streamline curvature effects on peristaltic pumping, *Int. J. Eng. Sci.*, 11 (1973) 681-699. [22] P.Tong and D. Vawter, An analysis of peristaltic pumping, *J. Appl. Mech.*, 39 (1972) 857-862. [23] R.E. Semleser, W.J. Shack and T.J. Lardner, The swimming of spermatozoa in an active channel, *J. Biomech.*, 7 (1974) 349-355. [24] T.K. Mitra and S.N. Prasad. Interaction of peristaltic motion with Poiseuille flow, *Bull. Math. Biol.*, 36 (1974) 127-141. [25] N. Liron, On peristaltic flow and its efficiency, *Bull. Math. Biol.*, 38 (1976) 573-596. [26] T.D. Brown and T.K.Hung, Computational and experimental investigations of two- dimensional nonlinear peristaltic flows, *J. Fluid Mech.*, 83 (1977) 249-272. [27] L.M. Srivastava and V.P. Srivastava, Peristaltic transport of a two-layered model of physiological fluid, *J. Biomech.*, 15 (1982) 257-265. [28] S. Nakanishi and M. Kawaguti, Numerical study on peristaltic flow of viscous fluid, *J. Phys. Soc. Jpn.* 52, (1983) 848-855. [29] S. Takabatake, K. Ayukawa and A. Mori, Peristaltic pumping in circular cylindrical tubes: a numerical study of fluid transport and its efficiency, *J. Fluid Mech.*, 193 (1988) 267-283. [30] Kh.S. Mekheimer, Peristaltic transport of a Newtonian fluid through a uniform and non- uniform annulus, *Arab. J. Sci. Eng.*, 30 (2005) 69-83. [31] A.R. Rao and M. Mishra, Nonlinear and curvature effects on peristaltic flow of a viscous fluid in an asymmetric channel, *Acta. Mech.*, 168 (2004) 35-59. [32] T. Hayat, M. Javed, and A.A. Hendi, Peristaltic transport of viscous fluid in a curved channel with compliant walls, *Int. J. Heat Mass Transf.*, 54 (2011) 1615-1621. [33] H.S. Lew, Peristaltic carrying and mixing of chyme in the small intestine (An analysis of a mathematical model of peristalsis of the small intestine), *J. Biomech.*, 4(1971) 297-315. [34] J.C. Misra and B.K. Sahu, Forced contraction and expansion of a valved blood vessel: A mathematical model, *Math. Comput. Model.*, 12 (1989) 761-776. [35] M. Patel and M.G. Timol, The stress strain relationship for viscoelastic non Newtonian fluids, *Int. J. Appl. Math. Mech.* 6 (2010) 79-93. [36] N.S. Akbar, S. Nadeem and Z.H. Khan, Numerical simulation of peristaltic flow of a Carreau nanofluid in an asymmetric channel, *Alexand. Eng. J.*, 53 (2014) 191-197. [37] R. Ellahi and F. Hussain, Simultaneous effects of MHD and partial slip on peristaltic flow of Jeffery fluid in a rectangular duct, *J. Mag. Magn. Mater.*, 393 (2015) 284-292. [38] M.M. Bhatti and M.A. Abbas, Simultaneous effects of slip and MHD on peristaltic blood flow of Jeffrey fluid model through a porous medium, *Alexand. Eng. J.*, 55 (2016) 1017- 1023. [39] R.G. Devi and R. Devanathan, Peristaltic transport of micropolar fluid, *Proc. Indian Acad. Sci.*, 81(A) (1975) 149-163. [40] M. Sheikholeslami, D.D. Ganji, R. Ashorynejad and H.B. Rokni, Analytical investigation of Jeffery-Hamel flow with high magnetic field and nanoparticle by Adomian decomposition method, *Appl. Math. Mech. - Engl. Ed.*, 33 (2012) 25-36. [41] G. Radhakrishnamacharya and V.R. Murthy, Heat transfer to peristaltic transport in a non-uniform channel, *Defence Sci. J.*, 43 (1993) 275-280. [42] V.P. Srivastava and M. Saxena, A two-fluid model of non-Newtonian blood flow induced by peristaltic waves, *Rheol. Acta.*, 34 (1995) 406-414. [43] E.F. Elshehawey, A. M. El Misery and A. E. H. Abd El Naby, Peristaltic motion of generalized Newtonian fluid in a non-uniform channel, *J. Phys. Soc. Jpn.*, 67 (1998) 434- 440. [44] A. Riaz, R. Ellahi and S. Nadeem, Peristaltic transport of a Carreau fluid in a compliant rectangular duct, *Alexand. Eng. J.*, 53

(2014) 475-484. [45] T. Hayat, R.J. Moitsheki and S. Abelman, Stokes' first problem for Sisko fluid over a porous wall, *Appl. Math. Comput.*, 217 (2010) 622-628. [46] T. Hayat, T. Muhammad, B. Ahmad and S.A. Shehzad, Impact of magnetic field in three dimensional flow of Sisko nanofluid with convective condition, *J. Mag. Magn. Mater.*, 413 (2016) 1-8. [47] A. Zaman, N. Ali and O.A. Bég, Numerical study of unsteady blood flow through a vessel using Sisko model, *Eng. Scien. Techn., an Int. J.*, 19 (2016) 538-547. 137 [48] T. Hayat, F.M. Abbasi and A. Alsaedi, Numerical analysis for MHD peristaltic transport of Carreau-Yasuda fluid in a curved channel with Hall effects, *J. Mag. Magn. Mater.*, 382 (2015) 104-110. [49] A. V. Mernone, J. N. Mazumdar and S. K. Lucas, A mathematical study of peristaltic transport of Casson fluid, *Math. Comput. Model.*, 35 (2002) 894-912. [50] O. Eytan and D. Elad, Analysis of intrauterine fluid motion induced by uterine contractions, *Bull. Math. Bio.*, 61 (1999) 221-238. [51] S. Nadeem and S. Akram, Peristaltic transport of a hyperbolic tangent fluid model in an asymmetric channel, *Z. Naturforsch.*, 64a (2009) 559-567. [52] S. Hina, M. Mustafa, T. Hayat and Naif D. Alotaibi, On peristaltic motion of pseudo-plastic fluid in a curved channel with heat/mass transfer and wall properties, *App. Math. Comp.*, 263 (2015) 378—391. [53] N. S. Akbar, S. Nadeem, C. Lee, Z. H. Khan and Rizwan Ul Haq, Numerical study of Williamson nano fluid flow in an asymmetric channel, *Res. Physics*, 3 (2013) 161-166. [54] A. Riaz, S. Nadeem, R. Ellahi and N. S. Akbar, The influence of wall flexibility on unsteady peristaltic flow of Prandtl fluid in a three dimensional rectangular duct, *Appl. Math. Comp.*, 241 (2014) 389—400. [55] T. Hayat, H. Zahir, A. Tanveer and A. Alsaedi, Influences of Hall current and chemical reaction in mixed convective peristaltic flow of Prandtl fluid, *J. Mag. Magn. Mater.*, 407 (2016) 321—327. [56] H.M. Shawky, Pulsatile flow with heat transfer of dusty magnetohydrodynamic Ree-Eyring fluid through a channel, *Heat/mass Tran.*, 45 (2009) 1261-1269. [57] M.M. Bhatti, M. Ali Abbas and M.M. Rashidi, Combine effects of Magnetohydrodynamics (MHD) and partial slip on peristaltic Blood flow of Ree-Eyring fluid with wall properties, *Eng. Sci. Tech. Int. J.*, 19 (2016) 1497-1502. [58] F.M. Abbasi, A. Alsaedi and T. Hayat, Peristaltic transport of Eyring-Powell fluid in a curved channel, *J. Aerosp. Eng.*, (2014) DOI: 10.1061/(ASCE)AS.1943-5525.0000354. 138 [59] S. Hina, M. Mustafa and T. Hayat and A. Alsaedi, Peristaltic transport of Powell-Eyring fluid in a curved channel with heat/mass transfer and wall properties, *Int. J. Heat Mass Transf.*, 101 (2016) 156-165. [60] A. C. Eringen, Nonlinear theory of simple micro-elastic solids-I, *Int. J. Eng. Sci.*, 2 (1964) 189-203. [61] M. W. Johnson and D. Segalman, A model for viscoelastic fluid behavior which allows non-affine deformation, *J. Non-Newtonian Fluid Mech.*, 2 (1977) 255-270. [62] P. Chaturani and R.P. Samy, A study of non-Newtonian aspects of blood flow through stenosed arteries and its application in arterial diseases, *J. Biorheol.*, 22 (1985) 521-531. [63] G. Bohme and R. Friedrich, Peristaltic flow of viscoelastic liquids, *J. Fluid Mech.*, 128 (1983) 109-122. [64] T. Hayat, A. Tanveer, H. Yasmin and A. Alsaedi, Effects of convective conditions and chemical reaction on peristaltic flow of Eyring-Powell fluid, *Appl. Bion. Biomech.*, 11 (2014) 221-233. [65] N. Alvi, T. Latif, Q. Hussain and S. Asghar, Peristalsis of nonconstant viscosity Jeffrey fluid with nanoparticles, *Results in Physics*, 6 (2016) 1109-1125. [66] T. Latif, N. Alvi, Q. Hussain and S. Asghar Variable properties of MHD third order fluid with peristalsis, *Results in Physics*, 6 (2016) 963-972. [67] R.L. Fosdick and K.R. Rajagopal, Thermodynamics and stability of fluids of third grade, *Proc. R. Soc. Lond. Ser. A*, 339 (1980) 351-377. [68] D. Tripathi, S.K. Pandey and S. Das, Peristaltic flow of viscoelastic fluid with fractional Maxwell model through a channel, *Applied Mathematics and Computation*, 215 (2010) 3645-3654. [69] K.S. Mekheimer and Y. Abd Elmaboud, Peristaltic flow of a couple stress fluid in an annulus: Application of an endoscope, *Physica A*, 387 (2008) 2403-2415. [70] G.C. Shit and M. Roy, Hydromagnetic effect on inclined peristaltic flow of a couple stress fluid, *Alex. Eng. J.* 53 (2014) 949-958. [71] K. Ramesh, Influence of heat and mass transfer on peristaltic flow of a couple stress fluid through porous medium in the presence of inclined magnetic field in an inclined asymmetric channel, *J. Mol. Liquids*, 219 (2016) 256-270. [72] D. C. Sanyal and N. K. Maji, Thermoregulation through skin under variable atmospheric and physiological conditions, *J. Theor. Biol.*, 208 (2001) 451-456. [73] M. D. Shera, A. S. Gladman, S. R. Davidson, J. Trachtenberg and M. R. Gertner, Helical antenna arrays for interstitial microwave thermal therapy for prostate cancer: tissue phantom testing and simulations for treatment, 46 (2001) 1905-1918. [74] G. Radhakrishnamacharya and

V.R. Murthy, Heat transfer to peristaltic transport in a non-uniform channel, *defence Sci. J.*, 43 (1993) 275-280. [75] K. Vajravelu, G. Radhakrishnamacharya and V. Radhakrishnamurty, Peristaltic flow and heat transfer in a vertical porous medium with long wave approximation, *Int. J. Nonlinear Mech.*, 42 (2007) 754-759. [76] J.R. Oleson, Hyperthermia by magnetic induction: I. Physical characteristics of the technique, *Int. J. Radiation Oncology (Biology and Physics)*, 8 (2001) 1747-1756. [77] P.A. Voltairas, D.I. Fotiadis and M.K. Michalis, Hydrodynamics of magnetic drug targeting, *J. Biomech.*, 35 (2002) 813-820. [78] A. Ogulu, Hydromagnetic heat transfer to blood flow in the microcirculation, *J. Fizik Malaysia*, 17 (1996) 135-140 [79] J. M. R. Carlton, C. A. Yowell, K. A. Sturrock and J. B. Dame, Biomagnetic separation of contaminating host leukocytes from plasmodium infected erythrocytes, *Exp. Parasitol.*, 97 (2001) 111-115. [80] V. K. Sud, G. S. Sekhon and R. K. Mishra, Pumping action on blood by a magnetic field, *Bull. Math. Biol.*, 39 (1977) 385-390. 140 [81] H. L. Agarwal and B. Anwaruddin, Peristaltic flow of blood in a branch, *Ranchi Univ. Math. J.*, 15 (1984) 111-121. [82] G. Radhakrishnamacharya and V. R. Murty, Heat transfer to peristaltic transport in a non-uniform channel, *Defence Sci. J.* 43 (1993) 275-280. [83] Y. Wang, T. Hayat, N. Ali and M. Oberlack, Magnetohydrodynamic peristaltic motion of a Sisko fluid in a symmetric or asymmetric channel, *Physica A: Stat. Mech. Appl.*, 387 (2008) 347-36. [84] T. Hayat, M. Shafique, A. Tanveer and A. Alsaedi, Magnetohydrodynamic effects on peristaltic flow of hyperbolic tangent nanofluid with slip conditions and Joule heating in an inclined channel, *Int. J. Heat Mass Transf.*, 102 (2016) 54-63. [85] M. Awais, S. Farooq, H. Yasmin, T. Hayat and A. Alsaedi, Convective heat transfer analysis for MHD peristaltic flow in an asymmetric channel, *Int. J. Biomath.*, 7 (2014) DOI: 10.1142/S1793524514500235 (15 pages). [86] F.M. Abbasi, Saba and S.A. Shehzad, Heat transfer analysis for peristaltic flow of Carreau-Yasuda fluid through a curved channel with radial magnetic field, *Int. J. Heat Mass Transf.*, 115 (2017) 777—783. [87] R. Ellahi, M.M. Bhatti and C.M. Khalique, Three-dimensional flow analysis of Carreau fluid model induced by peristaltic wave in the presence of magnetic field, *J. Mol. Liquids*, 241 (2017) 1059—1068. [88] S. Asghar, Q. Hussain, T. Hayat and F. Alsaadi, Hall and ion slip effects on peristaltic flow and heat transfer analysis with Ohmic heating, *Appl. Math. Mech.*, 35 (2014) 1509-1524. [89] T. Hayat, M. Shafique, A. Tanveer and A. Alsaedi, Hall and ion slip effects on peristaltic flow of Jeffrey nanofluid with Joule heating, *J. Magn. Mag. Materials*, 407 (2016) 51-59. [90] K. Nowar, Peristaltic flow of a nanofluid under the effect of Hall current and porous medium, *Math. Prob. Eng.*, DOI: 10.1155/2014/389581. [91] R. Ellahi, M. M. Bhatti and I. Pop, Effects of Hall and ion slip on MHD peristaltic flow of Jeffrey fluid in a non-uniform rectangular duct, *Int. J. Num. Meth. Heat and Fluid Flow*, 26 (2016) 1802 - 1820. [92] M. M. Bhatti, M. Ali Abbas and M. M. Rashidi, Effect of Hall and ion slip on peristaltic blood flow of Eyring Powell fluid in a non-uniform porous channel, *World J. Model. Simul.*, 12 (2016) 268-279. [93] S. Noreen and M. Qasim, Influence of Hall current and viscous dissipation on pressure driven flow of pseudoplastic fluid with heat generation: A mathematical study, *Plosone*, DOI: 10.1371/journal.pone.0129588. [94] M. Ganeswara Reddy, K. Venugopal Reddy and O.D. Makinde, Hydromagnetic peristaltic motion of a reacting and radiating couple stress fluid in an inclined asymmetric channel filled with a porous medium, *Alex. Eng. J.*, 55 (2016) 1841-1853. [95] A.A. Dar and K. Elangovan, Impact of an inclined magnetic field, heat generation/absorption and radiation on the peristaltic flow of a Micropolar fluid through a porous non-uniform channel with slip velocity, *NTMSCI*, 5 (2017), 227-244. [96] Y. A. Elmaboud, K. S. Mekheimer and M. S. Mohamed, Series solution of a natural convection flow for a Carreau fluid in a vertical channel with peristalsis, *J. Hydrodynamics, Ser. B*, 27 (2015) 969—979. [97] T. Hayat, S. Farooq and B. Ahmad, A. Alsaedi, Homogeneous-heterogeneous reactions and heat source/sink effects in MHD peristaltic flow of micropolar fluid with Newtonian heating in a curved channel, *J. Mol. Liq.*, 223 (2016) 469-488. [98] M. Rehman, S. Noreen, A. Haider and H. Azam, Effect of heat sink/source on peristaltic flow of Jeffrey fluid through a symmetric channel, *Alex. Eng. J.*, 54 (2015) 733-743. [99] E.P. Siva and A. Govindarajan, Thermal radiation and Soret effect on MHD peristaltic transport through a tapered asymmetric with convective boundary conditions, *Glob. J. Appl. Math.*, 12 (2016) 213-221. [100] T. Hayat, F. Shah, M.I. Khan and A. Alsaedi, Framing the performance of heat absorption/generation and thermal radiation in chemically reactive Darcy-Forchheimer flow, *Res.Physics*, 7 (2017)

3390-3395. [101] M.M. Bhatti, A.Zeeshan, N.Ijaz, O.Anwar Bég and A. Kadir, Mathematical modelling of nonlinear thermal radiation effects on EMHD peristaltic pumping of viscoelastic dusty fluid through a porous medium duct, *Eng. Sci. Tech. Int. J.*, 20 (2017) 1129-1139. [102] T. Hayat, S. Asad and A. Alsaedi, Non-uniform heat source/sink and thermal radiation effects on the stretched flow of cylinder in a thermally stratified medium, *J. Appl. Fluid Mech.*, 10 (2016) 915-924. [103] L. Lecoq, D. Flick, E. Derens, H.M. Hoang and O. Laguerre, Simplified heat and mass transfer modeling in a food processing plant, *J. Food Eng.*, 171 (2016) 1-13. [104] F. Gavelli, Computational fluid dynamics simulation of fog clouds due to ambient air vaporizers, *J. Loss Prevention Process Indust.*, 23 (2010) 773-780. [105] Z.G. Ariyan, V.M. Sadesh and B. Mojtaba, Numerical analysis of complicated heat and mass transfer inside a Wustite Pellet during reducing to sponge iron by H<sub>2</sub> and CO gaseous mixture, *J. Iron Steel Research, Int.*, 23 (2016) 1142-1150. [106] A.R. Goerke, J. Leung and S.R. Wickramasinghe, Mass and momentum transfer in blood oxygenators, *Chem. Eng. Scien.*, 57 (2002) 2035-2046. [107] S.G. Agrawal and R.N. Methekar, Mathematical model for heat and mass transfer during convective drying of pumpkin, *Food Bioprod. Proces.*, 101 (2017) 68-73. [108] A.R. Budu, G.L. Pavel and D.E. Moraru, Heat and mass transfer aspects in nuclear power generation, *Energy Proced.*, 112 (2017) 571-578. [109] A. Ogulu, Effect of heat generation on low Reynolds number fluid and mass transport in a single lymphatic blood vessel with uniform magnetic field, *Int. Commun. Heat Mass Transfer*, 33 (2006) 790-799. [110] S. Nadeem and N. S. Akbar, Influence of heat and mass transfer on a peristaltic motion of a Jeffrey-six constant fluid in an annulus, *Heat Mass Transfer*, 46 (2010) 485-493. [111] T. Hayat, S. Noreen, M. S. Alhothuali, S. Asghar and A. Alhomaidan, Peristaltic flow under the effects of an induced magnetic field and heat and mass transfer, *Int. J. Heat Mass Transfer*, 55 (2012) 443-452. [112] A. A. Shaaban and M. Y. Abou-zeid, Effects of heat and mass transfer on MHD peristaltic flow of a non-Newtonian fluid through a porous medium between two coaxial cylinders, *Math. Prob. Eng.*, 2013 (2013) 11 pages. [113] T. Hayat, F.M. Abbasi, M. Al-Yami and S. Monaqueel, Slip and Joule heating effects in mixed convection peristaltic transport of nanofluid with Soret and Dufour effects, *J. Mol. Liq.*, 194 (2014) 93-99. [114] M. Mustafa, S. Abbasbandy, S. Hina and T. Hayat, Numerical investigation on mixed convective peristaltic flow of fourth grade fluid with Dufour and Soret effects, *J. Taiwan Inst. Chem. Eng.*, 45 (2014) 308-316. [115] T. Hayat, R. Iqbal, A. Tanveer and A. Alsaed, Soret and Dufour effects in MHD peristalsis of pseudoplastic nanofluid with chemical reaction, *J. Mol. Liq.*, 220 (2016) 693-706. [116] S. Farooq, M. Awais, M. Naseem, T. Hayat and B. Ahmad, Magnetohydrodynamic peristalsis of variable viscosity Jeffrey liquid with heat and mass transfer, *Nucl. Eng. Technol.*, 49 (2017) 1396-1404. [117] T. Hayat, S. Farooq, M. Mustafa and B. Ahmad, Peristaltic transport of Bingham plastic fluid considering magnetic field, Soret and Dufour effects, *Res. Phys.*, 7 (2017) 2000-2011. [118] M. Mustafa, S. Abbasbandy, S. Hina and T. Hayat, Numerical investigation on mixed convective peristaltic flow of fourth grade fluid with Dufour and Soret effects, *J. Taiwan Inst. Chem. Eng.*, 45 (2014) 308-316. [119] T. Hayat, H. Yasmin and M. Al-Yami, Soret and Dufour effects in peristaltic transport of physiological fluids with chemical reaction: a mathematical analysis, *Comput. Fluids*, 89 (2015), 242-253. [120] G. Sankad and M. Dhange, Peristaltic pumping of an incompressible viscous fluid in a porous medium with wall effects and chemical reactions, *Alex. Eng. J.*, 55 (2016) 2015- 2021. [121] R. Muthuraj, K. Nirmala and S. Srinivas, Influences of chemical reaction and wall properties on MHD Peristaltic transport of a Dusty fluid with Heat and Mass transfer, *Alex. Eng. J.*, 55 (2016) 597-611. [122] T. Hayat, A. Tanveer and A. Alsaedi, Mixed convective peristaltic flow of Carreau—Yasuda fluid with thermal deposition and chemical reaction, *Int. J. Heat Mass Trans.*, 96 (2016) 474-481. [123] G. R. Machireddy and V. R. Kattamreddy, Impact of velocity slip and joule heating on MHD peristaltic flow through a porous medium with chemical reaction, *J. Nigerian Math. Soc.*, 35 (2016) 227-244. [124] M. G. Reddy, K. V. Reddy and O.D. Makinde, Hydro magnetic peristaltic motion of a reacting and radiating couple stress fluid in an inclined asymmetric channel filled with a porous medium, *Alex. Eng. J.*, 55 (2016) 1841-1853. [125] J. C. Misra, B. Mallick and A. Sinha, Heat and mass transfer in asymmetric channels during peristaltic transport of an MHD fluid having temperature-dependent properties, *Alex. Eng. J.*, <https://doi.org/10.1016/j.aej.2016.09.021>. [126] S. A. Shehzad, F. M. Abbasi, T. Hayat and F. Alsaadi, MHD

mixed convective peristaltic motion of nanofluid with Joule heating and thermophoresis effects, Plos One, DOI: <https://doi.org/10.1371/journal.pone.0111417>. [127] T. Hayat, M. Rafiq and B. Ahmad, Influences of rotation and thermophoresis on MHD peristaltic transport of Jeffrey fluid with convective conditions and wall properties, J. Magn. Mater., 410 (2016) 89-99. [128] A. Ali, S. Asghar and M. Awais, Thermophoresis and concentration effects in a fourth grade peristaltic flow with convective walls, J. Central South Univ., 24 (2017) 1654-1662. [129] A. Aziz, A similarity solution for laminar thermal boundary layer over a flat plate with a convective surface boundary condition, Commun. Nonlin. Sci. Numer. Simulat., 14 (2009) 1064-1068. [130] O. D. Makinde, Thermal stability of a reactive viscous flow through a porous saturated channel with convective boundary conditions, Appl. therm. Eng., 29 (2009) 1773-1777. [131] T. Hayat, H. Yasmin and M. Al-Yami, Soret and Dufour effects in peristaltic transport of physiological fluids with chemical reaction: A mathematical analysis, Comput. Fluids, 89 (2014) 242-253. [132] T. Hayat, A. Tanveer, H. Yasmin and A. Alsaedi, Effects of convective conditions and chemical reaction on peristaltic flow of Eyring-Powell fluid, Appl. Bionics Biomech., 11 (2014) 221-233. [133] F. M. Abbasi, T. Hayat and B. Ahmad, Peristaltic flow in an asymmetric channel with convective boundary conditions and Joule heating, J. Cent. South Univ., 21 (2014) 1411-1416. [134] N. S. Akbar, Natural convective MHD peristaltic flow of a nanofluid with convective surface boundary conditions, J. Comput. Theor. Nanosci., 12 (2015) 257-262. [135] T. Hayat, M. Iqbal, H. Yasmin, F. E. Alsaadi and H. Gao, Simultaneous effects of Hall and convective conditions on peristaltic flow of couple-stress fluid in an inclined asymmetric channel, Pranama J. Phys., 85 (2015) 125-148. [136] N. Ali, Q. Hussain, T. Hayat and S. Asghar, Slip effects on the peristaltic transport of MHD fluid with variable viscosity, Physics Lett. A, 372 (2008) 1477-1489. [137] T. Hayat, A. Tanveer and A. Alsaedi, Numerical analysis of partial slip on peristalsis of MHD Jeffrey nanofluid in curved channel with porous space, J. Mol. Liquids, 224 (2016) 944-953. [138] T. Hayat, S. Hina and N. Ali, Simultaneous effects of slip and heat transfer on the peristaltic flow, Commun. Nonlin. Sci. Numer. Simul., 15 (2010) 1526-1537. [139] K. Ramesh, Effects of slip and convective conditions on the peristaltic flow of couple stress fluid in an asymmetric channel through porous medium, Comp. Methods Prog. Biomed., 135 (2016) 1-14. [140] S. Hina, M. Mustafa and T. Hayat, Peristaltic motion of Johnson-Segalman fluid in a curved channel with slip conditions, Plos One, 9 (2014) e114168. [141] A. Yildirim and S.A. Sezer, Effects of partial slip on the peristaltic flow of a MHD Newtonian fluid in an asymmetric channel, Math. Comput. Model., 52 (2010) 618-625. [142] Y.V.K.R. Kumar, S.V.H.N.K. Kumari, M.V.R. Murthy and S. Sreenadh, Peristaltic transport of a power-law fluid in an asymmetric channel bounded by permeable walls, Adv. Appl. Sci. Res., 2 (2011) 396-406. [143] R. Ellahi and F. Hussain, Simultaneous effects of MHD and partial slip on peristaltic flow of Jeffrey fluid in a rectangular duct, J. Mag. Magn. Materials, 393 (2015) 284-292. [144] R. Saravana, R.H. Reddy, S. Sreenadh, S. Vekataramana and A. Kavitha, Influence of slip, heat and mass transfer on the peristaltic transport of a third order fluid in an inclined asymmetric channel, Int. J. Appl. Math. Mech., 9 (2013) 51-86. [145] K. Das, Slip effects on heat transfer and peristaltic pumping of a Johnson-Segalman fluid in an inclined asymmetric channel, Arab. J. Math., 1 (2012) 159-174. [146] B. Jyothi and P. K. Rao, Slip effects on MHD peristaltic transport of a Williamson fluid through a porous medium in a symmetric channel, J. Math. Comput., 3 (2013) 1306-1324. [147] A. Sinha, G.C. Shit and N.K. Ranjit, Peristaltic transport of MHD flow and heat transfer in an asymmetric channel: Effects of variable viscosity, velocity-slip and temperature jump, Alex. Eng. J., 54 (2015) 691-704. [148] S.I. Abdelsalam and K. Vafai, Combined effects of magnetic field and rheological properties on the peristaltic flow of a compressible fluid in a microfluidic channel, European J. Mech. B/Fluids, <https://doi.org/10.1016/j.euromechflu.2017.02.002>. [149] T. Hayat, M. Shafique, A. Tanveer and A. Alsaedi, Slip and Joule heating effects on radiative peristaltic flow of hyperbolic tangent nanofluid, Int. J. Heat Mass Trans., 112 (2017) 559-567. [150] A. M. Abd-Alla, S. M. Abo-Dahab and H. D. El-Shahrany, Effects of rotation and initial stress on peristaltic transport of fourth grade fluid with heat transfer and induced magnetic field, J. Mag. Magn. Mater., 349 (2014) 268-280. [151] A. M. Abd-Alla, S. M. Abo-Dahab and H. D. El-Shahrany, Effect of rotation on peristaltic flow of a micropolar fluid through a porous medium with an external magnetic field, J. Mag. Magn. Mater., 348 (2013) 33-43. [152] A. M. Abd-Alla and S. M.

Abo-Dahab, Magnetic field and rotation effects on peristaltic transport of a Jeffrey fluid in an asymmetric channel, *J. Mag. Magn. Mater.*, 374 (2015) 680—689. [153] N. Ali, M. Sajid, T. Javed and Z. Abbas, Peristalsis in a rotating fluid, *Scien. Essays*, 32 (2012) 2891-2897. [154] S.R. Mahmoud, Effect of rotation and magnetic field through porous medium on peristaltic transport of a Jeffrey fluid in tube, *Math. Prob. Eng.*, 2011 (2011) [155] T. Hayat, M. Rafiq and B. Ahmad, Soret and Dufour effects on MHD peristaltic flow of Jeffrey fluid in a rotating system with porous medium, *Plos One.*, DOI: 10.1371/journal.pone.0145525. [156] T. Hayat, M. Rafiq and A. Alsaedi, Investigation of Hall current and slip conditions on peristaltic transport of Cu-water nanofluid in a rotating medium, *Int. J. Thermal Sci.*, 112 (2017) 129-141. Fig. 10.4:

25Effect of  $\eta$  on  $\theta(\eta)$ . Fig. 10. 11: Effect of  $\eta$  on

$\theta(\eta)$ . Fig. 10.15:

25Effect of  $\eta$  on  $\theta(\eta)$ . Fig. 10. 19: Effect of  $\eta$  on  $\theta(\eta)$

$\theta(\eta)$ . 1 2 3 4 5 6 7 8 9 10 11 12 13 14 15 16 17 18 19 20 21 22 23 24 25 26 27 28 29 30 31 32 33 34 35 36  
37 38 39 40 41 42 43 44 45 46 47 48 49 50 51 52 53 54 55 56 57 58 59 60 61 62 63 64 65 66 67 68 69 70  
71 72 73 74 75 76 77 78 79 80 81 82 83 84 85 86 87 89 90 91 92 93 94 95 96 97 98 99 100 101 102 103  
104 105 106 107 108 109 110 111 112 113 114 115 116 117 118 119 120 121 122 123 124 125 126 127 128  
129 130 131 132 133 134 139 141 142 144 145 146 147 148